

---

UNIVERSITÀ  
DEGLI STUDI  
DI BRESCIA

DOTTORATO DI RICERCA IN PRECISION MEDICINE

---

MED 04

CICLO XXXVI

ROLE OF SPHINGOLIPID METABOLISM IN  
MELANOMA PROGRESSION

PhD candidate:  
Marzia Corli

SUPERVISOR: prof. Marco Presta



## TABLE OF CONTENTS

RIASSUNTO.....	1
ABSTRACT.....	3
List of abbreviation.....	5
1. SPHINGOLIPIDS AND THEIR METABOLISM.....	7
1.1 Sphingolipid metabolism .....	8
1.1.1 De novo synthesis of sphingolipids.....	9
1.1.2 The catabolism of sphingolipids.....	10
1.1.3 Zebra-Sphinx: modeling sphingolipidoses in zebrafish.....	11
1.2 The important balance between ceramide and sphingomyelin.....	38
1.2.1 Structure of neutral sphingomyelinase 2.....	39
1.2.2 Role of nSMase2 in cellular signalling.....	41
1.2.3 Biology of $\beta$ -galactosylceramidase.....	41
1.2.4 GALC as a key player in the sphingolipid homeostasis.....	43
1.2.5 Impact of an irreversible $\beta$ -galactosylceramidase inhibitor on the lipid profile of zebrafish embryos.....	44
2. SPHINGOLIPID METABOLIZING ENZYMES MODULATE TUMOR PROGRESSION.....	70
2.1 Role of nSMase2 in cancer progression.....	71
2.1.1 nSMase2 modulates the lipidomic profile in melanoma cells .....	71
2.2 GALC: tumor suppressor or pro-oncogenic protein?.....	74
2.2.1 Oncosuppressive and oncogenic activity of the sphingolipid-metabolizing enzyme $\beta$ -galactosylceramidase.....	74
3. CUTANEOUS MELANOMA.....	84
3.1 Cutaneous melanoma.....	84
3.2 Clinical management of melanoma.....	84
3.3 The origin of melanoma.....	85
3.4 Mechanism of melanoma progression and dissemination.....	87
4. GALC IN MELANOMA.....	89
4.1 The pro-oncogenic sphingolipid-metabolizing enzyme $\beta$ -galactosylceramidase modulates the proteomic landscape in BRAF(V600E)-mutated human melanoma cells.....	90
5. TUMOR ANGIOGENESIS.....	113

5.1 Angiogenesis in melanoma.....	114
5.2 Sphingolipid metabolizing enzymes modulate angiogenesis.....	115
5.2.1 GALC promotes angiogenesis in melanoma.....	116
5.2.2 GALC promotes tyrosine kinase receptor signalling cascades and VEGFR2 activation in HUVECs.....	125
6. DISCUSSION.....	128
7. REFERENCES.....	134
8. RINGRAZIAMENTI.....	145
9. MODULO DI EMBARGO.....	146





## RIASSUNTO

Gli sfingolipidi sono lipidi polari coinvolti in numerosi processi biologici. Ne consegue che sia gli sfingolipidi che gli enzimi coinvolti nel loro metabolismo, sono importanti per l'omeostasi cellulare e partecipano in numerosi processi fisio-patologici.

La mia ricerca mira ad investigare il ruolo degli enzimi GALC e SMPD3 nella progressione del melanoma.

*SMPD3* codifica per la sfingomielinasi neutra di tipo 2 (nSMase2) che promuove la rimozione della testa polare dalla sfingomielina, liberando il ceramide. Studi precedenti hanno dimostrato che l'espressione di *SMPD3* decresce al progredire del melanoma suggerendo un ruolo nella sopravvivenza. In questo lavoro, *SMPD3* è stato sovra-espresso in due linee di melanoma umano, le A2058 e le A375. Livelli aumentati di nSMase2 non hanno inficiato la proliferazione o la migrazione cellulare, tuttavia in un primo saggio di tumorigenesi *in vivo*, cellule che sovra-esprimono *SMPD3* hanno formato lesioni più piccole e meno vascolarizzate rispetto ai controlli, in linea con l'aumento di ceramide, e del suo ruolo protettivo, osservato in queste cellule.

GALC è un enzima lisosomiale che rimuove il  $\beta$ -galattosio dal  $\beta$ -galattosilceramide. Mutazioni nel suo gene codificante sono la causa della malattia neurodegenerativa di Krabbe. In letteratura sono presenti solo pochi studi sul profilo lipidico di modelli sperimentali o pazienti affetti da Krabbe. Per investigare come GALC modifichi la componente lipidica durante l'embriogenesi, embrioni di zebrafish sono stati trattati con un inibitore irreversibile di GALC. I risultati mostrano un'alterazione significativa della componente lipidica di questi embrioni, fornendo nuove conoscenze sul coinvolgimento della componente lipidica in questa patologia. Belleri et al., hanno mostrato che in campioni di melanoma umano c'è una correlazione inversa tra GALC e *SMPD3*, dimostrando che GALC esercita un'attività pro-oncogenica sulle cellule di melanoma murine sia *in vitro* che *in vivo*. Partendo da questi presupposti, *GALC* è stato sovra-espresso in due linee cellulari di melanoma umano, le A2058 e le A375. I dati indicano che cellule sovra-esprimenti GALC proliferano e migrano di più rispetto al controllo. Inoltre, analisi di proteomica rivelano che GALC modula l'espressione di diverse proteine coinvolte nella regolazione del melanoma, nell'evasione della risposta immunitaria, nella risposta da stress del reticolo endoplasmatico e ossidativo.

La progressione del melanoma è strettamente collegata all'angiogenesi. Per tanto il potenziale angiogenetico di queste cellule è stato valutato in un primo esperimento *in vivo*, dove cellule che sovra-esprimono GALC hanno prodotto lesioni più vascolarizzate.

In un contesto tumorale, le cellule secernono fattori pro-angiogenetici volti a innescare il processo di angiogenesi. E' stato verificato che GALC non promuove la secrezione di tali fattori, tuttavia, essendo GALC una proteina secreta, il terreno condizionato delle cellule che lo sovra-esprimono è stato utilizzato in saggi di angiogenesi *in vitro* e *in vivo*. Questi esperimenti hanno dimostrato per la prima volta che GALC, attraverso la sua attività enzimatica e l'internalizzazione in cellule endoteliali, promuove la risposta angiogenetica.

Questo lavoro si propone per tanto di fornire esempi esaustivi sul ruolo degli enzimi del metabolismo degli sfingolipidi nella progressione del melanoma.



## ABSTRACT

Sphingolipids and their metabolizing enzymes are involved in a variety of physiological and pathological conditions. During my PhD program I focused my research activity on the role of the sphingolipid metabolizing enzymes nSMase2 and GALC in cutaneous melanoma.

nSMase2, encoded by *SMPD3*, is the enzyme responsible for the breakdown of sphingomyelin into ceramide. Previous studies demonstrated an onco-suppressive role of nSMase2 in melanoma where *SMPD3* expression progressively decreases from primary to metastatic melanoma and is associated to short overall survival. Here, I overexpressed *SMPD3* in A2058 and A375 human melanoma cell lines to study the role of nSMase2 in this tumor. The upregulation of *SMPD3* did not impact their tumorigenic potential in *in vitro* assays even though preliminary *in vivo* results suggest an onco-protective role of nSMase2. Accordingly, A2058 nSMase2-overexpressing cells gave origin to smaller and less vascularized tumors in a tumorigenesis assay on the top of the chick embryo chorion allantoic membrane, consistent with the increased amount of ceramide that was observed in a lipidomic analysis on these cell lines.

GALC is a lysosomal enzyme that cleaves  $\beta$ -galactose from  $\beta$ -galactosylceramide. Historically, *GALC* has been studied as a causative gene of the neurodegenerative Krabbe disease. Currently, only a limited information is available about the effect of the modulation of GALC activity on the lipidome. For this purpose, zebrafish embryos were treated with an irreversible GALC inhibitor, leading to significant alterations of the lipidic profile.

Belleri et al. showed an inverse correlation between *GALC* and *SMPD3* expression in human melanoma, demonstrating that GALC critically modulates the oncogenic activity of melanoma cells *in vitro* and *in vivo*. On this basis, *GALC* was overexpressed in A2058 and A375 cell lines. Data indicate that *GALC* upregulation induces a significant increase in the proliferative potential and motility of *GALC*-overexpressing cells and proteomic analysis reveals that GALC modulates proteins involved in melanoma biology, tumor immune escape, ER stress responses, mitochondrial antioxidant activity, autophagy and/or apoptosis.

Melanoma progression strictly relies on angiogenesis. In this frame, previous studies demonstrated that GALC deficient mice have an impaired angio-architecture of brain vessels in post-natal angiogenesis and that their endothelium failed to respond to angiogenic factors, suggesting a role of GALC in neovascularization. Therefore, the angiogenic potential of A2058 and A375 *GALC*-overexpressing cells was investigated. Indeed, the s.c. grafting of these cells

in mice has led to more vascularized tumors compared to controls. By mimicking what happens in tumor microenvironment where GALC is secreted by melanoma cells, the conditioned medium of *GALC*-overexpressing cells exerted a significant angiogenic activity *in vitro* and *in vivo* that was hampered by inhibitors of its enzymatic activity. Finally, the conditioned medium of these cells triggers the phosphorylation of the angiogenic tyrosine kinase VEGF receptor 2 and of various downstream signaling pathways in human endothelial cells.

In conclusion, the data pointed out a prominent role of sphingolipid metabolizing enzymes in melanoma progression and angiogenesis.

In this thesis, I collected scientific articles and reviews to which I contributed. These works have been inserted in different points of the narration depending on the context to which they refer.

## LIST OF ABBREVIATION

aSMase: Acid sphingomyelinase  
C1P: Ceramide 1 phosphate (C1P)  
CAM: Chorion Allantoic Membrane  
CDH: Ceramide dihexoside  
CDKN2A: Cyclin-dependent kinase inhibitor 2A  
CE: Cholesterol ester  
Cer: Ceramide  
CerS: Ceramide synthase  
CERT: Ceramide transfer protein  
CHOL: Cholesterol  
CM: Conditioned medium  
CTLA-4: Cytotoxic T-lymphocyte antigen-4  
Dgal: D-galactal  
DH-Cer: Dihydroceramide  
DH-SM: Dihydro sphingomyelin  
ECs: Endothelial cells  
ER: Endoplasmatic reticulum  
FGF2: Fibroblast Growth Factor 2  
GALC:  $\beta$ -galactosylceramidase  
GalCer: Galactosylceramide  
GCP: GALC epoxide inhibitor Gal-cyclophellitol  
GCS: Glucosylceramide synthase  
GLD: Globoid cell leukodystrophy  
GluCer: Glucosylceramide  
HexCer: Hexosylceramide  
HIF1- $\alpha$ : Hypoxia-inducible factor 1-alpha  
INK4A: Inhibitor of kinase 4A  
LPC: Lyso-phosphatidylcholines  
LPE: Lyso-phosphatidylethanolamines  
M6P: Mannose-6-Phosphate  
M6PR: Mannose-6-Phosphate Receptor  
MAPK: Mitogen-activated protein kinase

MHC-I: Major histocompatibility complex I  
MITF: Microphthalmia-associated transcription factor  
MMPs: Matrix metalloproteases  
nSMase2: Neutral sphingomyelinase 2  
nSMases: Neutral sphingomyelinases  
PAF: Platelet-Activating Factor  
PAFR: Platelet-Activating Factor Receptor  
PC: Phosphatidylcholines  
PD-1: Programmed cell death 1  
PD-L1: Programmed cell death ligand 1  
PDGF-B: Platelet derived growth factor subunit b  
PE: Phosphatidylethanolamines  
PTEN: Phosphatase and tensin homologue  
S1P: Sphingosine 1 phosphate  
SapA: Saponin A  
SM: Sphingomyelin  
SMase: Sphingomyelinase  
SMS: Sphingomyelin synthase  
Sph: Sphingosine  
TAG: Triacylglycerols  
TLC: Thin Layer Chromatography  
UVR: UltraViolet Radiation  
VEGF-A: Vascular Endothelial Growth Factor A  
VEGFR2: VEGF Receptor 2

# 1. SPHINGOLIPIDS AND THEIR METABOLISM

Sphingolipids represent one of the major classes of eukaryotic lipids. The first sphingolipids were discovered in the brain in the late 19<sup>th</sup> century by Thudicum, who introduced the name ‘sphingosin’ after the Greek mythical creature, the Sphinx, out of respect for “the many enigmas which it presented to the inquirer” (Hannun and Obeid 2018).

Sphingolipids are important structural molecules of cell membranes. Their common structure is based on sphingosine, an eighteen carbon amino-alcohol. In 1947, H. E. Carter was the first who structurally characterized the sphingosine as S,3R,4E-2- aminooctadec-4-ene-1,3-diol (CARTER and HAINES 1947). Nowadays we refer to sphingolipids such as natural lipids comprised of a sphingoid base backbone with an N-acylated fatty acid chain and a polar head, absent in the sphingolipid precursor ceramide (Cer) (fig. 1.1) (Pralhada Rao et al. 2013).

Ceramides are the precursors for all the sphingolipid classes:

- 1) Sphingomyelins (SM), composed by Cer plus a polar phosphate head, such as phosphocholine. They are the most common sphingolipids and represent approximately 10-20% of membrane lipid composition (Goñi 2022).
- 2) Cerebrosides, composed by Cer with the addition of a single monosaccharide (glucose or galactose) (Dumoulin et al. 2002).
- 3) Gangliosides characterized by an oligosaccharidic head containing at least one sialic acid. They are located on cell surface and represent one of the main brain constituent, up to 6% (Dumoulin et al. 2002).

Sphingolipids are also involved in signal transduction. Indeed, sphingosine (Sph), sphingosine 1 phosphate (S1P), Cer, and ceramide 1 phosphate (C1P) can act as bioactive lipids and act as second messengers. Because of their chemical structure with only one aliphatic chain, Sph and S1P readily leave membranes once activated by their receptors. Instead, Cer and C1P remain in the membrane and are recruited by cytosolic proteins.

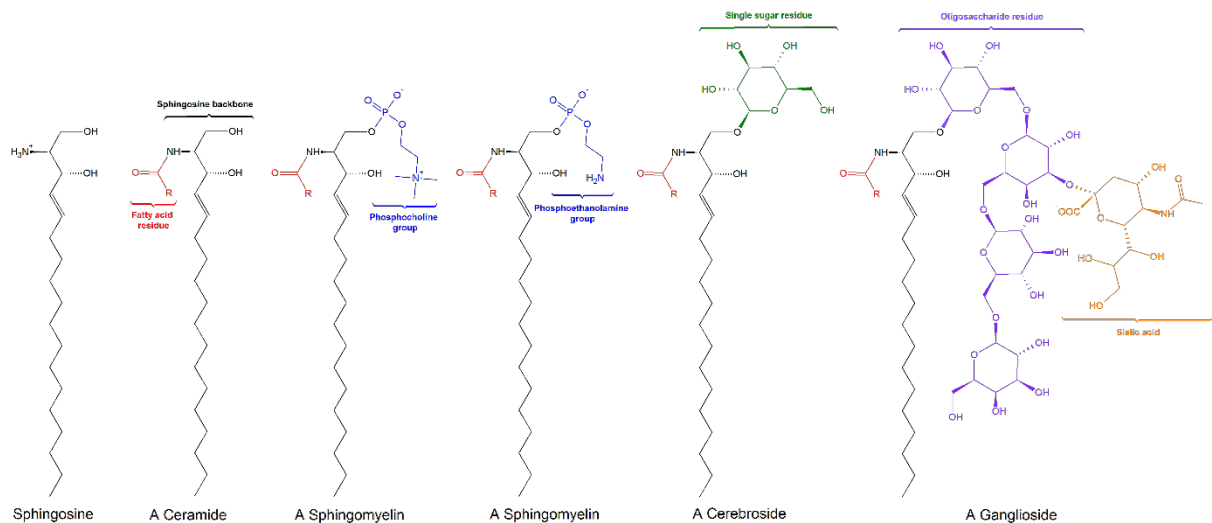


Figure 1.1 Structure of the common sphingolipid classes.

## 1.1 Sphingolipid metabolism

A complex network of enzymes and lipid transporter proteins is involved in the sphingolipid metabolism (fig. 1.2). Despite the diversity in function and structure, sphingolipids have common anabolic and catabolic synthetic pathways.

Sphingosine, the simplest form, serves as the backbone upon which further complexity is achieved. For example, sphingosine acylation results in several species of Cer based on the nature of the acylCoA molecules. The addition of a polar head (phosphocholine or phosphoethanolamine) to Cer gives origin to SM, whereas the addition of sugar residues give origin to glycosphingolipids (Hannun and Obeid 2018).

According to the length of the acyl chain and on the type of headgroup, sphingolipids can differ in complexity, function, and localization inside the cells. In particular, Sph and dihydro sphingosine (DH-Sph) are sufficiently amphipathic to diffuse freely in the cell membrane and flip inside the leaflets. However, the ionization of their free amino group allows them to accumulate in late endosome and lysosome. Cer, instead, relies on proteins for their transport. Among all the sphingolipids, SMs and glycosphingolipids are the most spatially restricted, they are unable to flip among the leaflets without dedicated flippases (Gault, Obeid and Hannun 2010).

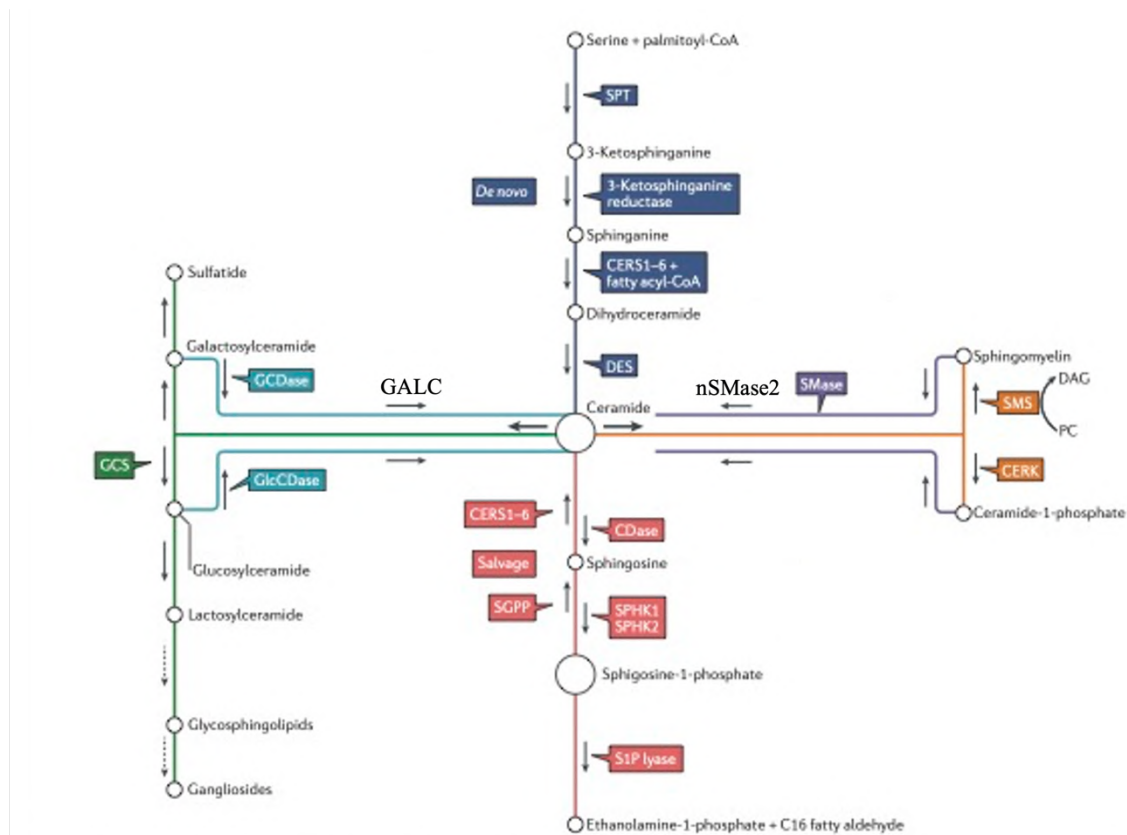


Figure 1.2 Main pathways of sphingolipid metabolism. Modified from (Ogretmen 2018)

### 1.1.1 De novo synthesis of sphingolipids

De novo synthesis of sphingolipids begins at the cytosolic face of the endoplasmic reticulum (ER) where the enzyme serine palmitoyltransferase promotes the condensation of serine and palmitoyl CoA into 3-ketodihydrosphingosine. The keto group is then reduced to a hydroxyl group (dihydrosphingosine) by the enzyme 3-ketodihydrosphingosine in a NADPH dependent manner (Menaldino et al. 2003).

Six different isoforms of ceramide synthases (CerS1-6) are mainly located in the cytoplasmic face of ER membrane and are responsible for the acylation of the previously formed DH-Sph, originating a molecule of dihydroceramide (DH-Cer). Recent evidence suggests that each CerS has a distinct fatty acyl CoA preference and, even though they are largely found in ER membrane, they localize also in the mitochondria and nuclear membranes. Moreover, the expression of different isoform varies among tissues and CerS activation can occur in response to stress stimuli (Wegner et al. 2016).

The newly form molecule of DH-Cer is modified by dihydroceramide  $\Delta$ 4-desaturase that produces a double bound between C4 and C5, thus originating Cer (Gault et al. 2010).

In ER lumen the enzyme ceramide galactosyltransferase transfers galactose from UDP-galactose to Cer, returning a molecule of galactosylceramide (GalCer). Finally, the synthesis of complex sphingolipids such as SMs, cerebrosides, and gangliosides occurs in the Golgi. Cer is delivered by ceramide transfer protein (CERT) or embedded in vesicles from ER to the Golgi where it can be modified into GluCer and SM by the enzymes glucosylceramide synthase (GCS) and sphingomyelin synthase (SMS), respectively (Gault et al. 2010, Ogretmen 2018). In the trans-Golgi, specific Golgi glycotransferases synthesize complex glycosphingolipids from GluCer and GalCer. See (D'Angelo et al. 2013) for further details about the synthesis of gangliosides.

### 1.1.2 The catabolism of sphingolipids

The breakdown of complex sphingolipids into Cer includes three different catabolic pathways (Gault et al. 2010):

1. The SM hydrolysis pathway
2. The salvage pathway
3. The catabolic pathway

The SM hydrolysis pathway involves the sphingomyelinase family that hydrolyzes the binding between the phosphocholine headgroup and Cer. The first sphingomyelinase (SMase) to be described was the acid SMase (aSMase), encoded by the gene *SMPD1*. aSMase works mainly in the lysosome where it metabolizes SM present on endosomal membranes, but it can be also secreted outside the cell. Among the neutral sphingomyelinases (nSMases), nSMase2 is localized in the cytosolic leaflet of Golgi apparatus or inside the plasma membrane (Marchesini, Luberto and Hannun 2003) whereas nSMase3 is mainly found in the ER (Cataldi et al. 2020).

Complex sphingolipids are partially degraded, and their components are recycled to form Cer in what is known as the salvage pathway. Glycosphingolipids are transported from the plasma membrane along endocytic routes to the lysosomes, where they are metabolized by specific glycohydrolases. Among them,  $\beta$ -galactosylceramidase (GALC) is responsible for the breakdown of GalCer in Cer (Kitatani, Idkowiak-Baldys and Hannun 2008). For the purpose of this thesis, the role of GALC in sphingolipid metabolism will be extensively discussed in the following paragraphs.



Cer is further degraded by ceramidases. In particular, the acid ceramidase, encoded by *ASAH1* gene, deacylates Cer in the lysosome, producing Sph. Neutral and alkaline ceramidases instead are located at the plasma membrane and in ER/Golgi complex, respectively. Notably, Sph is generated by the catabolism of more complex sphingolipids or *via* desaturation of DH-Cer, but not *via* de novo synthesis (Coant and Hannun 2019).

### **1.1.3 Zebra-Sphinx: modeling sphingolipidoses in zebrafish**

The enzymes involved in the catabolism of sphingolipids are crucial for cell homeostasis and physiology and their genetic deficiency results in various inborn errors of metabolism, named sphingolipidoses (Abed Rabbo et al. 2021). They represent a subgroup of lysosomal storage diseases characterized by the gradual lysosomal accumulation of the substrate of the defective proteins. Sphingolipidoses affect approximately 1 in 20,000 newborns (Eckhardt 2010) and the clinical presentation of the diseases ranges from a mild progression for some juvenile- or adult-onset forms to severe/fatal infantile forms. To gain a better understanding of the pathogenesis of sphingolipidoses and develop effective therapeutic strategies, it is important to establish new *in vivo* models.

The teleost zebrafish (*Danio rerio*) has emerged as a useful platform for studies in diverse fields of research. The high grade of genome conservation between human and zebrafish (Howe et al. 2013), combined with precise genome editing and the ease of manipulation, enable to model several human diseases in zebrafish, including sphingolipidoses.

In the following review, I briefly described the molecular and clinical features of genetic sphingolipidoses and the use of zebrafish as an animal model for the study of such diseases and for the search of novel therapeutic approaches.



Review

# Zebra-Sphinx: Modeling Sphingolipidoses in Zebrafish

Luca Mignani <sup>†</sup> , Jessica Guerra <sup>†</sup>, Marzia Corli, Davide Capoferri and Marco Presta <sup>\*†</sup>

Unit of Experimental Oncology and Immunology and Zebrafish Facility, Department of Molecular and Translational Medicine, University of Brescia, 25123 Brescia, Italy

\* Correspondence: marco.presta@unibs.it

<sup>†</sup> These authors contributed equally to this work.

**Abstract:** Sphingolipidoses are inborn errors of metabolism due to the pathogenic mutation of genes that encode for lysosomal enzymes, transporters, or enzyme cofactors that participate in the sphingolipid catabolism. They represent a subgroup of lysosomal storage diseases characterized by the gradual lysosomal accumulation of the substrate(s) of the defective proteins. The clinical presentation of patients affected by sphingolipid storage disorders ranges from a mild progression for some juvenile- or adult-onset forms to severe/fatal infantile forms. Despite significant therapeutic achievements, novel strategies are required at basic, clinical, and translational levels to improve patient outcomes. On these bases, the development of in vivo models is crucial for a better understanding of the pathogenesis of sphingolipidoses and for the development of efficacious therapeutic strategies. The teleost zebrafish (*Danio rerio*) has emerged as a useful platform to model several human genetic diseases owing to the high grade of genome conservation between human and zebrafish, combined with precise genome editing and the ease of manipulation. In addition, lipidomic studies have allowed the identification in zebrafish of all of the main classes of lipids present in mammals, supporting the possibility to model diseases of the lipidic metabolism in this animal species with the advantage of using mammalian lipid databases for data processing. This review highlights the use of zebrafish as an innovative model system to gain novel insights into the pathogenesis of sphingolipidoses, with possible implications for the identification of more efficacious therapeutic approaches.

**Keywords:** gene knockout; hereditary disease; lysosome; morpholino; sphingolipid; zebrafish



**Citation:** Mignani, L.; Guerra, J.; Corli, M.; Capoferri, D.; Presta, M. Zebra-Sphinx: Modeling Sphingolipidoses in Zebrafish. *Int. J. Mol. Sci.* **2023**, *24*, 4747. <https://doi.org/10.3390/ijms24054747>

Academic Editor: Taeg Kyu Kwon

Received: 20 January 2023

Revised: 24 February 2023

Accepted: 27 February 2023

Published: 1 March 2023



**Copyright:** © 2023 by the authors. Licensee MDPI, Basel, Switzerland. This article is an open access article distributed under the terms and conditions of the Creative Commons Attribution (CC BY) license (<https://creativecommons.org/licenses/by/4.0/>).

## 1. Introduction

Sphingolipids were first described during the second half of the nineteenth century [1]. The term “sphingolipid” was coined based on the complexity and sphinxlike nature of this class of lipids characterized by a core long chain aliphatic amino alcohol (sphingoid base). The most common member is represented by sphingosine, which can be functionalized by a fatty acid condensed at its aminic moiety and by polar molecules at its hydroxyl terminus, including small organic molecules, amino acids, or carbohydrates [2] (Figure 1).

De novo synthesis of sphingolipids begins in the endoplasmic reticulum (ER) and may move towards the Golgi apparatus. Finally, their mature forms are delivered to cell membranes [2–4]. Sphingolipids play a key structural role in cellular membranes and/or act as signaling molecules. Owing to their molecular structure, sphingolipids can organize within plasma membranes into ordered focal regions named lipid rafts, crucial for the arrangement of raftophilic molecules or transmembrane protein domains [5]. During recycling or after signaling events, sphingolipids may reach the lysosomes, where specific enzymes catabolize them to less-complex molecules, which can enter different metabolic pathways or act as novel signaling molecules [6]. Educated reviews have described the anabolic and metabolic pathways that characterize the sphingolipid metabolism and the involvement of the different sphingolipid species in physiological and pathological processes [7,8].

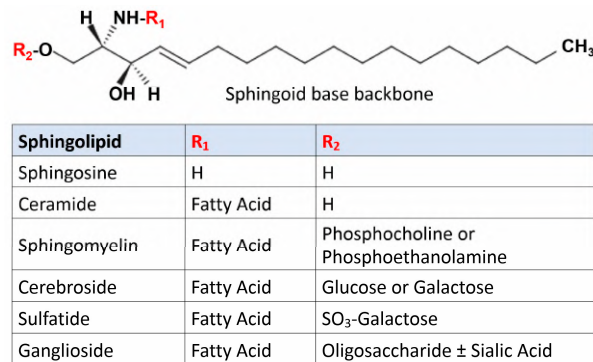


Figure 1. Schematic structure of sphingolipids.

Lysosomal storage diseases are a group of genetic disorders characterized by the gradual lysosomal accumulation of metabolites due to a defective lysosomal hydrolytic activity [9]. Among them, alterations of the lysosomal catabolic pathways responsible for the progressive breakdown of complex sphingolipids may translate into the accumulation of their corresponding undegraded substrates in lysosomes, leading to inherited sphingolipid storage diseases gathered under the name of sphingolipidoses [10]. In this review, we will focus our attention on zebrafish (*Danio rerio*) as an animal model for the study of this sub-class of lysosomal storage diseases and as a “zebra-sphinx” platform for a better understanding of the complex and, at least in part, still sphinxlike biology of sphingolipid metabolism (Figure 2).

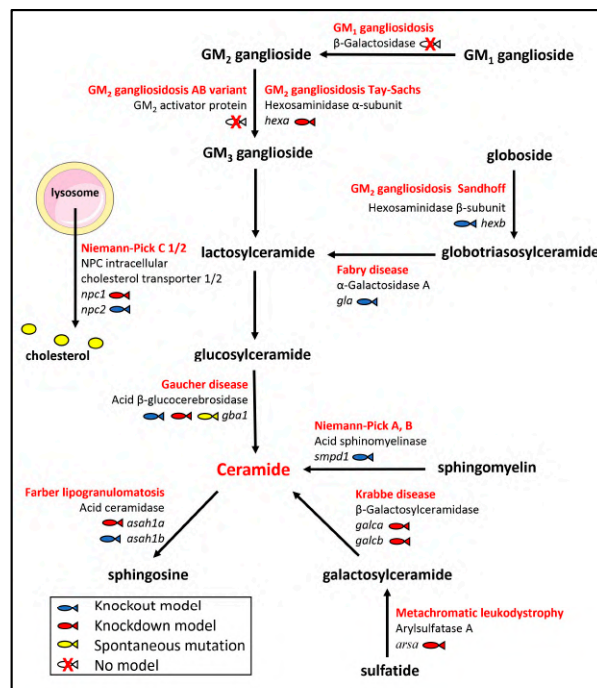
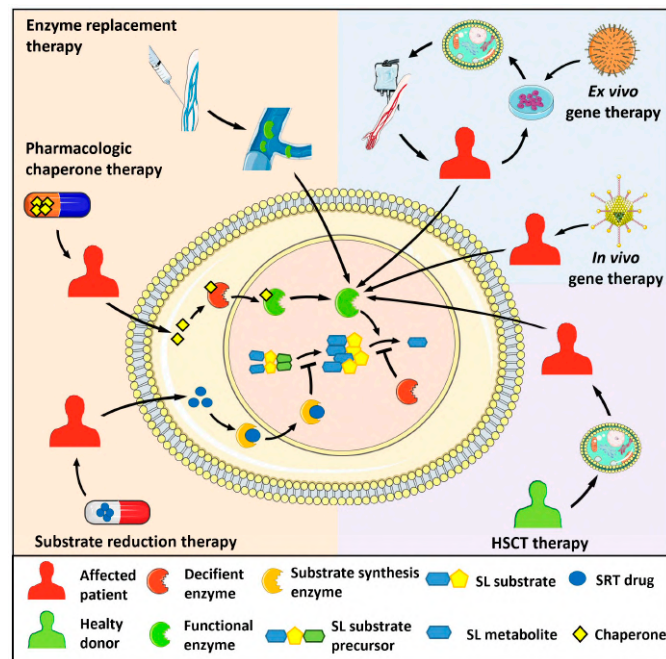


Figure 2. Sphingolipid catabolism. Schematic representation of the biochemical pathways of the sphingolipid catabolism related to hereditary human sphingolipidoses and corresponding non-functional enzymes. Zebrafish genes that have been knocked out or knocked down to generate models of sphingolipidoses are in italics. See text for details.

## 2. Sphingolipidoses

Sphingolipidoses affect approximately 1 in 20,000 newborns [11]. The clinical presentation of patients affected by sphingolipid storage disorders is quite diverse, ranging from a mild progression for some juvenile- or adult-onset forms to severe and fatal infantile forms.

To date, approved and investigational therapies for the treatment of lysosomal storage diseases, including sphingolipidoses, comprise hematopoietic stem cell transplantation (HSCT), in vivo and ex vivo gene therapy, enzyme replacement therapy (ERT), substrate reduction therapy (SRT), and pharmacologic chaperone therapy [12–14] (Figure 3). These strategies have improved the life of many affected patients by preventing progression or ameliorating various signs and symptoms. However, given the complexities resulting from the alterations of sphingolipid metabolism in different systemic organs, much is still needed at the basic, clinical, and translational levels to improve patient outcomes. For the purposes of the present paper, we will briefly describe the major types of human sphingolipidoses (Table 1). Diseases associated with deficiency of the sphingolipid activator proteins saposins A-D generated by proteolytic processing of the common precursor prosaposin will not be described here.



**Figure 3.** Therapeutic strategies for the treatment of sphingolipidoses. Enzyme replacement therapy consists of the intravenous administration of a bioactive recombinant form of the deficient enzyme. Pharmacologic chaperone therapy favours the proper folding of the mutated, misfolded enzyme and its lysosomal translocation, allowing the hydrolysis of the engulfing sphingolipid (SL) substrate. In substrate reduction therapy (SRT), drugs inhibit the activity of the enzyme responsible for the synthesis of the SL substrate of the deficient enzyme, hampering its lysosomal accumulation. In hematopoietic stem cell transplantation (HSCT), healthy donor-derived cells provide the patient with cells expressing the functional enzyme. Ex vivo gene therapy administers a bioactive enzyme by autologous transplantation of genetically modified hematopoietic stem cells. In vivo gene therapy consists of the injection of viral vectors encoding for the functional enzyme.

**Table 1.** Human sphingolipidoses.

Disease	OMIM	Affected Gene	Deficient Protein	Main Accumulated Metabolite
Gaucher	#230800 (type I) #230900 (type II) #231000 (type III)	<i>GBA1</i>	Acid $\beta$ -glucocerebrosidase	Glucosylceramide
Fabry	#301500	<i>GLA</i>	$\alpha$ -Galactosidase A	Globotriaosylceramide
Niemann–Pick	#257200 (type A) #607616 (type B)	<i>SMPD1</i>	Acid sphingomyelinase	Sphingomyelin
	#257220 (type C1)	<i>NPC1</i>	NPC intracellular cholesterol transporter 1	Cholesterol
	#607625 (type C2)	<i>NPC2</i>	NPC intracellular cholesterol transporter 2	
Krabbe	#245200	<i>GALC</i>	$\beta$ -Galactosylceramidase	$\beta$ -Galactosylsphingosine
Farber lipogranulomatosis	#228000	<i>ASAH1</i>	Acid ceramidase	Ceramide
GM1 gangliosidosis	#230500 (type I) #230600 (type II) #230650 (type III)	<i>GBL1</i>	$\beta$ -Galactosidase	GM1 ganglioside
GM2 gangliosidosis	#272750 (AB variant)	<i>GM2A</i>	GM2 activator protein	GM2 ganglioside
	#272800 (Tay-Sachs)	<i>HEXA</i>	Hexosaminidase $\alpha$ -subunit	
	#268800 (Sandhoff)	<i>HEXB</i>	Hexosaminidase $\beta$ -subunit	
Metachromatic leukodystrophy	#250100	<i>ARSA</i>	Arylsulfatase A	Sulfo-galactosylceramide

### 2.1. Gaucher Disease

Gaucher disease (GD) is one of the most common sphingolipidoses with an incidence ranging from 1:40,000 to 1:60,000 live births in the general population, with 1:850 in the Ashkenazi Jewish population [15]. GD is caused by recessive mutations in the *GBA1* gene that encodes for acid  $\beta$ -glucocerebrosidase, also known as  $\beta$ -glucosidase, a lysosomal enzyme responsible for the degradation of glucosylceramide.

The deficiency of acid  $\beta$ -glucocerebrosidase activity leads to the accumulation of its substrate primarily in the lysosomes of macrophages (Gaucher cells) found in the spleen, liver, bone marrow, lungs, and lymph nodes of affected patients [16].

Marked enlarged liver and splenomegaly are clear signs of the disease in children and teenagers that give rise to defects in the blood circulation with anemia and bleeding tendency [17]. Gene expression analysis of cultured skin fibroblasts from GD patients demonstrated that glucosylceramide accumulation triggers the activation of inflammatory responses via the upregulation of genes involved in cytokine and JAK-STAT signaling pathways, the downregulation of genes involved in cell-to-cell and cell-to-matrix interaction, and the inhibition of PI3K-Akt and survival signaling pathways [18].

Several factors may contribute to the severity of GD depending on the type of *GBA1* mutation, including the levels of ER stress and proteasomal degradation. In particular, ER stress responses may entail the accumulation of  $\alpha$ -synuclein aggregates, causative of neuronal injury and degeneration, as in Parkinson's disease [19,20].

According to the degree of severity and impairment, GD is classified into three main groups (GD type I–III) based on clinical presentation. The most frequent and less aggressive form of GD is type I, also known as nonneuropathic GD. The onset of the disease varies from childhood to adulthood, and is characterized by bone pain and fractures, splenomegaly,

hepatomegaly, anemia, leukopenia, and thrombocytopenia [17]. Although it is considered nonneuropathic, a continuum of clinical forms between GD types may exist, with some neuropathic defects also observed in GD type I patients [21].

GD type II and GD type III are historically classified as primary neurologic diseases. GD type II represents the most severe form as it affects children eliciting rapid degeneration that leads to death before 4 years of age. GD type III usually has a later onset with slower progression [22].

Nowadays, macrophage-directed ERT is the standard of care for symptomatic GD type I and type III patients. It is efficacious in reducing splenomegaly and hematological signs, favoring the growth of GD children, whereas, at variance with ERT, SRT based on the administration of glucosylceramide synthase inhibitors has been shown to be effective in also reducing the skeletal complications [23]. At present, no approved treatment exists for neuropathic GD, but recent studies suggest that the use of ambroxol, an over-the-counter drug that can cross the blood–brain barrier, might be effective [24].

## 2.2. Fabry Disease

The Fabry disease, also known as the Anderson–Fabry disease, was first described by W. Anderson and J. Fabry in 1898 as a systemic vascular disorder [25]. The Fabry disease is a X-linked disorder caused by mutations in the *GLA* gene encoding for  $\alpha$ -galactosidase A that catalyzes the hydrolysis of terminal non-reducing  $\alpha$ -D-galactose residues in  $\alpha$ -D-galactosides [26].

Pathogenic variants in *GLA* result in absent or non-functional  $\alpha$ -galactosidase A, leading to the accumulation of its substrate globotriaosylceramide (Gb3) and the deacylated derivative globotriaosylsphingosine in the lysosomes of endothelial cells, myocytes, renal cells, and neurons [27,28].

At the molecular level, the pathogenesis of Fabry disease is still unclear [29]. Gb3 accumulation results in the deregulation of the mitochondrial function and of mTOR and autophagy/lysosome pathways in peripheral blood mononuclear cells from Fabry patients. Of note, similar lysosomal, autophagy, and mitochondrial alterations were also observed in Faber cells, suggesting that a common pathogenic mechanism may exist for both sphingolipidoses [30]. Further confirmation that autophagy and mitochondrial dysfunctions may occur in Fabry disease comes from studies performed on cardiovascular endothelial cells derived from Fabry-induced pluripotent stem cells in which the *GLA* mutation was corrected by clustered regularly interspersed short palindromic repeats/CRISPR-associated 9 (CRISPR/Cas9) technology [31].

The Fabry disease is typically divided into the major classical or infantile phenotype and the late-onset phenotype. The classical form of Fabry disease affects males that have little or no residual  $\alpha$ -galactosidase A activity. It is characterized by clinical heterogeneity and symptoms arise around 1 to 3 years of age. Children with classical Fabry disease usually present acroparesthesia (“Fabry crisis”), angiokeratoma, hypohidrosis, and heat intolerance. The initial symptoms are followed by gastrointestinal disorders, ocular abnormalities, and Gb3 accumulation, causing renal, cardiac, and neurological complications. The milder late-onset Fabry disease involves only a single organ system, typically the heart or the kidneys. Female Fabry patients have a mosaic expression for *GLA* as a result of X chromosome inactivation and they usually show less severe symptoms [32].

Increasing evidence suggests that cardiovascular morbidity is the main cause of death in Fabry patients, mainly due to increased risk of sudden cardiac death and heart failure [33]. The identification of serum biomarkers derived from collagen type I metabolism has been proposed to predict early fibrotic damage in Fabry patients to be followed by a prompt ERT procedure [34–36]. A second currently approved medication is based on chaperone therapy to correct the misfolded enzyme, but an increase in enzymatic activity and a decrease in Gb3/lyso-Gb3 accumulation does not occur in all patients. Currently, SRT and mRNA-based therapy are under evaluation [37].

### 2.3. Niemann–Pick Disease

Niemann–Pick disease (NPD) is an autosomal recessive inherited disorder due to hydrolase deficiency or impaired intracellular cholesterol trafficking. Mutations in acid sphingomyelinase (aSMase), encoded by *SMPD1*, are causative of the NPD type A and B forms, whereas NPD type C, a lysosomal storage disease distinct from sphingolipidoses, is a cholesterol trafficking defect due to mutations in *NPC1* or *NPC2* genes [38].

aSMase catalyzes the breakdown of sphingomyelin in ceramide and phosphocholine. The degree of severity of NPD type A and B depends on the aSMase residual activity owing to the type of *SMPD1* mutation [39]. When aSMase is mutated, its primary substrate accumulates in the monocytes and macrophages (foam cells) of the liver, spleen, lymph nodes, adrenal cortex, and bone marrow [40]. In children with NPD type A, foam cells infiltrate the brain, causing structural changes, gliosis, demyelination, and neuronal cell loss. Thus, NPD type A is the most severe form of NPD and death occurs within the second or third year of age. NPD type A has a high incidence in the Ashkenazi Jewish population, with a carrier frequency of 1 in 90, whereas NPD type B is a pan-ethnic disease characterized by a later onset and milder symptoms [40,41]. Currently, there is no efficacious treatment for NPD type A and B. Recombinant human aSMase selectively reduces sphingomyelin accumulation in NPD type B fibroblasts in vitro [42] and ERT is now under clinical trial [43].

NPD type C is due to mutations in *NPC1*, which encodes for a transmembrane protein of the lysosomal membrane, or *NPC2*, which encodes for an intracellular cholesterol transporter. Both deficiencies lead to intracellular accumulation of unesterified cholesterol and glycosphingolipids [44]. Its incidence is about 1 in 100,000 live births and can be divided into neonatal, late infantile, and juvenile [45]. Neonatal presentation is rare and characterized by progressive liver disease, which represents the most common cause of death among neonatal-onset NPD type C patients [46]. Late infantile and juvenile forms are the most common, characterized by the outbreak of neurological disorders; in contrast to the infantile form, there is no liver or spleen enlargement. NPD type C is usually treated with anti-hypercholesterolemic drugs, but this does not ease the symptoms [47,48].

### 2.4. Krabbe Disease

Also known as globoid cell leukodystrophy, Krabbe disease is an autosomal recessive disorder characterized by the deficiency of the acid hydrolase  $\beta$ -galactosylceramidase (*GALC*) encoded by the *GALC* gene. *GALC* catalyzes the removal of  $\beta$ -galactose from  $\beta$ -galactosylceramide (a major component of myelin) and other terminal  $\beta$ -galactose-containing sphingolipids, including the neurotoxic metabolite  $\beta$ -galactosylsphingosine (psychosine) [49].

By acting at different cellular levels, *GALC* deficiency causes psychosine accumulation paralleled by neuroinflammation, degeneration of oligodendroglia, and progressive demyelination [50]. Psychosine has been shown to inhibit protein kinase C signaling, activate the caspase cascade, disrupt the trans Golgi network and endosomal vesicles, and impair mitochondria and peroxisome function [51]. In addition, the detergent-like action of psychosine may disturb the membrane microdomain organization of lipid rafts, causing demyelination [51–53]. Moreover, deregulation of brain neovascularization occurs in Krabbe patients and in *twitcher* mice, an authentic model of the disease [54], whereas neuroinflammation leads to increased levels of long pentraxin 3, an innate immune response mediator that acts at the site of inflammation [55].

The early infantile form (onset at birth to 5 months of age) represents the most common and severe type of Krabbe disease. It is characterized by fast progression and the symptoms include regression of psychomotor development followed by seizures, loss of vision and hearing, and early death [56]. The late-infantile onset occurs between 13 and 36 months and is characterized by motor regression, ataxia, and progressive blindness [57]. Adult forms of Krabbe disease are rare; they display progressive spastic paraplegia and sometimes neuropathy [58].

ERT is not the most effective treatment because of its poor ability to pass the blood brain barrier and the immune response against the recombinant *GALC* protein [51]. Currently, the standard of care is HSCT, which significantly improves the lifespan of Krabbe patients when performed before the outbreak of symptoms [57].

### 2.5. Farber Lipogranulomatosis

Farber disease is a rare autosomal inherited metabolic disorder caused by inactivating mutations in the *ASAHI* gene that encodes for the lysosomal acid ceramidase. Acid ceramidase promotes the breakdown of ceramide in sphingosine and fatty acid, and its deficiency leads to the progressive accumulation of ceramide in bone, cartilage, immune system, central nervous system, lungs, and other organs [59]. Farber lipogranulomatosis has a wide range of age onset and clinical features, even though subcutaneous nodules, made of ceramide engorged macrophages, arthritis, and dysphonia are the three major signs of the disease [60]. As for other sphingolipidosis, the infantile form is the most severe, characterized by progressive neurologic regression and lung disorders. Milder forms present only modest or no alterations of the central nervous system [61]. Unfortunately, no effective therapies are currently available for this disease [59].

### 2.6. GM1 and GM2 Gangliosidoses

Gangliosides are glycosphingolipids that account for up to 10% of brain lipid content and were isolated from the human brain for the first time in 1939 by E. Klenk [62]. They are composed of sialic-acid-containing oligosaccharide chains linked via a  $\beta$ -glycosidic bond to ceramide, which is responsible for their insertion into cell membranes. Deficiencies in enzymes involved in their metabolism cause an accumulation of unmetabolized gangliosides in lysosomes, mainly in neurons where ectopic neurite outgrowth may occur [63].

#### 2.6.1. GM1 Gangliosidosis

$\beta$ -Galactosidase is a lysosomal hydrolase that cleaves  $\beta$ -linked galactose residues from the non-reducing end of glycan moieties found in various glycoconjugates [62]. Deficiency in the  $\beta$ -galactosidase encoding gene *GBL1* leads to the accumulation of the GM1 ganglioside and its derivative GA1 mainly in lysosomes. Like all of the other lysosomal disorders, GM1 gangliosidosis is an inherited metabolic disease with an estimated incidence of 1 in 100,000–200,000 newborns [64].

The most severe form of the disease is the infantile type I GM1 gangliosidosis, characterized by hydrops fetalis developmental psychomotor regression and, as the child grows, hepatosplenomegaly and skeletal abnormalities. Type II GM1 gangliosidosis is named late infantile or juvenile, depending on the age at which the first symptoms arise: between 12 and 24 months for the late infantile form and 3–5 years for the juvenile form. Children quickly lose their ambulatory capacity and need a gastrostomy placement. In the juvenile form, ataxia and dysarthria follow the psychomotor decline [65]. The adult-onset type III GM1 gangliosidosis is characterized by milder and more varied symptoms, with a longer life expectancy [66].

Currently, no specific treatment exists for GM1 gangliosidosis; the therapy aims to relieve symptoms and is mostly palliative [67]. Recently, miglustat, a glucosylceramide synthase inhibitor, used for SRT in GD and NPD type C diseases [68,69], has also been proposed for the treatment of children affected by type II GM1 gangliosidosis [70].

#### 2.6.2. GM2 Gangliosidosis

The disease is due to the lysosomal accumulation of the GM2 ganglioside [71], which represents about 5% of all brain gangliosides [72]. The hydrolysis of GM2 to GM3 ganglioside is performed by  $\beta$ -hexosaminidase A (HEXA), a heterodimer whose  $\alpha$  and  $\beta$  subunits are encoded by *HEXA* and *HEXB* genes, respectively, and requires the GM2 activator protein (GM2AP) as a cofactor [73]. In an ERT prospective, an enzymatically active recombinant protein homodimer HexM has been developed that is able to interact with



the GM2AP–GM2 complex in vivo [73]. Currently, the use of HexM as ERT has not been transferred to the clinics and works are in progress to optimize an AAV vector for gene therapy [74,75] with reduced immune response reactions [76].

Three forms of GM2 gangliosidoses have been described: the AB variant, Tay–Sachs disease, and Sandhoff disease. They are characterized by neurological disorders that vary from hypotonia regression to cerebellar ataxia according to the age of onset [71].

#### AB Variant

The AB variant is the rarest form of GM2 gangliosidosis, with about 30 cases reported in the scientific literature. It is caused by inherited mutations of the *GM2A* gene that disrupt the activity of the GM2AP cofactor. The AB variant is characterized by severe cerebellar atrophy that causes dysphagia, muscle atrophy, psychotic episodes, and manic depression [72].

#### Tay–Sachs Disease

More than 130 mutations of the *HEXA* gene have been reported for Tay–Sachs disease, which has an incidence of 1 in 100,000 live births [77]. *HEXA* encodes for the  $\alpha$ -subunit of the enzyme and the disease presents an ample heterogeneity of clinical symptoms based on hexosaminidase residual activity [69].

Tay–Sachs disease can be divided according to the age of onset. The infantile form represents the most aggressive form and is associated with very low hexosaminidase activity. Developmental delay arises around the sixth month of age and is followed by blindness, cognitive impairment, seizures, and paralysis, resulting in death before 5 years of age [78]. The juvenile form is characterized by ataxia, dysarthria, and developmental delay; the survival time is usually around 14 years [79]. The adult form is less severe and has 5–20% of hexosaminidase residual activity. With the progression of the disease, patients complain of leg weakness, ataxia, tremor, and psychiatric disorders [80]. Current treatments for Tay–Sachs patients involve SRT, bone marrow transplantation, hematopoietic or neural stem cell transplantation, and the use of anti-inflammatory drugs. However, most of the treatments have failed to relieve neurological symptoms owing to the difficulty in restoring hexosaminidase activity in the brain [77].

#### Sandhoff Disease

Sandhoff disease accounts for approximately 7% of GM2 gangliosidoses. In this type of GM2 gangliosidoses, *HEXB* variants prevent the correct catabolism of GM2 ganglioside with its lysosomal accumulation in the central nervous system and somatic cells [62].

As for other sphingolipidoses, Sandhoff disease has been classified into infantile, juvenile, and adult forms according to the severity of the disease and the age of onset. The cardinal clinical features of infantile Sandhoff disease are seizure, muscle weakness, developmental delay, and regression; death occurs before 3 years of age [81]. Late onset forms are less common and characterized by lower motor neuron disease and neurological degeneration [82,83]. Clinical manifestations, mainly in juvenile and adult Sandhoff patients, are heterogeneous and based on residual hexosaminidase activity. A case report of two siblings with compound heterozygous *HEXB* mutations further confirmed the clinical heterogeneity of Sandhoff disease [84]. As in Tay–Sachs disease, efficacious therapy for Sandhoff patients is still lacking owing to poor diffusion of the drugs into the nervous system [83].

### 2.7. Metachromatic Leukodystrophy

Metachromatic leukodystrophy (MLD) is an autosomal-recessive inherited sphingolipidoses caused by deficiency of the enzyme arylsulfatase-A encoded by the *ARSA* gene. The enzyme cleaves sulfatides in galactosylceramide and its deficiency leads to the formation of sulfatide-engulfed metachromatic granules in oligodendrocytes, microglia, Schwann cell, neurons, and macrophages, causing myelin degradation and inflammation [85]. Motor neurons derived from induced pluripotent MLD stem cells are characterized by lysosomal

accumulation of sulfatides, mitochondrial fragmentation, and impaired autophagy, leading to premature cell death [86].

The worldwide incidence of MLD is around 1.5 in 100,000 live births, being much higher in Habbanite Jews (1:75) and Navajo Indians (1:2500) [85]. Different mutations in *ARSA* are associated with two groups with different residual arylsulfatase-A activity: the allele 459+1G>A is the most frequent mutation in Europe and belongs to group 0 with no residual activity, whereas the alleles 1277C>T and 536T>G represent the R group with minimal residual activity [87].

The disease can be also divided into four groups according to the age at onset: late infantile, early, and late juvenile, and adult forms. Late infantile and early juvenile MLD are the most frequent forms with severe and rapid progression; they arise during the second and fourth year of life, respectively, and the symptoms affect both the central and the peripheral nervous system [87]. Adult MLD is often misdiagnosed as early-onset dementia or schizophrenia because of its slow progression [85].

The most promising treatment is bone marrow transplantation or HSCT when performed before the onset of symptoms [85]. Moreover, HSCT leads to stabilization or reduced decline in motor and cognitive functions and the positive effects were particularly meaningful in the peripheral nervous system in patients with late-infantile MLD, refractory to other therapeutic interventions [88].

### 3. Sphingolipids in Zebrafish

Beginning with use as a vertebrate animal model during the 1980s [89], the teleost zebrafish has emerged as a useful platform for studies in diverse fields of research. The high grade of genome conservation between human and zebrafish (around 70%, and the percentage increases to 84% when focusing on genes associated with human diseases) [90], combined with precise genome editing and the ease of manipulation, enable to model several human diseases in zebrafish, such as cancer [91], neurodegenerative [92], cardiovascular [93], behavioral [94,95], and inherited [96,97] disorders, including sphingolipidoses. Indeed, lipidomic analysis has revealed the presence in zebrafish of all the principal lipid classes present in mammals (see [98,99] and Figure 4), supporting the possibility to model lipidic metabolism diseases in the fish with the advantage of using existing mammalian lipid databases for data processing [100]. In addition, zebrafish is useful to study lipidic changes after exposure to industrial pollutants [101], drugs [102], toxic compounds [103], or a high-cholesterol/high-fat diet [99]. Moreover, zebrafish larvae can be fed with fluorescent BODIPY-lipids to serve as metabolic tracers when incorporated in vivo into more complex lipid products [99].

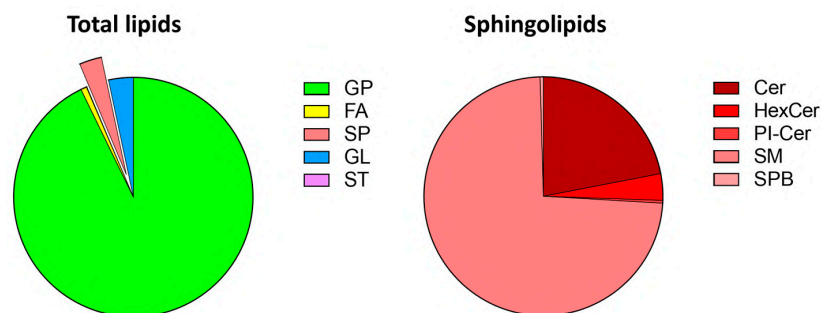


**Figure 4.** Lipid composition of zebrafish embryos. Untargeted lipidomic MS analysis of zebrafish embryos at 72 hpf identified 1377 lipid species. The relative amounts of the major classes of lipids are shown in the corresponding pie charts. Lipids were grouped into categories according to the LIPID MAPS consortium nomenclature [104]. Cer, ceramide; FA, fatty acyls; GL, glycerolipids; GP, glycerophospholipids; HexCer, hexosylceramides; PI-Cer, inositolphosphorylceramides; SM, sphingomyelins; SPB, sphingoid bases; SP, sphingolipids; ST, sterols.

### 3.1. Zebrafish Lipidomics

The dynamic composition of lipids in the body and yolk sac of zebrafish embryos was investigated during the first 5 days of development via liquid chromatography/mass spectrometry (LC/MS), demonstrating significant differences between the two embryonic compartments [98]. The results have shown that cholesterol, phosphatidylcholine, and triglycerides are the most abundant lipids in zebrafish embryos. Of note, the yolk not only represents simple storage of lipids to provide energy for the growing embryo, but also an active organ where lipids are remodeled before reaching the embryo body.

Desorption electrospray ionization MS imaging followed by nano-electrospray MS and tandem MS (MS/MS) were used to detect phosphatidylglycerols, phosphatidylcholines, phosphatidylinositols, free fatty acids, triacylglycerols, ubiquinone, squalene, and other lipids during zebrafish embryonic development from 0 to 96 h post fertilization (hpf) [105]. In addition, high-spatial-resolution matrix-assisted laser desorption/ionization (MALDI) MS imaging was applied to map and visualize the 3D spatial distribution of phosphatidylcholine, phosphatidylethanolamines, and phosphatidylinositol molecular species in zebrafish embryos at the one-cell stage, whereas high-spatial-resolution 2D MALDI MS imaging was used to analyze zebrafish embryos at the 1- to 16-cell stages [106]. These studies have allowed to investigate the composition and distribution of lipids in zebrafish, with insights about lipidic dynamics during embryonic development.

Given the growing interest in the study of the zebrafish lipidome, attempts have been performed to improve the quality of lipid analysis. For instance, conventional one-dimensional LC (1D-LC) was compared to comprehensive two-dimensional LC (2D-LC) coupled to a high-resolution time-of-flight mass spectrometer for a full-scale lipid characterization of lipid extracts from zebrafish embryos. The results demonstrate that 2D-LC is 2.5 times more efficient than 1D-LC, allowing the annotation of more than 1700 lipid species [107].

Recently, a direct infusion MS/MS approach using multiple reaction monitoring was applied to precisely quantify membrane lipid composition both in the yolk and in the zebrafish embryo body during the gastrula stage [108]. Around 700 membrane lipids were annotated, divided into two main lipid classes: sphingolipids and phospholipids, with the latter including phosphatidylcholine, phosphatidylinositol, phosphatidylserine, and phosphatidylethanolamine. The composition of the embryo body and yolk was quite similar, with phosphatidylcholine representing the most abundant species. However, major differences were found in the content of phosphatidylserine, dihydrosphingolipids, and sphingomyelin with short-chain fatty acids (significantly higher in the embryo body than in the yolk). Notably, the fine tuning of the sphingolipid synthesis appears to be related to the *wnt* pathway and is fundamental for proper orientation during cell division.

Lipidomic analysis can also be applied to specific organs from adult zebrafish. For instance, livers from 6-month-old animals were analyzed with different MS techniques, identifying 712 unique lipid species from four categories (fatty acyls, glycerolipids, glycerophospholipids, and sphingolipids) [109]. Moreover, adult zebrafish brains have been analyzed for changes in the lipid profile after exposure to different xenobiotics [102,110].

The central hub of the sphingolipid pathways ceramide and its derivatives play a pivotal role in different biological processes [3]. The ceramide profiles of adult zebrafish brain, 7-day-old zebrafish larvae, and human cells were compared using a parallel reaction monitoring approach in which a targeted quantification method was associated with high-resolution hybrid MS [111]. The results highlighted a significant overlapping in ceramide distribution, even though a scarcity of sphingadiene-containing ceramides was observed in zebrafish specimens, despite their biological importance in mammals. These results raised the hypothesis about possible alternative unexplored lipidic pathways in zebrafish that might pave the way for novel discoveries in human sphingolipid disorders. Targeted sphingolipidomics performed at various stages of embryonic development and in adult animals under different physiological and pathological conditions are required for a better understanding of sphingolipid metabolism and function in zebrafish.

### 3.2. Sphingolipid Metabolizing Enzymes in Zebrafish

Zebrafish and human genomes share a high homology [90], thus several lipid-metabolizing enzymes involved in human diseases have a zebrafish counterpart (Figure 2).

Ceramide synthases (*CERS*), the enzymes responsible for ceramide production, play a central role in the sphingolipid metabolism. Highly conserved through evolution, the *CERS* gene family encompasses six isoforms (*CERS1–6*) with diverse spatial/temporal expression in mammals. All *CERS*s except for *CERS1* show an *N*-terminal homeobox-like domain whose functions remain elusive [112]. In zebrafish, nine genes encoding for the six *cers* subtypes have been identified with a sequence homology with human and mouse counterparts ranging from 46% to 79% identity. Owing to the genome duplication typical of zebrafish, *cers2*, *cers3*, and *cers4* are present as double copy genes (*a* and *b*), while *cers1*, *cers5*, and *cers6* are present as single copy genes. As in mammals, all zebrafish orthologs display the Hox domain, except for the *Cers1* protein.

The tissue-/stage-dependent expression of the *cers* genes has been analyzed during zebrafish embryo development by whole mount in situ hybridization (WISH) [113]. The results suggest that these enzymes are involved in diverse biological processes and that the production of ceramides may dynamically vary in different tissues. For instance, only *cers2a* and *cers3b* are expressed in the embryonic zebrafish pronephros, congruent with the high expression of *Cers2* in murine kidney, while all *cers* are expressed in the nervous tissue, possibly pointing to the requirement for various ceramide species in the developing brain. Notably, the expression of *cers* can be modulated in zebrafish embryo when a perturbation in the lipidic composition occurs. Indeed, zebrafish embryo mutants for the sphingosine kinase gene *sphk2*, in which a potentially dangerous accumulation of the metabolite sphingosine occurs, upregulate the expression of *cers2b* to activate the sphingolipid salvage pathway and turn the excess of sphingosine in ceramide [114]. In this frame, the ortholog of the human peroxisome proliferator-activated receptor  $\gamma$ -responsive transmembrane gene *FAM57B*, involved in the regulation of ceramide metabolism, was found to maintain the homeostasis of sphingolipids and glycerol lipids during brain development in zebrafish [115]. Indeed, untargeted lipidomic analysis performed in the brain tissue of 7-day-old *fam57b* null and heterozygous zebrafish lines has revealed remarkable differences in the lipid profile with consequences on membrane composition and permeability when compared with wild type animals.

As described above, ceramide catabolism is catalyzed by the lysosomal acid ceramidase encoded by the *ASAH1* gene. In silico analysis has revealed the presence of two *ASAH1* co-orthologs in zebrafish (*asah1a* and *asah1b*) [116]. Genome editing techniques have revealed the importance of lysosomal acid ceramidase to maintain the physiological levels of ceramide in zebrafish. Indeed, *asah1a* and *asah1b* enzymes are both able to hydrolyze ceramide and the presence of either *asah1a* or *asah1b* prevents substrate accumulation, with ceramide being increased only in double *asah1a*<sup>-/-</sup>/*asah1b*<sup>-/-</sup> mutants [117].

Ceramide represents the substrate for the generation of more complex sphingolipids, such as sphingomyelin, a central component of myelin. The enzymes responsible for the production of sphingomyelin from ceramide are named sphingomyelin synthases (*SMS*s). As reported in the ZFIN database [118], two duplicated genes are predicted for the two human *SMS* genes in zebrafish (*sgms1a*, *sgms1b*, *sgms2a*, and *sgms2b*). Moreover, a gene ortholog for the human enzymatically inactive *SMS*-related protein (*SMSr*) has been reported in zebrafish, named *zgc:175139* [119]. *SMSr* represents a key regulator of ceramide homeostasis that may operate as a sensor rather than a converter of ceramides in the ER [120]. However, its role in zebrafish remains unexplored.

*SMases*, also named sphingomyelin phosphodiesterases, catalyze the production of ceramide and phosphocholine from sphingomyelin, representing one of the three ceramide production pathways together with the de novo synthesis and the salvage pathways [121]. In zebrafish, *smpd1* has been identified as a single ortholog of the *aSMase*-encoding gene *SMPD1*, which shares 59% identity with the human counterpart. A mutant line of *smpd1* was created in zebrafish via the CRISPR/Cas9 technique; the *SMase* enzymatic activity was

abolished by 93% at 5 days post fertilization (dpf) with a consequent increase in various sphingolipid metabolites [122].

*SMPD2* encodes for the membrane-bound  $Mg^{2+}$ -dependent neutral SMase1. Its *smpd2* ortholog has been cloned in zebrafish and it has been shown to mediate ceramide production and activation of apoptosis following heat stress in zebrafish embryonic cells [123]. Of note, neutral SMase1 is activated by phosphorylation at Ser-270 downstream of the c-Jun N-terminal kinase pathway in both zebrafish and human cells [124], and thalidomide exerts an antiangiogenic effect on zebrafish embryos due to the upregulation of neutral SMase activity and the consequent production of ceramides [125]. In addition, a mitochondrial neutral SMase (mtSMase) has been characterized in zebrafish. mtSMase was purified from zebrafish cells and tested for its enzymatic activity, showing an optimum working pH of 7.5 and sphingomyelin as the main substrate. Cell fractionation and immunofluorescence analysis demonstrated the mitochondrial localization of this novel SMase. Another neutral SMase has been identified in zebrafish that represents the ortholog of the human gene *SMPD3* with a conserved identity of 55% [126].

The sphingoid base sphingosine is an important component of sphingolipid metabolism. Its biologically active metabolite sphingosine-1-phosphate (S1P) is involved in a variety of physiological and pathological processes by binding specific G-coupled receptors (S1PRs) [127]. The study of sphingosine and related metabolites in zebrafish can provide novel information about the human counterparts, favoring a better understanding of the biological mechanisms involved in sphingolipidoses and other pathologies. Two S1P phosphatase (*spp1* and *spp2*), two sphingosine kinase (*sphk1* and *sphk2*), and one sphingosine lyase (*spl*) encoding genes have been identified in zebrafish, together with seven conserved *s1pr* orthologs corresponding to the five human *S1PRs* (*s1pr3* and *s1pr5* being duplicated in zebrafish). *s1pr1* is highly expressed in the brain, while *s1pr4* is expressed mainly in the kidney, which represents the zebrafish hematopoiesis site, thus reflecting the mammalian *S1PR* expression in lymphoid and hematopoietic tissues [128]. Knockdown (KD) and knockout (KO) approaches have shown that the S1P/S1PR pathway plays a pivotal role in vascular and cardiac development in the zebrafish embryo [129,130].

A single ortholog of the human *GLA* gene is present in zebrafish (*a-gal*) with significant similarities between human and zebrafish proteins (>70%). [131]. Enzymatic and immunohistochemical analyses have shown that the zebrafish protein retains significant  $\alpha$ -galactosidase activity and a distribution in zebrafish kidney like in humans, suggesting that it may retain the same biological functions. Finally, the zebrafish gene *arsa* is reported in the ZFIN database [118] as an ortholog of the human gene *ARSA* with a predicted arylsulfatase activity; however, its role in zebrafish remains to be investigated.

#### 4. Zebrafish as an Animal Model for Sphingolipidoses: The “Zebra-Sphinx” Platform

In the last decades, the use of zebrafish to study gene function has increased exponentially thanks to the multiple advantages offered by this model, such as a high number of offspring generated, embryo transparency, and quick genetic manipulation. The necessity to target distinct genes to study their function led to the development of different techniques to block gene function either in a transient manner or permanently. One of the most used commonly techniques involves the injection of antisense oligonucleotides complementary to specific genetic loci, named morpholinos (MOs), which temporarily KD protein production [132]. There are two different strategies by which MOs can interfere with protein expression. The first strategy is based on the block of the translation of the targeted gene (ATG-MO). The second one is aimed at interfering with the splicing process that occurs during mRNA maturation (splicing-MO) [96].

Genome editing techniques have been extensively applied in the zebrafish field. To date, the most used techniques are the Zinc-Finger Nuclease, the Transcription Activator Like Effector Nuclease (TALEN) [133,134], and a more recent approach based on the CRISPR/Cas9 system [135–137]. Briefly, these systems use different approaches to drive proteins with nuclease activity to a specific DNA sequence. Once bound to the locus, the

nucleases cut the double-stranded DNA, forcing the cell to activate double-strand break repair mechanisms. The repair process mediated by the non-homologous end-joining repair system can introduce deletions or insertions (indels) into the break-point region, which can lead to alterations of the reading frame and hence to an altered protein sequence and loss of gene function. Using these procedures, several models of inherited human diseases have been generated in zebrafish. In line with this review, we will discuss the phenotypes of the main models of sphingolipidoses in zebrafish (Table 2).

**Table 2.** Zebrafish models of sphingolipidoses.

Disease	Human Gene	Zebrafish Orthologous	Zebrafish Model
Gaucher	<i>GBA1</i>	<i>gba1</i>	MO [138] Spontaneous mutation [138] TALEN [139] CRISPR/Cas9 [117,140]
Fabry	<i>GLA</i>	<i>gla</i>	CRISPR/Cas9 [131]
Niemann–Pick	<i>SMPD1</i>	<i>smpd1</i>	CRISPR/Cas9 [122]
	<i>NPC1</i>	<i>npc1</i>	MO [141]
	<i>NPC2</i>	<i>npc2</i>	CRISPR/Cas9 [142–145]
Krabbe	<i>GALC</i>	<i>GALCa</i> <i>GALCb</i>	MO [146]
Farber lipogranulomatosis	<i>ASAH1</i>	<i>asah1a</i> <i>asah1b</i>	MO [147] CRISPR/Cas9 [111]
GM2 gangliosidosis	<i>HEXA</i> <i>HEXB</i>	<i>hexa</i> <i>hexb</i>	MO [148,149] CRISPR/Cas9 [150]
Metachromatic leukodystrophy	<i>ARSA</i>	<i>arsa</i>	MO [148]

#### 4.1. Gaucher Disease

Injection of a splicing-MOs directed against *gba1*, the zebrafish ortholog of the human *GBA1* gene, caused the appearance of specific alterations in 5 dpf embryos, including curvature of the trunk, defects of primary bone ossification with a decrease in *col10a1* and *runx2b* gene expression associated with a dysfunction of the osteoblast population, and severe erythropenia and thrombocytopenia caused by early hematopoietic defects. Microarray analysis demonstrated alterations in the expression of genes involved in different biological processes, including mitochondrial activity and intracellular vesicle trafficking. These defects were paralleled by increased oxidative stress and reduced signaling of the Wnt/ $\beta$ -catenin pathway [138]. In a different study, *gba1* KD led to an increased number of vacuolated macrophages, characterised by migratory defects and enlarged lysosomes, pointing to an impairment in the macrophage function due to the low levels of acid  $\beta$ -glucocerebrosidase activity [148].

The first KO model for GD was derived from a forward genetic screening that led to the identification of a *gba1*<sup>sa1621/sa1621</sup> mutant zebrafish line. The characterization of this mutant revealed a decrease in the body length and curvature of the spine at 7 dpf [138]. Like *gba1* morphants, *gba1*<sup>sa1621/sa1621</sup> mutants show a reduction in *col10a1* and *runx2b* expression related to osteoblast function, as well as erythropenia. In addition, splenomegaly and hepatomegaly can be observed in 3-month-old mutants.

To date, different zebrafish KO models of GD have been generated taking advantage of genome editing techniques. The first engineered *gba1* null mutant was obtained by TALEN approaches [139]. Mutants did not show any significant defect during the early stages of development, with the first alterations in the swimming behaviour occurring at 8 weeks of age and curvature of the spine at 12 weeks. Histopathological analysis revealed the presence of Gaucher-like cells in the brain, liver, thymus, and pancreas of

adult KO animals. Furthermore, dopaminergic neuron degeneration, the presence of cytoplasmic inclusions resembling Lewy bodies, an increased number of autophagosomes, and microglia activation were observed in KO brains. MS demonstrated the accumulation of sphingolipid metabolites in *gba1*<sup>-/-</sup> larvae at 5 dpf. They included hexosylsphingosine, glucosylceramide, lactosylceramide, and galactosylceramide, and their levels were further increased in juvenile brains.

A second zebrafish model of GD was generated by the CRISPR/Cas9 technique [140]. As observed for the *gba1* null zebrafish generated by TALEN, adult *gba1* KO mutants showed a curved back, and swimming and feeding impairment starting from 10 weeks of age. In addition, adults were characterized by the presence of Gaucher-like cells in the liver, spleen, and pancreas, together with an increase in glucosylsphingosine and glucosylceramide levels in the brain and liver. However, in this study, *gba1* KO larvae appeared to accumulate solely glucosylsphingosine at 5 dpf, and no altered levels of other glycosphingolipids were observed at this stage. Expression analysis of specific mRNAs in the brain of adult *gba1*<sup>-/-</sup> zebrafish mutants [117] revealed the upregulation of macrophage (*gpnmb*, *chia.6*), microglia (*apoeb*), and complement system (*c1qa*, *c3.1*, *c5*, *c5aR1*) markers, as well as the upregulation of proinflammatory cytokines (*il1-b*, *tnf-a2*), whereas downregulation of the dopaminergic neuron marker (*th1*) and of the myelin-related gene (*mbp*) were observed. Autophagy was also increased in these brains.

More recently, a further KO model was generated in zebrafish using TALEN [151]. Animals showed a reduction in dopaminergic and noradrenergic neurons at 3 months of age, confirming the importance of *gba1* function for neuronal survival.

Cytosol-facing GBA2 metabolizes cytosolic glucosylceramide. Genetic ablation of the *Gba2* gene exerts beneficial effects in murine models of GD and NPD type C [152,153]. In order to investigate the potential role of GBA2 in compensatory glucosylceramide metabolism during inadequate GBA1 activity, double *gba1* and *gba2* null animals were generated by CRISPR/Cas9 in zebrafish [140]. Lipid analysis performed on double mutants at 5 dpf showed increased glucosylceramide levels when compared with single *gba1*<sup>-/-</sup> larvae, but similar to those detected in single *gba2*<sup>-/-</sup> animals. Moreover, glucosylcholesterol was significantly decreased in the double KO animals and in single *gba2*<sup>-/-</sup> mutants. In addition, a significant accumulation of glucosylsphingosine occurs in double *gba1/gba2* null animals when compared with controls. Notably, in keeping with an SRT approach for the treatment of GD, the administration of the potent specific glucosylceramide synthase inhibitor eliglustat elicited a significant decrease in hexosylceramide and in the derived lipids glucosylsphingosine and hexosylcholesterol in *gba1*<sup>-/-</sup> larvae. Together, these data indicate that zebrafish larvae offer an attractive model to study glucosidase actions on glycosphingolipid metabolism in vivo.

To study the role of excessive glucosylsphingosine formation during acid  $\beta$ -glucocerebrosidase deficiency, KO zebrafish lines were generated for the two *ASAH1* orthologs *asah1a* and *asah2b* [117]. Of note, double *asah1a/asah1b* null larvae, but not single *asah1a* or *asah1b* mutants, accumulate the primary substrate ceramide. Nevertheless, only *asah1b* appears to be involved in the formation of glucosylsphingosine in a *gba1*-deficient background. Accumulation of glucosylsphingosine in *gba1*<sup>-/-</sup>/*asah1b*<sup>-/-</sup> zebrafish did not prevent the formation of Gaucher-like cells, glucosylceramide accumulation, or neuroinflammation. However, these double mutants show an ameliorated course of disease reflected by a delay in the appearance of locomotor abnormalities and curvature of the back, reduced loss of dopaminergic neurons, and increased lifespan, suggesting that the accumulation of glucosylsphingosine may play a role in the pathogenesis of GD.

A similar approach was used to investigate the impact of acid SMase activity on a glucocerebrosidase-deficient background by generating double *gba1*<sup>-/-</sup>/*smpd1*<sup>-/-</sup> zebrafish mutants [122]. Unexpectedly, double *gba1*<sup>-/-</sup>/*smpd1*<sup>-/-</sup> mutants showed a markedly prolonged survival, rescue of neuronal and mitochondrial damages, and normalization of the motor phenotype when compared with *gba1* KO animals. This occurred in the presence of an additive increase in the levels of various sphingolipid metabolites.

Both *GSC1* and *SMPD1* variants represent inherited risk factors for Parkinson's disease [154]. In keeping with the data obtained in double KO animals, human cells with combined glucocerebrosidase and  $\alpha$ SMase deficiency showed an unpredicted reduction in intracellular  $\alpha$ -synuclein levels. Together, these observations indicate that a better understanding of the crosstalk among sphingolipid metabolizing enzymes is required to dissect the pathogenesis of sphingolipid-related pathologies and for the development of efficacious therapeutic approaches.

#### 4.2. Fabry Disease

A model of Fabry disease was obtained in zebrafish by the generation of a  $\alpha$ -gal KO fish line using the CRISPR/Cas9 technique [131]. This led to the decrease in  $\alpha$ -gal protein expression in the kidney associated with a marked reduction in  $\alpha$ -galactosidase activity. Even though KO mutants did not show significant differences in body size when compared with wild type animals, they were characterized by an increased mortality during the early embryonic stages. A more in-depth analysis unveiled an increase in creatinine levels and the leak of high molecular weight proteins, suggesting that an impairment of glomerular filtration may occur in these mutants. Accordingly, microscopic analysis of the kidney revealed an increased glomerular size, dilated capillary loop, and thinner Bowman's space. In contrast with the results obtained in other animal models of Fabry disease that do not show renal abnormalities [155], these data are in keeping with the nephropathy that occurs in Fabry patients [156]. Notably, the absence of a Gb3 synthase encoding gene ortholog in zebrafish provides the unique opportunity to identify pathogenic processes that may work in concert with Gb3 accumulation in Fabry disease [131].

#### 4.3. Niemann–Pick Disease

A KO model of NPD type A was generated in zebrafish using the CRISPR/Cas9 system [122]. *Smpd1* KO animals showed a 93% reduction in the enzymatic activity at 5 dpf, with a consequent increase in sphingolipid metabolites, including sphingomyelin, ceramide, lactosylceramide, and sphinganine. However, despite the absence of enzyme activity and the significant increase in key glycolipid substrates, no obvious phenotype was observed in embryo and adult KO animals.

At variance with the paucity of zebrafish models for the  $\alpha$ SMase-deficient forms of NPD, various attempts have been made to model the type C form of NPD, a lysosomal storage disease distinct from sphingolipidoses that depends on cholesterol trafficking defects due to mutations in *NPC1* or *NPC2* genes. For instance, injection of specific MOs for *npc1*, the orthologous of *NPC1*, induces an accumulation of unesterified cholesterol at early embryonic stages [141]. Morphological evaluation of the zebrafish KD morphants injected at one cell stage or in the yolk syncytial layer revealed a disorganization of the actin cytoskeleton and a delay in the development during epiboly, unveiling a role for *npc1* in cell movement at this embryonic stage. Interestingly, a lower dose of MO was associated with a milder phenotype characterized by neuronal death, like in the human pathology. KD of *npc1* in zebrafish has also been associated with thrombocytopenia, as observed in some NPD patients [157].

Various KO models for NPD type C have been developed using the CRISPR/Cas9 technology to inactivate the *npc1* [142,143] or the *npc2* [144] gene. KO of *npc1* caused premature death of half of the animals during the embryonic and juvenile stages, with a significant reduction in body length, together with hepatomegaly, splenomegaly, neurological defects, and ataxia—features that resemble those observed in patients and other animal models of NPD type C. Moreover, analysis of hepatocytes unveils a massive accumulation of cholesterol and changes in the levels of different types of lipids, including ceramide, diacylglycerol, and lysophosphatidic acid [144,145]. At variance with *npc1* null animals, *npc2* KO fishes were able to reach adulthood, even though they showed a reduction in body size and impairment in the locomotor system starting from 2 months and 4 months of age, respectively [144]. Histopathological analysis of *npc2* KO adults revealed the presence of



foam cells in liver and kidney, defects in axonal myelination, and alterations of cerebellar Purkinje cells. Notably, significant alterations have also been observed in *npc2* null zebrafish at early stages of development [145]. They include the accumulation of unesterified cholesterol, upregulation of markers of inflammation and activated microglia, mitochondrial dysfunction, defects in the myelination process, and an anxiety-like behaviour. Like what was observed in *npc1* maternal mutants, *npc2* KO derived from homozygote females show an aberrant phenotype already at 30 hpf, such as a curved tail, absence or abnormalities of the otoliths, defects in the brain structures, and lack of circulating cells—defects that may arise from an impairment of the Notch3 signaling pathway [145].

As for NPD type C, zebrafish has been used as a platform to model lysosomal storage diseases other than sphingolipidoses, including mucopolidosis type II (MLII) and mucopolysaccharidosis type II (MPSII), providing novel information about the pathogenesis of these disorders.

Briefly, MLII is due to the mutation in the *GNPTAB* gene, encoding for the catalytic subunit of *N*-acetylglucosamine-1-phosphotransferase that catalyses the first step of the formation of mannose 6-phosphate (M6P)-tagged lysosomal soluble hydrolases. As a consequence of *GNPTAB* mutation, the lack of the M6P tag causes the missorting and secretion of such hydrolases, with lysosomal accumulation of their substrates. A first zebrafish model of MLII was obtained by MO injection. Morphant embryos showed craniofacial defects, impaired motility, and abnormal otolith and pectoral fin development. This model allowed to undercover alterations in the spatial-temporal expression of type II collagen and Sox9 [158]. Stable mutant lines for the *gnptab* gene were obtained by TALEN and site-directed mutagenesis technologies. Zebrafish mutants showed a craniofacial phenotype and elevated levels of cathepsin K activity associated with abnormal cartilage development and heart and valve malformations [159,160].

MPSII is caused by mutation in the *IDS* gene, encoding for the lysosomal enzyme iduronate 2-sulfatase, leading to the toxic accumulation of glycosaminoglycans into lysosomes (mainly dermatan and heparan sulphates) and multi-organ damage. An MO approach in zebrafish targeting *ids*, the single ortholog for human *IDS*, caused early defects in embryonic development. In particular, the abnormal migration and differentiation of neural crest cells into chondroblasts were responsible for craniofacial cartilage defects, while sonic hedgehog pathway disruption led to congenital heart defects [161,162]. In addition, KO of *ids* in zebrafish has provided novel information about the role of early deregulation of the fibroblast growth factor signaling pathway in the occurrence of irreversible skeletal defects before glycosaminoglycans' accumulation [163]. With a different approach, human-mutated *IDS* mRNAs have been injected into zebrafish embryos for a rapid preliminary study about novel *IDS* point mutations associated with MPSII [164].

#### 4.4. Krabbe Disease

Two *GALC* co-orthologs have been identified in zebrafish (*GALCa* and *GALCb*) that share a high identity with their human counterpart [148]. Further analysis confirmed that both isoforms are endowed with enzymatic activity and are localised in the lysosome. Moreover, WISH analysis revealed their co-expression in the central nervous system during embryonic development. Injection of single *GALCa* or *GALCb* specific MOs in zebrafish resulted in the partial reduction in enzymatic  $\beta$ -galactosylceramidase activity, which was completely abolished by the simultaneous injection of both MOs. Nevertheless, no evident morphological alterations were observed in both single- and double-injected morphants during embryonic development. Notably, no alterations in psychosine levels were detected in double *GALCa/GALCb* morphants, suggesting that the transient abrogation of *GALC* activity is not sufficient to accumulate this metabolite [146].

Relevant to this point, myelination in zebrafish starts in the hindbrain at day 4 of development and is not completed at day 10 [165], making the study of the effect of  $\beta$ -galactosylceramidase deficiency on myelination in zebrafish morphants unfeasible. However, analysis of the expression pattern of a set of neuronal marker genes unveiled a

significant reduction and partial disorganization in *neurod1* expression and neuronal death in double *GALCa/GALCb* morphants, in keeping with the neurodegenerative features of Krabbe disease. These data suggest that *GALC* loss-of-function may have pathological consequences independent of psychosine accumulation, thus providing new insights into the pathogenesis of Krabbe disease. This possibility is supported by the observation that psychosine levels do not correlate with nervous system regions exhibiting demyelination and axonopathy in *twi-5J* mice harboring a spontaneous missense *GALC* mutation [166]. Thus, double *GALCa/GALCb* zebrafish morphants may represent an interesting option for addressing previously unrecognized psychosine-independent key aspects of the pathogenesis of Krabbe disease.

#### 4.5. Farber Lipogranulomatosis

Transient downregulation of *asah1b* using an ATG-MO approach led to a 74% decrease in acid-ceramidase activity in zebrafish embryos [147]. Embryo morphants develop macroscopic phenotypic alterations by 48 hpf. Further analysis has disclosed increased neuronal apoptosis localised only in the spinal cord, leading to a reduction in the number of motor neuron branches. This defect does not affect peripheral projections, indicating a specific susceptibility of motor neurons to the reduced levels of lysosomal acid-ceramidase [147].

A more recent zebrafish model of Farber disease was generated using the CRISPR/Cas9 technique [111]. Three different mutant lines were generated: single KOs for each of the two co-orthologs (*asah1a* or *asah1b*) and a double *asah1a/asah1b* KO. At variance with the MO model, the abrogation of only one gene (*asah1a* or *asah1b*) did not lead to the appearance of an evident phenotype until adulthood, whereas double KO animals display a progressive reduction in body size when compared with wild type and single KO siblings. These differences became more evident 3 months after birth and double KO animals died within 4 months [111]. Accordingly, sphingolipid analysis performed on the brain of 3.5-month-old fishes revealed a significant accumulation of ceramide only in double KO animals. These results indicate that the activity of a single *asah1* ortholog is sufficient to maintain physiological levels of ceramide and to guarantee a normal phenotype in zebrafish. At variance, reminiscent of the joint deformations observed in Farber patients [61], the complete abrogation of acid-ceramidase activity impairs the normal growth of the skeletal system in zebrafish and induces a premature death, probably due to heart failure or seizure related to progressive ceramide accumulation.

#### 4.6. GM2 Gangliosidosis

##### 4.6.1. Tay–Sachs Disease

During a multi-gene analysis to understand the role of macrophages in tuberculosis progression, a zebrafish model for Tay–Sachs disease was generated by injecting an MO targeting *hexa*, the ortholog of human *HEXA*. This model was characterized by augmented macrophages that show migratory defects and enlarged lysosomes [148].

##### 4.6.2. Sandhoff Disease

Analysis of different MOs in a wide range screening for angiogenesis inhibitors in zebrafish revealed that downregulation of *hexb*, the *HEXB* ortholog, induces defects in the vascular system at 48–56 hpf, as shown by FITC-dextran microangiography and by WISH analysis of the expression of the endothelial cadherin-5 encoding gene *cdh5* in the intersegmental vessels [149].

More recently, a KO model of Sandhoff disease was generated using a CRISPR/Cas9 approach targeting *hexb* [150]. The enzymatic activity of *hexa*<sup>+/+</sup>/*hexb*<sup>-/-</sup> animals was reduced by 99% compared with controls, indicating that the *hexa* does not contribute significantly to the total  $\beta$ -hexosaminidase activity in zebrafish. Despite the lack of enzymatic activity, *hexb* null adult fishes are viable and show a normal morphological phenotype. However, mutant fishes showed an accumulation of different oligosaccharides in the brain and various internal organs. A more in-depth analysis performed on *hexb* KO embryos at

5 dpf evidenced abnormality in the lysosome morphology of the microglia and radial glia, probably associated with defects in the lysosome fusing process. A behavioural analysis of 4.5 and 6 dpf embryos showed a reduced locomotor activity of *hexb* KO animals compared with controls, an alteration that resembles the impaired locomotor function observed in Sandhoff patients [167]. Interestingly, the manifestation of this locomotor alteration is simultaneous with the appearance of lysosomal abnormalities in the radial glia, suggesting a correlation between glial function and locomotor activity. Moreover, *hexb* KO animals exhibit a slight increase in neuronal loss at 5 dpf that partially mimics the neurodegeneration observed in humans.

#### 4.7. Metachromatic Leukodystrophy

The only zebrafish model established so far for MLD was obtained by injection of a splicing-MO specific for the *arsa* gene [148]. An initial characterization of this KD model showed an increased number of vacuolated macrophages presenting enlarged lysosomes compared with control embryos. Moreover, as observed in *gba1* and *hexa* null animals, abnormal macrophages showed an impairment of movement associated with migratory defects. These results indicate that diverse lysosomal storage disorders may impair macrophage function with an impact on their anti-microbial function [148].

### 5. Concluding Remarks

In this review, we have highlighted the use of zebrafish to develop new animal models of sphingolipidoses. Starting from a gene knockdown approach via MO injection at the one–two cell stage of embryonic development, the more recent use of the TALEN and CRISPR/Cas9 gene editing techniques has allowed to knock out enzymes involved in sphingolipid metabolism whose deficiency is responsible for various human hereditary sphingolipid disorders. Notably, many of these models recapitulate, at least in part, the phenotypic defects observed in patients (Figure 5). In addition, lipidomic analysis has allowed the study of the impact of enzymatic deficiencies on the sphingolipid metabolism in zebrafish, providing useful insights into the pathogenesis of these diseases. It must be pointed out that these studies can be performed not only in adult animals, but also in zebrafish embryos, thus providing invaluable information about the early biochemical alterations that may occur in patients before birth.

At present, different therapeutic approaches, including HSCT, ERT, SRT, pharmacological chaperones, and in vivo and ex vivo gene therapy, are envisaged for patients affected by sphingolipidoses. However, given the complexities resulting from the alterations of sphingolipid metabolism in different systemic organs and the early appearance of serious pathological alterations in the infantile forms of various sphingolipidoses, more efficacious therapeutic strategies are required to improve patient outcomes.

As described in numerous reviews [96,97], the zebrafish system includes several advantages that make this organism a powerful platform for the study of the pathogenesis of human hereditary diseases and for the development of novel drug-based therapeutic strategies. Indeed, as also pointed out in this review, most of the pathogenic processes of genetic diseases are conserved between humans and zebrafish, with high similarity among possible drug targets. Compared with cell-based and biochemical screening of putative drug candidates, zebrafish models offer the great advantage of providing a whole organism response to the delivery of drug candidates, thus also allowing the evaluation of side effects such as teratogenicity, toxicity, and metabolic alterations, as well as the study of drug pharmacokinetics and pharmacodynamics [168]. In addition, the zebrafish embryo offers multiple advantages that make this model attractive for a cost-effective drug screening, including external fertilisation, high fecundity, and ease of use; furthermore, embryo transparency enables imaging at cellular resolution and internal organ visualization. Given these features, zebrafish has been used as a tool for high-throughput screening of different drug candidates relevant to a broad range of human diseases [169]. Many of these

molecules have reached the clinical trial phase, confirming the possibility of using zebrafish as a platform for the development of new potential therapeutic strategies.

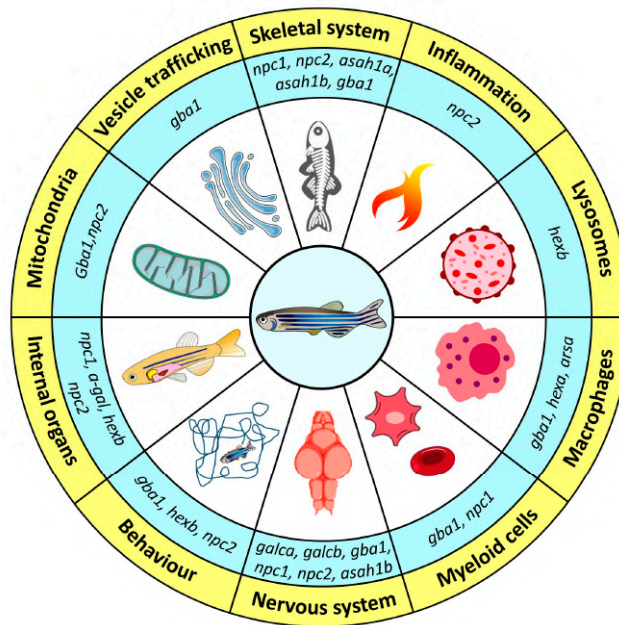


**Figure 5.** Main phenotypic alterations in zebrafish models of sphingolipidoses. Schematic summary of the major biological systems affected in zebrafish embryos or adults following the knockdown or knockout of the indicated genes encoding for different sphingolipid metabolizing enzymes. See text for details.

In this frame, even though some of the approaches envisioned for the therapy of sphingolipidoses cannot be modelled in zebrafish (like HSCT and gene therapy), various studies indicate the possibility to assess, in KO zebrafish mutants, the therapeutic potential of novel drugs to be used in an SRT approach. In addition, double KO zebrafish mutants harbouring the pathogenic mutation together with the genetic deficit of an upstream enzyme involved in the synthesis of the accumulating substrate may provide useful information about the possible efficacy of drug-driven SRT strategies. Moreover, zebrafish models of sphingolipidoses might be useful for the screening of pharmacological chaperones in zebrafish lines obtained by CRISPR/Cas9-based point mutation gene editing that harbour the identical pathogenic mutation detected in human patients.

Clearly, given the obvious differences with humans, zebrafish models may not fully reflect the pathophysiology of the human disease. In addition, the duplication of the zebrafish genome may result in the presence of two co-orthologs of the human pathogenic gene. This may require the understanding of the biological role of both proteins encoded by the two orthologs during zebrafish development and in adults to evaluate how and to what extent the single or double KO mutants may mimic the human disease. Despite these and other drawbacks, the “zebra-sphinx” system represents an innovative and informative tool to gain insights into the biology of sphingolipid metabolism for a better comprehension of the pathological processes contributing to sphingolipid disorders, thus enabling the development of novel potential therapies and their translation to patients.

**Author Contributions:** Conceptualization, M.P.; formal analysis, L.M., J.G., M.C. and D.C.; writing—original draft preparation, L.M., J.G., M.C. and D.C.; writing—review and editing, M.P.; funding acquisition, M.P. All authors have read and agreed to the published version of the manuscript.

**Funding:** This work was supported by Associazione Italiana per la Ricerca sul Cancro (AIRC IG 23116 to M.P.). J.C. is supported by an AIRC fellowship (ID 26633).

**Institutional Review Board Statement:** Not applicable.

**Informed Consent Statement:** Not applicable.

**Data Availability Statement:** Not applicable.

**Acknowledgments:** We wish to thank T. Cox (University of Cambridge, Cambridge, UK) for his encouragement to write this review and M. Manfredi (Department of Translational Medicine, University of Piemonte Orientale, Novara, Italy) for the lipidomic analysis of zebrafish embryos shown in Figure 4.

**Conflicts of Interest:** The authors declare no conflict of interest.

### Abbreviations

aSMase, acid sphingomyelinase; *CERS*, ceramide synthases; CRISPR/Cas9, clustered regularly interspersed short palindromic repeats/CRISPR-associated 9; dpf, days post fertilization; ER, endoplasmic reticulum; ERT, enzyme replacement therapy; *GALC*,  $\beta$ -galactosylceramidase; Gb3, globotriaosylceramide; GD, Gaucher disease; GM2AP, GM2 activator protein; HEXA,  $\beta$ -hexosaminidase A; HSCT, hematopoietic stem cell transplantation; hpf, hours post fertilization; KD, knockdown; KO, knockout; LC, liquid chromatography; M6P, mannose 6-phosphate; MLD, metachromatic leukodystrophy; MO, morpholino; MS, mass spectrometry; NPD, Niemann–Pick disease; S1P, sphingosine-1-phosphate; S1PR, S1P receptor; *SMS*, sphingomyelin synthase; SRT, substrate reduction therapy; TALEN, transcription activator like effector nuclease; WISH, whole mount in situ hybridization.

### References

1. Thudichum, J.L.W. A Treatise on the Chemical Constitution of the Brain: Based Throughout upon Original Researches. *Glasgow Med. J.* **1884**, *22*, 363–364.
2. Breslow, D.K. Sphingolipid homeostasis in the endoplasmic reticulum and beyond. *Cold Spring Harb. Perspect. Biol.* **2013**, *5*, a013326. [[CrossRef](#)]
3. Futerman, A.H.; Riezman, H. The ins and outs of sphingolipid synthesis. *Trends Cell Biol.* **2005**, *15*, 312–318. [[CrossRef](#)]
4. Gault, C.R.; Obeid, L.M.; Hannun, Y.A. An overview of sphingolipid metabolism: From synthesis to breakdown. *Adv. Exp. Med. Biol.* **2010**, *688*, 1–23. [[CrossRef](#)]
5. Sezgin, E.; Levental, I.; Mayor, S.; Eggeling, C. The mystery of membrane organization: Composition, regulation and roles of lipid rafts. *Nat. Rev. Mol. Cell Biol.* **2017**, *18*, 361–374. [[CrossRef](#)]
6. Kitatani, K.; Idkowiak-Baldys, J.; Hannun, Y.A. The sphingolipid salvage pathway in ceramide metabolism and signaling. *Cell. Signal.* **2008**, *20*, 1010–1018. [[CrossRef](#)]
7. Hannun, Y.A.; Obeid, L.M. Sphingolipids and their metabolism in physiology and disease. *Nat. Rev. Mol. Cell Biol.* **2018**, *19*, 175–191. [[CrossRef](#)]
8. Grassi, S.; Chiricozzi, E.; Mauri, L.; Sonnino, S.; Prinetti, A. Sphingolipids and neuronal degeneration in lysosomal storage disorders. *J. Neurochem.* **2019**, *148*, 600–611. [[CrossRef](#)]
9. Platt, F.M.; d’Azzo, A.; Davidson, B.L.; Neufeld, E.F.; Tiffit, C.J. Lysosomal storage diseases. *Nat. Rev. Dis. Primers.* **2018**, *4*, 27. [[CrossRef](#)]
10. Abed Rabbo, M.; Khodour, Y.; Kaguni, L.S.; Stiban, J. Sphingolipid lysosomal storage diseases: From bench to bedside. *Lipids. Health Dis.* **2021**, *20*, 44. [[CrossRef](#)]
11. Eckhardt, M. Pathology and current treatment of neurodegenerative sphingolipidoses. *Neuromolecular Med.* **2010**, *12*, 362–382. [[CrossRef](#)]
12. Santos, R.; Amaral, O. Advances in Sphingolipidoses: CRISPR-Cas9 editing as an option for modelling and therapy. *Int. J. Mol. Sci.* **2019**, *20*, 5897. [[CrossRef](#)]
13. Fernandez-Pereira, C. Therapeutic approaches in lysosomal storage diseases. *Biomolecules* **2021**, *11*, 1775. [[CrossRef](#)]
14. Grabowski, G.A.; Mistry, P.K. Therapies for lysosomal storage diseases: Principles, practice, and prospects for refinements based on evolving science. *Mol. Genet. Metab.* **2022**, *137*, 81–91. [[CrossRef](#)]

15. Andrade-Campos, M.M. Identification of risk features for complication in Gaucher's disease patients: A machine learning analysis of the Spanish registry of Gaucher disease. *Orphanet. J. Rare Dis.* **2020**, *15*, 256. [CrossRef]
16. Cox, T.M.; Cachón-González, M.B. The cellular pathology of lysosomal diseases. *J. Pathol.* **2021**, *226*, 241–254. [CrossRef]
17. Roh, J.; Subramanian, S.; Weinreb, N.J.; Kartha, R.V. Gaucher disease—more than just a rare lipid storage disease. *J. Mol. Med.* **2022**, *100*, 499–518. [CrossRef]
18. Ługowska, A. Gene expression profile in patients with Gaucher disease indicates activation of inflammatory processes. *Sci. Rep.* **2019**, *9*, 6060. [CrossRef]
19. Maor, G. The contribution of mutant GBA to the development of Parkinson disease in Drosophila. *Hum. Mol. Genet.* **2016**, *25*, 2712–2727. [CrossRef]
20. Riboldi, G.M.; Di Fonzo, A.B. Gaucher Disease, and Parkinson's Disease: From Genetic to Clinic to New Therapeutic Approaches. *Cells* **2019**, *8*, 364. [CrossRef]
21. Alaei, M.; Jafari, N.; Rohani, F.; Ahmadabadi, F.; Azadi, R. Are There Neurological Symptoms in Type 1 of Gaucher Disease? *Iran. J. Child. Neurol.* **2018**, *12*, 99–106. [PubMed]
22. Stone, W.L.; Basit, H.; Master, S.R. Gaucher disease. In *StatPearls*; StatPearls Publishing: Treasure Island, FL, USA, 2022. Available online: <https://www.ncbi.nlm.nih.gov/books/NBK448080/> (accessed on 19 November 2022).
23. Limgala, R.P.; Goker-Alpan, O. Effect of Substrate Reduction Therapy in Comparison to Enzyme Replacement Therapy on Immune Aspects and Bone Involvement in Gaucher Disease. *Biomolecules* **2020**, *10*, 526. [CrossRef]
24. Istiti, M. Upgrading the evidence for the use of amroxol in Gaucher disease and GBA related Parkinson: Investigator initiated registry based on real life data. *Am. J. Hematol.* **2021**, *96*, 545–551. [CrossRef] [PubMed]
25. Schiffmann, R. Chapter 17—Fabry disease. *Handb. Clin. Neurol.* **2015**, *132*, 231–248. [CrossRef] [PubMed]
26. Turkmen, K.; Baloglu, I. Fabry disease: Where are we now? *Int. Urol. Nephrol.* **2020**, *52*, 2113–2122. [CrossRef]
27. Germain, D.P. Challenging the traditional approach for interpreting genetic variants: Lessons from Fabry disease. *Clin. Genet.* **2022**, *101*, 390–402. [CrossRef]
28. Stamerra, C.A.; Del Pinto, R.; di Giosia, P.; Ferri, C.; Sahebkar, A. Anderson-Fabry Disease: From Endothelial Dysfunction to Emerging Therapies. *Adv. Pharmacol. Pharm. Sci.* **2021**, *2021*, 5548445. [CrossRef]
29. Li, X. Fabry disease: Mechanism and therapeutics strategies. *Front. Pharmacol.* **2022**, *13*, 1025740. [CrossRef]
30. Ivanova, M.M.; Changsila, E.; Iaconou, C.; Goker-Alpan, O. Impaired autophagic and mitochondrial functions are partially restored by ERT in Gaucher and Fabry diseases. *PLoS ONE.* **2019**, *14*, e0210617. [CrossRef]
31. Song, H.Y. reversal of the inflammatory responses in Fabry Patient iPSC-Derived cardiovascular endothelial cells by CRISPR/Cas9-Corrected mutation. *Int. J. Mol. Sci.* **2021**, *22*, 2381. [CrossRef]
32. Kok, K. Fabry Disease: Molecular basis, pathophysiology, diagnostics and potential therapeutic directions. *Biomolecules* **2021**, *11*, 271. [CrossRef] [PubMed]
33. Wang, S.C.; Tapia, D.; Kimonis, V.E.; Lombardo, D.M. Regional strain pattern and correlation with cardiac magnetic resonance imaging in Fabry Disease. *J. Cardiovasc. Echogr.* **2021**, *31*, 131–136. [CrossRef]
34. Aguiar, P. Biomarkers of Myocardial Fibrosis: Revealing the Natural History of Fibrogenesis in Fabry Disease Cardiomyopathy. *J. Am. Heart Assoc.* **2018**, *7*, e007124. [CrossRef] [PubMed]
35. Weidemann, F. Long-term effects of enzyme replacement therapy on Fabry cardiomyopathy: Evidence for a better outcome with early treatment. *Circulation* **2009**, *119*, 524–529. [CrossRef] [PubMed]
36. Lenders, M.; Brand, E. Fabry disease: The current treatment landscape. *Drugs* **2021**, *81*, 635–645. [CrossRef] [PubMed]
37. van der Veen, S.J.; Hollak, C.E.M.; van Kuilenburg, A.B.P.; Langeveld, M. Developments in the treatment of Fabry disease. *J. Inher. Metab. Dis.* **2020**, *43*, 908–921. [CrossRef]
38. Torres, S. Lysosomal and mitochondrial liaisons in Niemann-Pick disease. *Front. Physiol.* **2017**, *8*, 982. [CrossRef]
39. Hollak, C.E. Acid sphingomyelinase (Asm) deficiency patients in The Netherlands and Belgium: Disease spectrum and natural course in attenuated patients. *Mol. Genet. Metab.* **2012**, *107*, 526–533. [CrossRef]
40. Schuchman, E.H.; Desnick, R.J. Types A and B Niemann-Pick disease. *Mol. Genet. Metab.* **2017**, *120*, 27–33. [CrossRef]
41. McGovern, M.M.; Avetisyan, R.; Sanson, B.J.; Lidove, O. Disease manifestations and burden of illness in patients with acid sphingomyelinase deficiency (ASMD). *Orphanet J. Rare Dis.* **2017**, *12*, 41. [CrossRef]
42. Aldosari, M.H. Liposome-targeted recombinant human acid sphingomyelinase: Production, formulation, and in vitro evaluation. *Eur. J. Pharm. Biopharm.* **2019**, *137*, 185–195. [CrossRef]
43. Diaz, G.A. One-year results of a clinical trial of olipudase alfa enzyme replacement therapy in pediatric patients with acid sphingomyelinase deficiency. *Genet. Med.* **2021**, *23*, 1543–1550. [CrossRef]
44. Sitarska, D.; Tylki-Szymańska, A.; Ługowska, A. Treatment trials in Niemann-Pick type C disease. *Metab. Brain Dis.* **2021**, *36*, 2215–2221. [CrossRef]
45. Geberhiwot, T. Consensus clinical management guidelines for Niemann-Pick disease type C. *Orphanet J. Rare Dis.* **2018**, *13*, 50. [CrossRef] [PubMed]
46. Gumus, E. Niemann-Pick disease type C in the newborn period: A single-center experience. *Eur. J. Pediatr.* **2017**, *176*, 1669–1676. [CrossRef]

47. Kim, S.J.; Lee, B.H.; Lee, Y.S.; Kang, K.S. Defective cholesterol traffic and neuronal differentiation in neural stem cells of Niemann-Pick type C disease improved by valproic acid, a histone deacetylase inhibitor. *Biochem. Biophys. Res. Commun.* **2007**, *360*, 593–599. [[CrossRef](#)]
48. Lee, S.E. Human iNSC-derived brain organoid model of lysosomal storage disorder in Niemann-Pick disease type C. *Cell Death Dis.* **2020**, *11*, 1059. [[CrossRef](#)]
49. Bradbury, A.M.; Bongarzone, E.R.; Sands, M.S. Krabbe disease: New hope for an old disease. *Neurosci Lett.* **2021**, *752*, 135841. [[CrossRef](#)] [[PubMed](#)]
50. Rafi, M.A. Krabbe disease: A personal perspective and hypothesis. *Bioimpacts* **2022**, *12*, 3–7. [[CrossRef](#)] [[PubMed](#)]
51. Feltri, M.L. Mechanisms of demyelination and neurodegeneration in globoid cell leukodystrophy. *Glia* **2021**, *69*, 2309–2331. [[CrossRef](#)]
52. Hawkins-Salsbury, J.A. Psychosine, the cytotoxic sphingolipid that accumulates in globoid cell leukodystrophy, alters membrane architecture. *J. Lipid. Res.* **2013**, *54*, 3303–3311. [[CrossRef](#)]
53. White, A.B. Psychosine accumulates in membrane microdomains in the brain of Krabbe patients, disrupting the raft architecture. *J. Neurosci.* **2009**, *29*, 6068–6077. [[CrossRef](#)] [[PubMed](#)]
54. Belleri, M.; Ronca, R.; Coltrini, D.; Nico, B.; Ribatti, D.; Poliani, P.L.; Giacomini, A.; Alessi, P.; Marchesini, S.; Santos, M.B.; et al. Inhibition of angiogenesis by  $\beta$ -galactosylceramidase deficiency in globoid cell leukodystrophy. *Brain.* **2013**, *136*, 2859–2875. [[CrossRef](#)] [[PubMed](#)]
55. Coltrini, D.; Chandran, A.M.K.; Belleri, M.; Poliani, P.L.; Cominelli, M.; Pagani, F.; Capra, M.; Calza, S.; Prioni, S.; Mauri, L.; et al.  $\beta$ -Galactosylceramidase deficiency causes upregulation of long pentraxin-3 in the central nervous system of Krabbe patients and Twitcher Mice. *Int. J. Mol. Sci.* **2022**, *23*, 9436. [[CrossRef](#)] [[PubMed](#)]
56. Kwon, J.M. Consensus guidelines for newborn screening, diagnosis and treatment of infantile Krabbe disease. *Orphanet J. Rare Dis.* **2018**, *13*, 30. [[CrossRef](#)] [[PubMed](#)]
57. Yoon, I.C.; Bascou, N.A.; Poe, M.D.; Szabolcs, P.; Escolar, M.L. Long-term neurodevelopmental outcomes of hematopoietic stem cell transplantation for late-infantile Krabbe disease. *Blood* **2021**, *137*, 1719–1730. [[CrossRef](#)] [[PubMed](#)]
58. Zhang, T.; Yan, C.; Ji, K.; Lin, P.; Chi, L.; Zhao, X.; Zhao, Y. Adult-onset Krabbe disease in two generations of a Chinese family. *Ann. Transl. Med.* **2018**, *6*, 174. [[CrossRef](#)]
59. Elsea, S.H.; Solyom, A.; Martin, K.; Harmatz, P.; Mitchell, J.; Lampe, C.; Grant, C.; Selim, L.; Mungan, N.O.; Guelbert, N.; et al. ASAH1 pathogenic variants associated with acid ceramidase deficiency: Farber disease and spinal muscular atrophy with progressive myoclonic epilepsy. *Hum. Mutat.* **2020**, *41*, 1469–1487. [[CrossRef](#)]
60. Sands, M.S. Farber disease: Understanding a fatal childhood disorder and dissecting ceramide biology. *EMBO Mol. Med.* **2013**, *5*, 799–801. [[CrossRef](#)]
61. Ehlert, K.; Frosch, M.; Fehse, N.; Zander, A.; Roth, J.; Vormoor, J. Farber disease: Clinical presentation, pathogenesis and a new approach to treatment. *Pediatr. Rheumatol. Online J.* **2007**, *5*, 15. [[CrossRef](#)] [[PubMed](#)]
62. Sandhoff, K.; Harzer, K. Gangliosides and gangliosidoses: Principles of molecular and metabolic pathogenesis. *J. Neurosci.* **2013**, *33*, 10195–10208. [[CrossRef](#)]
63. Breiden, B.; Sandhoff, K. Ganglioside Metabolism and Its Inherited Diseases. *Methods Mol. Biol.* **2018**, *1804*, 97–141. [[CrossRef](#)] [[PubMed](#)]
64. Nicoli, E.R.; Annunziata, I.; d’Azzo, A.; Platt, F.M.; Tifft, C.J.; Stepien, K.M. GM1 Gangliosidosis-A Mini-Review. *Front. Genet.* **2021**, *12*, 734878. [[CrossRef](#)] [[PubMed](#)]
65. Nestrail, L.; Ahmed, A.; Utz, J.M.; Rudser, K.; Whitley, C.B.; Jarnes-Utz, J.R. Distinct progression patterns of brain disease in infantile and juvenile gangliosidoses: Volumetric quantitative MRI study. *Mol. Genet. Metab.* **2018**, *123*, 97–104. [[CrossRef](#)]
66. Jarnes Utz, J.R.; Kim, S.; King, K.; Ziegler, R.; Schema, L.; Redtree, E.S.; Whitley, C.B. Infantile gangliosidoses: Mapping a timeline of clinical changes. *Mol. Genet. Metab.* **2017**, *121*, 170–179. [[CrossRef](#)]
67. Rha, A.K.; Maguire, A.S.; Martin, D.R. GM1 Gangliosidosis: Mechanisms and Management. *Appl. Clin. Genet.* **2021**, *14*, 209–233. [[CrossRef](#)] [[PubMed](#)]
68. Pineda, M.; Walterfang, M.; Patterson, M.C. Miglustat in Niemann-Pick disease type C patients: A review. *Orphanet J. Rare. Dis.* **2018**, *13*, 140. [[CrossRef](#)] [[PubMed](#)]
69. Aerts, J.M.; Hollak, C.E.; Boot, R.G.; Groener, J.E.; Maas, M. Substrate reduction therapy of glycosphingolipid storage disorders. *J. Inherit. Metab. Dis.* **2006**, *29*, 449–456. [[CrossRef](#)]
70. Fischetto, R.; Palladino, V.; Mancardi, M.; Giacomini, T.; Palladino, S.; Gaeta, A.; Di Rocco, M.; Zampini, L.; Lassandro, G.; Favia, V.; et al. Substrate reduction therapy with Miglustat in pediatric patients with GM1 type 2 gangliosidosis delays neurological involvement: A multicenter experience. *Mol. Genet. Genomic. Med.* **2020**, *8*, e1371. [[CrossRef](#)]
71. Leal, A.F.; Benincore-Flórez, E.; Solano-Galarza, D.; Garzón Jaramillo, R.G.; Echeverri-Peña, O.Y.; Suarez, D.A.; Almérciga-Díaz, C.J.; Espejo-Mojica, A.J. GM2 Gangliosidoses: Clinical Features, Pathophysiological Aspects, and Current Therapies. *Int. J. Mol. Sci.* **2020**, *21*, 6213. [[CrossRef](#)]
72. Ganne, B.; Dauriat, B.; Richard, L.; Lamari, F.; Ghorab, K.; Magy, L.; Benkirane, M.; Perani, A.; Marquet, V.; Calvas, P.; et al. GM2 gangliosidosis AB variant: First case of late onset and review of the literature. *Neurol. Sci.* **2022**, *43*, 6517–6527. [[CrossRef](#)] [[PubMed](#)]

73. Tropak, M.B.; Yonekawa, S.; Karumuthil-Meilethil, S.; Thompson, P.; Wakarchuk, W.; Gray, S.J.; Walia, J.S.; Mark, B.L.; Mahuran, D. Construction of a hybrid  $\beta$ -hexosaminidase subunit capable of forming stable homodimers that hydrolyze GM2 ganglioside in vivo. *Mol. Ther. Methods. Clin. Dev.* **2016**, *3*, 15057. [[CrossRef](#)]
74. Ou, L.; Przybilla, M.J.; Tåbåran, A.F.; Overn, P.; O'Sullivan, M.G.; Jiang, X.; Sidhu, R.; Kell, P.J.; Ory, D.S.; Whitley, C.B. A novel gene editing system to treat both Tay-Sachs and Sandhoff diseases. *Gene Ther.* **2020**, *27*, 226–236. [[CrossRef](#)] [[PubMed](#)]
75. Flotte, T.R.; Cataltepe, O.; Puri, A.; Batista, A.R.; Moser, R.; McKenna-Yasek, D.; Douthwright, C.; Gernoux, G.; Blackwood, M.; Mueller, C.; et al. AAV gene therapy for Tay-Sachs disease. *Nat. Med.* **2022**, *28*, 251–259. [[CrossRef](#)] [[PubMed](#)]
76. Kot, S.; Karumuthil-Meilethil, S.; Woodley, E.; Zaric, V.; Thompson, P.; Chen, Z.; Lykken, E.; Keimel, J.G.; Kaemmerer, W.F.; Gray, S.J. Investigating Immune Responses to the scAAV9-. *Int. J. Mol. Sci.* **2021**, *22*, 6751. [[CrossRef](#)]
77. Solovyeva, V.V.; Shaimardanova, A.A.; Chulpanova, D.S.; Kitaeva, K.V.; Chakrabarti, L.; Rizvanov, A.A. New Approaches to Tay-Sachs Disease Therapy. *Front. Physiol.* **2018**, *9*, 1663. [[CrossRef](#)]
78. Ihsan Fazal, M.; Kacprzyk, R.; Timson, D.J. *In silico* analysis of the effects of disease-associated mutations of  $\beta$ -hexosaminidase A in Tay-Sachs disease. *J. Genet.* **2020**, *99*, 42. [[CrossRef](#)]
79. Maegawa, G.H.; Stockley, T.; Tropak, M.; Banwell, B.; Blaser, S.; Kok, F.; Giugliani, R.; Mahuran, D.; Clarke, J.T. The natural history of juvenile or subacute GM2 gangliosidosis: 21 New cases and literature review of 134 previously reported. *Pediatrics* **2006**, *118*, e1550–e1562. [[CrossRef](#)]
80. Májovská, J.; Hennig, A.; Nestržil, I.; Schneider, S.A.; Jahnová, H.; Vaněčková, M.; Magner, M.; Dušek, P. Pontocerebellar atrophy is the hallmark neuroradiological finding in late-onset Tay-Sachs disease. *Neurol. Sci.* **2022**, *43*, 3273–3281. [[CrossRef](#)]
81. Tim-Aroon, T.; Wichajarn, K.; Katanyuwong, K.; Tanpaiboon, P.; Vatanavicharn, N.; Sakpichaisakul, K.; Kongkrapan, A.; Eu-Ahsunthornwattana, J.; Thongpradit, S.; Moolsuwan, K.; et al. Infantile onset Sandhoff disease: Clinical manifestation and a novel common mutation in Thai patients. *BMC Pediatr.* **2021**, *21*, 22. [[CrossRef](#)]
82. García Morales, L.; Mustelier Bécquer, R.G.; Pérez Joglar, L.; Zaldivar Vaillant, T. Sandhoff disease in the elderly: A case study. *Amyotroph. Lateral Scler. Front. Degener* **2022**, *23*, 137–138. [[CrossRef](#)]
83. Masingue, M.; Dufour, L.; Lenglet, T.; Saleille, L.; Goizet, C.; Ayrygnac, X.; Ory-Magne, F.; Barth, M.; Lamari, F.; Mandia, D.; et al. Natural History of Adult Patients with GM2 Gangliosidosis. *Ann. Neurol.* **2020**, *87*, 609–617. [[CrossRef](#)]
84. Alonso-Pérez, J.; Casasús, A.; Gimenez-Muñoz, Á.; Duff, J.; Rojas-García, R.; Illa, I.; Straub, V.; Töpf, A.; Díaz-Manera, J. Late onset Sandhoff disease presenting with lower motor neuron disease and stuttering. *Neuromuscul. Disord.* **2021**, *31*, 769–772. [[CrossRef](#)]
85. Shaimardanova, A.A.; Chulpanova, D.S.; Solovyeva, V.V.; Mullagulova, A.I.; Kitaeva, K.V.; Allegrucci, C.; Rizvanov, A.A. Metachromatic Leukodystrophy: Diagnosis, Modeling, and Treatment Approaches. *Front. Med.* **2020**, *7*, 576221. [[CrossRef](#)]
86. Hossain, M.A.; Hasegawa-Ogawa, M.; Manome, Y.; Igarashi, M.; Wu, C.; Suzuki, K.; Igarashi, J.; Iwamoto, T.; Okano, H.J.; Eto, Y. Generation and characterization of motor neuron progenitors and motor neurons using metachromatic leukodystrophy-induced pluripotent stem cells. *Mol. Genet. Metab. Rep.* **2022**, *31*, 100852. [[CrossRef](#)]
87. Biffi, A.; Lucchini, G.; Rovelli, A.; Sessa, M. Metachromatic leukodystrophy: An overview of current and prospective treatments. *Bone Marrow Transplant.* **2008**, *42* (Suppl. S2), S2–S6. [[CrossRef](#)] [[PubMed](#)]
88. Fumagalli, F.; Calbi, V.; Natali Sora, M.G.; Sessa, M.; Baldoli, C.; Rancoita, P.M.V.; Ciotti, F.; Sarzana, M.; Frascini, M.; Zambon, A.A.; et al. Lentiviral haematopoietic stem-cell gene therapy for early-onset metachromatic leukodystrophy: Long-term results from a non-randomised, open-label, phase 1/2 trial and expanded access. *Lancet* **2022**, *399*, 372–383. [[CrossRef](#)] [[PubMed](#)]
89. Streisinger, G.; Walker, C.; Dower, N.; Knauber, D.; Singer, F. Production of clones of homozygous diploid zebra fish (*Brachydanio rerio*). *Nature* **1981**, *291*, 293–296. [[CrossRef](#)] [[PubMed](#)]
90. Howe, K.; Clark, M.D.; Torroja, C.F.; Torrance, J.; Berthelot, C.; Muffato, M.; Collins, J.E.; Humphray, S.; McLaren, K.; Matthews, L.; et al. The zebrafish reference genome sequence and its relationship to the human genome. *Nature* **2013**, *496*, 498–503. [[CrossRef](#)] [[PubMed](#)]
91. Dudziak, K.; Nowak, M.; Sozoniuk, M. One Host-Multiple Applications: Zebrafish (*Danio rerio*) as Promising Model for Studying Human Cancers and Pathogenic Diseases. *Int. J. Mol. Sci.* **2022**, *23*, 10255. [[CrossRef](#)]
92. Chia, K.; Klingseisen, A.; Sieger, D.; Priller, J. Zebrafish as a model organism for neurodegenerative disease. *Front. Mol. Neurosci.* **2022**, *15*, 940484. [[CrossRef](#)]
93. Bowley, G.; Kugler, E.; Wilkinson, R.; Lawrie, A.; van Eeden, F.; Chico, T.J.A.; Evans, P.C.; Noël, E.S.; Serbanovic-Canic, J. Zebrafish as a tractable model of human cardiovascular disease. *Br. J. Pharmacol.* **2022**, *179*, 900–917. [[CrossRef](#)]
94. Fontana, B.D.; Norton, W.H.J.; Parker, M.O. Modelling ADHD-Like Phenotypes in Zebrafish. *Curr. Top. Behav. Neurosci.* **2022**, *57*, 395–414. [[CrossRef](#)]
95. Canzian, J.; Gonçalves, F.L.S.; Müller, T.E.; Franscescon, F.; Santos, L.W.; Adedara, I.A.; Rosemberg, D.B. Zebrafish as a potential non-traditional model organism in translational bipolar disorder research: Genetic and behavioral insights. *Neurosci. Biobehav. Rev.* **2022**, *136*, 104620. [[CrossRef](#)]
96. Phillips, J.B.; Westerfield, M. Chapter 47—Zebrafish as a Model to Understand Human Genetic Diseases. In *The Zebrafish in Biomedical Research: Biology, Husbandry, Diseases, and Research Applications*; American College of Laboratory Animal Medicine: Chester, NH, USA, 2020; pp. 619–626. [[CrossRef](#)]
97. Crouzier, L.; Richard, E.M.; Sourbron, J.; Lagae, L.; Maurice, T.; Delprat, B. Use of Zebrafish Models to Boost Research in Rare Genetic Diseases. *Int. J. Mol. Sci.* **2021**, *22*, 13356. [[CrossRef](#)]



98. Fraher, D.; Sanigorski, A.; Mellett, N.A.; Meikle, P.J.; Sinclair, A.J.; Gibert, Y. Zebrafish Embryonic Lipidomic Analysis Reveals that the Yolk Cell Is Metabolically Active in Processing Lipid. *Cell Rep.* **2016**, *14*, 1317–1329. [[CrossRef](#)]
99. Quinlivan, V.H.; Wilson, M.H.; Ruzicka, J.; Farber, S.A. An HPLC-CAD/fluorescence lipidomics platform using fluorescent fatty acids as metabolic tracers. *J. Lipid. Res.* **2017**, *58*, 1008–1020. [[CrossRef](#)]
100. Zhang, T.; Peterson, R.T. Modeling Lysosomal Storage Diseases in the Zebrafish. *Front. Mol. Biosci.* **2020**, *7*, 82. [[CrossRef](#)]
101. Xu, M.M.; Legradi, J.; Leonards, P. Using comprehensive lipid profiling to study effects of PFHxS during different stages of early zebrafish development. *Sci. Total. Environ.* **2022**, *808*, 151739. [[CrossRef](#)]
102. Zhang, W.; Song, Y.; Chai, T.; Liao, G.; Zhang, L.; Jia, Q.; Qian, Y.; Qiu, J. Lipidomics perturbations in the brain of adult zebrafish (*Danio rerio*) after exposure to chiral ibuprofen. *Sci. Total. Environ.* **2020**, *713*, 136565. [[CrossRef](#)]
103. Hachicho, N.; Reithel, S.; Miltner, A.; Heipieper, H.J.; Küster, E.; Luckenbach, T. Body Mass Parameters, Lipid Profiles and Protein Contents of Zebrafish Embryos and Effects of 2,4-Dinitrophenol Exposure. *PLoS ONE* **2015**, *10*, e0134755. [[CrossRef](#)]
104. Liebisch, G.; Fahy, E.; Aoki, J.; Dennis, E.A.; Durand, T.; Ejsing, C.S.; Fedorova, M.; Feussner, I.; Griffiths, W.J.; Köfeler, H.; et al. Update on LIPID MAPS classification, nomenclature, and shorthand notation for MS-derived lipid structures. *J. Lipid. Res.* **2020**, *61*, 1539–1555. [[CrossRef](#)]
105. Pirro, V.; Guffey, S.C.; Sepúlveda, M.S.; Mahapatra, C.T.; Ferreira, C.R.; Jarmusch, A.K.; Cooks, R.G. Lipid dynamics in zebrafish embryonic development observed by DESI-MS imaging and nano-electrospray-MS. *Mol. Biosyst.* **2016**, *12*, 2069–2079. [[CrossRef](#)]
106. Dueñas, M.E.; Essner, J.J.; Lee, Y.J. 3D MALDI Mass Spectrometry Imaging of a Single Cell: Spatial Mapping of Lipids in the Embryonic Development of Zebrafish. *Sci Rep.* **2017**, *7*, 14946. [[CrossRef](#)]
107. Xu, M.; Legradi, J.; Leonards, P. Evaluation of LC-MS and LCxLC-MS in analysis of zebrafish embryo samples for comprehensive lipid profiling. *Anal. Bioanal. Chem.* **2020**, *412*, 4313–4325. [[CrossRef](#)]
108. Castanon, I.; Hannich, J.T.; Abrami, L.; Huber, F.; Dubois, M.; Muller, M.; van der Goot, F.G.; Gonzalez-Gaitan, M. Wnt-controlled sphingolipids modulate Anthrax Toxin Receptor palmitoylation to regulate oriented mitosis in zebrafish. *Nat. Commun.* **2020**, *11*, 3317. [[CrossRef](#)]
109. da Silva, K.M.; Iturraspe, E.; van den Boom, R.; van de Lavoie, M.; Robeyns, R.; Vergauwen, L.; Knapen, D.; Cuykx, M.; Covaci, A.; van Nuijs, A.L.N. Lipidomics profiling of zebrafish liver through untargeted liquid chromatography-high resolution mass spectrometry. *J. Sep. Sci.* **2022**, *45*, 2935–2945. [[CrossRef](#)]
110. Choi, J.; Leonard, S.W.; Kasper, K.; McDougall, M.; Stevens, J.F.; Tanguay, R.L.; Traber, M.G. Novel function of vitamin E in regulation of zebrafish (*Danio rerio*) brain lysophospholipids discovered using lipidomics. *J. Lipid. Res.* **2015**, *56*, 1182–1190. [[CrossRef](#)]
111. Zhang, T.; Trauger, S.A.; Vidoudez, C.; Doane, K.P.; Pluimer, B.R.; Peterson, R.T. Parallel Reaction Monitoring reveals structure-specific ceramide alterations in the zebrafish. *Sci. Rep.* **2019**, *9*, 19939. [[CrossRef](#)]
112. Zelnik, I.D.; Rozman, B.; Rosenfeld-Gur, E.; Ben-Dor, S.; Futerman, A.H. A Stroll Down the CerS Lane. *Adv. Exp. Med. Biol.* **2019**, *1159*, 49–63. [[CrossRef](#)]
113. Brondolin, M.; Berger, S.; Reinke, M.; Tanaka, H.; Ohshima, T.; Fuβ, B.; Hoch, M. Identification and expression analysis of the zebrafish homologs of the ceramide synthase gene family. *Dev. Dyn.* **2013**, *242*, 189–200. [[CrossRef](#)]
114. Mendelson, K.; Pandey, S.; Hisano, Y.; Carellini, F.; Das, B.C.; Hla, T.; Evans, T. The ceramide synthase 2b gene mediates genomic sensing and regulation of sphingosine levels during zebrafish embryogenesis. *eLife* **2017**, *6*, e21992. [[CrossRef](#)]
115. Tomasello, D.L.; Kim, J.L.; Khodour, Y.; McCammon, J.M.; Mitalipova, M.; Jaenisch, R.; Futerman, A.H.; Sive, H. FAM57B is a modulator of ceramide synthesis that regulates sphingolipid homeostasis and synaptic composition in the developing brain. *bioRxiv* **2021**. [[CrossRef](#)]
116. Zerbino, D.R.; Achuthan, P.; Akanni, W.; Amode, M.R.; Barrell, D.; Bhai, J.; Billis, K.; Cummins, C.; Gall, A.; Girón, C.G.; et al. Ensembl 2018. *Nucleic Acids Res.* **2018**, *46*, D754–D761. [[CrossRef](#)]
117. Lelieveld, L.T.; Gerhardt, S.; Maas, S.; Zwieters, K.C.; de Wit, C.; Beijck, E.H.; Ferraz, M.J.; Artola, M.; Meijer, A.H.; Tudorache, C.; et al. Consequences of excessive glucosylsphingosine in glucocerebrosidase-deficient zebrafish. *J. Lipid Res.* **2022**, *63*, 100199. [[CrossRef](#)]
118. Bradford, Y.M.; Van Slyke, C.E.; Ruzicka, L.; Singer, A.; Eagle, A.; Fashena, D.; Howe, D.G.; Frazer, K.; Martin, R.; Paddock, H.; et al. Zebrafish information network, the knowledgebase for *Danio rerio* research. *Genetics* **2022**, *220*, iyac016. [[CrossRef](#)]
119. Taniguchi, M.; Okazaki, T. The role of sphingomyelin and sphingomyelin synthases in cell death, proliferation and migration—from cell and animal models to human disorders. *Biochim. Biophys. Acta* **2014**, *1841*, 692–703. [[CrossRef](#)]
120. Vacaru, A.M.; Tafesse, F.G.; Ternes, P.; Kondylis, V.; Hermansson, M.; Brouwers, J.F.; Somerharju, P.; Rabouille, C.; Holthuis, J.C. Sphingomyelin synthase-related protein SMSr controls ceramide homeostasis in the ER. *J. Cell. Biol.* **2009**, *185*, 1013–1027. [[CrossRef](#)]
121. Ogretmen, B. Sphingolipid metabolism in cancer signalling and therapy. *Nat. Reviews. Cancer* **2018**, *18*, 33–50. [[CrossRef](#)]
122. Keatinge, M.; Gegg, M.E.; Watson, L.; Mortiboy, H.; Li, N.; Dunning, M.; Ailani, D.; Bui, H.; van Rens, A.; Lefeber, D.J.; et al. Unexpected opposing biological effect of genetic risk factors for Parkinson’s disease. *bioRxiv* **2020**. [[CrossRef](#)]
123. Yabu, T.; Imamura, S.; Yamashita, M.; Okazaki, T. Identification of Mg<sup>2+</sup>-dependent neutral sphingomyelinase 1 as a mediator of heat stress-induced ceramide generation and apoptosis. *J. Biol. Chem.* **2008**, *283*, 29971–29982. [[CrossRef](#)]

124. Yabu, T.; Shiba, H.; Shibasaki, Y.; Nakanishi, T.; Imamura, S.; Touhata, K.; Yamashita, M. Stress-induced ceramide generation and apoptosis via the phosphorylation and activation of nSMase1 by JNK signaling. *Cell Death Differ.* **2015**, *22*, 258–273. [[CrossRef](#)] [[PubMed](#)]
125. Yabu, T.; Tomimoto, H.; Taguchi, Y.; Yamaoka, S.; Igarashi, Y.; Okazaki, T. Thalidomide-induced antiangiogenic action is mediated by ceramide through depletion of VEGF receptors, and is antagonized by sphingosine-1-phosphate. *Blood* **2005**, *106*, 125–134. [[CrossRef](#)]
126. Yabu, T.; Shimizu, A.; Yamashita, M. A novel mitochondrial sphingomyelinase in zebrafish cells. *J. Biol. Chem.* **2009**, *284*, 20349–20363. [[CrossRef](#)]
127. Bravo, G.Á.; Cedeño, R.R.; Casadevall, M.P.; Ramió-Torrentà, L. Sphingosine-1-Phosphate (S1P) and S1P Signaling Pathway Modulators, from Current Insights to Future Perspectives. *Cells* **2022**, *11*, 2058. [[CrossRef](#)] [[PubMed](#)]
128. Mendelson, K.; Zygmunt, T.; Torres-Vázquez, J.; Evans, T.; Hla, T. Sphingosine 1-phosphate receptor signaling regulates proper embryonic vascular patterning. *J. Biol. Chem.* **2013**, *288*, 2143–2156. [[CrossRef](#)]
129. Hisano, Y.; Inoue, A.; Okudaira, M.; Taimatsu, K.; Matsumoto, H.; Kotani, H.; Ohga, R.; Aoki, J.; Kawahara, A. Maternal and Zygotic Sphingosine Kinase 2 Are Indispensable for Cardiac Development in Zebrafish. *J. Biol. Chem.* **2015**, *290*, 14841–14851. [[CrossRef](#)] [[PubMed](#)]
130. Zhu, X.; Ren, K.; Zeng, Y.Z.; Zheng, Z.; Yi, G.H. Biological function of SPNS2: From zebrafish to human. *Mol. Immunol.* **2018**, *103*, 55–62. [[CrossRef](#)]
131. Elsaid, H.O.A.; Furriol, J.; Blomqvist, M.; Diswall, M.; Leh, S.; Gharbi, N.; Anonsen, J.H.; Babickova, J.; Tøndel, C.; Svarstad, E.; et al. Reduced  $\alpha$ -galactosidase A activity in zebrafish (*Danio rerio*) mirrors distinct features of Fabry nephropathy phenotype. *Mol. Genet. Metab. Rep.* **2022**, *31*, 100851. [[CrossRef](#)] [[PubMed](#)]
132. Nasevicius, A.; Ekker, S.C. Effective targeted gene ‘knockdown’ in zebrafish. *Nat. Genet.* **2000**, *26*, 216–220. [[CrossRef](#)] [[PubMed](#)]
133. Huang, P.; Xiao, A.; Zhou, M.; Zhu, Z.; Lin, S.; Zhang, B. Heritable gene targeting in zebrafish using customized TALENs. *Nat. Biotechnol.* **2011**, *29*, 699–700. [[CrossRef](#)] [[PubMed](#)]
134. Sander, J.D.; Cade, L.; Khayter, C.; Reyon, D.; Peterson, R.T.; Joung, J.K.; Yeh, J.R. Targeted gene disruption in somatic zebrafish cells using engineered TALENs. *Nat. Biotechnol.* **2011**, *29*, 697–698. [[CrossRef](#)] [[PubMed](#)]
135. Chang, N.; Sun, C.; Gao, L.; Zhu, D.; Xu, X.; Zhu, X.; Xiong, J.W.; Xi, J.J. Genome editing with RNA-guided Cas9 nuclease in zebrafish embryos. *Cell Res.* **2013**, *23*, 465–472. [[CrossRef](#)] [[PubMed](#)]
136. Hwang, W.Y.; Fu, Y.; Reyon, D.; Maeder, M.L.; Kaini, P.; Sander, J.D.; Joung, J.K.; Peterson, R.T.; Yeh, J.R. Heritable and precise zebrafish genome editing using a CRISPR-Cas system. *PLoS ONE* **2013**, *8*, e68708. [[CrossRef](#)] [[PubMed](#)]
137. Gagnon, J.A.; Valen, E.; Thyme, S.B.; Huang, P.; Akhmetova, L.; Pauli, A.; Montague, T.G.; Zimmerman, S.; Richter, C.; Schier, A.F. Efficient mutagenesis by Cas9 protein-mediated oligonucleotide insertion and large-scale assessment of single-guide RNAs. *PLoS ONE* **2014**, *9*, e98186. [[CrossRef](#)]
138. Zancan, L.; Bellesso, S.; Costa, R.; Salvalaio, M.; Stroppiano, M.; Hammond, C.; Argenton, F.; Filocamo, M.; Moro, E. Glucocerebrosidase deficiency in zebrafish affects primary bone ossification through increased oxidative stress and reduced Wnt/ $\beta$ -catenin signaling. *Hum. Mol. Genet.* **2015**, *24*, 1280–1294. [[CrossRef](#)] [[PubMed](#)]
139. Keatinge, M.; Bui, H.; Menke, A.; Chen, Y.C.; Sokol, A.M.; Bai, Q.; Ellett, F.; Da Costa, M.; Burke, D.; Gegg, M.; et al. Glucocerebrosidase 1 deficient *Danio rerio* mirror key pathological aspects of human Gaucher disease and provide evidence of early microglial activation preceding alpha-synuclein-independent neuronal cell death. *Hum. Mol. Genet.* **2015**, *24*, 6640–6652. [[CrossRef](#)]
140. Lelieveld, L.T.; Mirzaian, M.; Kuo, C.L.; Artola, M.; Ferraz, M.J.; Peter, R.E.A.; Akiyama, H.; Greimel, P.; van den Berg, R.; Overkleeft, H.S.; et al. Role of  $\beta$ -glucosidase 2 in aberrant glycosphingolipid metabolism: Model of glucocerebrosidase deficiency in zebrafish. *J. Lipid. Res.* **2019**, *60*, 1851–1867. [[CrossRef](#)]
141. Schwend, T.; Loucks, E.J.; Snyder, D.; Ahlgren, S.C. Requirement of Npc1 and availability of cholesterol for early embryonic cell movements in zebrafish. *J. Lipid. Res.* **2011**, *52*, 1328–1344. [[CrossRef](#)]
142. Tseng, W.C.; Loeb, H.E.; Pei, W.; Tsai-Morris, C.H.; Xu, L.; Cluzeau, C.V.; Wassif, C.A.; Feldman, B.; Burgess, S.M.; Pavan, W.J.; et al. Modeling Niemann-Pick disease type C1 in zebrafish: A robust platform for in vivo screening of candidate therapeutic compounds. *Dis. Model. Mech.* **2018**, *11*, dmm034165. [[CrossRef](#)]
143. Lin, Y.; Cai, X.; Wang, G.; Ouyang, G.; Cao, H. Model construction of Niemann-Pick type C disease in zebrafish. *Biol. Chem.* **2018**, *399*, 903–910. [[CrossRef](#)]
144. Wiweger, M.; Majewski, L.; Adamek-Urbanska, D.; Wasilewska, I.; Kuznicki, J. npc2-Deficient Zebrafish Reproduce Neurological and Inflammatory Symptoms of Niemann-Pick Type C Disease. *Front. Cell. Neuro.* **2021**, *15*, 647860. [[CrossRef](#)] [[PubMed](#)]
145. Tseng, W.C.; Johnson Escauriza, A.J.; Tsai-Morris, C.H.; Feldman, B.; Dale, R.K.; Wassif, C.A.; Porter, F.D. The role of Niemann-Pick type C2 in zebrafish embryonic development. *Development* **2021**, *148*, dev194258. [[CrossRef](#)] [[PubMed](#)]
146. Zizioli, D.; Guarienti, M.; Tobia, C.; Gariano, G.; Borsani, G.; Bresciani, R.; Ronca, R.; Giacomuzzi, E.; Preti, A.; Gaudenzi, G.; et al. Molecular cloning and knockdown of galactocerebrosidase in zebrafish: New insights into the pathogenesis of Krabbe’s disease. *Biochim. Biophys. Acta* **2014**, *1842*, 665–675. [[CrossRef](#)]
147. Zhou, J.; Tawk, M.; Tiziano, F.D.; Veillet, J.; Bayes, M.; Nolent, F.; Garcia, V.; Servidei, S.; Bertini, E.; Castro-Giner, F.; et al. Spinal muscular atrophy associated with progressive myoclonic epilepsy is caused by mutations in ASAH1. *Am. J. Hum. Genet.* **2012**, *91*, 5–14. [[CrossRef](#)]

148. Berg, R.D.; Levitte, S.; O'Sullivan, M.P.; O'Leary, S.M.; Cambier, C.J.; Cameron, J.; Takaki, K.K.; Moens, C.B.; Tobin, D.M.; Keane, J.; et al. Lysosomal Disorders Drive Susceptibility to Tuberculosis by Compromising Macrophage Migration. *Cell* **2016**, *165*, 139–152. [[CrossRef](#)] [[PubMed](#)]
149. Kalén, M.; Wallgard, E.; Asker, N.; Nasevicius, A.; Athley, E.; Billgren, E.; Larson, J.D.; Wadman, S.A.; Norseng, E.; Clark, K.J.; et al. Combination of reverse and chemical genetic screens reveals angiogenesis inhibitors and targets. *Chem. Biol.* **2009**, *16*, 432–441. [[CrossRef](#)]
150. Kuil, L.E.; López Martí, A.; Carreras Mascaro, A.; van den Bosch, J.C.; van den Berg, P.; van der Linde, H.C.; Schoonderwoerd, K.; Ruijter, G.J.G.; van Ham, T.J. Hexb enzyme deficiency leads to lysosomal abnormalities in radial glia and microglia in zebrafish brain development. *Glia* **2019**, *67*, 1705–1718. [[CrossRef](#)]
151. Matsui, H.; Ito, J.; Matsui, N.; Uechi, T.; Onodera, O.; Kakita, A. Cytosolic dsDNA of mitochondrial origin induces cytotoxicity and neurodegeneration in cellular and zebrafish models of Parkinson's disease. *Nat. Commun.* **2021**, *12*, 3101. [[CrossRef](#)]
152. Marques, A.R.; Aten, J.; Ottenhoff, R.; van Roomen, C.P.; Herrera Moro, D.; Claessen, N.; Vinueza Veloz, M.F.; Zhou, K.; Lin, Z.; Mirzaian, M.; et al. Reducing GBA2 Activity Ameliorates Neuropathology in Niemann-Pick Type C Mice. *PLoS ONE* **2015**, *10*, e0135889. [[CrossRef](#)]
153. Mistry, P.K.; Liu, J.; Sun, L.; Chuang, W.L.; Yuen, T.; Yang, R.; Lu, P.; Zhang, K.; Li, J.; Keutzer, J.; et al. Glucocerebrosidase 2 gene deletion rescues type 1 Gaucher disease. *Proc. Natl. Acad. Sci. USA* **2014**, *111*, 4934–4939. [[CrossRef](#)]
154. Robak, L.A.; Jansen, I.E.; van Rooij, J.; Uitterlinden, A.G.; Kraaij, R.; Jankovic, J.; International Parkinson's Disease Genomics Consortium (IPDGC); Heutink, P.; Shulman, J.M. Excessive burden of lysosomal storage disorder gene variants in Parkinson's disease. *Brain* **2017**, *140*, 3191–3203. [[CrossRef](#)]
155. Toyooka, K. Chapter 37—Fabry disease. *Handb. Clin. Neurol.* **2013**, *115*, 629–642. [[CrossRef](#)] [[PubMed](#)]
156. Hayashi, T.; Okamoto, R.; Kawano, T.; Iwasaki, T. Development of Organelle Replacement Therapy Using a Stearyl-Polyhistidine Peptide against Lysosomal Storage Disease Cells. *Molecules* **2019**, *24*, 2995. [[CrossRef](#)]
157. Spiegel, R.; Raas-Rothschild, A.; Reish, O.; Regev, M.; Meiner, V.; Bargal, R.; Sury, V.; Meir, K.; Nadjari, M.; Hermann, G.; et al. The clinical spectrum of fetal Niemann-Pick type C. *Am. J. Med. Genet. A* **2009**, *149A*, 446–450. [[CrossRef](#)] [[PubMed](#)]
158. Flanagan-Steet, H.; Sias, C.; Steet, R. Altered chondrocyte differentiation and extracellular matrix homeostasis in a zebrafish model for mucopolidosis II. *Am. J. Pathol.* **2009**, *175*, 2063–2075. [[CrossRef](#)]
159. Lu, P.N.; Moreland, T.; Christian, C.J.; Lund, T.C.; Steet, R.A.; Flanagan-Steet, H. Inappropriate cathepsin k secretion promotes its enzymatic activation driving heart and valve malformation. *JCI Insight* **2020**, *5*. [[CrossRef](#)]
160. Qian, Y.; van Meel, E.; Flanagan-Steet, H.; Yox, A.; Steet, R.; Kornfeld, S. Analysis of mucopolidosis ii/iii gntab missense mutations identifies domains of udp-glcna:lysosomal enzyme glcna-1-phosphotransferase involved in catalytic function and lysosomal enzyme recognition. *J. Biol. Chem.* **2015**, *290*, 3045–3056. [[CrossRef](#)]
161. Moro, E.; Tomanin, R.; Friso, A.; Modena, N.; Tiso, N.; Scarpa, M.; Argenton, F. A novel functional role of iduronate-2-sulfatase in zebrafish early development. *Matrix Biol.* **2010**, *29*, 43–50. [[CrossRef](#)]
162. Costa, R.; Urbani, A.; Salvalaio, M.; Bellesso, S.; Cieri, D.; Zancan, I.; Filocamo, M.; Bonaldo, P.; Szabò, I.; Tomanin, R.; et al. Perturbations in cell signaling elicit early cardiac defects in mucopolysaccharidosis type II. *Hum. Mol. Genet.* **2017**, *26*, 1643–1655. [[CrossRef](#)]
163. Bellesso, S.; Salvalaio, M.; Lualdi, S.; Tognon, E.; Costa, R.; Braghetta, P.; Giraud, C.; Stramare, R.; Rigon, L.; Filocamo, M.; et al. Fgf signaling deregulation is associated with early developmental skeletal defects in animal models for mucopolysaccharidosis type II (mpsII). *Hum. Mol. Genet.* **2018**, *27*, 2262–2275. [[CrossRef](#)]
164. Lin, C.Y.; Lin, H.Y.; Chuang, C.K.; Zhang, P.H.; Tu, R.Y.; Lin, S.P.; Tsai, H.J. Effect of mutated ids overexpression on ids enzyme activity and developmental phenotypes in zebrafish embryos: A valuable index for assessing critical point-mutations associated with mucopolysaccharidosis type II occurrence in humans. *Diagnostics* **2020**, *10*, 854. [[CrossRef](#)]
165. White, A.B.; Galbiati, F.; Givogri, M.I.; Lopez Rosas, A.; Qiu, X.; van Breemen, R.; Bongarzone, E.R. Persistence of psychosine in brain lipid rafts is a limiting factor in the therapeutic recovery of a mouse model for Krabbe disease. *J. Neurosci. Res.* **2011**, *89*, 352–364. [[CrossRef](#)]
166. MacMillan, C.J.; Furlong, S.J.; Doucette, C.D.; Chen, P.L.; Hoskin, D.W.; Easton, A.S. Bevacizumab diminishes experimental autoimmune encephalomyelitis by inhibiting spinal cord angiogenesis and reducing peripheral T-cell responses. *J. Neuropathol. Exp. Neurol.* **2012**, *71*, 983–999. [[CrossRef](#)]
167. Cachon-Gonzalez, M.B.; Zaccariotto, E.; Cox, T.M. Genetics and Therapies for GM2 Gangliosidosis. *Curr. Gene Ther.* **2018**, *18*, 68–89. [[CrossRef](#)] [[PubMed](#)]
168. Wiley, D.S.; Redfield, S.E.; Zon, L.I. Chemical screening in zebrafish for novel biological and therapeutic discovery. *Methods Cell. Biol.* **2017**, *138*, 651–679. [[CrossRef](#)]
169. Patton, E.E.; Zon, L.I.; Langenau, D.M. Zebrafish disease models in drug discovery: From preclinical modelling to clinical trials. *Nat. Rev. Drug Discov.* **2021**, *20*, 611–628. [[CrossRef](#)]

**Disclaimer/Publisher's Note:** The statements, opinions and data contained in all publications are solely those of the individual author(s) and contributor(s) and not of MDPI and/or the editor(s). MDPI and/or the editor(s) disclaim responsibility for any injury to people or property resulting from any ideas, methods, instructions or products referred to in the content.

## Highlights:

- Sphingolipidoses arise from inborn errors of genes that encode for sphingolipid metabolism. They represent a subgroup of lysosomal storage diseases characterized by the gradual lysosomal accumulation of the substrate of the defective protein.
- The incidence of sphingolipidoses is approximately 1 in 20.000 newborns. The clinical presentation is quite diverse ranging from a mild progression for some juvenile or adult-onset forms to severe and fatal infantile forms.
- Given the complexities resulting from alterations of sphingolipid metabolism, much is still needed at the basic, clinical, and translational levels to improve patient outcomes.
- Lipidomic analyses have revealed the presence in zebrafish of all the principal lipid classes present in mammals, supporting the possibility to model lipidic metabolism diseases in this animal model.

## Take home message:

The “zebra-sphinx” system represents an innovative and informative tool to acquire knowledge about the biology of sphingolipid metabolism for a better comprehension of the pathological processes contributing to sphingolipid disorders, thus enabling the development of novel potential therapies and their translation to patients.

## 1.2 The important balance between ceramide and sphingomyelin

SM is one of the main components of plasma membrane, endocytic recycling compartment and the *trans* Golgi. SM is present also in the nucleus where, together with cholesterol (CHOL), is associated to proteins in the chromatin structure (Albi et al. 1994). In addition, mitochondrial SM has been proposed to participate in initiation of apoptosis via Cer generation (Dai et al. 2004).

The SMS enzyme exerts its activity mainly in the luminal *trans* Golgi and plasma membrane, resulting in SM enrichment in the membranes of the endosomal recycling compartment (Devaux and Morris 2004).

In plasma membrane, SM is biochemically more stable than most phospholipids and its melting point above 37°C consolidates membrane order. Moreover, SM is often the only fully saturated

phospholipid and for this reason CHOL is more prone to bind SM, creating SM-CHOL enriched domains (Goñi 2022). The interaction between SM and CHOL can affect CHOL homeostasis. For example, addition of SM to cells increases CHOL biosynthesis (Gatt and Bierman 1980). Conversely, enhanced SM degradation leads to free CHOL that it is transported to ER and inhibits its synthesis (Slotte et al. 1990). In addition, SM-CHOL enriched membrane domains specifically accommodate several transmembrane proteins and are crucial structural components of caveolae (Slotte 2013).

Through the degradation pathway, SM is metabolized in Cer that, beside playing a structural role in the cell membranes, may mediate several cell responses, such as regulation of apoptosis, differentiation, senescence, and cell-cycle arrest (Morad and Cabot 2013). Of note, the length of the acyl chain is critical to address different Cer molecules towards a particular signaling pathway. The “many ceramides” hypothesis postulates that each structural change in Cer leads to specific sphingolipid derivatives with distinct subcellular localization and function (Hannun and Obeid 2011).

As described above, aSMase catabolizes the reaction inside the lysosome, and it has been reported to be activated by various cellular stressors to promote Cer formation. Furthermore, the levels of its secreted form are increased in mouse and human serum in response to pro-inflammatory cytokines (Jenkins et al. 2011). Accordingly, various stimuli, such as TNF- $\alpha$ , PMA, H<sub>2</sub>O<sub>2</sub>, and cell confluence, may increase nSMase2 activity and induce its translocation from the Golgi to the plasma membrane (Airola and Hannun 2013). In addition, nSMase2 can induce cell growth arrest *via* p53 following DNA damage (Shamseddine et al. 2015b).

### 1.2.1 Structure of neutral sphingomyelinase 2

nSMase2 (E.C.3.1.4.12) is a Mg<sup>2+</sup>-dependent phosphodiesterase that catalyzes the hydrolytic cleavage of SM to Cer and phosphocholine at a neutral pH (Marchesini et al. 2003).

nSMase2 is encoded by the *SMPD3* gene that maps on chromosome 16 and consists of 13 exons. Both the human and murine nSMase2 are 655 amino acid long, resulting in a molecular mass of 71 kDa. The structure of the human protein has been resolved in 2017 (fig. 1.3) (Airola et al. 2017). The N-terminal domain contains two helical hydrophobic segments that anchor the protein in the membrane. This region acts as allosteric activator and binds the lipid activator phosphatidylserine which is necessary for full nSMase2 activity. The activity of nSMase2 is also mediated by the DK switch domain that consists in an extended loop adopting several conformations obstructing or unleashing the hydrophobic groove. The C-terminal catalytic

domain originates a DNase-I-type fold with a  $\beta$ -sandwich core and connecting loops and secondary structure elements forming the active pocket. This site contains all the residues predicted to bind the phosphodiester group of SM that is stabilized by  $Mg^{2+}$ . The remaining portion forms two  $\beta$ -strands on the periphery of the site: one of them contains the binding motif for the calmodulin-activated phosphatase calcineurin, important for nSMase2 regulation (Filosto et al. 2010, Airola et al. 2017). In addition to calcineurin regulation, nSMase2 is modulated by phosphorylation of five conserved serine residues (Filosto et al. 2012). Finally, the catalytic region of nSMase2 harbors two palmitoylation sites that contribute to nSMase2 membrane association and stability (Airola and Hannun 2013).

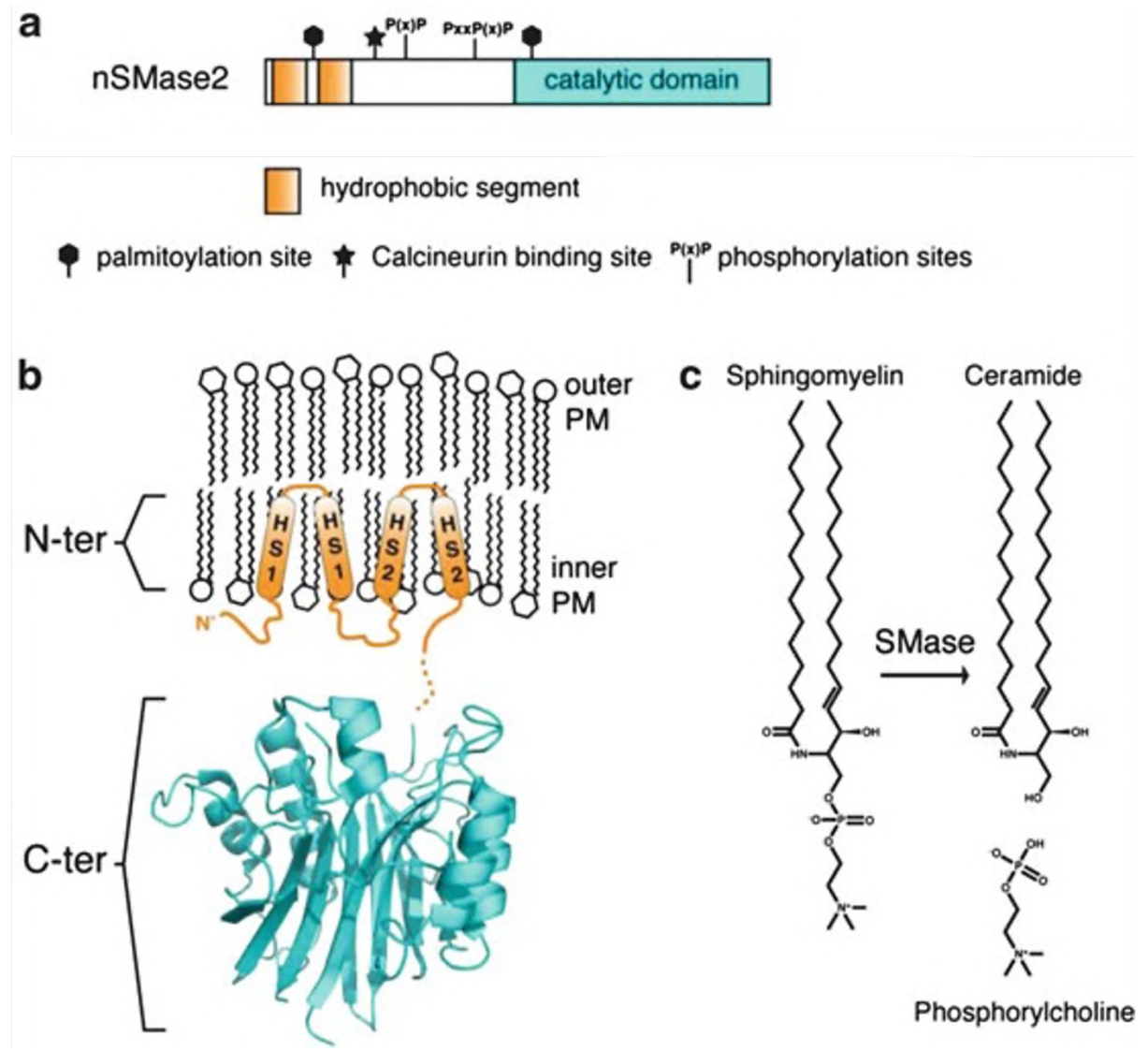


Figure 1.3 A) Domain architecture and topology of nSMase2. B) Overview of nSMase2 structure and localization in the cell membrane: the N-terminal domains, in orange, associate to the membrane whereas the catalytic C-terminal site, in blue, localizes in the cytoplasm. c) nSMase2 catalyzes the hydrolysis of SM to generate Cer and phosphocholine. Modified from (Airola and Hannun 2013)

### 1.2.2 Role of nSMase2 in cellular signalling

As reviewed in (Airola and Hannun 2013), the modulation of nSMase2 activity in response to various cellular stresses and cytokines, including TNF- $\alpha$  IL-1 $\beta$  and IFN- $\gamma$  (Shamseddine, Airola and Hannun 2015a), may affect several biological processes in physiological and pathological conditions.

Activation by TNF- $\alpha$  is currently the best-studied pathway. Decreased amounts of glutathione (Liu et al. 1998), as well as phosphorylation by p38 mitogen-activated protein kinase (MAPK) and Protein Kinase C delta are critical for TNF- $\alpha$ -induced activation of nSMase2, leading to a rapid SM hydrolysis (Clarke, Truong and Hannun 2007, Clarke, Guthrie and Hannun 2008).

The involvement of nSMase2 in pathology and in neuropathology is well established. For example, nSMase2-derived Cer mediates apoptosis after lung and cardiac insults. At the same time, overexpression of nSMase2 is associated with hypertension (Airola and Hannun 2013, Chaube et al. 2012). Recently, the role of nSMase2 in Alzheimer's disease has been investigated. Chronic increase of brain nSMase2 activity and related exosome release causes accumulation of amyloid- $\beta$  and treatment with nSMase2 inhibitors has been proposed as therapy for Alzheimer's disease (Tohumeken et al. 2023, Šála et al. 2020)

Despite the great interest in nSMase2 there is a lack of lipidomic studies. How *SMPD3* overexpression may modulate melanoma progression and lipidic profile will be cover later in this thesis.

### 1.2.3 Biology of $\beta$ -galactosylceramidase

$\beta$ -galactosylceramidase (GALC; EC 3.2.1.46) is a lysosomal hydrolase responsible for the catabolism of several  $\beta$ -galactosphingolipids (Won, Singh and Singh 2016) including GalCer, one of the main component of myelin (Luzi, Rafi and Wenger 1995).

In humans, the *GALC* gene maps on chromosome 14 and consists of 17 exons ranging from 39 to 181 nucleotides that encode for a 685 amino acid protein. More than 70 mutations in *GALC* are associated with globoid cell leukodystrophy (GLD), a sever neurodegenerative disease also named Krabbe disease (Deane et al. 2011).

GALC is highly conserved: the murine ortholog retains 83% homology with the human counterpart (Deane et al. 2011) and the two co-orthologs zebrafish *galca* and *galb* share the same 17 exons/16 introns structure of human and murine genes and display 61% homology with human *GALC* (Zizioli et al. 2014).

GALC is a 80 kDa protein translated in the ER and N-glycosylated at specific asparagine residues in the ER/trans-Golgi network (Nagano et al. 1998). The addition of a mannose 6-phosphate (M6P) moiety allows the binding of GALC to M6P receptors (M6PRs) and its transport *via* the M6P pathway. M6P-tagged GALC is transferred to the late endosome compartment where it is released by the receptor and delivered to the lysosome. Once in the lysosome, GALC is cleaved in two 50 and 30 kDa fragments (Nagano et al. 1998). The presence of both subunits and the binding to the saposin-A (SapA) co-factor are essential for its enzymatic activity in the lysosome (Nagano et al. 1998, Hill et al. 2018). However, GALC may follow an alternative secretory pathway and be released in the extracellular environment (Nagano et al. 1998).

3D structure analyses of murine GALC protein revealed three domains: a central TIM barrel, a  $\beta$ -sandwich, and a unique lectin domain not observed in other hydrolases. The central TIM barrel is composed of eight parallel  $\beta$ -strands surrounded by  $\alpha$ -helices (fig 1.4) and it allocates the core of the catalytic site (Deane et al. 2011). The hydroxyl groups of galactose make multiple specific contacts with the enzyme, however there is no conformational change, suggesting that the catalytic site is highly preorganized (Hill et al. 2018). A specific hydrogen bond between one of the hydroxyl groups of galactose and the residue T93 allows the enzyme to distinguish galactose from glucose. Moreover, the active pocket accommodates only the sugar group and does not have space for the lipid tails.

The presence of the lectin domain is atypical. It is a carbohydrate recognition domain, not observed in other hydrolases. This region may involve binding of glycosylated proteins during the translation and maturation process and it might provide an additional uptake mechanism

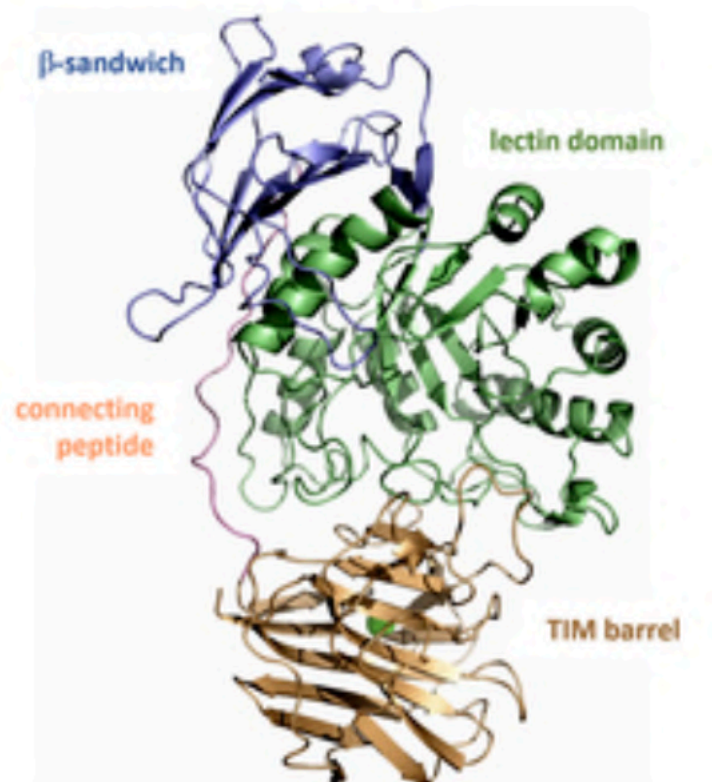


Figure 1.4 Ribbon diagram colored by protein domain showing the overall structure of murine GALC. TIM barrel (brown),  $\beta$ -sandwich (blue), lectin domain (green). (Belleri et al. 2022)



(Deane et al. 2011). Although the catalytic site lies in the C-terminal face of the TIM barrel, loops from both the  $\beta$ -sandwich and lectin domains contribute to the formation of the active pocket. Finally, X-ray crystallography demonstrates that the non-enzymatic sphingolipid activator protein saposin-A forms a 2:2 heterotetramer with GALC. SapA-GALC complex creates a hydrophobic cavity that accommodates the polar headgroup of galactosphingolipids but not their tails, further explaining how this hydrolase can cleave the sugar moiety from Cer (Hill et al. 2018).

#### **1.2.4 GALC as a key player in the sphingolipid homeostasis**

As mentioned above, GALC removes  $\beta$ -galactose from galactosylsphingolipids, mainly from GalcCer. Further GALC substrates are psychosine (or  $\beta$ -galactosyl-sphingosine), lactosylceramide and the seminolipid precursor galactosyl-alkyl-acyl-glycerol. GLD is caused by inborn genetic errors in *GALC* that lead to accumulation of the neurotoxic metabolite psychosine, followed by degeneration of oligodendroglia and progressive demyelination. Sphingolipidome analysis suggests that, beside psychosine, other sphingolipids are modified in *twitcher* mice, an authentic model of GLD. For example, in their central nervous system the levels of psychosine, C16:0 Cer and C18:0 GalcCer were increased compared to wild-type animals, whereas S1P and long chain Cer (C18:0, C22:0, C24:0) were reduced. Saturated long chain GalCers were similar between *twitcher* and control mice, conversely there was a trend toward decreased levels of C24:1 GalCer (Esch et al. 2003). Analysis on fatty acid chain further confirmed this tendency (Zanfini et al. 2014). Finally in murine hematopoietic stem cells, downregulation of *Galc* results in decrease levels of Cer and Sph, whereas its upregulation causes a significant increase of these sphingolipids and S1P, in the absence of significant changes in the intracellular levels of psychosine, SM, and sulphatides (Visigalli et al. 2010). Remarkably, downregulation of *GALC* also impacts phospholipid and CHOL, as demonstrated by two independent studies. Weinstock et al. performed a metabolomic analyses on *twitcher* mice brain revealing that phospholipids and CHOL precursors are reduced (Weinstock et al. 2016). More recently, Belleri et al, downregulated *Galc* in murine melanoma B16F10 cells. Surprisingly, a significant increase of intracellular Cer mirrored by a decrease of SM was observed. This occurred together with a significant reduction of phosphatidylethanolamines and cholesteryl esters, accompanied by an increased concentration of diacylglycerols (Belleri et al. 2020).

Further studies are needed to fully understand the role of GALC in sphingolipid metabolism. Here I include an example of the use of a GALC inhibitor to study the effect of GALC modulation on the lipid profile in zebrafish.

### **1.2.5 Impact of an irreversible $\beta$ -galactosylceramidase inhibitor on the lipid profile of zebrafish embryos**

The sphingolipidosis Krabbe disease is characterized by the genetic deficiency of the acid hydrolase GALC. The majority of the studies elucidating the biological role of GALC performed on Krabbe patients and *twitcher* mice reveals that the pathogenesis of this disorder is the consequence of the accumulation of the neurotoxic GALC substrate psychosine (Li et al. 2019). Despite this, there is little information available about how GALC downregulation affects the cell lipidome in adult and developing organisms (Martin et al. 1981, Suchlandt, Schlote and Harzer 1982).

The teleost zebrafish has emerged as a useful platform for lipidomic studies. This animal can be used to model genetic disorders of lipid metabolism, including sphingolipidoses, due to the high genome conservation between humans and zebrafish, the presence of the main mammalian lipid classes and the use of lipid databases for data processing (Mignani et al. 2023). Indeed, two *GALC* co-orthologs have been identified in zebrafish that share a high identity with their human counterpart and are co-expressed in the central nervous system during embryonic development (Zizioli et al. 2014). On this basis, in the following article we have investigated the effect of the competitive and irreversible GALC-inhibitor Gal-cyclophellitol (GCP) (Marques et al. 2017) on the lipid profile in zebrafish embryos. Docking and molecular dynamics simulation show the ability of GCP to compete with the natural product  $\beta$ -D-galactose for the binding to the catalytic residues of human GALC and zebrafish Galca and Galcb proteins. In *in vitro* and *in vivo* experiments, GCP binds and inhibits  $\beta$ -galactosylceramide activity of zebrafish resulting in significant changes in lipid profile of zebrafish embryos.

The results indicate for the first time that GALC may be more than a psychosine “scavenger” since the lack of GALC activity deeply affects the lipidome of developing zebrafish embryos.

## Impact of an irreversible $\beta$ -galactosylceramide inhibitor on the lipid profile of zebrafish embryos

Jessica Guerra<sup>1,7</sup>, Mirella Belleri<sup>1,7</sup>, Giulia Paiardi<sup>1,2,7</sup>, Chiara Tobia<sup>1</sup>, Davide Capoferri<sup>1</sup>, Luca Mignani<sup>1</sup>, Marzia Corli<sup>1</sup>, Elisa Scalvini<sup>1</sup>, Marco Ghirimoldi<sup>3,4</sup>, Marcello Manfredi<sup>3,4</sup>, Rebecca Wade<sup>2,5</sup>, and Marco Presta<sup>1,6</sup>

<sup>1</sup> *Department of Molecular and Translational Medicine, University of Brescia, Brescia, Italy.*

<sup>2</sup> *Molecular and Cellular Modeling Group, Heidelberg Institute for Theoretical Studies, Heidelberg, Germany.*

<sup>3</sup> *Department of Translational Medicine, University of Piemonte Orientale, Novara, Italy.*

<sup>4</sup> *Center for Allergic and Autoimmune Diseases, University of Piemonte Orientale, Novara, Italy.*

<sup>5</sup> *Zentrum für Molekulare Biologie, DKFZ-ZMBH Alliance, Heidelberg University, Heidelberg, Germany.*

<sup>6</sup> *Consorzio Interuniversitario Biotecnologie (CIB), Unit of Brescia, Italy.*

<sup>7</sup> *These authors contributed equally to this work.*

**Short title:** GALC inhibition in zebrafish embryo

**Funding sources:** This work was supported by “Associazione Italiana per la Ricerca sul Cancro” [AIRC IG 23116 to M.P] and by NextGenerationEU [PNRR M4C2-Investimento 1.4- CN00000041]. J.G. is supported by an AIRC fellowship [ID 26633]. M.M. is supported by the AGING Project – Department of Excellence – DIMET, Università del Piemonte Orientale. G.P. and R.C.W. thanks the Klaus Tschira Foundation. G.P was supported by a Joachim Herz Foundation Fellowship and by the Artificial Intelligence Health Innovation Cluster. This publication was supported through state funds approved by the State Parliament of Baden-Württemberg for the Innovation Campus Health + Life Science Alliance Heidelberg Mannheim.

### Abbreviations

GCP,  $\beta$ -galactose-cyclophellitol;  $\beta$ -D-galactose,  $\beta$ -D-Gal; hpf, hours post fertilization; LRh-6-GalCer, lissamine-rhodaminyl-6-aminohexanoyl-galactosylceramide; MD, molecular dynamics; psychosine,  $\beta$ -galactosylsphingosine; RMSD, root-mean-square deviation.

## Abstract

Krabbe disease is a sphingolipidosis characterized by the genetic deficiency of the acid hydrolase  $\beta$ -galactosylceramidase (GALC). Most of the studies concerning the biological role of GALC performed on Krabbe patients and *Galc*-deficient *twitcher* mice (an authentic animal model of the disease) indicate that the pathogenesis of this disorder is the consequence of the accumulation of the neurotoxic GALC substrate  $\beta$ -galactosylsphingosine (psychosine), ignoring the possibility that this enzyme may exert a wider biological impact. Indeed, limited information is available about the effect of GALC downregulation on cell lipidome in adult and developing organisms. The teleost zebrafish (*Danio rerio*) has emerged as a useful platform to model human genetic diseases, including sphingolipidoses, and two *GALC* co-orthologs have been identified in zebrafish (*galca* and *galcb*). Here, we have investigated the effect of the competitive and irreversible GALC inhibitor  $\beta$ -galactose-cyclophellitol (GCP) on the lipid profile of zebrafish embryos. Molecular modelling indicates that GCP can be sequestered in the catalytic site of the enzyme and covalently binds human GALC, zebrafish Galca, and Galcb proteins in a similar manner. Accordingly, GCP inhibits the  $\beta$ -galactosylceramide hydrolase activity of zebrafish *in vitro* and *in vivo*, leading to significant alterations of the lipidome of zebrafish embryos. These results demonstrate for the first time that the lack of GALC activity may deeply affect the lipidome during the early stages of embryonic development, providing further insights about the pathogenesis of Krabbe disease.

**Keywords:** lipidomics, galactosylceramidase, Krabbe disease, molecular modeling, zebrafish.

## INTRODUCTION

Krabbe disease, also known as globoid cell leukodystrophy (OMIM #245200), is an autosomal recessive sphingolipidosis characterized by the deficiency of the acid hydrolase  $\beta$ -galactosylceramidase (GALC) encoded by the *GALC* gene. GALC catalyzes the removal of  $\beta$ -galactose from  $\beta$ -galactosylceramide, a major component of myelin, and other terminal  $\beta$ -Gal-containing sphingolipids (1). The early infantile form of the disease is characterized by fast progression and early death; the symptoms include irritability, regression of psychomotor development, feeding difficulties, followed by hypertonicity, seizures, and loss of vision and hearing (2). The standard of care of Krabbe disease is hematopoietic stem cell transplantation that improves the lifespan of Krabbe patients only when performed before symptoms outbreak (3).

Based on a long-held and recently confirmed “psychosine hypothesis” (4), Krabbe disease may manifest because of the accumulation of the neurotoxic GALC substrate  $\beta$ -galactosylsphingosine (psychosine) in the central and peripheral nervous system, leading to neuroinflammation, degeneration of oligodendroglia, and progressive demyelination (5). In this frame, most of the studies concerning the biological role of GALC performed on Krabbe patients and *Galc*-deficient *twitcher* mice (an authentic animal model of the disease (6), have led to the envision that the major biological function of GALC may consist in its psychosine “scavenging” activity, neglecting the possibility that this enzyme may exert a wider biological impact.

The teleost zebrafish (*Danio rerio*) has emerged as a useful platform to model human genetic diseases due to the high grade of genome conservation between human and zebrafish. In addition, lipidomic studies have allowed the identification in zebrafish of all the main classes of lipids present in mammals, supporting the possibility to model diseases of the lipidic metabolism in this animal species, including sphingolipidoses, using mammalian lipid databases for data processing (7).

Two *GALC* co-orthologs have been identified in zebrafish (*galca* and *galcb*) that share a high identity with their human counterpart and are co-expressed in the central nervous system during embryonic development (8). Double *galca/galcb* knockdown by oligonucleotide morpholino injection caused alterations of the central nervous system in the absence of a significant accumulation of psychosine, suggesting that *GALC* loss-of-function may have pathological consequences during early developmental processes independent of psychosine accumulation (8). Indeed, alterations of the myelinated regions of the spinal cord, brain stem, and peripheral nerves have been reported in 20-23-week-old Krabbe fetuses analyzed after therapeutic abortion, before a significant accumulation of psychosine may occur (9, 10). However, at present no data are available about the impact of *GALC* deficiency on the lipidome of developing organisms.

In contrast to the murine models of Krabbe disease, in which the intrauterine gestation makes it difficult to follow possible alterations in early developmental processes, zebrafish has significant advantages over mice in producing hundreds of externally fertilized eggs that develop *in vitro* as optically transparent embryos. This makes zebrafish particularly suitable for studying the effects of *GALC* deficiency on the lipid landscape during embryonic development. On this basis, in the present paper we have investigated the effect of the competitive and irreversible activity-based *GALC* inhibitor Gal-cyclophellitol (GCP) (11) on the lipid profile of zebrafish embryos. Docking and molecular dynamics (MD) simulations show the ability of GCP to compete with the natural product  $\beta$ -D-galactose ( $\beta$ -D-Gal) for the binding to the catalytic residues of zebrafish *Galca* and *Galcb* proteins. Accordingly, GCP inhibits the  $\beta$ -galactosylceramide hydrolase activity of zebrafish *in vitro* and *in vivo*, leading to significant alterations of the lipid profile of zebrafish embryos.

These results demonstrate for the first time that the lack of *GALC* activity deeply affects the lipidome during the early stages of embryonic development, providing further insights about the pathogenesis of Krabbe disease and setting the bases for a better comprehension of the alterations of the central and peripheral nervous system observed human Krabbe fetuses.

## **MATERIALS AND METHODS**

### **Molecular docking studies**

Human *GALC* (h*GALC*) protein (Uniprot P54803) was modelled on the Swiss-Model website (<https://swissmodel.expasy.org/>) (12) based on the *GALC* mouse structure determined by x-ray diffraction (PDBid: 4CCE; sequence identity 82.6%) (13). Similarly, the initial models of the zebrafish *Galca* (Uniprot Q5SNX7) and *Galcb* (Uniprot Q7ZUD5) proteins were modelled on the Swiss-Model website based on the murine *GALC*/saposin-A crystal structure (PDBid: 5NXB; sequence identity 64.48% and 64.99%,

respectively) (14). The high sequence identity and the conservation of the catalytic sites enabled the generation of high-quality models as evaluated by the MolProbity tool (15). The protein structures were then prepared using the Protein Preparation Wizard in Maestro (Schödinger Release 2019-1) (16) and protonated at pH 4.4 using PROPKA. Prior to docking calculation,  $\beta$ -D-Gal and GCP were prepared with LigPrep (16) and ionized at pH 4.4 using Epik (17). Flexible non-covalent docking (hereafter referred to as flexible docking) studies were performed with Glide 4.8 (16) in Standard Precision mode with default parameters at pH 4.4. The grid box was centered on the active site pockets: G63, T109, N197, E198, E274, W307, Y319, and W541 for human GALC (UniProt P54803); G41, T87, N175, E176, E251, W284, F296, and W517 for zebrafish Galca (Uniprot Q5SNX7); G45, T91, N179, E180, E256, W289, F301, and W521 for zebrafish Galcb (Uniprot Q7ZUD5). Notably, E198 in human GALC, or alternatively E176 and E180 in zebrafish Galca and Galcb respectively, were protonated. Covalent docking studies were performed with Glide.4.8 (16) in covalent docking mode and default parameters at pH 4.4. The grid box was centered as previously described. The reaction type selected is the *epoxide opening* while the reacting residue selected was E274 in human GALC or alternatively E251 and E256 in zebrafish Galca and Galcb respectively (13). Thirty-two poses were collected and ranked according to their Gscore value for all ligands in the flexible or covalent docking procedures. The poses selected for  $\beta$ -D-Gal and GCP in the flexible docking and in the covalent docking were the top-ranked, overlapping with the orientation of the crystal structure with  $\beta$ -D-Gal (PDBid: 4CCE) (13).

### **All-atom Molecular Dynamics (MD) simulation**

The Amber18 package (18) was used to carry out the simulations for the modelled systems starting from the top ranked docking poses. Three replica all-atom MD simulations of 100 ns duration in explicit solvent and 150 mM NaCl salt concentration were run for each system. Parameters for GALC were assigned with the ff14SB force field (19). Ligands were parameterized with GAFF (20) along with AM1-BCC for assigning partial charges (21). The models were placed in a periodic-cubic water box using the TIP3P water model (22) with 10 Å between the solutes and the edges of the box. Na<sup>+</sup> and Cl<sup>-</sup> ions were added to neutralize the systems and to immerse them in solvent with an ionic strength of 150 mM. Each system was energy minimized in 4 consecutive minimization steps, each of 100 steps of steepest descent followed by 900 steps of conjugate gradient, with decreasing positional restraints from 10 to 0 kcal mol<sup>-1</sup> Å<sup>-2</sup> on all the atoms of the systems excluding waters, counterions, and hydrogens, with a cut-off for non-bonded interactions of 8 Å. The systems were then subjected to two consecutive steps of heating, each of 10,000 steps, from 10 to 100 K and from 100 to 310 K in an NVT ensemble with a Langevin thermostat. Bonds involving hydrogen atoms were constrained with the SHAKE algorithm and 2 fs time step was used. The systems were then equilibrated at 310 K for 2.5 ns in the NPT ensemble with a Langevin thermostat with random velocities assigned at the beginning of each step. During the MD simulations, a cutoff of 8 Å for the evaluation of short-range non-bonded interactions was used and the Particle Mesh Ewald method was employed for the long-range electrostatic

interactions. The temperature was kept constant at 310 K with a Langevin thermostat. MD trajectories were analyzed using CPPTRAJ from AmberTools20 (18) and Visual Molecular Dynamics (VMD) (23).

### **Zebrafish maintenance**

Zebrafish embryos were handled according to relevant national and international guidelines. Current Italian rules do not require approval for research on zebrafish embryos. Zebrafish were raised and maintained under standard laboratory conditions as described (24). Briefly, the wildtype AB strain was maintained at 28°C on a 14 h light/10 h dark cycle. Immediately after spawning, the fertilized eggs were harvested, washed, and placed in 10 cm Petri dishes in fish water. The developing embryos were incubated at 28°C and staged as described (25).

### **GALC activity assay**

GALC-mediated hydrolysis of the fluorescent GALC substrate lissamine-rhodaminyl-6-aminohexanoyl-galactosylceramide (LRh-6-GalCer) was quantified by thin-layer chromatography (TLC) (26) following its incubation with 20-50 µg of the extracts of zebrafish embryos or of adult zebrafish or mouse brains. Briefly, 3 nmoles of LRh-6-GalCer in 3:2 chloroform/methanol were concentrated and dissolved in 5 µl of DMSO and 25 µl of 0.2 M citrate phosphate buffer, pH 4.4. The enzyme source and water were added to a final volume of 100 µl and incubated overnight at 37°C. The reaction was extracted with 1.9 ml of 3:2 v/v chloroform/methanol and 0.4 ml of water. The lower phase was collected and evaporated under nitrogen. Samples were spotted on glass-coated silica gel plates and developed in 25:25:25:9:16 volumes chloroform:ethyl acetate:*n*-propanol:0.25 M KCl:methanol. The fluorescent ceramide spots (LRh-6-Cer) were visualized under an ultraviolet lamp and photographed. Next, the bands corresponding to the enzyme product were extracted in 6:4 volumes chloroform:methanol and fluorescence of the solubilized product was measured at the spectrofluorometer (Excitation: 565 nm; Emission: 575 nm).

### **LC-MS lipidomic analysis of zebrafish embryos**

Zebrafish embryos at 1-2 cell stage were injected with GCP (160 pmoles/embryo) or vehicle (4 nanoliters of 10% DMSO in water). At 96 hours post-fertilization (hpf), embryos were harvested and grouped in 3 pools of GCP or vehicle treated animals, each formed by 4-8 embryos. Next, pools were processed for GALC activity assay and lipidomic analysis. Lipids were extracted using two different cold organic solvents. Embryos were sonicated, and 5 µl of a methanol mix of deuterated standards (Splash Lipidomix®) was added. Then, 225 µl of cold methanol were added and the sample was vortexed for 10 s, followed by the addition of 750 µl of cold MTBE and vortexed for 10 s. The samples were then shaken at 4 °C for 6 min at 2000 rpm and 100 µl of water were added and vortexed. After 2 min of centrifugation at 14,000 rpm and 4 °C, 500 µl of supernatant were collected and evaporated using a SpeedVac. The dried sample was reconstituted with 50 µl of a solution MeOH/toluene 9:1 (v/v) containing the internal standard CUDA (12.5 ng/ml). For the lipidomic analysis a UHPLC Vanquish system (Thermo Scientific, Rodano, Italy) coupled with an Orbitrap Q-Exactive

Plus (Thermo Scientific, Rodano, Italy) was used. A reverse phase column was used for the separation of lipids (Hypersil Gold™ 150 x 2.1 mm, particle size 1.9 µm). Mass spectrometry analysis was performed in both positive and negative ion modes. The source voltage was maintained at 3.5 kV in the positive ion mode and 2.8 kV in the negative ion mode. All other interface settings were identical for the two types of analysis. The injection volume was 3 µl. Lockmass and regular inter-run calibrations were used for accurate mass-based analysis. An exclusion list for background ions was generated by analyzing the same procedural blank sample, for both the positive and negative ESI modes. More details on the chromatographic and mass spectrometry conditions can be found here (27). To ensure good reproducibility during the analysis, different quality control procedures were adopted: a quality control sample, represented by a pool of all the samples, was analyzed at the beginning of the batch, after every 5 samples, and at the end of the batch. Internal standards that cover several analyte classes at appropriate levels (Avanti SPLASH Lipidomix), and an internal standard (CUDA) added before the LC-MS analysis were used. Instrument variations were then monitored and corrected ensuring the good reproducibility of all the batches. Raw data acquired from untargeted analysis were processed with MSDIAL software (Yokohama City, Kanagawa, Japan), version 4.24. Peaks were detected, MS<sup>2</sup> data were deconvoluted, compounds were identified, and peaks were aligned across all samples. For quantification, the peak areas for the different molecular species detected were normalized using the deuterated internal standard for each lipid class. To obtain an estimated concentration expressed in nmol/4 embryos, the normalized areas were multiplied by the concentration of the internal standard. An in-house library of standards was also used for lipid identification. MetaboAnalyst 4.0 software ([www.metaboanalyst.org](http://www.metaboanalyst.org)) was used for the statistical analysis.

### **Statistical analysis**

Statistics were performed using Microsoft Excel 365 and Graphpad Prism 8. P-values were calculated by two-tailed uncoupled t-test and P-values  $\leq 0.10$  were considered statistically significant.

## **RESULTS**

### **MD simulations and covalent docking elucidate the activity of the GCP inhibitor on human GALC.**

To investigate the mechanisms exerted by the selective inhibitor GCP, a preliminary set of experiments was performed to model by homology the structure of human GALC (hereinafter named hGALC) on the murine GALC crystal structure (PDBid: 4CCE) (13) using the Swiss-Model webserver (12). The global amino acid sequence identity between the two proteins is 82.6% and the local identity in the catalytic site increases up to 100% (UniProt P54818 and P54803 for murine and human sequences, respectively). The binding mode of the natural product  $\beta$ -D-Gal and of the irreversible inhibitor GCP on hGALC was investigated by performing flexible docking with the Glide docking software [14] at pH 4.4, in keeping with the lysosomal pH [15]. The top-ranked poses for both ligands perfectly overlapped in the binding mode with the crystallographic data for the mouse model. Indeed, the root-mean-square deviation (RMSD) computed



between mouse and human proteins for  $\beta$ -D-Gal was equal to 0 Å and between  $\beta$ -D-Gal and GCP with the human enzyme was equal to 0.5 Å. This indicates that the catalytic pocket is conserved between the murine and human enzymes and points to a similar binding mode for  $\beta$ -D-Gal and GCP.  $\beta$ -D-Gal establishes hydrogen bonds with T109, W151, N197, E198, E274, S277, and R396 residues of human GALC, while GCP interacts with G63, T109, W151, N197, E198, E274, and S277 residues (**Table 1**). The docking scores indicate a slightly better binding affinity for GCP (Gscore= -7.846) when compared to  $\beta$ -D-Gal (Gscore= -7.348).

Molecular dynamics (MD) simulations were then performed to evaluate the stability of the  $\beta$ -D-Gal/hGALC and GCP/hGALC complexes and to confirm the binding pose of the ligands. Both ligands are steadily anchored to the hGALC active site during the simulation, with an average deviation from the starting structure of less than 0.5 Å (**Supplementary Fig. S1**). The orientation of  $\beta$ -D-Gal is maintained *via* hydrogen bonds among the hydroxyl groups of the ligand and the catalytic residues E198 and E274 (proton donor and active site nucleophile, respectively) and the non-catalytic product binding residues T109, W151, N197, S277, and R396, with an occupancy over 90% along all the replicas (**Fig. 1A** and **Table 1**). Simulations confirmed the ability of GCP to establish stable polar contacts with all the catalytic and non-catalytic residues involved in the interaction of  $\beta$ -D-Gal for more than 90% of the replica simulations (**Fig. 1B**). The orientation of GCP is further maintained by interaction with T109 and G64, which confers specificity to the ligand. The only contact not conserved upon GCP engagement is with the R396 residue due to the lower flexibility of the epoxide compared to the hydroxyl groups exposed by the natural product at this interface (**Fig. 1A,B** and **Table 1**). This interaction strongly reflects on the binding free energy equal to  $-46.92 \pm 0.65$  and  $-32.05 \pm 1.59$  kcal/mol for  $\beta$ -D-Gal and GCP, respectively (**Table 2**). The favorable solvation component resulting from the exposure to the solvent of the epoxide of GCP does not compensate the strong electrostatic term derived from the salt bridge established between the hydroxyl group of  $\beta$ -D-Gal and R396 (**Fig.1A,B** and **Table 2**).

To obtain insights into the irreversible binding mode of GCP on GALC, the opening of the oxirane of GCP upon nucleophilic attack was investigated by performing covalent docking with Glide. The top-ranked poses show how the covalent linkage between the C3 of GCP exposed upon opening of the oxirane and the O<sup>e2</sup> atom of nucleophile E274 is unambiguous and only requires a minor conformational change of E274. All the interactions identified with classic docking followed by MD simulations are conserved and further interaction with Y254, Y319, and R396 are established (**Fig. 1C**). Notably, interaction with R396 is important for the binding of  $\beta$ -D-Gal (**Fig. 1A**). The covalent docking score is -8.719. The conservation of the contacts established with GCP prior and upon opening of the oxirane and limited conformational changes on the active site loops indicate that the binding pocket of hGALC is highly preorganized and the flexible docking procedure followed by MD simulation enabled the identification of the orientation of GPC prior the nucleophilic attack.

Overall, our findings suggest that GPC can be accommodated in the catalytic pocket with the closed-epoxide and the subsequent nucleophilic attack exerted by E274 triggers the formation of an irreversible linkage.

## GCP sequesters the pharmacophoric residues within the catalytic pocket of zebrafish GALC orthologues.

The protocol described above was applied to investigate the interaction of  $\beta$ -D-Gal and GCP with the two GALC zebrafish orthologues Galca and Galcb (8). The zebrafish Galca and Galcb were modelled in Swiss-Model based on the x-ray murine GALC/saposin-A crystal structure (PDBid: 5NXB) [16] and the Galca (Uniprot Q5SNX7) and Galcb (Uniprot Q7ZUD5) sequences. Flexible docking was used to set up the systems for both zebrafish orthologues with  $\beta$ -D-Gal or GCP simulated at pH 4.4. The top-ranked poses of  $\beta$ -D-Gal in Galca and Galcb overlap with those of the ligand in the murine GALC crystal structure (RMSD < 0.2 Å) while the two top-ranked poses for GCP are slightly rotated (RMSD < 0.8 Å) although they maintain the interaction with all the key residues within the catalytic pocket. Indeed,  $\beta$ -D-Gal interacts with T87, W129, N175, E176, E251, S254, and R373 residues in Galca and with T91, W133, N179, E180, E256, S259, and R378 residues in Galcb. while GCP establishes contacts with G42, W129, N175, E176, E251, S254, and R373 in Galca and with residues G46, W133, N179, E180, E256, S259, and R378 in Galcb (**Table 1**). As observed for hGALC, docking scores show better binding affinity of GCP for Galca and Galcb (Gscore= -8.069 and -8.063, respectively) when compared to the natural ligand  $\beta$ -D-Gal (Gscore= -7.138 and -7.29).

Multiple replica MD simulations were then performed to evaluate the stability of the systems and to confirm the binding pose of the ligands. In agreement with the docking scores, all ligands in both zebrafish orthologues were stable along the simulations with a deviation from the starting structure of less than 0.5 Å (**Fig. 1D,E,G,H** and **Supplementary Fig. S1**). The orientation of  $\beta$ -D-Gal was maintained *via* hydrogen bonds between the hydroxyl groups of the ligand and Galca or Galcb non catalytic residues (T87, W129, N175, S254, and R373 for Galca; T91, W133, N179, S259, and R378 for Galcb) and with the proton donor and the active site nucleophile (E176 and E251 in Galca; E180 and E256 in Galcb) for more than 90% of all the replicas (**Fig. 1D,G** and **Table 1**). The computed binding free energy values were equal to  $-43.14 \pm 4.28$  and  $-42.11 \pm 3.41$  kcal/mol for  $\beta$ -D-Gal/Galca and  $\beta$ -D-Gal/Galcb, respectively (**Table 2**). As observed for the human model, GCP demonstrates the ability to sequester the catalytic pocket of both zebrafish GALC orthologues maintaining interactions with key residues for more than 90% of the simulations (**Fig. 1D,E** and **Table 1**). In the system with Galca, the orientation of GCP is stabilized by an intricate hydrogen bond network involving the hydroxyl groups of the inhibitor and T87, N175, E176, E251, and R373 residues, *plus* a pi-pi interaction with W284 (**Fig. 1E** and **Table 1**). In the system with Galcb, the orientation of GCP is slightly shifted and the hydrogen bond network involves the hydroxyl groups of the inhibitor and T91, Y236, E256, and R378 residues, *plus* a pi-pi interaction with W289 (**Fig. 1H** and **Table 1**). Remarkably, the salt bridge between the hydroxyl group of the inhibitor and the Galca residue R373 results in a more favorable electrostatic component with an increased binding free energy when compared to the GCP/hGALC complex, with values equal to  $-35.36 \pm 4.46$  kcal/mol (**Table 2**). Conversely, although the correspondent salt bridge is maintained in the GCP/Galcb complex, the loss of other interactions results in a lower binding free energy equal to  $-27.71 \pm 2.19$  kcal/mol (**Table 2**).

Then, covalent docking was performed to investigate the putative formation of an irreversible linkage between GPC and Galca or Galcb upon nucleophilic attack in the catalytic pocket, as seen in hGALC. Top-ranked poses show that, upon nucleophilic attack and oxirane-opening, C4 or C3 of GPC established covalent linkage with the O<sup>e2</sup> atom of E251 in Galca or E256 in Galcb, respectively. In Galca, the orientation of GPC is slightly rotated compared to  $\beta$ -D-Gal, although the inhibitor interacts with all the pharmacophoric residues previously identified and, in addition, with G42 and Y231 (**Figure. 1D,F**). In Galcb, the orientation of GPC perfectly overlaps the binding mode of  $\beta$ -D-Gal, and the irreversible inhibitor interacts with all the pharmacophoric residues of Galcb plus G46 (**Figure. 1G,I**). Covalent docking scores are -7.372 and -8.629 for Galca and Galcb, respectively. In summary, despite the preservation of the catalytic pocket in both Galca and Galcb, differences in their surrounding regions, combined with the rigidity of GPC before the oxirane opening, hindered the precise determination of the GPC orientation that triggers the nucleophilic attack by flexible docking followed by MD simulation. However, the covalent docking results allow the identification of the interactions established by GPC on Galca and Galcb, suggesting the ability of the inhibitor to establish a covalent binding with the zebrafish orthologues in an arrangement corresponding to that seen for hGALC.

### **GCP inhibits GALC activity in zebrafish embryos.**

The *in-silico* data prompted us to assess the capacity of GCP to inhibit GALC activity in zebrafish. In a first set of experiments, the extracts of zebrafish embryos at 96 hpf and of adult zebrafish brain harvested at 3 months of age were incubated with increasing concentrations of GCP. Next, GALC activity was measured by an enzymatic TLC assay using the fluorescent GALC substrate LRh-6-GalCer (26). As shown in **Fig. 2A,B**, GCP inhibits the activity of GALC in both zebrafish extracts in a dose-dependent manner, with a potency similar to that exerted on the GALC activity of a murine brain extract and on the activity of recombinant human GALC transduced in human HEK293 cells.

On this basis, the impact of GCP on GALC activity was assessed *in vivo* in zebrafish embryos. To this aim, zebrafish embryos at 1-2 cell stage were microinjected with GCP (160 pmoles/embryo) or vehicle (10% DMSO in water). The enzymatic TLC assay performed on the whole embryo extracts at 96 hpf confirmed the capacity to GCP to inhibit GALC activity *in vivo* when compared to DMSO-treated embryos (**Fig. 2C**). No significant differences in embryo mortality and macroscopic morphologic alterations were observed between the two experimental groups (data not shown).

### **GCP modulates the lipid profile of zebrafish embryos.**

Untargeted lipidomic analysis was used to assess the effect of GALC inhibition on the lipid composition in 96 hpf embryos microinjected at 1-2 cell stage with 160 pmoles/embryo of GCP or vehicle. The analysis identified 766 lipid species in both experimental groups, representing various classes of lipids, including: bis(monoacylglycerol)phosphate (BMP, 1 species), fatty acids (FA, 8 species), fatty acyl carnitines (CAR, 17 species), N-acyl-ethanolamines (NAE, 9 species), sterols (ST, 3 species), free cholesterol, cholesteryl esters (CE, 2 species), diacylglycerols (DG, 58 species), and triglycerides (TG, 179 species); the sphingolipids

ceramides (Cer, 20 species), sphingomyelins (SM, 52 species), and sphingoid bases (SPB, 1 species); the phospholipids phosphatidylcholines (PC, 193 species), phosphatidylethanolamines (PE, 102 species), phosphatidylglycerols (PG, 2 species), phosphatidylinositols (PI, 39 species), and phosphatidylserines (PS, 24 species); the lysophospholipids lyso-PC (LPC, 27 species), lyso-PE (LPE, 15 species), lyso-PI (LPI, 5 species), and lyso-PS (LPS, 3 species) (**Supplementary Table S1**).

When GCP-treated embryos were compared to vehicle-treated animals, significant differences were observed for the levels of TG and ST classes, as well as for the levels of Cer and SM, all increased in GCP-treated animals with respect to controls, whereas the levels of CE were decreased by GCP. In addition, significant changes were observed for the levels of various classes of phospholipids, that included an increase of the amount PC and LPE, paralleled by a decrease of PI, LPI, LPS, and PI-Cer (**Fig. 3A**). Moreover, analysis of the metabolic pathways affected by GCP treatment using the BioPan platform (29) identified 77 activated and 43 suppressed reactions. Among them, DG→TG and PS→PE→PC→LPC pathways accounted for 68% of the activated reactions (53/77) whereas TG→DG and PE→PS represented 50% of the suppressed reactions (21/43) (**Fig. 3C** and **Supplementary Table S2**).

Analysis of the individual molecular species confirmed the capacity of GCP to modulate the lipid composition of zebrafish embryos. Indeed, among the 766 lipid species identified in the two experimental groups, 186 lipids were present at different levels in GCP-treated embryos when compared to controls (**Fig. 3B** and **Supplementary Table S3**). Many of these lipid species were in the TG and PC classes [74/179 (41%) and 42/193 (22%), respectively] (**Fig. 4A,B**). Among them, BioPan analysis pointed to the activation of the synthesis of TG 62:8, 58:11, and 54:8 species from DG 40:2, 36:5, and 34:3, respectively, whereas the degradation of TG 58:11 and 54:8 to DG 42:11 and 38:8 was suppressed. Similarly, the production of PC 40:2, 38:3, 36:5 and 36:4 species was increased from different substrates whereas the degradation of PC 40:2 and 36:4 to DG 40:2 and LPC 20:4 was suppressed (**Fig 4H**).

Lipid species in classes other than TG and PC were affected as well. Among phospholipid classes other than PC, various PE species (17/102; 16%) were significantly increased, including PE 36:4 (more than two-fold increase), and PE 42:7 *plus* the corresponding LPE 20:1 (both increased by 80%). Accordingly, PE 36:4 conversion from LPC 16:0 was activated in parallel with a suppression of its degradation to LPE 20:4 (**Fig 4C,H**). Conversely, 9 out of 39 PI species (23%) and 3 out of 5 LPI species (60%) were decreased following GCP administration. Among them, the PI 38:4 and 38:3 species were decreased by 70% as a result of an augmented conversion to LPI 18:0 whereas LPI 20:5 and 20:4 species decreased by approximately 50%, LPI 20:4 being converted to PI 40:8 (**Fig. 4D,H**). Similarly, PS 38:6 and 40:7, as well as LPS 16:0, were also decreased by 30 to 50% following their conversion to PC 38:6 and 40:7, respectively, together with a reduction in their synthesis reactions (**Fig. 4E,H**). As for sterols, CE 22:5 and 22:6 were decreased by 40% and 50% respectively, whereas ST 24:1;O2;T and 24:1;O3;T were increased significantly, no changes being observed for free cholesterol (**Fig. 4F**). Finally, among sphingolipids, the levels of 3 out of 20 Cer species were more abundant in GCP-treated embryos, Cer 40:2;20, 37:3;20, and 41:1;20 species being increased by more than 60%, 25%, and 20%, respectively. Similarly, among the 52 detected SM species, the levels of SM 32:1;20,

33:1;20, and 35:1;20 were increased by more than 50% following GCP treatment (**Fig. 4G**). Together, the data indicate that inhibition of GALC activity by GCP exerts a significant impact on the lipid profile of zebrafish embryo.

## DISCUSSION

The  $\beta$ -galactopyranose-configured cyclophellitol-epoxide GCP has been demonstrated to exert a covalent and irreversible inhibition of the enzymatic activity of recombinant and rodent GALC (11). Here, *in-silico* analysis indicates that GCP shares the same pharmacophoric points in hGALC and in the zebrafish orthologues Galca and Galcb, indicating its capacity to exert an inhibitory effect by trapping the catalytic residues of the active site of the zebrafish enzymes. Based on our *in-silico* prediction and on experimental evidence about an irreversible binding of GCP with GALC (11), we demonstrated that once the GCP epoxide is accommodated within the catalytic site of the enzyme, the lysosomal acid environment promotes the protonation of the oxirane while the nucleophile residue within the catalytic pocket (E274, E251, and E256 in hGALC, Galca, and Galcb, respectively) triggers its opening and the formation of a covalent bond (**Figure. 1C,F,I**), thus leading to an irreversible inhibition of human and zebrafish enzymes.

In keeping with this hypothesis, GCP inhibits the GALC activity present in zebrafish embryos and adult brain extracts with a potency similar to that exerted on human and murine GALC. Accordingly, injection of GCP into the zebrafish embryos at 1-2 cell stage leads to a significant inhibition of GALC activity that it is retained for at least 96 hours after injection. Of note, no significant changes in embryo survival and morphology were observed between GCP-treated animals and vehicle-injected control embryos. Previous observations had shown that double *galca/galcb* knockdown by oligonucleotide morpholino injection caused reduction and partial disorganization of the expression of the neuronal marker *neuroD* in the central nervous system of zebrafish morphants (8). Such alterations were not observed in GCP-treated embryos (data not shown) and may represent off-target effects consequent to the double morpholino injection. Further studies will be required to evaluate the consequence of GALC deficiency on the spatial-temporal transcriptome of zebrafish during embryonic development.

Taking advantage of the capacity of GCP to exert a long-lasting inhibition of GALC activity when injected in zebrafish at the 1-2 cell stage, we analyzed the lipid profile of zebrafish embryos at 96 hpf to assess a possible impact of GALC deficiency on the lipidome during the early phases of embryonic development. Indeed, even though scattered evidence indicated that alterations of the central and peripheral nervous system may occur in human Krabbe fetuses (9, 10), no data are available about the effects of the lack of GALC activity on the lipidome of developing organisms.

Untargeted lipidomic analysis identified 766 lipid species in the whole extracts of zebrafish embryos at 96 hpf in both GCP-treated and control animals. Even though embryos still rely on the yolk contents for nutrition at this developmental stage, the lipid content of the yolk sac is remarkably decreased at 96 hpf while

it is increased in the embryo body, lipid metabolism representing a dynamic process that occurs between the two embryonic compartments (30). Thus, the results of our analysis reflect the effect of GCP on the balance between lipid remodeling that occurs in the yolk sac and their metabolism in the embryo proper.

Among the various classes of lipids, GCP treatment caused a significant increase of the levels of TG, possibly because of a reduced lipid remodeling in the yolk sac. This increase was due to an increased amount of 74 out of the 179 TG species identified in zebrafish embryos, indicating a specificity of the effect. As for sterols, while no changes in the levels of free cholesterol were observed between GCP-treated and control animals, the decrease in the levels of the CE species 22:5 and 22:6 resulted in a significant decrease in the total amount of CE following GCP treatment. This observation goes along with the decrease of CE levels that occurs in murine melanoma B16-F10 cells following shRNA mediated *Galc* knockdown (31). In GCP-treated embryos, CE reduction was paralleled by an increase of the levels of the taurine-conjugated bile acids ST 24:1;O2;T and 24:1;O3;T. Maturation of the liver occurs in zebrafish embryos at 72-120 hpf (32). These data suggest that a decrease in GALC activity may affect liver metabolism in zebrafish embryos, in keeping with the alterations observed in the liver of adult GALC-deficient *twitcher* mice, an authentic model of Krabbe disease (33, 34).

Notably, significant changes were observed for the levels of various classes of phospholipids following GCP treatment. They included an increase of PC, PE, and LPE levels, paralleled by a decrease of PI, LPI, LPS, and PI-Cer. As observed for TG changes, the effect of GCP on these phospholipid classes was restricted to defined lipid species, pointing again to a specific effect of GALC inhibition on phospholipid metabolism in zebrafish embryos. In keeping with these observations, a significant reduction of PE was observed in *Galc* knockdown B16 cells (31) and alterations of the phospholipid profile and membrane turnover have been reported in the brain of *twitcher* mice (35) as a possible consequence of the tight crosstalk that occurs between phospholipid and sphingolipid metabolism [reviewed in (36)]. Indeed, significant changes in the levels of Cer and SM were detected in GCP-treated animals. They included Cer 40:2;20, 37:3;20, and 41:1;20, as well as SM 32:1;20, 33:1;20, and 35:1;20, the increased amount of SM reflecting the higher content of its biosynthetic precursors PC and Cer.

The effect of GCP on Cer deserves further discussion. Previous observations had shown that the total levels of Cer are decreased in *Galc* null murine hematopoietic stem cells (37) whereas they are increased in *Galc* knockdown murine melanoma B16 cells (31). On the other hand, a lipidomic approach has shown that the levels of Cer 16:0 were increased in the central nervous system of *twitcher* mice when compared to wildtype animals, whereas the levels of Cer 18:0, 22:0, and 24:0 were reduced, no difference being observed for Cer 24:0 (38). The Cer species affected by GCP in zebrafish belong to both long acyl chain (C18:0) and very long acyl chain (22:0; 23:0, and 24:0) species. Nine highly conserved homologs of the vertebrate *Cer* synthase gene family have been identified in the zebrafish genome (39). Since the six members of the mammalian *Cer* synthase family show substrate preference for different lengths of FA chains (40), it seems possible to hypothesize that GALC deficiency may affect different *Cer* synthases in a context-dependent manner with a consequent impact on different *Cer* species.

GCP is a competitive and irreversible GALC inhibitor with no anti- $\alpha$ -galactosidase nor anti- $\beta$ -glucosidase activity, its selectivity arising from its absolute configuration (11, 41). However, we cannot rule out the possibility that its effect on zebrafish embryo lipidomic may be due, at least in part, on its possible interaction with  $\beta$ -galactosidase(s) distinct from GALC, including acid  $\beta$ -galactosidase (11). Experiments on *galca/galcb* single and double knockout animals will be required to elucidate this point.

In Krabbe patients and *twitcher* mice, the lack of GALC activity is characterized by a progressive increase of the neurotoxic GALC substrate psychosine after birth. Here, the levels of hexosylsphingosines (including psychosine) were below the limits of detection in both control and GCP-treated embryos. These data are in keeping with the lack of psychosine accumulation in double *galca/galcb* zebrafish embryo morphants and human Krabbe fetuses (8-10), possibly as a consequence of the early developmental time at which such analyses were performed.

Thus far, only a limited information is available about the effect of the modulation of GALC activity on the lipidome, mainly obtained by the analysis of tissues harvested from adult *twitcher* mice or genetically modified cell lines [reviewed in (42)]. Our data extend these observations and indicate for the first time that GALC plays a non-redundant role in lipid metabolism also during embryonic development, in line with clinical evidence about alterations of the central and peripheral nervous system of human Krabbe fetuses (9, 10).

## DATA STATEMENT

The data supporting the findings of this study are available from the corresponding author upon reasonable request.

### *Supplemental data*

This article contains supplemental data.

### *Acknowledgements*

The GALC inhibitor GCP was kindly provided by M. Artola and H.S. Overkleeft (Department of Medical Biochemistry, Leiden Institute of Chemistry, Leiden University, Leiden, The Netherlands). This work was supported by Associazione Italiana per la Ricerca sul Cancro (AIRC IG 23116 to M.P.). J.C. is supported by an AIRC fellowship (ID 26633). G.P. and R.C.W. thank the Klaus Tschira Foundation.

### *Author contributions*

Conceptualization, M.P. and J.G.; methodology, J.G. and G.P.; formal analysis, R.C.W.; investigation, J.G., M.B., G.P., C.T., L.M., M.C., E.S. and M.G.; data curation, D.C., M.M. and L.M.; writing—original draft preparation, M.P.; writing—review and editing, M.P.; supervision, M.P.; funding acquisition, M.P.

## References

1. Bradbury, A.M., Bongarzone, E.R., Sands, M.S. (2021) Krabbe disease: New hope for an old disease. *Neurosci Lett.* **752**, 135841
2. Kwon, J.M., Matern, D., Kurtzberg, J., Wrabetz, L., Gelb, M.H., Wenger, D.A., Ficiocioglu, C., Waldman, A.T., Burton, B.K., Hopkins, P.V., Orsini, J.J. (2018) Consensus guidelines for newborn screening, diagnosis and treatment of infantile Krabbe disease. *Orphanet J Rare Dis.* **13**, 30
3. Yoon, I.C., Bascou, N.A., Poe, M.D., Szabolcs, P., Escolar, M.L. (2021) Long-term neurodevelopmental outcomes of hematopoietic stem cell transplantation for late-infantile Krabbe disease. *Blood.* **137**, 1719-1730
4. Li, Y., Xu, Y., Benitez, B.A., Nagree, M.S., Dearborn, J.T., Jiang, X., Guzman, M.A., Woloszynek, J.C., Giaramita, A., Yip, B.K., Elsbernd, J., Babcock, M.C., Lo, M., Fowler, S.C., Wozniak, D.F., Vogler, C.A., Medin, J.A., Crawford, B.E., Sands, M.S. (2019) Genetic ablation of acid ceramidase in Krabbe disease confirms the psychosine hypothesis and identifies a new therapeutic target. *Proc Natl Acad Sci U S A.* **116**, 20097-20103
5. Rafi, M.A. (2022) Krabbe disease: A personal perspective and hypothesis. *Bioimpacts.* **12**, 3-7
6. Suzuki, K., Suzuki, K. (1995) The twitcher mouse: a model for Krabbe disease and for experimental therapies. *Brain Pathol.* **5**, 249-258
7. Mignani, L., Guerra, J., Corli, M., Capoferri, D., Presta, M. (2023) Zebra-Sphinx: Modeling Sphingolipidoses in Zebrafish. *Int J Mol Sci.* **24**, 4747
8. Zizioli, D., Guarienti, M., Tobia, C., Gariano, G., Borsani, G., Bresciani, R., Ronca, R., Giacomuzzi, E., Preti, A., Gaudenzi, G., Belleri, M., Di Salle, E., Fabrias, G., Casas, J., Ribatti, D., Monti, E., Presta, M. (2014) Molecular cloning and knockdown of galactocerebrosidase in zebrafish: new insights into the pathogenesis of Krabbe's disease. *Biochim Biophys Acta.* **1842**, 665-675
9. Suchlandt, G., Schlote, W., Harzer, K. (1982) [Ultrastructural findings in 9 fetuses following prenatal diagnosis of neuropilidoses]. *Arch Psychiatr Nervenkr (1970).* **232**, 407-426
10. Martin, J.J., Leroy, J.G., Ceuterick, C., Libert, J., Dodinval, P., Martin, L. (1981) Fetal Krabbe leukodystrophy. A morphologic study of two cases. *Acta Neuropathol.* **53**, 87-91
11. Marques, A.R., Willems, L.I., Herrera Moro, D., Florea, B.I., Scheij, S., Ottenhoff, R., van Roomen, C.P., Verhoek, M., Nelson, J.K., Kallemeijn, W.W., Biela-Banas, A., Martin, O.R., Cachón-González, M.B., Kim, N.N., Cox, T.M., Boot, R.G., Overkleeft, H.S., Aerts, J.M. (2017) A Specific Activity-Based Probe to Monitor Family GH59 Galactosylceramidase, the Enzyme Deficient in Krabbe Disease. *Chembiochem.* **18**, 402-412
12. Waterhouse, A., Bertoni, M., Bienert, S., Studer, G., Tauriello, G., Gumienny, R., Heer, F.T., de Beer, T.A P., Rempfer, C., Bordoli, L., Lepore, R., Schwede, T. (2018) SWISS-MODEL: homology modelling of protein structures and complexes. *Nucleic Acids Research.* **46**, W296-W303



13. Hill, C.H., Graham, S.C., Read, R.J., Deane, J.E. (2013) Structural snapshots illustrate the catalytic cycle of  $\beta$ -galactocerebrosidase, the defective enzyme in Krabbe disease. *Proc Natl Acad Sci U S A*. **110**, 20479-20484
14. Hill, C.H., Cook, G.M., Spratley, S.J., Fawke, S., Graham, S.C., Deane, J.E. (2018) The mechanism of glycosphingolipid degradation revealed by a GALC-SapA complex structure. *Nat Commun*. **9**, 151
15. Williams, C.J., Headd, J.J., Moriarty, N.W., Prisant, M.G., Videau, L.L., Deis, L.N., Verma, V., Keedy, D.A., Hintze, B.J., Chen, V.B., Jain, S., Lewis, S.M., Arendall III, W.B., Snoeyink, J., Adams, P.D., Lovell, S.C., Richardson, J.S., Richardson, D.C. (2018) MolProbity: More and better reference data for improved all-atom structure validation. *Protein Sci*. **27**, 293-315
16. Sastry, G.M., Adzhigirey, M., Day, T., Annabhimoju, R., Sherman, W. (2013) Protein and ligand preparation: parameters, protocols, and influence on virtual screening enrichments. *J Comput Aided Mol Des*. **27**, 221-234
17. Shelley, J.C., Cholleti, A., Frye, L.L., Greenwood, J.R., Timlin, M.R., Uchimaya, M. (2007) Epik: a software program for pK<sub>a</sub> prediction and protonation state generation for drug-like molecules. *J Comput Aided Mol Des*. **21**, 681-691
18. Case, D.A., Ben-Shalom, I.Y., Brozell, S.R., Cerutti, D.S., Cheatham, T.E.III, Cruzeiro, V.W.D., Darden, T.A., Duke, R.E., Ghoreishi, D., Gilson, M.K., Gohlke, H., Goetz, A.W., Greene, D., Harris, R., Homeyer, N., Huang, Y., Izadi, S., Kovalenko, A., Kurtzman, T., Lee, T.S., LeGrand, S., Li, P., Lin, C., Liu, J., Luchko, T., Luo, R., Mermelstein, D.J., Merz, K.M., Miao, Y., Monard, G., Nguyen, C., Nguyen, H., Omelyan, I., Onufriev, A., Pan, F., Qi, R., Roe, D.R., Roitberg, A., Sagui, C., Schott-Verdugo, S., Shen, J., Simmerling, C.L., Smith, J., SalomonFerrer, R., Swails, J., Walker, R.C., Wang, J., Wei, H., Wolf, R.M., Wu, X., Xiao, L., York D.M. and Kollman P.A. (2018) *AMBER 18*. San Francisco, CA, USA: University of California.
19. Maier, J.A., Martinez, C., Kasavajhala, K., Wickstrom, L., Hauser, K.E., Simmerling, C. (2015) ff14SB: Improving the Accuracy of Protein Side Chain and Backbone Parameters from ff99SB. *J Chem Theory Comput*. **11**, 3696-3713
20. Wang, J., Wolf, R.M., Caldwell, J.W., Kollman, P.A., Case, D.A. (2004) Development and testing of a general amber force field. *J Comput Chem*. **25**, 1157-1174
21. Jakalian, A., Jack, D.B., Bayly, C.I. (2002) Fast, efficient generation of high-quality atomic charges. AM1-BCC model: II. Parameterization and validation. *J Comput Chem*. **23**, 1623-1641
22. Jorgensen, W.L., Chandrasekhar, J., Madura, J.D., Impey, R.W., Klein, M.L. (1983) Comparison of simple potential functions for simulating liquid water. *J Chem Phys*. **79**, 926-935
23. Humphrey, W., Dalke, A., Schulten, K. (1996) VMD: Visual molecular dynamics. *J Mol Graphics*. **14**, 33-38
24. Westerfield, M. (1995) *The Zebrafish Book. A Guide for the Laboratory Use of Zebrafish (Danio rerio)*. 3rd edition ed. University of Oregon Press, Eugene.

25. Kimmel, C.B., Ballard, W.W., Kimmel, S.R., Ullmann, B., Schilling, T.F. (1995) Stages of embryonic development of the zebrafish. *Dev Dyn.* **203**, 253-310
26. Marchesini, S., Preti, A., Aleo, M.F., Casella, A., Dagan, A., Gatt, S. (1990) Synthesis, spectral properties and enzymatic hydrolysis of fluorescent derivatives of cerebroside sulfate containing long-wavelength-emission probes. *Chem Phys Lipids.* **53**, 165-175
27. Consonni, F.M., Durante, B., Manfredi, M., Bleve, A., Pandolfo, C., Garlatti, V., Vanella, V.V., Marengo, E., Barberis, E., Bottazzi, B., Bombace, S., My, I., Condorelli, G., Torri, V., Sica, A. (2023) Immunometabolic interference between cancer and COVID-19. *Front Immunol.* **14**, 1168455
28. Zeng, J., Shirihai, O.S., Grinstaff, M.W. (2020) Modulating lysosomal pH: a molecular and nanoscale materials design perspective. *J Life Sci.* **2**, 25-37
29. Gaud, C., B, C.S., Nguyen, A., Fedorova, M., Ni, Z., O'Donnell, V.B., Wakelam, M.J.O., Andrews, S., Lopez-Clavijo, A.F. (2021) BioPAN: a web-based tool to explore mammalian lipidome metabolic pathways on LIPID MAPS. *F1000Res.* **10**, 4
30. Fraher, D., Sanigorski, A., Mellett, N.A., Meikle, P.J., Sinclair, A.J., Gibert, Y. (2016) Zebrafish Embryonic Lipidomic Analysis Reveals that the Yolk Cell Is Metabolically Active in Processing Lipid. *Cell Rep.* **14**, 1317-1329
31. Belleri, M., Paganini, G., Coltrini, D., Ronca, R., Zizioli, D., Corsini, M., Barbieri, A., Grillo, E., Calza, S., Bresciani, R., Maiorano, E., Mastropasqua, M.G., Annese, T., Giacomini, A., Ribatti, D., Casas, J., Levade, T., Fabrias, G., Presta, M. (2020)  $\beta$ -Galactosylceramidase Promotes Melanoma Growth via Modulation of Ceramide Metabolism. *Cancer Res.* **80**, 5011-5023
32. Cheng, Y.C., Wu, T.S., Huang, Y.T., Chang, Y., Yang, J.J., Yu, F.Y., Liu, B.H. (2021) Aflatoxin B1 interferes with embryonic liver development: Involvement of p53 signaling and apoptosis in zebrafish. *Toxicol.* **458**, 152844
33. Kobayashi, T., Yamanaka, T., Jacobs, J.M., Teixeira, F., Suzuki, K. (1980) The Twitcher mouse: an enzymatically authentic model of human globoid cell leukodystrophy (Krabbe disease). *Brain Res.* **202**, 479-483
34. Contreras, M.A., Haq, E., Uto, T., Singh, I., Singh, A.K. (2008) Psychosine-induced alterations in peroxisomes of twitcher mouse liver. *Arch Biochem Biophys.* **477**, 211-218
35. Weinstock, N.I., Wrabetz, L., Feltri, M.L., Shin, D. (2016) Metabolic profiling reveals biochemical pathways and potential biomarkers associated with the pathogenesis of Krabbe disease. *J Neurosci Res.* **94**, 1094-1107
36. Rodriguez-Cuenca, S., Pellegrinelli, V., Campbell, M., Oresic, M., Vidal-Puig, A. (2017) Sphingolipids and glycerophospholipids - The "ying and yang" of lipotoxicity in metabolic diseases. *Prog Lipid Res.* **66**, 14-29
37. Visigalli, I., Ungari, S., Martino, S., Park, H., Cesani, M., Gentner, B., Sergi Sergi, L., Orlacchio, A., Naldini, L., Biffi, A. (2010) The galactocerebrosidase enzyme contributes to the maintenance of a functional hematopoietic stem cell niche. *Blood.* **116**, 1857-1866

38. Esch, S.W., Williams, T.D., Biswas, S., Chakrabarty, A., LeVine, S.M. (2003) Sphingolipid profile in the CNS of the twitcher (globoid cell leukodystrophy) mouse: a lipidomics approach. *Cell Mol Biol.* **49**, 779-787
39. Brondolin, M., Berger, S., Reinke, M., Tanaka, H., Ohshima, T., Fuß, B., Hoch, M. (2013) Identification and expression analysis of the zebrafish homologs of the ceramide synthase gene family. *Dev Dyn.* **242**, 189-200
40. Ho, Q.W.C., Zheng, X., Ali, Y. (2022) Ceramide Acyl Chain Length and Its Relevance to Intracellular Lipid Regulation. *Int J Mol Sci.* **23**,
41. Schröder, S.P., van de Sande, J.W., Kallemeijn, W.W., Kuo, C.L., Artola, M., van Rooden, E.J., Jiang, J., Beenakker, T.J.M., Florea, B.I., Offen, W.A., Davies, G.J., Minnaard, A.J., Aerts, J., Codée, J.D.C., van der Marel, G.A., Overkleeft, H.S. (2017) Towards broad spectrum activity-based glycosidase probes: synthesis and evaluation of deoxygenated cyclophellitol aziridines. *Chem Commun.* **53**, 12528-12531
42. Belleri, M., Chiodelli, P., Corli, M., Capra, M., Presta, M. (2022) Oncosuppressive and oncogenic activity of the sphingolipid-metabolizing enzyme  $\beta$ -galactosylceramidase. *Biochim Biophys Acta Rev Cancer.* **1877**, 188675

## Legends to Figures.

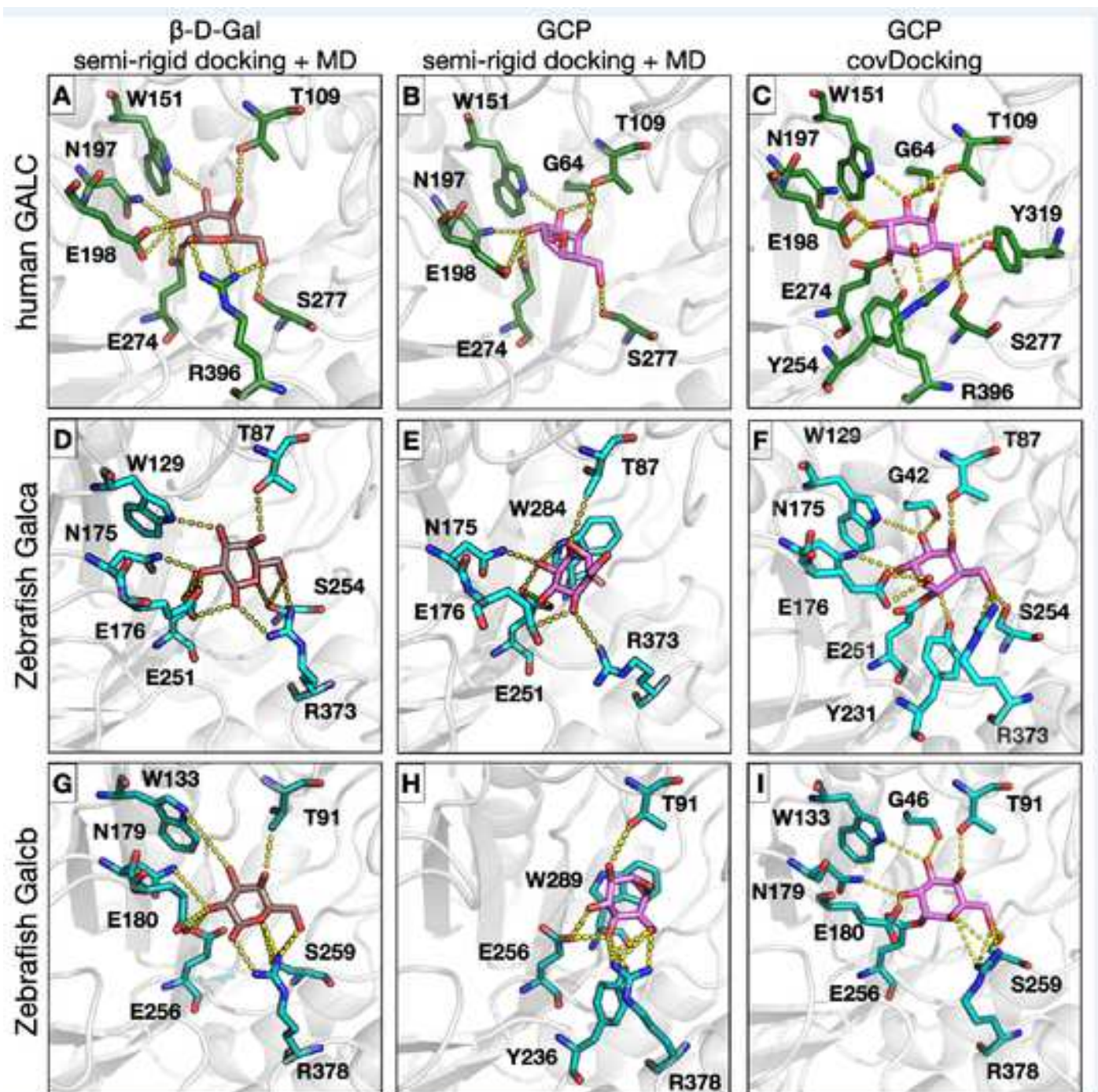
**Figure. 1. Binding modes from molecular docking and molecular dynamics simulations of the interaction of  $\beta$ -D-Gal and GCP with human and zebrafish GALC proteins.** The active site pockets of hGALC (A,B,C), zebrafish Galca (D,E,F), and zebrafish Galcb (G,H,I) proteins are shown with the orientation of  $\beta$ -D-Gal (left panels) and GCP (center panels) obtained after MD simulation and for GCP obtained upon covalent docking (right panels). Proteins are shown in grey cartoon representation while residues involved in the interactions are shown in stick representation colored by element with green, cyan, or turquoise carbons for hGALC, Galca, and Galcb, respectively.  $\beta$ -D-Gal and GCP are shown in stick representation with carbons colored brown or magenta, respectively. H-bond interactions are shown as yellow dashed lines. The covalent bond between the ligand and the protein is shown as extended connection between GCP and the neutrophile residue (E274 for human GALC, E251 or E256 for zebrafish Galca or Galcb, respectively).

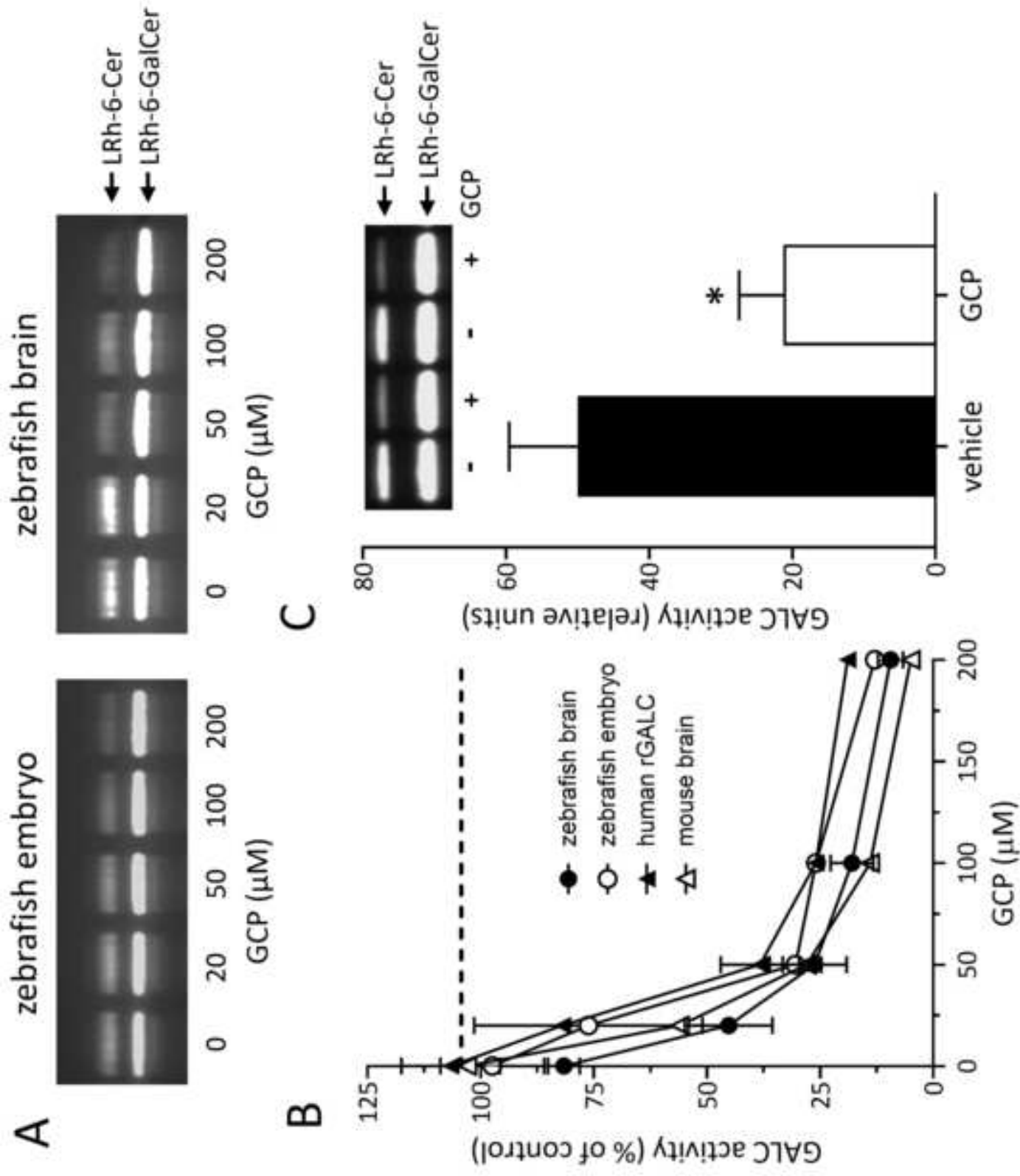
**Figure. 2. Effect of GCP on GALC activity in zebrafish.** A) Extracts of 96 hpf zebrafish embryos (50  $\mu$ g/sample) and of adult zebrafish brain (20  $\mu$ g/sample) were incubated at room temperature with increasing concentrations of GCP in the presence of the GALC substrate LRh-6-GalCer. After overnight incubation, the GALC product LRh-6-Cer was separated from its substrate by TLC, visualized under an ultraviolet lamp, and photographed. B) Extracts of zebrafish embryos, zebrafish and murine adult brains, and recombinant human GALC expressed in HEK 293 cells (rGALC) were incubated with GCP as in A. The GALC product LRh-6-Cer was quantified following its extraction from the silica gel plates. Data are the mean  $\pm$  S.E.M of 3-4 independent experiments. C) Zebrafish embryos at 1-2 cell stage were injected with 160 pmoles of GCP/embryo or vehicle. At 96 hpf, embryos were harvested and grouped in pools of GCP or vehicle-treated animals, each formed by 8 embryos. Next, pools were processed for GALC activity assay as in panel B. Data are the mean  $\pm$  S.E.M of 4 independent experiments. *Inset*: Image of the TLC analysis performed on two pools of vehicle (-) or GCP (+) treated animals.

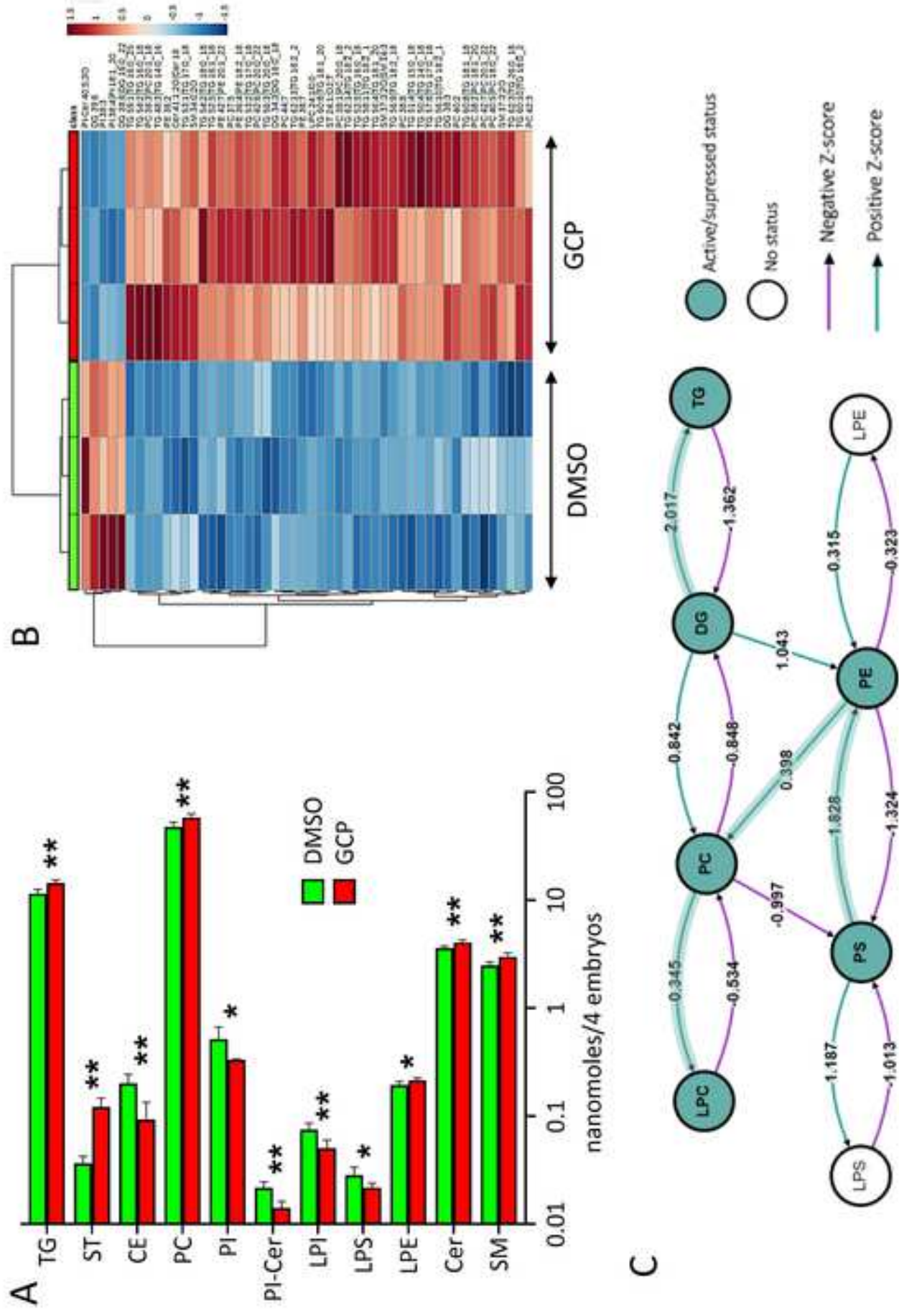
**Figure. 3. Effect of GCP on the lipid profile of zebrafish embryos.** A) Levels of the different classes of lipids detected in DMSO and GCP-treated embryos. Embryos were treated at the 1-2 cell stage and lipid analysis was performed 96 hpf. Data are expressed as nanomoles/pool of 4 embryos. \*,  $P < 0.1$ ; \*\*,  $P < 0.05$ , Student's t test. B) Heatmap showing hierarchical clustering of the lipid species between GCP-treated zebrafish embryos and control animals (DMSO). Only the 50 most important lipid species are displayed based on their t-test p-values. Color coding represents the  $-\log p$ -value. C) Lipid subclass correlation network of GCP-treated embryos compared to controls.

**Figure. 4. GCP affects the levels of various lipid species in zebrafish embryos.** A-G) Levels of the different species of lipids whose amount was significantly affected by GCP treatment when compared to controls. Embryos were treated at the 1-2 cell stage and lipid analysis was performed 96 hpf. Data are expressed as

nanomoles/pool of 4 embryos. H) Z-score representation of the reactions that involve the most GCP-modulated species of lipids following BioPan analysis of lipidomic data. Positive z-score indicates an activated reaction, negative z-score indicates a suppressed reaction.









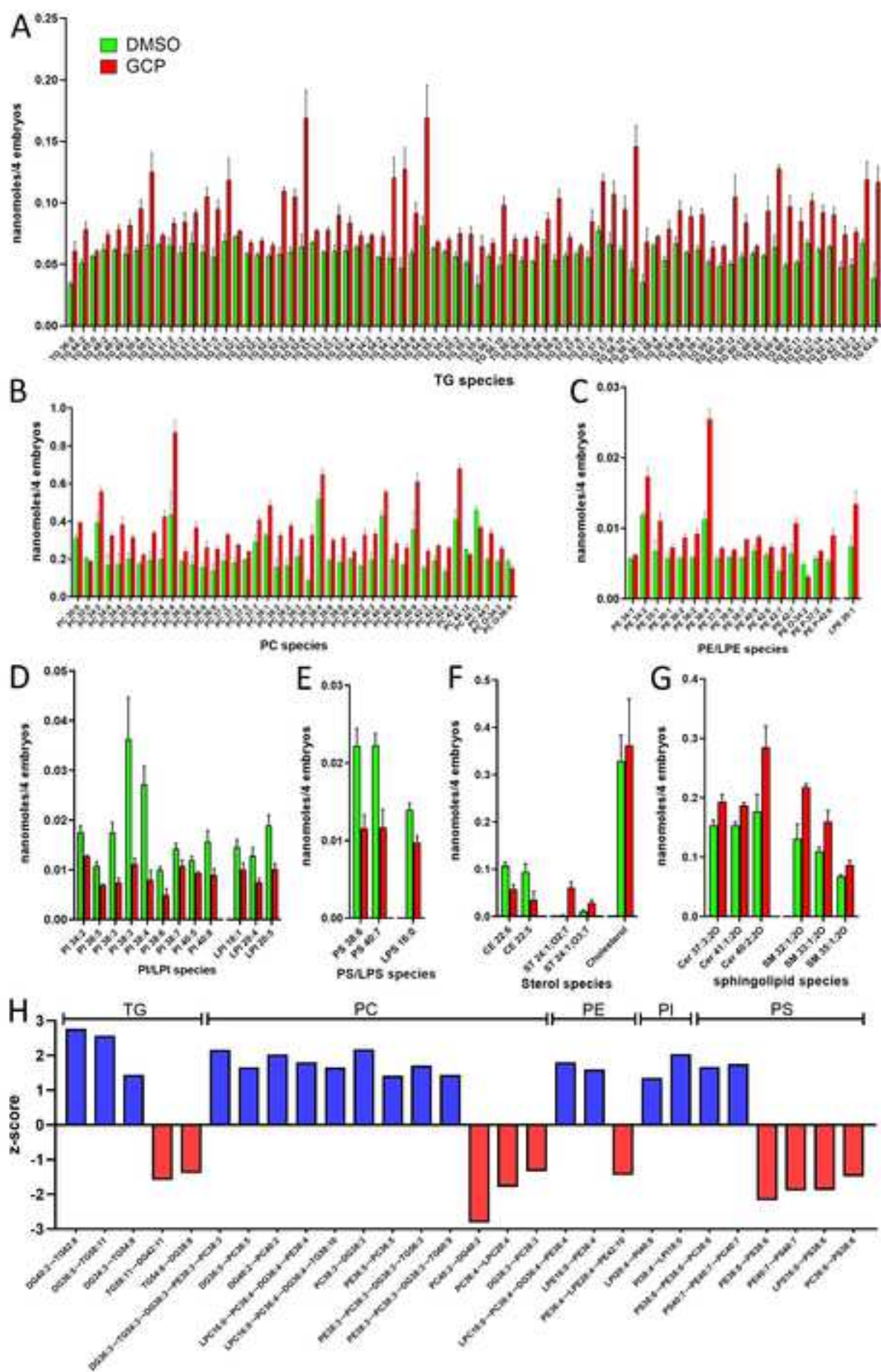


TABLE 2. Computed binding free energy for the human and zebrafish simulated systems <sup>[a]</sup>

Enzyme	Ligand	$\Delta G^{total}$	$\Delta G^{el}$	$\Delta G^{VdW}$	$\Delta G^{solv}$
hGALC	$\beta$ -D-Gal	$-46.92 \pm 0.65$	$-79.58 \pm 0.72$	$-22.20 \pm 0.76$	$54.87 \pm 0.47$
	GCP	$-32.05 \pm 1.59$	$-48.32 \pm 3.65$	$-20.70 \pm 3.52$	$38.51 \pm 2.01$
Zebrafish Galca	$\beta$ -D-Gal	$-43.14 \pm 4.28$	$-85.00 \pm 3.04$	$-18.91 \pm 3.46$	$60.77 \pm 4.63$
	GCP	$-35.36 \pm 4.46$	$-69.61 \pm 3.83$	$-19.31 \pm 3.35$	$53.57 \pm 4.66$
Zebrafish Galcb	$\beta$ -D-Gal	$-42.11 \pm 3.41$	$-79.34 \pm 7.08$	$-18.41 \pm 0.52$	$55.64 \pm 8.67$
	GCP	$-27.71 \pm 2.19$	$-62.99 \pm 4.12$	$-17.50 \pm 1.3$	$52.79 \pm 2.51$

<sup>[a]</sup> Molecular mechanics-generalized Born surface area (MM/GBSA) energies (kcal/mol) and their component computed for  $\beta$ -D-Gal or GCP bound to hGALC, Galca, or Galcb show that the GCP inhibitor accommodates within the catalytic site of the enzyme with energetically favorable interactions that trigger the formation of a covalent bond (see **Fig. 1C,F,I**). The average binding free energy ( $\Delta G^{total}$ ) is computed as the sum of the electrostatic ( $\Delta G^{el}$ ), Van der Waals ( $\Delta G^{VdW}$ ) and solvation-free ( $\Delta G^{solv}$ ) energies. The mean and standard deviations of the energies are computed from three replica simulations for each system.

TABLE 1. Amino acid residues of human GALC and zebrafish orthologues involved in the interaction with  $\beta$ -D-Gal and GCP in the simulated systems <sup>[a]</sup>

Enzyme	Ligand	Amino acid residues
hGALC	$\beta$ -D-Gal	T109, W151, N197, <b>E198</b> , <b>E274</b> , S277, R396
	GCP	T109, W151, N197, <b>E198</b> , <b>E274</b> , S277, R396
Zebrafish Galca	$\beta$ -D-Gal	G64, T109, W151, N197, <b>E198</b> , <b>E274</b> , S277
	GCP	G64, T109, W151, N197, <b>E198</b> , <b>E274</b> , S277
Zebrafish Galcb	$\beta$ -D-Gal	T87, W129, N175, <b>E176</b> , <b>E251</b> , S254, R373
	GCP	T87, W129, N175, <b>E176</b> , <b>E251</b> , S254, R373

<sup>[a]</sup> Comparison between docking and MD simulation results confirms that both  $\beta$ -D-Gal and GCP are stably anchored to the catalytic pockets of hGALC and the zebrafish orthologues. Docking results represent the top-ranked poses then submitted to MD simulation. Contacts from MD simulations shown in the table are conserved in more than 90% of the simulations and in at least two out of the three replicas performed for each simulated system. Residue numbering follows the FASTA numbering (UniProt P54803) for the human enzyme and the Ensembl numbering for the Galc (Uniprot Q5SNX7) and Galcb (Uniprot Q7ZUD5) zebrafish orthologues.

## Highlights:

- Molecular docking simulation on human GALC and zebrafish Galca and Galcb demonstrated that once GCP epoxide is accommodated within the catalytic site of the enzyme, the lysosomal acid environment triggers the formation of a covalent bond.
- GCP competes with the natural product  $\beta$ -D-Galactose for the binding to the catalytic residues of human and zebrafish GALC.
- GCP inhibits zebrafish Galca and Galcb activity both *in vitro* and *in vivo*.
- Lipid profile of zebrafish embryos at 96 hours post fertilization reveals that GCP treatment caused a significant increase of TG and decrease CE. Among phospholipids, an increase of PC, PE and LPE, paralleled by a decrease of PI, LPI, LPS and PI-Cer were observed.
- 3 out of 20 Cer species and 3 out of 52 SM species were significantly more abundant in GCP-treated embryos.

## Take home message:

*In silico* analyses demonstrate for the first time that the catalytic site of GALC is conserved among human, murine and zebrafish counterparts and that the GALC inhibitor GCP competes with the natural substrate. The teleost zebrafish allowed the study of the effect of GALC modulation in a developing organism and our data show that GALC plays a non-redundant role in lipid metabolism also during embryonic development.

## 2. SPHINGOLIPID METABOLIZING ENZYMES MODULATE TUMOR PROGRESSION

Sphingolipids have opposing roles in regulating cancer cell death and survival. In general, ceramides are linked to apoptosis, cell cycle arrest, senescence, and autophagy. However, the length of the acyl chain, the metabolic pathway activated, the subcellular localization and even the cell type can affect these responses (Hannun and Obeid 2018).

In this scenario, the CerS family are usually downregulated. For instance, both CerS2 and CerS6 are inhibited by the mitochondrial associated anti apoptotic protein BCL2L13 in glioblastoma cell lines and xenograft tumors (Jensen et al. 2014). CerS6 is also downregulated in colon cancer cells resistant to chemotherapy. Additionally, *CERS1* is inhibited in head and neck cancer cells, therefore C18 ceramide-induced apoptosis is repressed (Meyers-Needham et al. 2012). Conversely, CerS6-generated C16 ceramide in the same tumor protects from ER-stress (Senkal et al. 2011).

Upregulation of acid ceramidase is linked to a pro-oncogenic phenotype in many cancers (Beckham et al. 2013, Tirodkar et al. 2015). In prostate cancer, acid ceramidase promotes nuclear export of PTEN through S1P-mediated AKT signalling. Moreover, its expression is increased in patients who had relapsed from radiotherapy (Cheng et al. 2013, Beckham et al. 2013). In colon cancer cells, acid ceramidase mediates pro-survival S1P signalling through activation of CerS6 (Tirodkar et al. 2015).

In keeping with the hypothesis that Cer orchestrates cancer responses, also glycosphingolipid metabolism may be impaired. Expression of GCS is associated to poor prognosis in patients with oral cavity cancer. Moreover, GCS-dependent accumulation of GluCer is important for maintenance of breast cancer stem cell pluripotency, whereas inhibition of GCS in ovarian cancer restores p53-mediated apoptosis (Ogretmen 2018).

Finally, loss of CERT is linked to heightened epidermal growth factor receptor which is up regulated in 70% of triple negative breast cancer (Heering et al. 2012). In contrast, CERT expression is induced in ovarian tumors treated with paclitaxel, thereby protecting cells from Cer-induced apoptosis (Swanton et al. 2007).

## 2.1 Role of nSMase2 in cancer progression

*SMPD3* is located on chromosome 16q22.1 that represents a common site of loss of heterozygosity in breast and prostate cancer, thus suggesting a tumor suppressor role for this gene. Accordingly, lack of nSMase2 has been observed in a murine osteosarcoma cell line and *SMPD3* hypermethylation occurs in basal MDA-MB-231 adenocarcinoma cells (Clarke 2018). Moreover, higher *SMPD3* methylation correlates with larger tumors and higher tumor grade in renal carcinoma (Wang et al. 2015) and low levels of nSMase2 are associated to earlier recurrence in hepatocellular carcinoma (Revill et al. 2013).

Conversely, anti-cancer drugs, including danorubicin, doxorubicin, cisplatin and oxaliplatin, may increase nSMase2 activity and Cer production (Clarke 2018). nSMase2 promotes cell growth arrest in G1. Accordingly, the induction of nSMase2 is necessary for retinoic acid-induced G1 arrest in breast cancer cells (Clarke et al. 2011) and cell growth blockage by doxorubicin requires *SMPD3* expression and activity (Shamseddine et al. 2015b).

Recently, nSMase2 has been investigated in cutaneous melanoma. *SMPD3* expression and Cer levels progressively decrease from primary to metastatic melanoma (Belleri et al. 2020) and its low expression is associated with short overall survival. *Smpd3* upregulation in murine melanoma cells is associated to a strong decrease in tumor growth in immunocompetent C57BL/6 mice but not in CD8a-deficient animals. In immunocompetent animals, the number of tumor-infiltrating leukocytes is significantly higher in *SMPD3* overexpressing tumors and nSMase2 has been shown to enhance the effect of both anti-programmed cell death 1 (PD-1) and anti-cytotoxic T-lymphocyte antigen-4 (CTLA-4) therapies in melanoma (Montfort et al. 2021)

### 2.1.1 nSMase2 modulates the lipidomic profile in melanoma cells

At present, no lipidomic studies have been performed to evaluate the impact of nSMase2 on melanoma lipidic profile. On this basis, during my PhD program, *SMPD3* was overexpressed in two human melanoma cell lines harboring the BRAF<sup>V600E</sup> driver mutation, frequently observed in human melanoma. The upregulation of nSMase2 in A2058 and A375 cells (nSMase2 cells) was confirmed by Western blot analysis (fig. 2.1 A). Increased levels of nSMase2 do not result in reduced cell proliferation neither in basal nor starving conditions (fig. 2.1 B-D). Similarly, the migratory capacity of these cells, evaluated in a wound healing assay

and in a Boyden chamber migration assay, was not affected by *SMPD3* overexpression (fig. 2.1 E-F).

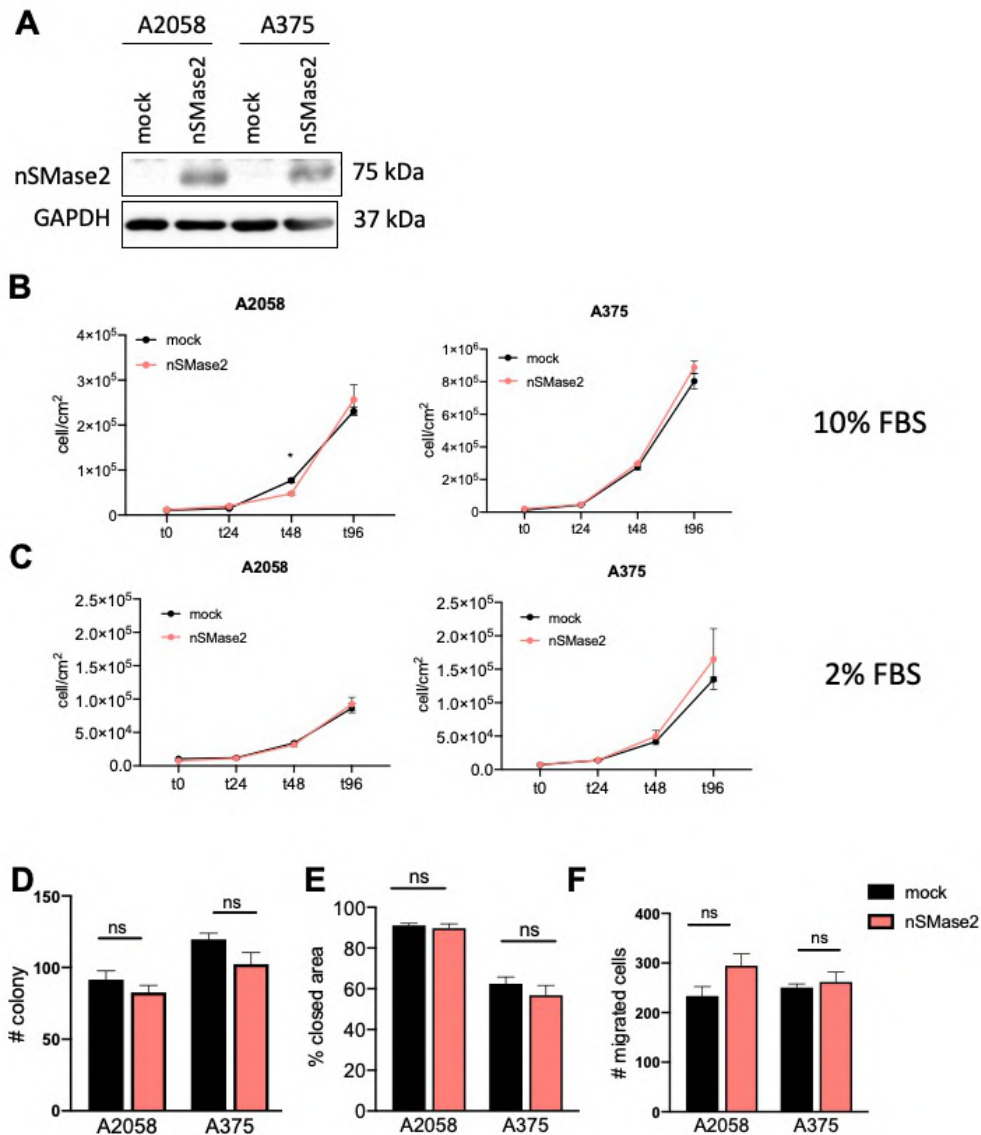


Figure 2.1 *SMPD3* overexpression in A2058 and A375 human melanoma cells does not affect their tumorigenic potential *in vitro*. A) Western blot analysis of *SMPD3*-upregulated cells. B, C) *nSMase2* does not delay cell growth at basal (10% FBS) or starving (2% FBS) conditions. D) Colony formation on 2D plastic support is similar in mock and *nSMase2* cells. E, F) Migration rate after wound healing and chemotaxis response in a Boyden chamber assay are not affected by *SMPD3* upregulation.

Despite the lack of phenotype *in vitro*, lipidomic analysis revealed that *nSMase2* upregulation does modulate sphingolipid and lipid levels in melanoma cells (fig. 2.2). Cer and DH-Cer were significantly increased in both cell lines, paralleled by a decrease of SM and DH-SM. A2058 melanoma cells also showed a significant decrease in the levels of hexosyl- and dihexosyl-Cer,

phosphatidylcholine, and CHOL. A trend toward a decrease in hexosyl- and dihexosyl-Cer was observed also in nSMase2 A375 cells with no effect on lipid levels.

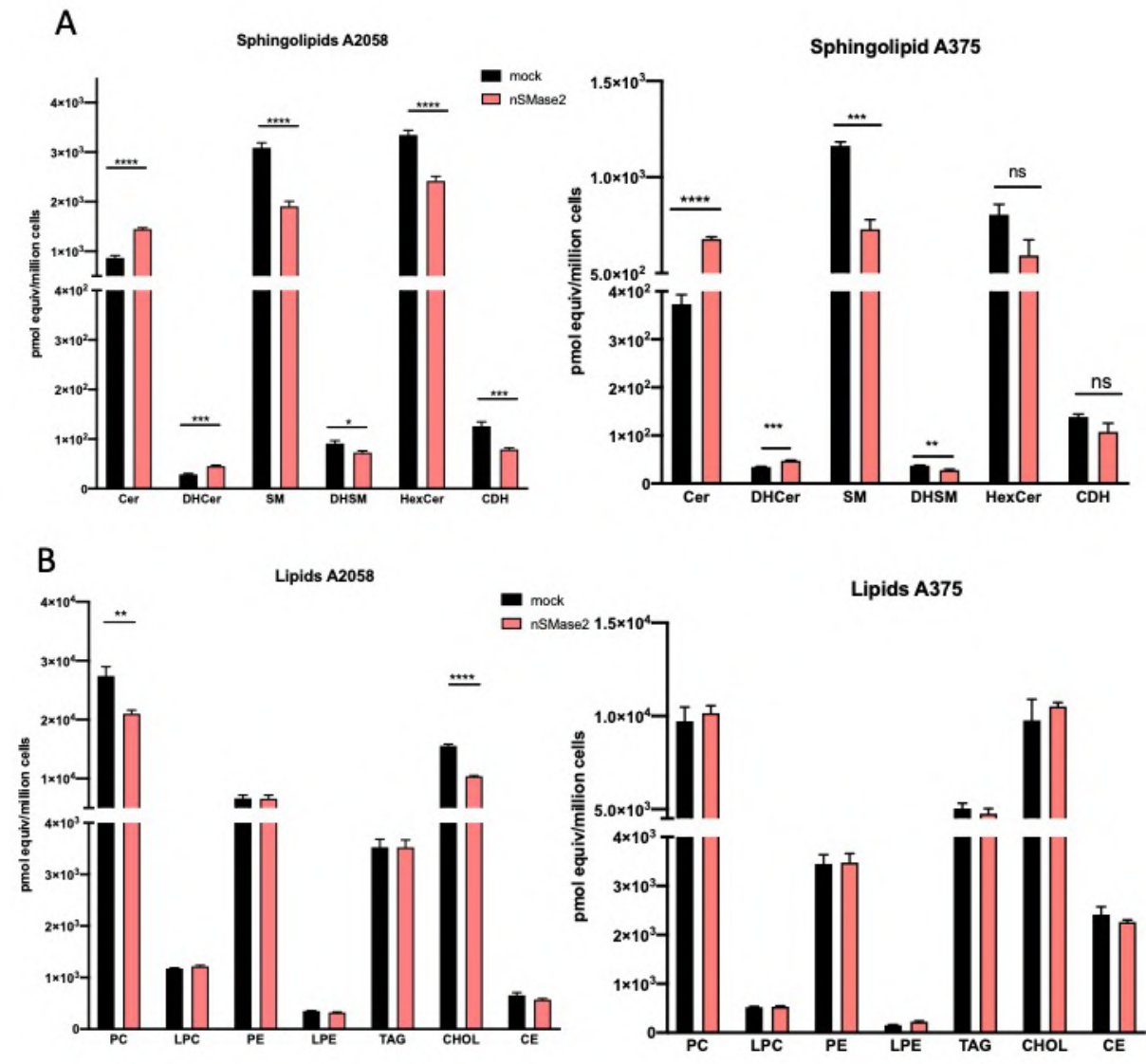


Figure 2.2 nSMase2 upregulation modulates sphingolipid and lipid levels in human melanoma cell lines. Sphingolipidomics (A) and lipidomics (B) analyses on A2058 (left) and A375 (right) cells overexpressing SMPD3. Cer: ceramide, SM: sphingomyelin, DH-Cer: dihydroceramide, DH-SM: dihydrosphingomyelin, HexCer: hexosylceramide, CDH: dihexosylceramide, PC: phosphatidylcholines, LPC: lyso-phosphatidylcholine, PE: phosphatidylethanolamines, LPE: lyso-phosphatidylcholine, TAG: triacylglycerols, CHOL: cholesterol, CE: cholesterol ester

To evaluate the impact of nSMase2 upregulation on the tumorigenic activity of melanoma cells, nSMase2 and control A2058 cells were implanted on the top of the chick embryo chorion allantoic membrane (CAM). As shown in fig. 2.3, preliminary results suggest that nSMase2 upregulation causes a significant decrease in the growth and neovascularization of nSMase2 A2058 tumor grafts when compared to control lesions.



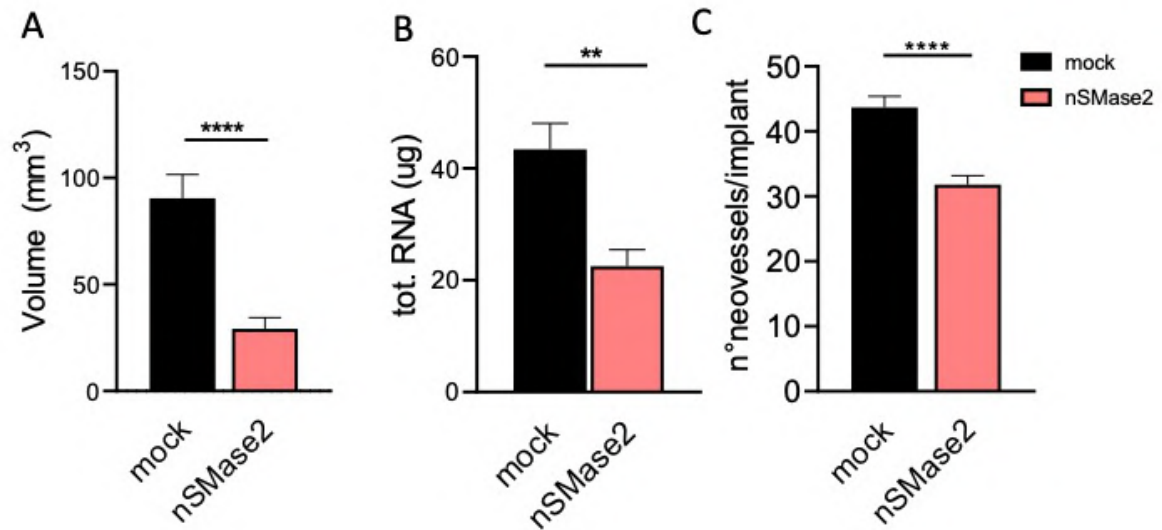


Figure 2.3 Reduced tumorigenic and angiogenic capacity of melanoma nSMase2 A2058 cells. Mock and nSMase2 cells were implanted on the top of the chick embryo CAM at day 7 post fertilization. A, B) After 10 days, volume and total RNA of the explanted grafts were measured. C) The number of neo-vessels converging versus the graft was assessed before the explant.

## 2.2 GALC: tumor suppressor or pro-oncogenic protein?

### 2.2.1 Oncosuppressive and oncogenic activity of the sphingolipid-metabolizing enzyme $\beta$ -galactosylceramidase

At variance with *SMPD3*, *GALC* seems to have a dual role in cancer progression. *GALC* is heavily downregulated by promoter hypermethylation in laryngeal squamous cell carcinoma and head and neck tumors, as well as in nasopharyngeal carcinoma where promoter demethylation is associated with decreased cell proliferation and migration (Görögh et al. 1999, Peng et al. 2015, Zhao et al. 2015). Conversely, *GALC* appears to be upregulated and increases tumorigenesis in cutaneous melanoma, colorectal cancer, non-small cell lung cancer and cervical cancer (Belleri et al. 2020, Yang et al. 2020, Liu et al. 2018, Atilla-Gokcumen et al. 2014).

Further studies are needed to unravel the role of *GALC* in cancer where it may behave as onco-suppressor or pro-oncogenic protein depending on the modulation it exerts on sphingolipids, in particular on Cer.

The dual role of *GALC* in cancer progression has been reviewed in the following article that I co-authored.



Contents lists available at ScienceDirect

BBA - Reviews on Cancer

journal homepage: [www.elsevier.com/locate/bbcan](http://www.elsevier.com/locate/bbcan)

Review

## Oncosuppressive and oncogenic activity of the sphingolipid-metabolizing enzyme $\beta$ -galactosylceramidase

Mirella Belleri<sup>a,\*</sup>, Paola Chiodelli<sup>a,1</sup>, Marzia Corli<sup>a</sup>, Miriam Capra<sup>a</sup>, Marco Presta<sup>a,b,\*</sup><sup>a</sup> Department of Molecular and Translational Medicine, University of Brescia, Italy<sup>b</sup> Italian Consortium for Biotechnology (CIB), Unity of Brescia, Italy

## ARTICLE INFO

## Keywords:

Ceramide  
Galactosylceramide  
Galactosylceramidase  
Lipidome  
Melanoma  
Sphingolipids

## ABSTRACT

$\beta$ -galactosylceramidase (GALC) is a lysosomal enzyme that removes  $\beta$ -galactose from  $\beta$ -galactosylceramide, leading to the formation of the oncosuppressor metabolite ceramide. Recent observations have shown that GALC may exert opposite effects on tumor growth by acting as an oncosuppressive or oncogenic enzyme depending on the different experimental approaches, *in vitro* versus *in vivo* observations, preclinical versus clinical findings, and tumor type investigated. This review will recapitulate and discuss the contrasting experimental evidence related to the impact of GALC on the biological behavior of cancer and stromal cells and its contribution to tumor progression.

## 1. Introduction

$\beta$ -Galactosylceramidase (GALC; EC 3.2.1.46) [1] is a lysosomal acid hydrolase that catalyzes the removal of  $\beta$ -galactose from  $\beta$ -galactosylceramide (GalCer, a major component of myelin) and other terminal  $\beta$ -galactose-containing sphingolipids, including  $\beta$ -galactosylsphingosine (psychosine). In humans, GALC deficiency causes globoid cell leukodystrophy (also named Krabbe disease; OMIM #245200), an autosomal recessive sphingolipidosis characterized by degeneration of oligodendroglia and progressive demyelination due to the accumulation of the neurotoxic metabolite psychosine. In its infantile form, Krabbe disease manifests in early infancy and results in a severe neurological dysfunction that often leads to death by 2 years of age [2].

Sphingolipid metabolism occurs in different subcellular compartments due to the activity of a variety of enzymes that form a complex lipid landscape that regulates various biological processes in different tumor types [3]. Among them, the GALC enzymatic product ceramide acts as a tumor suppressor metabolite and alterations in ceramide metabolism contribute to tumor cell survival and resistance to chemotherapy [4]. Ceramide is at the center of various interrelated metabolic pathways that include, among others, the *de novo*, sphingomyelin

hydrolysis, salvage, and catabolic pathways (Fig. 1). Thus, intracellular levels and localization of ceramide are the result of the orchestrated activity of more than 30 sphingolipid-metabolizing enzymes [5]. In this frame, recent observations have shown that the ceramide-generating enzyme GALC may exert opposite effects on tumor growth and differentiation [6]. Here, we will recapitulate and discuss the contrasting experimental evidence related to the contribution of GALC to the sphingolipid metabolism in cancer and its role in tumor progression.

## 2. Biology of GALC

## 2.1. GALC gene and protein

## 2.1.1. GALC gene

The human GALC gene maps on chromosome 14 and consists of 17 exons ranging from 39 to 181 nucleotides that encode for a 685 amino acid protein [7]. Murine GALC protein retains 83% identity with human GALC and two GALC co-orthologs (named *galca* and *galcb*) are expressed in zebrafish [8]. Zebrafish *galca* and *galcb* genes share the same 17 exons/16 introns structure of human and murine genes. A comparison of Galca and Galcb zebrafish polypeptides with mammalian GALC revealed a 61% amino acid sequence identity, with phylogenetic tree analysis

**Abbreviations:** ER, endoplasmic reticulum; GALC,  $\beta$ -galactosylceramidase; GalCer,  $\beta$ -galactosylceramide; IGF2R, insulin-like growth factor 2 receptor; M6P, mannose-6-phosphate; M6PR, M6P receptor; SMPD3, sphingomyelin phosphodiesterase 3; VEGF, vascular endothelial growth factor.

\* Corresponding authors at: Department of Molecular and Translational Medicine, University of Brescia, viale Europa 11, 25123 Brescia, Italy.

E-mail addresses: [mirella.belleri@unibs.it](mailto:mirella.belleri@unibs.it) (M. Belleri), [marco.presta@unibs.it](mailto:marco.presta@unibs.it) (M. Presta).

<sup>1</sup> The two authors contributed equally to this work.

<https://doi.org/10.1016/j.bbcan.2021.188675>

Received 4 August 2021; Received in revised form 7 December 2021; Accepted 27 December 2021

Available online 31 December 2021

0304-419X/© 2021 Published by Elsevier B.V.

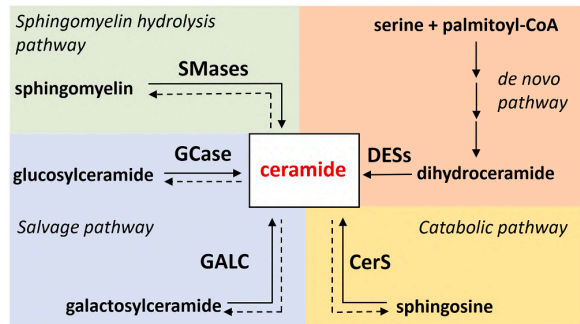


**Fig. 1.** Ceramide metabolism. Schema of the main ceramide metabolic pathways. Only the major ceramide precursors and ceramide-generating enzymes are shown. GALC, involved in the salvage pathway, generates ceramide by removing galactose from galactosylceramide. In Krabbe disease, GALC activity deficiency leads to the accumulation of toxic metabolites, including psychosine. CerSs, ceramide synthases; DESs, dihydroceramide desaturases; GCCase, glucosylceramidase; SMases, sphingomyelinases. See [5] for a detailed description of ceramide as the central hub of sphingolipid metabolism.

showing that vertebrate GALC has been highly conserved during evolution [8].

The untranslated 5' flanking region  $-176$  to  $-24$  of the human *GALC* gene is GC-rich, it includes potential YY1 (AAATGG) and Sp1 (CCCCC) binding sites and is endowed with promoter activity. However, at variance with other lysosomal enzyme promoters, the minimal promoter region in human *GALC* does not contain a housekeeping gene-typical GC-box nor TATA or CAAT box types. In addition, the 5' end of intron 1 contains six potential Sp1 binding sites, one AP1 binding site, and eight AP2 binding sites [9]. As described in section 3.1., promoter methylation modulates the expression of *GALC* in some types of cancer. However, to the best of our knowledge no published data are available about the transcription factors/suppressors and intracellular signaling pathway(s) that control *GALC* gene expression under physiological and pathological conditions.

### 2.1.2. *GALC* protein structure and cellular trafficking

The 3D structures of *GALC* protein and of the *GALC*-product complex have been solved by X-ray crystallography [10,11]. *GALC* contains a TIM barrel domain responsible for the enzymatic activity, a  $\beta$ -sandwich domain, and a unique carbohydrate recognition lectin domain not observed in other hydrolyses (Fig. 2A). In addition, these studies revealed how the active site of *GALC* recognizes and accommodates the sugar moiety of galactose-containing lipids (Fig. 2B) and provided insight into Krabbe disease-associated *GALC* mutations that affect the activity, stability, folding, glycosylation, and trafficking of the mutated protein (see [10] for a description of the protein regions perturbed by such mutations). The characterization of *GALC* structure in complex with substrate, product, and covalent intermediate has elucidated the catalytic cycle of the enzyme [11]. Finally, recent X-ray crystallography studies have revealed how *GALC* and the nonenzymatic sphingolipid activator protein saposin A form a heterotetrametric complex that accommodates the acyl moiety of glycosphingolipids in a hydrophobic patch of the saposin A dimer while the hydrophilic glycosyl head group interacts with the *GALC* active site [12].

The *GALC* protein is produced and *N*-glycosylated at specific asparagine residues in the endoplasmic reticulum (ER)/trans-Golgi network. Then, the addition of mannose-6-phosphate (M6P) groups allows its binding to M6P receptors (M6PR). This is followed by the transport of the M6P-tagged protein from the early to the late endosome compartment from where the enzyme is delivered to the lysosome after dissociation from the receptor [13]. Once in the lysosome, the 80 kDa *GALC* protein is cleaved in two 50 and 30 kDa fragments [7,13], originating a

complex that maintains its enzymatic activity [14]. M6P-tagged *GALC* may also enter an alternative secretory pathway to be released in the extracellular environment [13]. Once in the extracellular milieu, *GALC* can be recycled via the M6PR-dependent pathway and delivered to the lysosomes (Fig. 2C). It has been hypothesized that the reuptake of extracellular *GALC* may occur also via M6P-independent mechanism(s) [13], possibly due to the presence of the lectin domain in its protein structure [see [10] for further details].

### 2.2. Enzymatic activity of *GALC*

Sphingolipids are a family of lipids with a sphingoid backbone. Their metabolism occurs in different subcellular compartments via the activity of a variety of enzymes that form a complex lipid landscape [3,5,15]. In this frame, *GALC* acts inside the lysosomes and removes  $\beta$ -galactose primarily from GalCer, thus generating ceramide. Psychosine, lactosylceramide, and the seminolipid precursor galactosyl-alkyl-acyl-glycerol represent further *GALC* substrates. GalCer is synthesized following galactosylation of ceramide by the action of UDP-ceramide:galactose galactosyltransferase whereas psychosine is synthesized by galactosylation of sphingosine, which is generated from the deacylation of ceramide by acid ceramidase (Fig. 2D) [see [2] and references therein]. Recent observations have shown that acid ceramidase may also synthesize psychosine from GalCer and have confirmed the long-held “psychosine hypothesis” indicating that the pathogenesis of Krabbe disease is due to the accumulation of this neurotoxic metabolite [16].

Despite the pivotal role exerted by psychosine in *GALC* deficient animal models of Krabbe disease, scattered experimental evidence suggests that *GALC* may act not only as a psychosine “scavenger”, indicating that this enzyme may exert also psychosine-independent effects. For instance, downregulation of *GALC* expression results in a significant decrease in the response of endothelial cells to vascular endothelial growth factor (VEGF) with negligible modifications of the intracellular levels of psychosine [17]. Similarly, double *galca/galcb* knockdown in zebrafish embryos induces apoptosis and causes an altered expression of the neuronal marker *neuroD* in the absence of any significant accumulation of this metabolite [8]. Relevant to this point, *galcb* zebrafish morphants also show a delay in melanoblast/melanocyte differentiation consequent to the downregulation of the *dopachrome tautomerase* and *tyrosinase* genes, a finding that paved the way to further studies about the role of *GALC* in melanoma [18] (see section 3.2.). In addition, *twitche* mice, an authentic model of Krabbe disease [19], accumulate psychosine when generated in the C57BL/6 J background but not in the mixed C57BL/6 J/129SvEv background characterized by the accumulation of the alternative *GALC* substrate lactosyl-ceramide [20], a lipid raft component implicated in cell differentiation, development, apoptosis, and oncogenesis [21]. These data suggest that modulation of *GALC* may exert a more general impact on the sphingolipid profile under different physiological and pathological conditions.

Unfortunately, only limited information is available about the effect of *GALC* up/downregulation on the sphingolipidome. A lipidomic approach has shown that the levels of psychosine, C 16:0 ceramide, and C 18:0 GalCer were increased in the central nervous system of *twitche* mice compared to wild-type animals, whereas the levels of sphingosine-1-phosphate, C18:0 ceramide, C22:0 ceramide, and C24:0 ceramide were reduced. At variance, the levels of C22:0 and C24:0 GalCer were similar in the two groups with a trend toward reduced levels of C24:1 GalCer and C24:1 hydroxy-GalCer in *twitche* specimens [22]. Further studies have indicated a possible impact of *GALC* deficiency on fatty acid composition in *twitche* mice [23] and a decrease in phospholipid and membrane turnover in the brain of these animals [24]. In addition, *Galc* downregulation decreases the levels of ceramide and sphingosine in murine hematopoietic stem cells whereas its upregulation causes a significant increase of these sphingolipids and of sphingosine-1-phosphate, in the absence of significant changes in the intracellular levels of psychosine, sphingomyelin, and sulphatides [25]. More recently, the

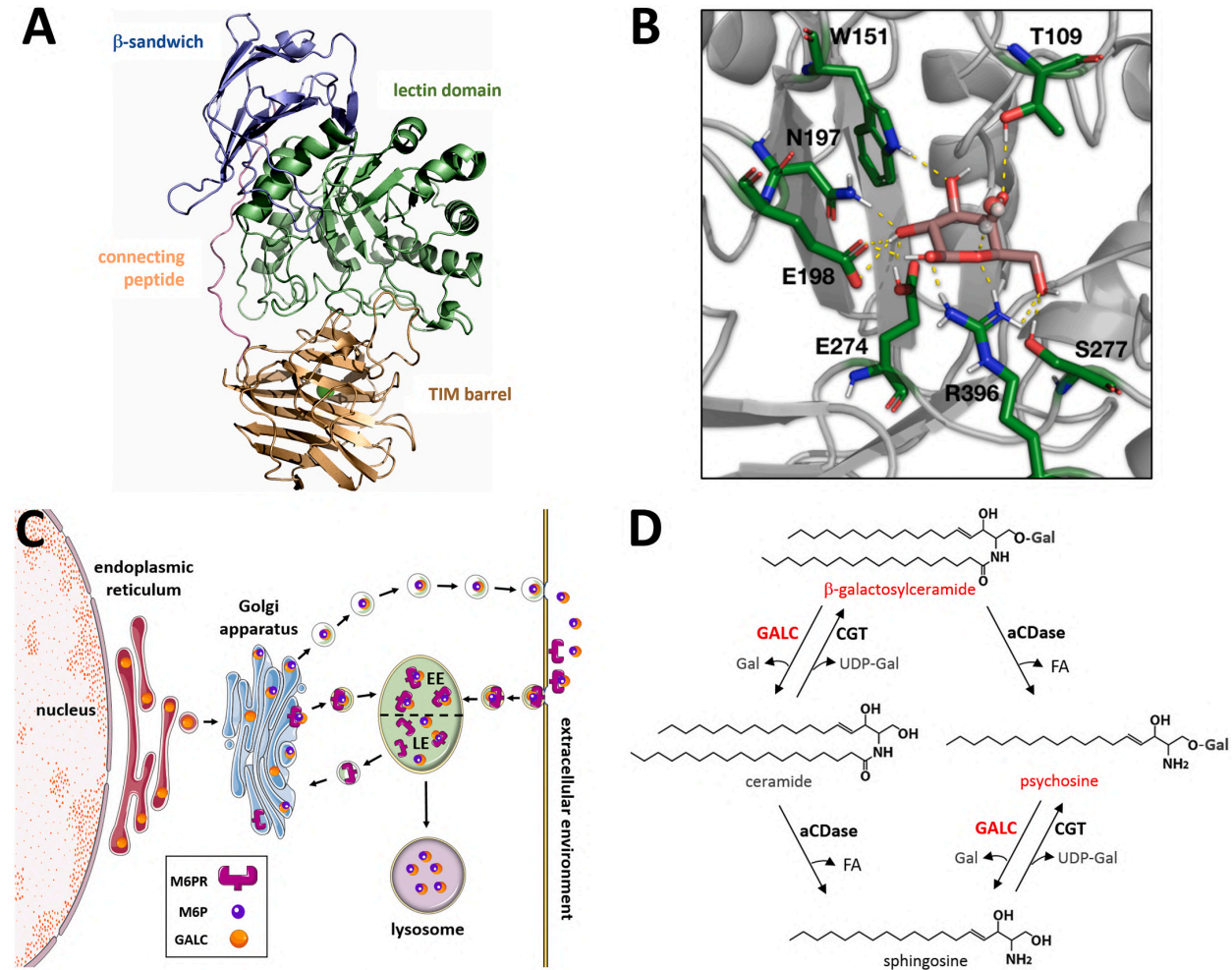


**Fig. 2.** 3D structure, intracellular trafficking, and role of GALC in sphingolipid metabolism. A) Ribbon diagram colored by protein domain showing the overall structure of murine GALC (PDB 3ZR5) [10]. TIM barrel (brown),  $\beta$ -sandwich (blue), lectin domain (green). B) Molecular modeling of the active site pocket of human GALC showing its interaction with D-galactose. In line with crystallographic data [10], D-galactose interacts with Thr<sup>109</sup>, Trp<sup>151</sup>, Asn<sup>197</sup>, Glu<sup>198</sup>, Glu<sup>274</sup>, Ser<sup>277</sup> and Arg<sup>396</sup> residues of GALC protein (grey cartoon). Amino acid residues involved in D-galactose interaction are shown as sticks colored by elements (green for carbons); polar hydrogens are in white. D-galactose is shown by stick representation (carbons in brown) and H-bond interactions as yellow dashes. C) GALC is produced in the endoplasmic reticulum/trans-Golgi network where it is modified by the addition of mannose-6-phosphate (M6P) groups, thus allowing its binding to M6P receptors (M6PR) and its transport to the early endosomal compartment (EE). In the late endosomal compartment (LE), GALC dissociates from M6PR and translocates to the lysosome. Alternatively, M6P-tagged GALC enters the secretory pathway and is released in the extracellular environment from where it can be recycled to the lysosomes following its binding to cell surface M6PRs. D) GalCer and psychosine are synthesized through the galactosylation of ceramide and sphingosine by the action of UDP-ceramide:galactose galactosyltransferase (CGT). In turn, GALC removes  $\beta$ -galactose from its major substrates GalCer and psychosine, thus generating ceramide and sphingosine, respectively. Acid ceramidase (aCDase), that generates sphingosine from ceramide, may synthesize psychosine from GalCer. FA, fatty acid. (For interpretation of the references to colour in this figure legend, the reader is referred to the web version of this article.)

sphingolipid, phospholipid, and neutral lipid composition of murine melanoma B16 cells have been investigated following shRNA mediated *Galc* knockdown [18]. Unexpectedly, *Galc* downregulation was found to result in a significant increase of intracellular ceramide mirrored by a decrease of sphingomyelins. This occurred together with a significant reduction of phosphatidylethanolamines and cholesteryl esters, accompanied by an increased concentration of diacylglycerols. No alterations were instead observed for the levels of sphingosine-1-phosphate, as well as of monohexosyl- and lactosyl-ceramides [18]. Further studies will be required to fully elucidate the impact of the modulation of GALC activity on ceramide metabolism, as well on the overall sphingolipidome, as compared to the other sphingolipid-metabolizing enzymes.

### 3. GALC in cancer

#### 3.1. GALC as an oncosuppressor enzyme

In 1999, T. Gorogh et al. [26] showed that the expression of *GALC* is strongly downregulated in laryngeal squamous cell carcinoma cell lines and tumor specimens when compared to benign keratinocytes. This was confirmed by the reduced transcriptional activity of a 152 bp regulatory promoter element of the 5' flanking region of the *GALC* gene when transduced in laryngeal squamous cell carcinoma cells in respect to benign keratinocytes. In keeping with these observations, methylation and expression analysis of the *GALC* gene in a limited number of head and neck cancer (HNC) and lung cancer cell lines revealed that the low

levels of *GALC* expression observed in approximately 50% of the samples were paralleled by heavy CpG island promoter methylation and were rescued by treatment with the demethylating agent 5-Aza-2'-deoxycytidine. Accordingly, *GALC* promoter hypermethylation was observed in a small set of HNC specimens, absent in normal mucosa [27]. *GALC* downregulation linked to promoter hypermethylation has been reported also in Epstein-Barr virus-associated nasopharyngeal carcinoma [28]. Accordingly, low levels of *GALC* protein in nasopharyngeal primary tumors correlated with a higher risk of lymph node metastases [28].

With a reductionist approach, these data suggest that *GALC* may behave as an oncosuppressor enzyme, *GALC* downregulation leading to a decrease of the levels of ceramide derived by GalCer hydrolysis, thus allowing tumor progression [29]. Based on this hypothesis, a reduced *GALC* activity may also cause an increase of its substrate GalCer. In this frame, the capacity of GalCer to favor tumor growth and metastatic activity of breast cancer cells by inhibiting apoptosis appears to be in line with this premise [30]. Accordingly, high levels of the GalCer synthesizing enzyme UDP-ceramide:galactose galactosyltransferase contribute to the aggressiveness of basal-like breast cancer [31], even though, in apparent contrast with these observations, treatment with C12:0 or C18:0 GalCer inhibited the growth of HPV16 E6/E7-transformed murine lung TC-1 cells and human lung cancer A559 cells, respectively [32,33].

### 3.2. *GALC* as an oncogenic enzyme

Despite the above-mentioned experimental observations pointing to a possible oncosuppressive role of *GALC*, recent data indicate that this enzyme might also exert pro-tumorigenic effects. Tumor growth depends on bi-directional interactions between tumor and non-malignant cells, including immune, stromal, and endothelial cells. *In vitro* and *in vivo* experimental evidence suggest that *GALC* may affect both stromal and parenchymal tumor compartments in a pro-tumorigenic manner. A first evidence for a possible impact of *GALC* on tumor stroma came from the observation that the loss of *GALC* activity deeply affects the microvasculature of the brain and bone marrow of *twitcher* mice and of the brain cortex of Krabbe patients [17,34], pointing to a role for *GALC* in the neovascularization process, a hallmark of cancer. Accordingly, *ex vivo* and *in vivo* angiogenesis models demonstrated that the *Galc*-null endothelium fails to respond to pro-angiogenic stimuli. Indeed, as stated above, *GALC* silencing prevents the capacity of human umbilical vein endothelial cells to migrate and proliferate following stimulation by the major tumor-derived angiogenic factor VEGF [17].

*GALC* may also affect the activity of cancer-associated fibroblasts, important players in tumor progression [35]. Indeed, *GALC*-overexpressing fibroblasts undergo senescence and stimulate the proliferation, motility, and tumorigenic potential of co-cultured colorectal cancer (CRC) cells. Moreover, transcriptome analysis of CRC cells co-cultured with *GALC*-overexpressing fibroblasts demonstrated the enrichment of various Gene Ontology pathways associated with tumor cell survival and metastasis [36].

These data raise the question as to whether such stimulatory effects are exerted by pro-tumorigenic factors released by *GALC*-overexpressing cells and/or are due to an extracellular activity of *GALC* released in the extracellular milieu. Relevant to this point, sphingolipid metabolites and sphingolipid-metabolizing enzymes may function not only at the intracellular level but also on the cell surface and in the extracellular microenvironment [37]. For instance, extracellular acid sphingomyelinase retains a significant, albeit decreased enzymatic activity at neutral pH when compared to optimal pH 5.5 and can catalyze the hydrolysis of sphingomyelin present in lipid rafts when localized in the outer leaflet of the plasma membrane [37]. Of note, GalCer is abundant at the extracellular surface of the multilayered myelin sheath and it is present in the outer layer of the cell membrane, contributing to its nanomechanical properties (see [38] and references therein). Given the role of lipid rafts

in receptor activity and intracellular signaling, it is tempting to hypothesize that extracellular *GALC* may modulate GalCer composition on the cell surface, thus affecting the behavior of both tumor parenchyma and stroma. Moreover, recent observations have shown that the M6P/insulin-like growth factor 2 receptor (IGF2R), usually considered to act as a IGF2-scavenging oncosuppressor protein, binds a variety of ligands, including M6P-tagged proteins, and may exert a pro-tumorigenic function in cancer [see [39] and references therein]. The possibility that extracellular M6P-tagged *GALC* may modify the cell membrane milieu and/or that its M6P/IGF2R interaction may affect tumor progression remains unexplored.

In keeping with the hypothesis that *GALC* may favor tumor growth by affecting the behavior of cancer parenchymal cells, immunohistochemical data have shown that high levels of *GALC* immunoreactivity are associated with poor prognosis in CRC patients [36]. Accordingly, the levels of *GALC* expression in circulating tumor cells correlate closely with the presence of distant metastases and tumor number in non-small cell lung cancer (NSCLC) patients. In addition, higher *GALC* expression levels in circulating NSCLC tumor cells correlated with a poor response to therapy, thereby suggesting that *GALC* may represent a predictor of tumor progression and prognosis in these patients [40]. Finally, studies aimed at investigating the lipid composition and localization during the cell cycle of cervix cancer HeLa-S3 cells provided evidence that RNAi *GALC* knockdown results in metaphase delay, cytokinesis failure, and altered cell shape and actin morphology [41].

In line with the data obtained on HeLa-S3 cells, *Galc* silencing results also in a significant inhibition of the tumorigenic and metastatic activity of murine melanoma B16-F10 cells [18]. As described in section 2.2., *Galc*-silenced cells showed alterations of the sphingolipid profile characterized by an increase of the intracellular levels of the anti-oncometabolite ceramide. This was paralleled by a non-redundant upregulation of *sphingomyelin phosphodiesterase 3* (*Smpd3*). At variance, no changes were observed in the expression levels of various other genes involved in sphingolipid metabolism, including *Smpd1*, *Sgms1*, *Sgms2*, *Gba1*, *Asah1*, *Cerk*, and *Sphk1* that encode for acid lysosomal sphingomyelinase, sphingomyelin synthase 1, sphingomyelin synthase 2, acid  $\beta$ -glucosylceramidase, acid ceramidase, ceramide kinase, and sphingosine kinase 1, respectively.

*Smpd3* encodes for the SMPD3 protein, also named neutral sphingomyelinase 2 (nSMase2), an enzyme that catalyzes the hydrolysis of sphingomyelin to form ceramide and phosphocholine. Thus, its upregulation may result in increased intracellular levels of ceramide. Indeed, in keeping with the data obtained in *Galc*-silenced murine melanoma cells, *GALC* downregulation caused *SMPD3* upregulation and ceramide accumulation also in human melanoma A2058 cells. Conversely, RNA *in situ* hybridization followed by morphometric image analysis of human specimens ranging from common nevi to stage IV melanoma demonstrated that the gradual increase of *GALC* mRNA levels that occurs during melanoma progression goes along with a decrease of ceramide and *SMPD3* immunoreactivity and with increased protein levels of the melanocyte differentiation markers microphthalmia transcription factor and tyrosinase, both involved in melanoma progression [18] (Fig. 3). Notably, Human Protein Atlas mining ([www.proteinatlas.org](http://www.proteinatlas.org)) of TCGA Skin Cutaneous Melanoma data set shows that melanomas with low levels of *GALC* expression are associated to a better 3-year patient survival (50%) when compared to tumors with high levels of *GALC* expression (0%). Nevertheless, the same Atlas reports low or absent *GALC* immunoreactivity in human melanoma specimens, possibly because of the lower sensitivity of the immunohistochemistry techniques when compared to gene expression analysis.

Experimental evidence indicates that *SMPD3* may act as a tumor suppressor gene by regulating tumor cell proliferation, survival, and response to chemotherapy (reviewed in [42]). In addition, *Smpd3* overexpression directly inhibits the growth of murine melanoma and breast tumor grafts in syngeneic immunocompetent mice by increasing anti-tumor immune responses and by potentiating the efficacy of

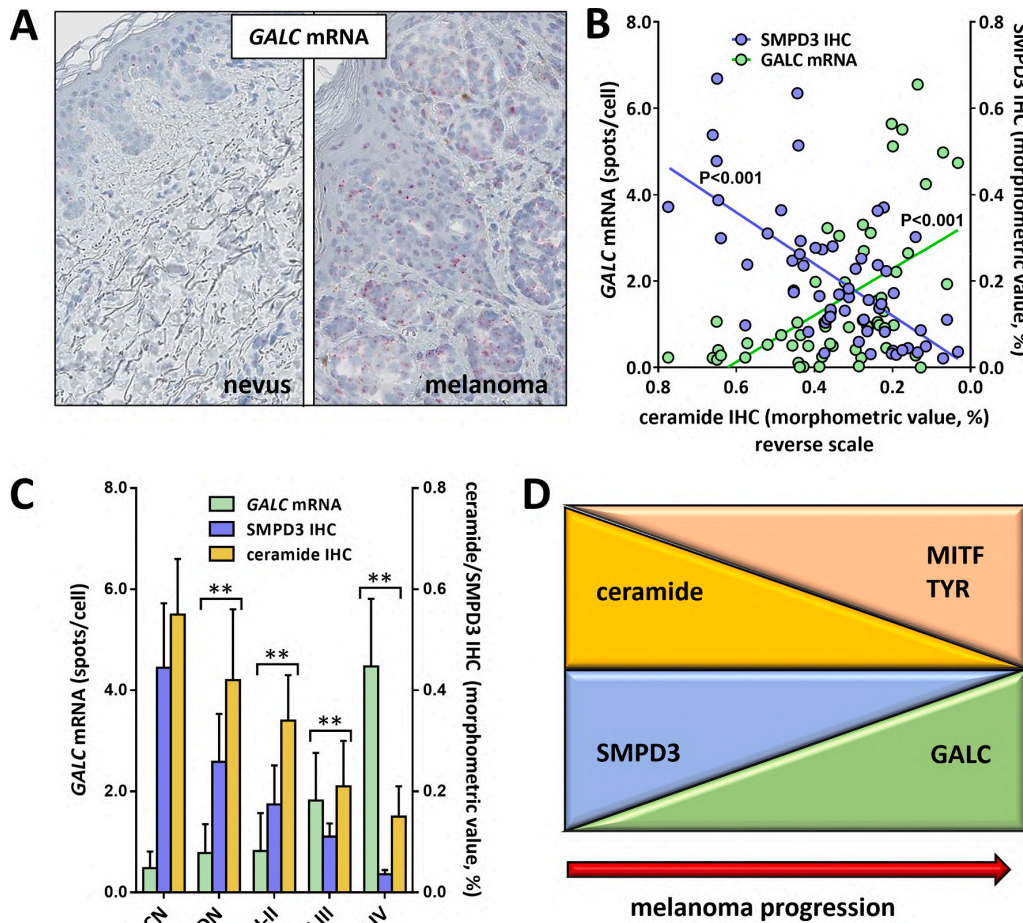


**Fig. 3.** GALC in human melanoma. A) RNA *in situ* hybridization analysis shows an increase of GALC mRNA levels (pink spots) in human skin melanoma (right panel) when compared to nevus (left panel). B) Ceramide immunoreactivity (x axis, reverse scale) is directly related to SMPD3 immunoreactivity (right y axis) and inversely related to GALC mRNA levels (left y axis) in skin specimens from 60 melanoma patients. Morphometric image analysis was used to quantify the GALC mRNA *in situ* hybridization signal that was expressed as spots per cell. See [18] for a detailed description of the *in situ* hybridization analysis of GALC expression in human melanoma. C) When clustered according to tumor stage, data shown in panel B indicate that GALC expression increases during melanoma progression. This was paralleled by a progressive decrease of the levels of SMPD3 and ceramide immunoreactivity. \*\*,  $P < 0.01$  versus earlier stage. D) Schematic representation of the relationship among GALC expression, SMPD3, ceramide, microphthalmia transcription factor (MITF), and tyrosinase (TYR) immunoreactivity during melanoma progression. ICH, immunohistochemistry; CN, common nevi; DN, dysplastic nevi; M I-IV, melanoma stages. See [18] for details. (For interpretation of the references to colour in this figure legend, the reader is referred to the web version of this article.)

immune check point inhibitors [43]. Together, these findings suggest that the oncosuppressive effects exerted by GALC downregulation in melanoma might be mediated, at least in part, by a parallel increase of SMPD3 activity, with a consequent increase of ceramide levels, inhibition of tumor growth, and immune escape. This hypothesis is supported by the observation that the neutral sphingomyelinase inhibitor GW4869 causes a significant stimulation of the tumorigenic activity of *Galc*-silenced murine melanoma cells paralleled by decreased levels of ceramide [18]. On the other hand, the above-mentioned impact of *Galc* downregulation on the sphingolipid profile of murine melanoma cells, that includes increased concentrations of diacylglycerols and the reduction of phosphatidylethanolamines/lyso-phosphatidylethanolamines, cholesteryl esters and phosphatidylcholines [18], indicates that this enzyme may also exert a more direct effect on melanoma cells.

SMPD3 deficiency may disrupt the homeostasis of ceramide, diacylglycerol, and sphingomyelin in the Golgi compartment [44]. As stated above, *Galc* downregulation in murine melanoma cells causes an increase of both ceramide and diacylglycerols. These observations raise the

question as to whether GALC might be involved directly (or indirectly via the modulation of SMPD3 activity) in the regulation of ER/Golgi intracellular pathways related to tumor progression, such as autophagy and ER stress [45,46]. Relevant to this point, cBioPortal for Cancer Genomics data mining indicates an enrichment of Gene Ontology terms related to ER/Golgi cellular components for the top 25 genes co-expressed with GALC in the TCGA melanoma data set [6]. Among these genes, *SEL1L* and *TMED10* encode for proteins involved in protein transport and quality control of ER export of misfolded proteins [47,48].

Chemotherapeutics, all-trans-retinoic acid, p53-mediated response to DNA damage, and inflammatory cytokines can modulate SMPD3 expression at the transcriptional level. In addition, various kinases regulate intracellular stability and trafficking of the SMPD3 protein [42]. However, the molecular mechanisms responsible for the SMPD3 upregulation that occurs in murine melanoma cells in response to GALC silencing remain unknown. In addition, the possibility exists that the modulation of GALC and SMPD3 expression in melanoma may depend also on common upstream signaling pathways affecting the two genes in

an opposite manner.

It must be pointed out that the inverse correlation between *GALC* and *SMPD3* expression observed in melanoma cells might not necessarily hold true for all types of cancer. Indeed, TCGA data mining via the cBioPortal for Cancer Genomics platform indicates that such inverse correlation occurs in brain lower grade glioma, renal clear cell carcinoma and thymoma, whereas no correlation (e.g., in stomach and pancreatic adenocarcinoma) or a direct correlation (e.g., in esophageal, breast, and liver carcinoma) can be found in other tumor types. Further studies aimed at understanding the mechanism(s) that regulate the *GALC/SMPD3* balance in different cancers and its impact on ceramide metabolism in tumor progression are eagerly required.

#### 4. Concluding remarks

Growing experimental evidence indicates that sphingolipid

metabolism plays a pivotal role in cancer [3,15]. Enzymes affecting the levels of the anti-oncometabolite ceramide may act as tumor promoting or oncosuppressive mediators, depending on their negative or positive impact of the intracellular concentration of this sphingolipid [3,4]. In addition, the tight crosstalk between the mechanisms involved in neoplastic transformation and cell differentiation, including but not limited to the epithelial-to-mesenchymal transition process, emphasizes the importance of dissecting the role of bioactive lipids and of the corresponding metabolizing enzymes in embryonic development, cell fate specification, and differentiation. Such understanding may pave the way to novel therapeutic strategies in cancer.

As described in this article, the scientific literature provides contrasting findings about a possible dual role of *GALC* in cancer progression, indicating that this sphingolipid-metabolizing enzyme may exert both oncosuppressive and oncogenic functions in tumor biology. It is conceivable that such discrepancies may be due to different

**Table 1**  
Oncosuppressive and oncogenic activity of *GALC*. Preclinical and clinical observations.

Cancer type	<i>GALC</i> expression	Experimental preclinical observations		Observations in human tumors	Impact on the sphingolipidome	Reference
		<i>In vitro</i>	<i>In vivo</i>			
<b>Oncosuppressive activity</b>						
Laryngeal squamous cell carcinoma (LSCC)	Downregulated	Transcriptional repression by promoter hypermethylation in LSCC cell lines <i>versus</i> normal keratinocytes.	n.a.	Transcriptional repression in LSCC specimens <i>versus</i> normal mucosa.	n.a.	[26]
Epstein-Barr virus-associated nasopharyngeal carcinoma (NPC)	Downregulated	Transcriptional repression by promoter hypermethylation in NPC cell lines. Promoter demethylation inhibits NPC cell proliferation and migration.	n.a.	<i>GALC</i> protein expression in NPC specimens more frequently detectable in tumors with latent EBV infection <i>versus</i> tumors without EBV latent infection.	n.a.	[28]
Head and neck cancer (HNC)	Downregulated	Transcriptional repression by promoter hypermethylation in HNC cell lines <i>versus</i> immortalized normal keratinocytes.	n.a.	Promoter hypermethylation in primary HNC specimens <i>versus</i> normal oral tissues.	n.a.	[27]
lung adenocarcinoma	Downregulated	Promoter hypermethylation in a few cancer cell lines.	n.a.	n.a.	n.a.	[27]
<b>Oncopromotive activity</b>						
Melanoma	Increased	<i>GALC</i> downregulation inhibits murine and human melanoma cell growth and motility.	<i>GALC</i> downregulation inhibits the tumorigenic and metastatic activity of murine and human melanoma cells.	<i>GALC</i> expression is positively correlated to tumor stage in human skin melanoma specimens.	<i>GALC</i> downregulation alters the sphingolipid profile and increases ceramide levels in murine and human melanoma cell lines. <i>GALC</i> mRNA levels are inversely related to ceramide levels at different stages of human skin melanoma.	[18]
Colorectal cancer (CRC)	Increased in senescent CRC-associated fibroblasts	<i>GALC</i> overexpressing fibroblasts undergo senescence and induce CRC cell proliferation and migration.	<i>GALC</i> overexpressing fibroblasts contribute to the grafting and growth of CRC xenografts in immunodeficient mice.	High levels of <i>GALC</i> immunoreactivity in CRC specimens are associated with poor prognosis.	n.a.	[36]
Non-small cell lung cancer (NSCLC)	Expressed by circulating NSCLC cells	n.a.	n.a.	<i>GALC</i> expression in circulating NSCLC cells positively correlates with tumor number, distant metastases, and poor response to therapy.	n.a.	[40]
Cervical cancer	Expressed by HeLa cells	Cell division failure in <i>GALC</i> silenced cells.	n.a.	n.a.	Accumulation of specific side-chain hexosylceramides in <i>GALC</i> silenced cells.	[41]

See text for details. n.a., not available.

experimental approaches, *in vitro* versus *in vivo* observations, preclinical versus clinical findings, and tumor type investigated (Table 1). Clearly, further studies are required to dissect the impact of GALC on cancer and to assess whether such enzyme may represent a therapeutic target.

In its infantile form, inherited GALC deficiency causes the lethal neurodegenerative Krabbe disease, leading the progressive loss of myelin and death by 2–4 years of age. In addition, loss of GALC activity has been shown to induce mitochondrial and peroxisomal defects [2] as well as microvascular alterations [17]. In addition, liver damage [49], lymphoid organ atrophy [50], and impairment of the hematopoietic stem cell niche [25] have been observed in *Galc* null *twitcher* mice. Moreover, even though the most relevant changes in myelination occur in humans between midgestation and the end of the second postnatal year, myelination may continue for the next 30–40 years in some areas of the central nervous system [2]. These data indicate that GALC inhibitors to be used as potential chemotherapy drugs for GALC-dependent tumors might be endowed with significant side effects. Thus, tumor-targeting, nano-based drug delivery approaches [51] should be envisaged to overcome possible organ-specific and/or systemic side effects consequent to the administration of GALC-targeting agents. Conversely, gene or microRNA delivery *via* tumor-targeting viral and non-viral vectors [52] might be used for those tumors in which GALC exerts an oncosuppressive activity.

In conclusion, much remains to be achieved to understand the impact exerted by GALC on cancer. The envision of GALC as a mere “psychosine scavenger” neglects a potentially wider impact of this enzyme on the sphingolipid metabolism, including the ceramide hub, in cancer cells. Few data, if any, are available about the impact of GALC activity on tumor and stromal cell lipidome, metabolome, transcriptome, and proteome. Also, the mechanism(s) regulating GALC expression during tumor progression and metastasis are largely unknown. Relevant to this point, it is unknown if and how oncogene and oncosuppressor driver mutations affect GALC expression and activity in different tumor types. Finally, the impact, if any, of extracellular GALC in tumor biology remains unexplored. Only such a level of understanding will allow a precise delineation of the role of GALC in cancer and of its clinical implications for improving anticancer therapy.

#### Author contributions

All authors contributed to the conception of the study and the preparation and approval of the manuscript.

#### Funding

This work was supported by Associazione Italiana per la Ricerca sul Cancro (AIRC IG grant n° 23116) to M. Presta.

#### Declaration of competing interest

None.

#### Acknowledgements

The authors wish to thank Dr. T. Annese (Department of Basic Medical Sciences, Neurosciences, and Sensory Organs, University of Bari, Italy) for *in situ* hybridization images and melanoma specimen analysis, Dr. G. Paiardi (Molecular and Cellular Modeling Group, Heidelberg Institute for Theoretical Studies, Heidelberg, Germany) for GALC modeling images, and Prof. T. Levade (Cancer Research Center of Toulouse, France) for helpful suggestions and criticisms.

#### References

- [1] K. Suzuki, Y. Suzuki, Globoid cell leucodystrophy (Krabbe's disease): deficiency of galactocerebroside beta-galactosidase, *Proc. Natl. Acad. Sci. U. S. A.* 66 (1970) 302–309, <https://doi.org/10.1073/pnas.66.2.302>.
- [2] J.S. Won, A.K. Singh, I. Singh, Biochemical, cell biological, pathological, and therapeutic aspects of Krabbe's disease, *J. Neurosci. Res.* 94 (2016) 990–1006, <https://doi.org/10.1002/jnr.23873>.
- [3] B. Ogretmen, Sphingolipid metabolism in cancer signalling and therapy, *Nat. Rev. Cancer* 18 (2018) 33–50, <https://doi.org/10.1038/nrc.2017.96>.
- [4] S.A. Morad, M.C. Cabot, Ceramide-orchestrated signalling in cancer cells, *Nat. Rev. Cancer* 13 (2013) 51–65, <https://doi.org/10.1038/nrc3398>.
- [5] A. Gomez-Larrauri, U. Das Adhikari, M. Aramburu-Nunez, A. Custodia, A. Ouro, Ceramide metabolism enzymes-therapeutic targets against cancer, *Medicina* 57 (2021) 729, <https://doi.org/10.3390/medicina57070729>.
- [6] M. Presta, beta-Galactosylceramidase in cancer: friend or foe? *Trends Cancer* 7 (2021) 974–977, <https://doi.org/10.1016/j.trecan.2021.08.001>.
- [7] Y.Q. Chen, M.A. Rafi, G. de Gala, D.A. Wenger, Cloning and expression of cDNA encoding human galactocerebroside, the enzyme deficient in globoid cell leukodystrophy, *Hum. Mol. Genet.* 2 (1993) 1841–1845, <https://doi.org/10.1093/hmg/2.11.1841>.
- [8] D. Zizioli, M. Guarienti, C. Tobia, G. Gariano, G. Borsani, R. Bresciani, R. Ronca, E. Giacomuzzi, A. Preti, G. Gaudenzi, M. Belleri, E. Di Salle, G. Fabrias, J. Casas, D. Ribatti, E. Monti, M. Presta, Molecular cloning and knockdown of galactocerebroside in zebrafish: new insights into the pathogenesis of Krabbe's disease, *Biochim. Biophys. Acta* 2014 (2014) 665–675, <https://doi.org/10.1016/j.bbdis.2014.01.008>.
- [9] N. Sakai, H. Fukushima, K. Inui, L. Fu, T. Nishigaki, I. Yanagihara, N. Tatsumi, K. Ozono, S. Okada, Human galactocerebroside gene: promoter analysis of the 5'-flanking region and structural organization, *Biochim. Biophys. Acta* 1395 (1998) 62–67, [https://doi.org/10.1016/s0167-4781\(97\)00140-1](https://doi.org/10.1016/s0167-4781(97)00140-1).
- [10] J.E. Deane, S.C. Graham, N.N. Kim, P.E. Stein, R. McNair, M.B. Cachon-Gonzalez, T.M. Cox, R.J. Read, Insights into krabbe disease from structures of galactocerebroside, *Proc. Natl. Acad. Sci. U. S. A.* 108 (2011) 15169–15173, <https://doi.org/10.1073/pnas.1105639108>.
- [11] C.H. Hill, S.C. Graham, R.J. Read, J.E. Deane, Structural snapshots illustrate the catalytic cycle of beta-galactocerebroside, the defective enzyme in krabbe disease, *Proc. Natl. Acad. Sci. U. S. A.* 110 (2013) 20479–20484, <https://doi.org/10.1073/pnas.1311990110>.
- [12] C.H. Hill, G.M. Cook, S.J. Spratley, S. Fawke, S.C. Graham, J.E. Deane, The mechanism of glycosphingolipid degradation revealed by a GALC-SapA complex structure, *Nat. Commun.* 9 (2018) 151, <https://doi.org/10.1038/s41467-017-02361-y>.
- [13] S. Nagano, T. Yamada, N. Shinnoh, H. Furuya, T. Taniwaki, J. Kira, Expression and processing of recombinant human galactosylceramidase, *Clin. Chim. Acta* 276 (1998) 53–61, [https://doi.org/10.1016/s0009-8981\(98\)00095-3](https://doi.org/10.1016/s0009-8981(98)00095-3).
- [14] W.C. Lee, D. Kang, E. Causevic, A.R. Herdt, E.A. Eckman, C.B. Eckman, Molecular characterization of mutations that cause globoid cell leukodystrophy and pharmacological rescue using small molecule chemical chaperones, *J. Neurosci.* 30 (2010) 5489–5497, <https://doi.org/10.1523/JNEUROSCI.6383-09.2010>.
- [15] Y.A. Hannun, L.M. Obeid, Sphingolipids and their metabolism in physiology and disease, *Nat Rev Mol Cell Biol* 19 (2018) 175–191, <https://doi.org/10.1038/nrm.2017.107>.
- [16] Y. Li, Y. Xu, B.A. Benitez, M.S. Nagree, J.T. Dearborn, X. Jiang, M.A. Guzman, J. C. Woloszynek, A. Giaramita, B.K. Yip, J. Elsbernd, M.C. Babcock, M. Lo, S. C. Fowler, D.F. Wozniak, C.A. Vogler, J.A. Medin, B.E. Crawford, M.S. Sands, Genetic ablation of acid ceramidase in krabbe disease confirms the psychosine hypothesis and identifies a new therapeutic target, *Proc. Natl. Acad. Sci. U. S. A.* 116 (2019) 20097–20103, <https://doi.org/10.1073/pnas.1912108116>.
- [17] M. Belleri, R. Ronca, D. Coltrini, B. Nico, D. Ribatti, P.L. Poliani, A. Giacomini, P. Alessi, S. Marchesini, M.B. Santos, E.R. Bongarzone, M. Presta, Inhibition of angiogenesis by beta-galactosylceramidase deficiency in globoid cell leukodystrophy, *Brain* 136 (2013) 2859–2875, <https://doi.org/10.1093/brain/awt215>.
- [18] M. Belleri, G. Paganini, D. Coltrini, R. Ronca, D. Zizioli, M. Corsini, A. Barbieri, E. Grillo, S. Calza, R. Bresciani, E. Maiorano, M.G. Mastropasqua, T. Annese, A. Giacomini, D. Ribatti, J. Casas, T. Levade, G. Fabrias, M. Presta, Beta-galactosylceramidase promotes melanoma growth via modulation of ceramide metabolism, *Cancer Res.* 80 (2020) 5011–5023, <https://doi.org/10.1158/0008-5472.CAN-19-3382>.
- [19] K. Suzuki, The twitcher mouse: a model for krabbe disease and for experimental therapies, *Brain Pathol.* 5 (1995) 249–258, <https://doi.org/10.1111/j.1750-3639.1995.tb00601.x>.
- [20] K. Tominaga, J. Matsuda, M. Kido, E. Naito, I. Yokota, K. Toida, K. Ishimura, K. Suzuki, Y. Kuroda, Genetic background markedly influences vulnerability of the hippocampal neuronal organization in the “twitcher” mouse model of globoid cell leukodystrophy, *J. Neurosci. Res.* 77 (2004) 507–516, <https://doi.org/10.1002/jnr.20190>.
- [21] S. Chatterjee, A. Pandey, The yin and Yang of lactosylceramide metabolism: implications in cell function, *Biochim. Biophys. Acta* 1780 (2008) 370–382, <https://doi.org/10.1016/j.bbagen.2007.08.010>.
- [22] S.W. Esch, T.D. Williams, S. Biswas, A. Chakrabarty, S.M. LeVine, Sphingolipid profile in the CNS of the twitcher (globoid cell leukodystrophy) mouse: a lipidomics approach, *Cell. Mol. Biol.* 49 (2003) 779–787.



- [23] A. Zanfini, E. Dreassi, A. Berardi, P. Piomboni, E. Costantino-Ceccarini, A. Luddi, GC-ESI-MS analysis of fatty acid composition in brain and serum of twitcher mouse, *Lipids* 49 (2014) 1115–1125, <https://doi.org/10.1007/s11745-014-3945-0>.
- [24] N.I. Weinstock, L. Wrabetz, M.L. Feltri, D. Shin, Metabolic profiling reveals biochemical pathways and potential biomarkers associated with the pathogenesis of krabbe disease, *J. Neurosci. Res.* 94 (2016) 1094–1107, <https://doi.org/10.1002/jnr.23789>.
- [25] I. Visigalli, S. Ungari, S. Martino, H. Park, M. Cesani, B. Gentner, L. Sergi Sergi, A. Orlicchio, L. Naldini, A. Biffi, The galactocerebrosidase enzyme contributes to the maintenance of a functional hematopoietic stem cell niche, *Blood* 116 (2010) 1857–1866, <https://doi.org/10.1182/blood-2009-12-256461>.
- [26] T. Gorogh, H. Rudert, B.M. Lippert, S. Gottschlich, S. Maune, K. Heidorn, J. Maass, M. Hoffmann, J.E. Meyer, I.O. Rathcke, B.J. Folz, T. Hortobagyi, J.A. Werner, Transcriptional repression of the human galactocerebrosidase gene in squamous cell carcinomas of the larynx, *Int. J. Cancer* 83 (1999) 750–754, [https://doi.org/10.1002/\(sici\)1097-0215\(19991210\)83:6<750::aid-ijc9>3.0.co;2-v](https://doi.org/10.1002/(sici)1097-0215(19991210)83:6<750::aid-ijc9>3.0.co;2-v).
- [27] J. Peng, B. Chen, Z. Shen, H. Deng, D. Liu, X. Xie, X. Gan, X. Xu, Z. Huang, J. Chen, DNA promoter hypermethylation contributes to down-regulation of galactocerebrosidase gene in lung and head and neck cancers, *Int. J. Clin. Exp. Pathol.* 8 (2015) 11042–11050.
- [28] Y. Zhao, Y. Guo, Z. Wang, Z. Xiao, R. Li, A. Luo, C. Wu, Z. Jing, N. Sun, X. Chen, H. Du, Y. Zeng, GALC gene is downregulated by promoter hypermethylation in Epstein-Barr virus-associated nasopharyngeal carcinoma, *Oncol. Rep.* 34 (2015) 1369–1378, <https://doi.org/10.3892/or.2015.4134>.
- [29] U.H. Beier, T. Gorogh, Implications of galactocerebrosidase and galactosylceramide metabolism in cancer cells, *Int. J. Cancer* 115 (2005) 6–10, <https://doi.org/10.1002/ijc.20851>.
- [30] T.B. Owczarek, J. Suchanski, B. Pula, A.M. Kmiecik, M. Chadalski, A. Jethon, P. Dziegiel, M. Ugorski, Galactosylceramide affects tumorigenic and metastatic properties of breast cancer cells as an anti-apoptotic molecule, *PLoS One* 8 (2013), e84191, <https://doi.org/10.1371/journal.pone.0084191>.
- [31] Q. Cao, X. Chen, X. Wu, R. Liao, P. Huang, Y. Tan, L. Wang, G. Ren, J. Huang, C. Dong, Inhibition of UGT8 suppresses basal-like breast cancer progression by attenuating sulfate- $\alpha$ -V $\beta$ 5 axis, *J. Exp. Med.* 215 (2018) 1679–1692, <https://doi.org/10.1084/jem.20172048>.
- [32] J. Simova, M. Indrova, J. Bieblova, R. Mikyskova, J. Bubenik, M. Reinis, Therapy for minimal residual tumor disease: beta-galactosylceramide inhibits the growth of recurrent HPV16-associated neoplasms after surgery and chemotherapy, *Int. J. Cancer* 126 (2010) 2997–3004, <https://doi.org/10.1002/ijc.24887>.
- [33] H. Oku, C. Li, M. Shimatani, H. Iwasaki, T. Toda, T. Okabe, H. Watanabe, Tumor specific cytotoxicity of beta-glucosylceramide: structure-cytotoxicity relationship and anti-tumor activity in vivo, *Cancer Chemother. Pharmacol.* 64 (2009) 485–496, <https://doi.org/10.1007/s00280-008-0896-2>.
- [34] M. Belleri, D. Coltrini, M. Righi, C. Ravelli, S. Taranto, P. Chioldelli, S. Mitola, M. Presta, A. Giacomini, Beta-galactosylceramidase deficiency causes bone marrow vascular defects in an animal model of krabbe disease, *Int. J. Mol. Sci.* 21 (2019) 251, <https://doi.org/10.3390/ijms21010251>.
- [35] R.S. Joshi, S.S. Kanugula, S. Sudhir, M.P. Pereira, S. Jain, M.K. Aghi, The role of cancer-associated fibroblasts in tumor progression, *Cancers* 13 (2021) 1399, <https://doi.org/10.3390/cancers13061399>.
- [36] M. Yang, Z. Jiang, G. Yao, Z. Wang, J. Sun, H. Qin, H. Zhao, GALC triggers tumorigenicity of colorectal cancer via senescent fibroblasts, *Front. Oncol.* 10 (2020) 380, <https://doi.org/10.3389/fonc.2020.00380>.
- [37] M. Tani, M. Ito, Y. Igarashi, Ceramide/sphingosine/sphingosine 1-phosphate metabolism on the cell surface and in the extracellular space, *Cell. Signal.* 19 (2007) 229–237, <https://doi.org/10.1016/j.cellsig.2006.07.001>.
- [38] B. Gumi-Audenis, F. Sanz, M.I. Giannotti, Impact of galactosylceramides on the nanomechanical properties of lipid bilayer models: an AFM-force spectroscopy study, *Soft Matter* 11 (2015) 5447–5454, <https://doi.org/10.1039/c5sm01252j>.
- [39] T. Takeda, M. Komatsu, F. Chiwaki, R. Komatsuzaki, K. Nakamura, K. Tsuji, Y. Kobayashi, E. Tominaga, M. Ono, K. Banno, D. Aoki, H. Sasaki, Upregulation of IGF2R evades lysosomal dysfunction-induced apoptosis of cervical cancer cells via transport of cathepsins, *Cell Death Dis.* 10 (2019) 876, <https://doi.org/10.1038/s41419-019-2117-9>.
- [40] D.G. Liu, L. Xue, J. Li, Q. Yang, J.Z. Peng, Epithelial-mesenchymal transition and GALC expression of circulating tumor cells indicate metastasis and poor prognosis in non-small cell lung cancer, *Cancer Biomark* 22 (2018) 417–426, <https://doi.org/10.3233/CBM-170995>.
- [41] G.E. Atilla-Gokcumen, E. Muro, J. Relat-Goberna, S. Sasse, A. Bedigian, M. L. Coughlin, S. Garcia-Manyes, U.S. Eggert, Dividing cells regulate their lipid composition and localization, *Cell* 156 (2014) 428–439, <https://doi.org/10.1016/j.cell.2013.12.015>.
- [42] A.A. Shamseddine, M.V. Airola, Y.A. Hannun, Roles and regulation of neutral sphingomyelinase-2 in cellular and pathological processes, *Adv. Biol. Regul.* 57 (2015) 24–41, <https://doi.org/10.1016/j.jbior.2014.10.002>.
- [43] A. Montfort, F. Bertrand, J. Rochotte, J. Gilhodes, T. Filleron, J. Milhes, C. Dufau, C. Imbert, J. Riond, M. Tosolini, C.J. Clarke, F. Dufour, A.A. Constantinescu, N. de Franca Junior, V. Garcia, M. Record, P. Cordelier, P. Brousset, P. Rochemaux, S. Silvente-Poirot, N. Therville, N. Andrieu-Abadie, T. Levade, Y.A. Hannun, H. Benoist, N. Meyer, O. Micheau, C. Colacios, B. Segui, Neutral sphingomyelinase 2 heightens anti-melanoma immune responses and anti-PD-1 therapy efficacy, *cancer, Immunol. Res.* 9 (2021) 568–592, <https://doi.org/10.1158/2326-6066.CCR-20-0342>.
- [44] W. Stoffel, I. Hammels, B. Jenke, E. Binczek, I. Schmidt-Soltan, S. Brodesser, A. Schauss, J. Etich, J. Heilig, F. Zaucke, Neutral sphingomyelinase (SMPD3) deficiency disrupts the golgi secretory pathway and causes growth inhibition, *Cell Death Dis.* 7 (2016), e2488, <https://doi.org/10.1038/cddis.2016.385>.
- [45] M. Lai, V. La Rocca, R. Amato, G. Freer, M. Pistello, Sphingolipid/Ceramide pathways and autophagy in the onset and progression of melanoma: novel therapeutic targets and opportunities, *Int. J. Mol. Sci.* 20 (2019) 3436, <https://doi.org/10.3390/ijms20143436>.
- [46] W.J. Park, J.W. Park, The role of sphingolipids in endoplasmic reticulum stress, *FEBS Lett.* 594 (2020) 3632–3651, <https://doi.org/10.1002/1873-3468.13863>.
- [47] A. Bhattacharya, L. Qi, ER-associated degradation in health and disease - from substrate to organism, *J. Cell Sci.* 132 (2019) jcs232850, <https://doi.org/10.1242/jcs.232850>.
- [48] R. Aber, W. Chan, S. Mugisha, L.A. Jerome-Majewska, Transmembrane emp24 domain proteins in development and disease, *Genet. Res.* 101 (2019), e14, <https://doi.org/10.1017/S0016672319000090>.
- [49] M.A. Contreras, E. Haq, T. Uto, I. Singh, A.K. Singh, Psychosine-induced alterations in peroxisomes of twitcher mouse liver, *Arch. Biochem. Biophys.* 477 (2008) 211–218, <https://doi.org/10.1016/j.abb.2008.06.012>.
- [50] F. Galbiati, V. Basso, L. Cantuti, M.I. Givogri, A. Lopez-Rosas, N. Perez, C. Vasu, H. Cao, R. van Breemen, A. Mondino, E.R. Bongarzone, Autonomic denervation of lymphoid organs leads to epigenetic immune atrophy in a mouse model of krabbe disease, *J. Neurosci.* 27 (2007) 13730–13738, <https://doi.org/10.1523/JNEUROSCI.3379-07.2007>.
- [51] T. Briolay, T. Petithomme, M. Fouet, N. Nguyen-Pham, C. Blanquart, N. Boisgerault, Delivery of cancer therapies by synthetic and bio-inspired nanovectors, *Mol. Cancer* 20 (2021) 55, <https://doi.org/10.1186/s12943-021-01346-2>.
- [52] B. Caffery, J.S. Lee, A.A. Alexander-Bryant, Vectors for Glioblastoma Gene Therapy: Viral & Non-Viral Delivery Strategies, *Nanomaterials* 9 (2019) 105, <https://doi.org/10.3390/nano9010105>.

**Highlights:**

- Downregulation of *GALC* by promoter hypermethylation suggests its role as an oncosuppressive protein.
- The expression of *GALC* correlates with a worst prognosis in cutaneous melanoma, colorectal cancer and non-small cell lung cancer.
- Downregulation of *GALC* in murine melanoma cells is linked to increased level of SMPD3 expression and ceramide production, leading to tumor protection.

**Take home message:**

*GALC* exerts a dual role in cancer progression. It may have both oncosuppressive and oncogenic activity depending on the type of the tumor. Understanding the role of *GALC* in tumor progression will be achieved by elucidating its mechanisms of expression and regulation and its impact on tumor sphingolipid metabolism.

### **3. CUTANEOUS MELANOMA**

#### **3.1 Cutaneous melanoma**

Cutaneous melanoma is a malignant skin cancer that occurs from the uncontrolled proliferation of melanocytes. Melanocytes are specialized cells that produce the melanin pigment and are found mostly in skin, but also in eyes, ears, leptomeninges, gastrointestinal tract and mucous membranes (Centeno, Pavet and Marais 2023). Since melanocytes are mainly present in the derma, cutaneous melanoma is the most common diagnosis for bulk melanoma in white population. In Europe, the incidence of cutaneous melanoma (hereafter referred as melanoma) is approximately 25 new cases per 100'000. The incidence is higher in the USA with 30 cases per 100'000 inhabitants and 60 per 100'000 in Australia (Long et al. 2023).

A family history of melanoma, sun sensitivity, exposure to ultraviolet radiation (UVR) and immunosuppression are the main risk factors for this tumor. Melanoma may account for 90% of all skin cancer-related death each year (Garbe et al. 2010). This high mortality is explained by its tendency towards metastasis. Melanoma is one of the most aggressive cancers and even relatively small tumors are able to disseminate throughout the body. Moreover, its progression is also linked to immune escape mechanisms and resistance to chemotherapy and immunotherapy (Braeuer et al. 2014).

At a first glance, melanoma presents as typically dark pigmented lesions because of melanin production, but it can also be clear (amelanotic), a situation that delays its detection. Biopsy and histopathology are generally required to confirm the diagnosis. Early-stage melanoma appears as radial growth phase lesions upon the superficial layers of the epidermis. However, this localized lesion can easily convert to the vertical growth phase: it first invades the dermis and then migrates and metastasized into distant organs (Miller and Mihm 2006).

#### **3.2 Clinical management of melanoma**

Primary melanoma tumors are removed with surgical excision. The size of the excision is usually determined by histological analyses, and it varies between 1 or 2 cm radial surgical margin. The excision generally reaches the underlying muscular fascia, which might be modified to accommodate the mass. Apart from excision of primary tumor, assessment of

patient's sentinel lymph node is established. These procedures are curative in the majority of cases (Ross and Gershenwald 2011).

Nowadays advanced and metastatic tumors remain a therapeutic challenge with high risk of recurrence and the 5 years survival at this stage is about 30% (Centeno et al. 2023, Leonardi et al. 2018). Currently, the gold standard of cure for metastatic tumors are BRAF and MEK kinase inhibitors and the use of immune checkpoint inhibitors such as anti-PD-1 combined with anti CTLA-4 (Amaria et al. 2018). This has allowed durable disease control in approximately 50% of patients with advance or metastatic melanoma. Consequently, chemotherapy is considered a second-line treatment option (Leonardi et al. 2018).

Despite remarkable initial response, the limiting factor of BRAF-targeted therapy is the acquired resistance. About 50% of patients develop resistance within 1 year and 80% of patients gain resistance within 5 years. At the basis of different mechanisms of resistance there are, among others, MAPK re-activation through secondary NRAS or MEK mutations and amplification. Clinical studies have shown that combined BRAF and MEK inhibitors effectively prevent the development of acquire resistance and led to high response rates, with a progression free survival of nearly 12 months and an overall survival significantly higher than monotherapy (Liu et al. 2017).

Although immune checkpoint inhibitors have less initial activity than target therapy, they have improved 5-year overall survival up to 50% and their capability to control the disease is higher. However, responses to immune therapy remain unpredictable and depends on tumor microenvironment, genetic and epigenetic alterations and on the type of immune infiltrate into the tumor (Carlino, Larkin and Long 2021, Leonardi et al. 2018).

### **3.3 The origin of melanoma**

The origin of melanoma is still a matter of debate since it presents high heterogeneity and recapitulates distinct melanocyte developmental states. Melanocytes derive from the neural crest and they migrate towards the extremity of the developing embryo. At this stage the microphthalmia-associated transcription factor (MITF) is responsible for cell survival and proliferation. For this reason, melanocyte stem cells are considered as the putative source of melanoma (Centeno et al. 2023, Prager et al. 2019). However also mature melanocytes can de-differentiate and give origin to tumors (Köhler et al. 2017).

In 1969, W.H Clark first described the histogenesis of three melanoma forms: the superficial spreading melanoma, the nodular melanoma, and the lentigo malignant melanoma (fig 3.1).

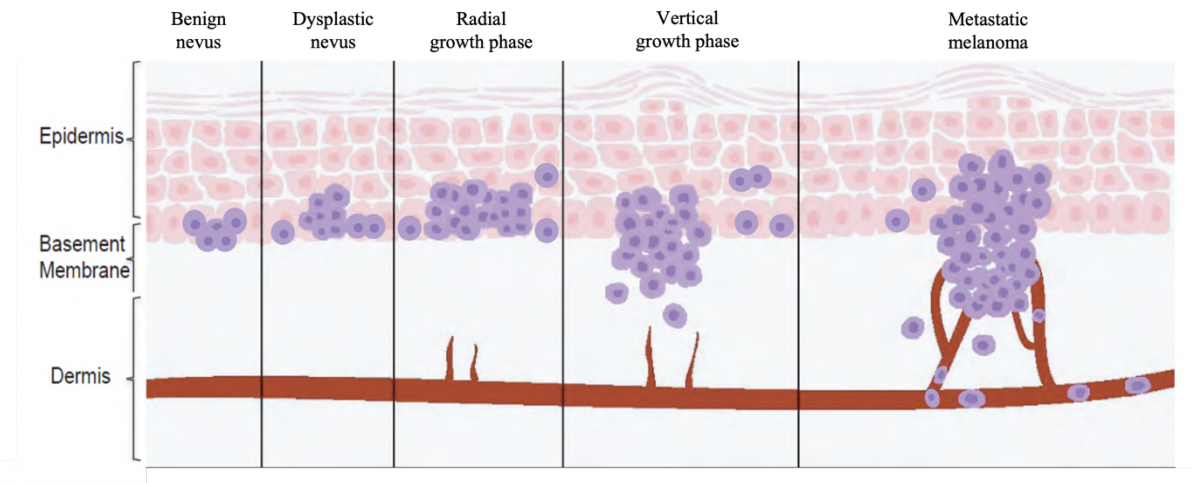


Figure 3.1 The Clark model of the progression of melanoma emphasizes the stepwise transformation of melanocytes to melanoma. The model depicts the proliferation of melanocytes in the process of forming nevi and the subsequent development of dysplasia, hyperplasia, invasion, and metastasis. Modified from (Qendro et al. 2014)

The first event described in the model is the formation of benign nevi by proliferation of structurally normal melanocytes. The abnormal activation of the MAPK hijacks melanocyte proliferation and it is driven by N-RAS or BRAF mutation in 15 and 80% of tumors, respectively (Centeno et al. 2023). Accordingly, melanocyte specific expression of mutant BRAF in animal models causes an ectopic proliferation similar to human nevi (Köhler et al. 2017, Baggiolini et al. 2021). However, neither NRAS nor BRAF mutations are capable of driving melanoma progression to the next stage. This static phase is probably due to oncogene-induced cell senescence (Michaloglou et al. 2005), a phenomenon linked to downstream activation of the cell-cycle inhibitor of kinase 4A (INK4A).

The second stage of the Clark model is characterized by the formation of dysplastic nevi in preexisting ones or in a new location. Lesions undergo aberrant growth and may appear asymmetric, with random and discontinuous cytologic atypia. At a molecular level, this stage is characterized by the acquisition of a second mutation distinct from BRAF or NRAS mutations. In familial melanoma, cyclin-dependent kinase inhibitor 2A (CDKN2A) is usually inactivated in 25 to 40% of tumors and results in low expression of the tumor suppressor protein p16<sup>INK4A</sup> and p19<sup>ARF</sup>. Concerning sporadic melanoma, phosphatase and tensin homologue (PTEN) is often inactivated.

The radial growth phase occurs because of the increased expression of CD1 that allows cells to proliferate intraepidermally. A progressive transition from epithelial to mesenchymal feature allows melanocytes to cross the basement membrane and form nodules, the so-called vertical growth phase. Metastatic melanoma is the final stage of the Clark model characterized by migration of tumor cells into distal tissues and organs (Miller and Mihm 2006).

Nowadays, the Clark’s model is applied only for tumors with < 1 mm thickness. The clinical staging is based on the American Joint Comitee on cancer system (Keung and Gershenwald 2018) and European guidelines (Garbe et al. 2010) (Table 3.1).

Table 3.1 Clinical melanoma stages. Modified from (Garbe et al. 2010)

Stage	Primary tumour (pT)	Regional lymph node metastases (N)	Distant metastases (M)
0	In situ tumour	None	None
IA	<1.0 mm, no ulceration	None	None
IB	<1.0 mm with ulceration or Clark Level IV or V	None	None
	1.01–2.0 mm, no ulceration	None	None
IIA	1.01–2.0 mm with ulceration	None	None
	2.01–4.0 mm, no ulceration	None	None
IIB	2.01–4.0 mm with ulceration	None	None
	>4.0 mm, no ulceration	None	None
IIC	>4.0 mm with ulceration	None	None
IIIA	Any tumour thickness, no ulceration	Micrometastases	None
IIIB	Any tumour thickness with ulceration	Micrometastases	None
	Any tumour thickness, no ulceration	Up to three macrometastases	None
	Any tumour thickness ± ulceration	None but satellite and/or in-transit metastases	None
IIIC	Any tumour thickness with ulceration	Up to three macrometastases	None
	Any tumour thickness ± ulceration	Four or more macrometastases, or lymph node involvement extending beyond capsule, or satellite and/or in-transit metastases with lymph node involvement	None
IV			Distant metastases

### 3.4 Mechanisms of melanoma progression and dissemination

As previously described, melanoma is highly metastatic and accounts for the majority of the cancer-related death among all skin cancers.

Melanoma cells usually metastasize to the lung, brain or liver (Braeuer et al. 2014). Therefore, they can respond and adapt to different organ microenvironments by acquiring specific characteristics. For example, human A375SM amelanotic melanoma cells grafted in different mouse organs showed the upregulation of neurological signalling genes only in cells implanted in brain (Park et al. 2011). In addition, tumor cells prepare the distant metastatic environment by priming the pre-metastatic niche throughout the so called “tumor exosome-driven education”. According to Hood et al., melanoma-derived exosomes educate endothelial cells (ECs) and lymph nodes by inducing expression of factors responsible for cell recruitment, matrix remodeling, and angiogenesis even in the absence of tumor cells (Hood et al. 2009, Hood, San and Wickline 2011). Moreover, melanoma cells are able to create a specific supporting microenvironment through the secretion of paracrine factors that allow them to grow, migrate and evade the immune response. The pro-inflammatory lipid Platelet-Activating Factor (PAF) activates keratinocytes, ECs, macrophages, fibroblasts, and cancer cells

promoting both cell survival and angiogenesis. Moreover, PAF is secreted by keratinocytes after UVR exposure and the binding of PAF to its receptor PAFR on keratinocytes induces the expression of other pro-inflammatory molecules such as COX-2, IL-6, and IL-8. The signal transduction of PAF in melanoma cells stimulates the production of matrix metalloproteases (MMPs) that play a critical role in the degradation of the basement membrane and the extracellular matrix to allow the invasion of melanoma cells (Zhang et al. 2006, Im et al. 1996). The transcription factor AP-2 $\alpha$  is generally downregulated during the vertical growth phase. Loss of AP-2 $\alpha$  correlates with decreased p21 levels and it is linked to poor prognosis. The transcription of the adhesion molecule MCAM/MUC18 is generally inhibited by the binding of AP-2 $\alpha$  to the *MCAM/MUC18* promoter. Consequently, reduced AP-2 $\alpha$  levels result in increased *MCAM/MUC18* expression on plasma membrane. In addition, the signal cascade of the activated PAFR leads to phosphorylation of CREB and subsequent expression of MCAM/MUC18 (Braeuer et al. 2011). Of note, the expression of this cell adhesion molecule augments as the tumor progresses. In this frame, *MCAM/MUC18* is highly expressed in advance primary melanoma, regional lymph nodes and metastasis, whereas it is barely expressed on normal epidermal melanocytes (Lehmann et al. 1987, Denton et al. 1992). In addition, the upregulation of several adhesion proteins such as MCAM/MUC18, L1-CAM, N-cadherin, VCAM, PECAM and VE-cadherin allows melanoma cells to start the intravasation process into the blood circulation as well as to adhere to the blood vessel wall and extravasate into the parenchyma (Zhang et al. 2019).

Both melanoma and stromal cells secrete immunosuppressive cytokines that abrogate the immune response. TNF- $\alpha$ , IL-8, and TGF- $\beta$  are expressed at very low levels in nevi and thin primary melanoma, whereas they are upregulated in thick primary tumors and metastases (Moretti et al. 1999, Mattei et al. 1994). TGF- $\beta$  negatively regulates T-cell proliferation, inhibits antigen presenting cells and promotes the differentiation and activation of T-reg that suppresses physiological and pathological immune responses (Braeuer et al. 2014). Moreover, melanoma cells may express specific T cell antigens. Physiologically, CTLA-4 is normally expressed on T cells, and it is involved in dampening their activation. Thus, melanoma cells expressing CTLA-4 can modulate the immune response. Likewise, programmed cell death ligand 1 (PD-L1) is highly expressed on malignant and stromal cells and its binding to PD-1 on the surface of T cells allows the downregulation of the immune response (Amaria et al. 2018). Accordingly, as described above, targeting PD-1 and/or CTLA-4 can significantly increase the immune response against melanoma.

Finally, to evade cytotoxicity, melanoma cells can also downregulate major histocompatibility complex I (MHC-I) components (Degenhardt et al. 2010) and this mechanism is at the basis of the resistance to anti-PD1 inhibitors in MITF<sup>low</sup>/AXL<sup>high</sup> de-differentiated tumors (Lee et al. 2020).

#### 4. GALC IN MELANOMA

As previously described, GALC may exert either an onco-suppressive or pro-tumorigenic role in cancer progression. Experimental evidence suggests that GALC may play an oncogenic role in melanoma.

Indeed, downregulation of *Galc* causes a decrease in the proliferation rate of silenced B16F10 murine melanoma cells (shGALC cells) compared to controls. Likewise, shGALC cells show a reduced colony formation ability, motility, and invasion capacity when compared to mock and wild-type cells. In addition, shGALC cells implanted in C57BL/6 mice exhibited a delay in tumor growth and a significant reduction in lung metastases when compared to controls. Interestingly, lipidomic analysis revealed increased levels of Cer and decreased amount of SM in these cells, possibly as a consequence of the upregulation of *Smpd3* expression. In keeping with this hypothesis, the administration of the neutral sphingomyelinase inhibitor GW4869 (Luberto et al. 2002) restored the rate of growth of shGALC grafts (Belleri et al. 2020).

In keeping with these observations in a murine melanoma model, Human Protein Atlas (["http://www.proteinatlas.org"](http://www.proteinatlas.org)) and Gene Expression Omnibus (<https://www.ncbi.nlm.nih.gov/geo>) data mining indicates that *GALC* expression levels in human specimens are related to melanoma progression. Accordingly, RNAscope analysis performed on 60 human melanoma specimens indicated that *GALC* expression levels positively correlate with melanoma progression and are paralleled to a progressive increase of MITF and tyrosinase immunoreactivity in the same samples (Belleri et al. 2020). In addition, the overexpression of *GALC* in the A2058 melanoma cell line leads to a higher proliferative capacity *in vitro* or when cells were grafted in NOD/Scid mice (Belleri et al. 2020).



#### **4.1 The pro-oncogenic sphingolipid-metabolizing enzyme $\beta$ -galactosylceramidase modulates the proteomic landscape in BRAF(V600E)-mutated human melanoma cells**

The mutation BRAF<sup>V600E</sup> is a tumor-driving mutation in approximately 50% of human cutaneous melanomas (Ascierto et al. 2012). The overexpression of catalytically active *GALC* in A2058 and A375 human melanoma cells harboring the BRAF<sup>V600E</sup> mutation leads to higher proliferation and migration in *in vitro* assays. At the proteomic level, the upregulation of GALC modulates the expression of proteins involved in different aspects of tumor progression, including melanoma biology, tumor invasion and metastatic dissemination, tumor immune escape, mitochondrial antioxidant activity, endoplasmic reticulum stress responses, autophagy. Notably, analysis of the expression of the corresponding genes in human skin cutaneous melanoma samples (TCGA, Firehose Legacy) using the cBioPortal for Cancer Genomics platform demonstrated a positive correlation between *GALC* expression and the expression levels of 14 out of the 27 genes identified by proteomic analysis, thus supporting our findings. Overall, these data indicate for the first time that the expression of the lysosomal sphingolipid-metabolizing enzyme GALC may exert a pro-oncogenic impact on the proteomic landscape in *BRAF*-mutated human melanoma.



Article

# The Pro-Oncogenic Sphingolipid-Metabolizing Enzyme $\beta$ -Galactosylceramidase Modulates the Proteomic Landscape in BRAF(V600E)-Mutated Human Melanoma Cells

Davide Capoferri <sup>1</sup> , Paola Chiodelli <sup>1,†</sup>, Marzia Corli <sup>1</sup>, Mirella Belleri <sup>1</sup>, Elisa Scalvini <sup>1</sup>, Luca Mignani <sup>1</sup>, Jessica Guerra <sup>1</sup>, Elisabetta Grillo <sup>1</sup> , Veronica De Giorgis <sup>2,3</sup>, Marcello Manfredi <sup>2,3</sup> and Marco Presta <sup>1,4,\*</sup>

<sup>1</sup> Unit of Experimental Oncology and Immunology, Department of Molecular and Translational Medicine, University of Brescia, 25123 Brescia, Italy; davide.capoferri@unibs.it (D.C.); luca.mignani@unibs.it (L.M.)

<sup>2</sup> Department of Translational Medicine, University of Piemonte Orientale, 28100 Novara, Italy; marcello.manfredi@uniupo.it (M.M.)

<sup>3</sup> Center for Allergic and Autoimmune Diseases, University of Piemonte Orientale, 28100 Novara, Italy

<sup>4</sup> Consorzio Interuniversitario Biotecnologie (CIB), Unit of Brescia, 25123 Brescia, Italy

\* Correspondence: marco.presta@unibs.it

† Current address: Dipartimento di Scienze della Vita e Sanità Pubblica, Università Cattolica del Sacro Cuore, 00168 Roma, Italy.



**Citation:** Capoferri, D.; Chiodelli, P.; Corli, M.; Belleri, M.; Scalvini, E.; Mignani, L.; Guerra, J.; Grillo, E.; De Giorgis, V.; Manfredi, M.; et al. The Pro-Oncogenic Sphingolipid-Metabolizing Enzyme  $\beta$ -Galactosylceramidase Modulates the Proteomic Landscape in BRAF(V600E)-Mutated Human Melanoma Cells. *Int. J. Mol. Sci.* **2023**, *24*, 10555. <https://doi.org/10.3390/ijms241310555>

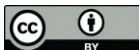
Academic Editors: Elisabetta Meacci and Paola Ghiorzo

Received: 18 May 2023

Revised: 13 June 2023

Accepted: 20 June 2023

Published: 23 June 2023



**Copyright:** © 2023 by the authors. Licensee MDPI, Basel, Switzerland.

This article is an open access article distributed under the terms and conditions of the Creative Commons Attribution (CC BY) license (<https://creativecommons.org/licenses/by/4.0/>).

**Abstract:**  $\beta$ -Galactosylceramidase (GALC) is a lysosomal enzyme involved in sphingolipid metabolism by removing  $\beta$ -galactosyl moieties from  $\beta$ -galactosylceramide and  $\beta$ -galactosylsphingosine. Previous observations have shown that GALC may exert pro-oncogenic functions in melanoma and *Galc* silencing, leading to decreased oncogenic activity in murine B16 melanoma cells. The tumor-driving BRAF(V600E) mutation is present in approximately 50% of human melanomas and represents a major therapeutic target. However, such mutation is missing in melanoma B16 cells. Thus, to assess the impact of GALC in human melanoma in a more relevant BRAF-mutated background, we investigated the effect of GALC overexpression on the proteomic landscape of A2058 and A375 human melanoma cells harboring the BRAF(V600E) mutation. The results obtained by liquid chromatography-tandem mass spectrometry (LC-MS/MS) demonstrate that significant differences exist in the protein landscape expressed under identical cell culture conditions by A2058 and A375 human melanoma cells, both harboring the same BRAF(V600E)-activating mutation. GALC overexpression resulted in a stronger impact on the proteomic profile of A375 cells when compared to A2058 cells (261 upregulated and 184 downregulated proteins versus 36 and 14 proteins for the two cell types, respectively). Among them, 25 proteins appeared to be upregulated in both A2058-upGALC and A375-upGALC cells, whereas two proteins were significantly downregulated in both GALC-overexpressing cell types. These proteins appear to be involved in melanoma biology, tumor invasion and metastatic dissemination, tumor immune escape, mitochondrial antioxidant activity, endoplasmic reticulum stress responses, autophagy, and/or apoptosis. Notably, analysis of the expression of the corresponding genes in human skin cutaneous melanoma samples (TCGA, Firehose Legacy) using the cBioPortal for Cancer Genomics platform demonstrated a positive correlation between GALC expression and the expression levels of 14 out of the 27 genes investigated, thus supporting the proteomic findings. Overall, these data indicate for the first time that the expression of the lysosomal sphingolipid-metabolizing enzyme GALC may exert a pro-oncogenic impact on the proteomic landscape in BRAF-mutated human melanoma.

**Keywords:** melanoma; proteomics;  $\beta$ -galactosylceramidase

## 1. Introduction

$\beta$ -Galactosylceramidase (GALC; EC 3.2.1.46) is a lysosomal acid hydrolase that catalyzes the removal of the  $\beta$ -galactose moiety from  $\beta$ -galactosylceramide and other sphingolipids [1]. Recent observations have shown that a progressive increase in GALC

expression occurs during melanoma progression in human pathological skin specimens ranging from common nevi to stage IV melanoma [1]. These data suggest that GALC might act as an oncogenic enzyme during melanoma progression. In keeping with this hypothesis, *Galc* knockdown causes a decrease in the tumorigenic and metastatic potential of murine melanoma B16 cells that also showed significant alterations in their lipidomic profile, characterized by increased levels of the oncosuppressive sphingolipid ceramide and of diacylglycerols, mirrored by a decrease in sphingomyelins, phosphatidylethanolamines, and cholesteryl esters. Accordingly, increased levels of ceramide were observed in GALC-silenced human melanoma A2058 cells and tumor xenografts, with a consequent decrease in their tumorigenic potential [1]. However, the mechanism(s) by which GALC exerts its pro-tumorigenic functions in melanoma remains poorly understood.

Mass spectrometry (MS)-based proteomics has been emerging as a core technique for largescale protein characterization in cells and tissue samples by providing a qualitative and quantitative analysis of proteins produced under different physiological and pathological conditions, including cancer [2]. Recently, analysis of the proteome has been considered as a tool for the advancement of diagnostic and prognostic biomarkers in melanoma, as well as for the identification of biological pathways leading to melanoma progression [3–5].

The BRAF(V600E)-activating mutation is present in approximately 50% of human melanomas and represents a major target for melanoma therapy [6]. However, such mutation is missing in murine melanoma B16 cells [7]. To obtain further insights into the role of GALC in human melanoma, liquid chromatography-tandem mass spectrometry (LC-MS/MS) was used in the present work to investigate the impact of *GALC* overexpression on the proteomic profile of BRAF-mutated human melanoma cells. To this aim, *GALC* was stably overexpressed in BRAF(V600E)-mutated A2058 and A375 human melanoma cells that express intermediate levels of *GALC* when compared to other human melanoma cell lines (Supplementary Figure S1). The use of two cell lines harboring the same driver mutation appeared to be necessary given the well-known tumor heterogeneity and would have allowed us to define common and individual protein profiles modulated by *GALC* overexpression in BRAF-mutated human melanoma cells.

The results of the present work extend previous observations about a pro-oncogenic role of GALC in *Braf* wildtype murine melanoma cells [1] by demonstrating that *GALC* overexpression increases the tumorigenic potential of human melanoma cells harboring the tumor-driving BRAF(V600E) mutation. Moreover, LC-MS/MS proteomic analysis, supported by transcriptomic data mining, demonstrates for the first time that *GALC* upregulation exerts a significant impact on the proteomic landscape of BRAF-mutated human melanoma cells, leading to the modulation of the expression of proteins involved in different aspects of tumor progression, including endoplasmic reticulum responses, the metastatic process, and tumor immune escape.

## 2. Results

### 2.1. *GALC* Overexpression in A2058 and A375 Melanoma Cells

A2058-upGALC and A375-upGALC cells, together with the corresponding control A2058-mock and A375-mock cells, were obtained by lentiviral infection, and *GALC* overexpression was confirmed by semiquantitative RT-PCR and enzymatic activity assays (Figure 1A,B). As shown in Figure 1C,D, A2058-upGALC and A375-upGALC cells showed a significant increase in their proliferative potential and their anchorage-independent growth ability when compared to the corresponding mock cells. In addition, *GALC*-overexpressing cells were characterized by increased motility when assessed in wound healing and Boyden chamber assays (Figure 1E,F). Together, these data indicate that *GALC* upregulation exerts a pro-oncogenic function on both A2058 and A375 cells. On this basis, LC-MS/MS proteomic analysis was performed on the cell extracts of mock and upGALC cells originating from both cell lines.

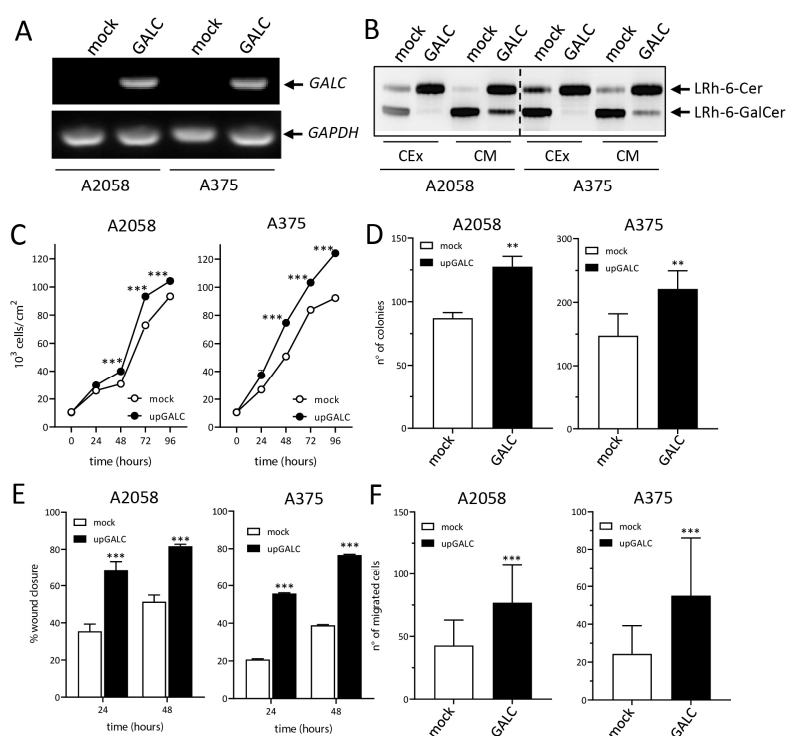


**Figure 1.** GALC upregulation affects the proliferative and migratory potential of human melanoma cells. RT-PCR (A) and enzymatic activity TLC (B) assays show the increased expression and activity of GALC in A2058-upGALC and A375-upGALC cell extracts (CEx) and conditioned media (CM) when compared to mock cells. GALC upregulation stimulates the growth (C) and colony formation capacity (D) of A2058 and A375 cells. GALC upregulation stimulates the migratory potential of A2058 and A375 cells after a mechanical scratch of the cell monolayer (E) and in a Boyden chamber chemotaxis assay (F). Data are the mean  $\pm$  SEM, \*\*  $p < 0.01$ , \*\*\*  $p < 0.001$ .

## 2.2. Analysis of A2058 and A375 Cell Proteomics

Given the well-known heterogeneity of the proteomic landscape even among cell lines originating from the same tumor type [8], a preliminary analysis was performed to compare the proteomic profile of A2058-mock and A375-mock cells. LC-MS/MS resulted in the identification (protein-level FDR below 1%) of 1471 and 1483 proteins for mock A2058 and A375 cells, respectively (Figure 2A,D). Among them, 1437 proteins were detected in both cell types. Comparative quantitative analysis of averaged spectral count values for the identified proteins resulted in 666 proteins equally expressed and 771 proteins differentially expressed in the two cell types. Among the differentially expressed proteins (Supplementary Table S1), 349 proteins were expressed at higher levels in A2058-mock cells and 422 proteins in A375-mock cells. Proteins that showed expression levels above the sensitivity threshold of the LC-MS/MS procedure in only one of the two cell types (13 and 22 proteins for A2058-mock and A375-mock cells, respectively) were included in the corresponding list of upregulated proteins, resulting in 362 and 444 entries for A2058-mock cells and A375-mock cells, respectively.

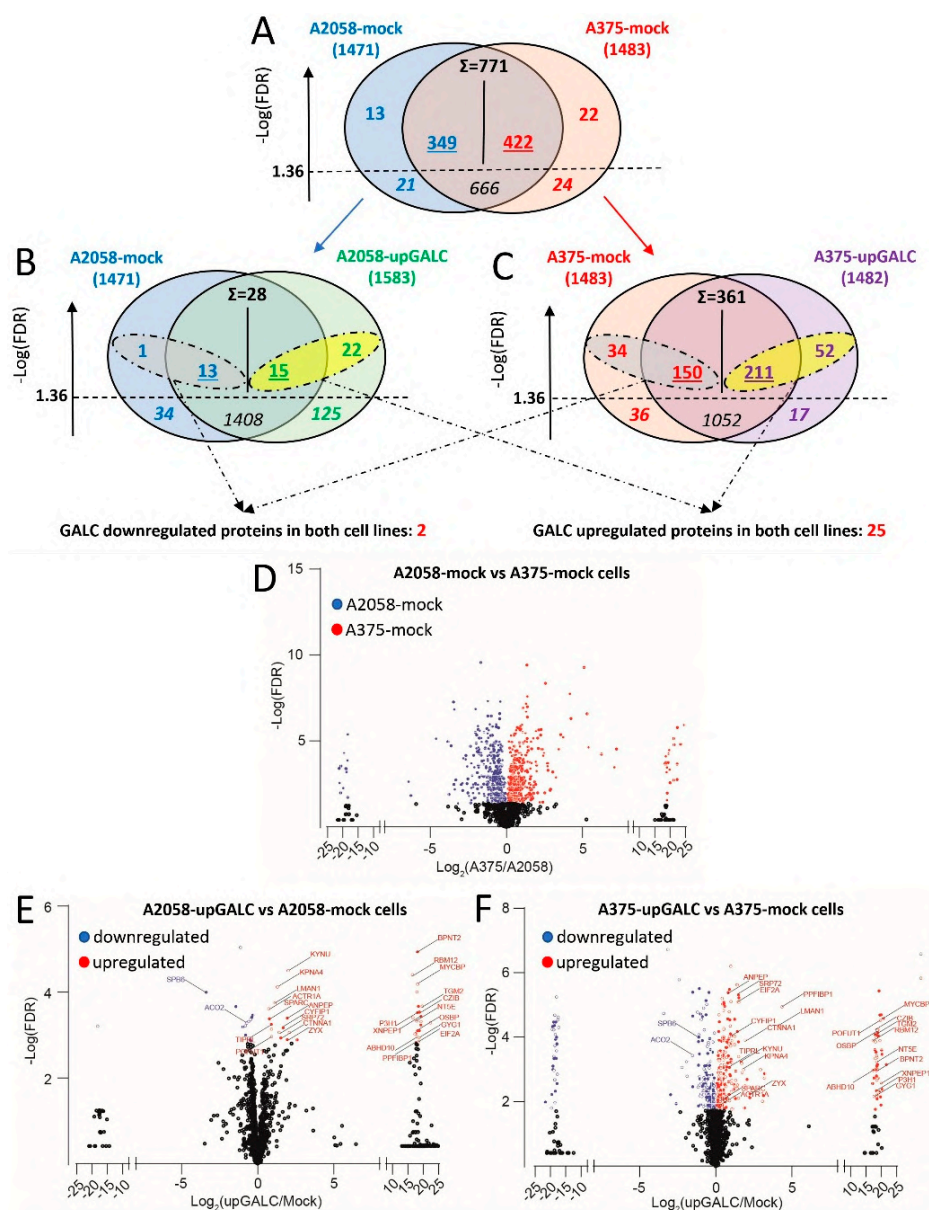


**Figure 2.** Summary of the quantitative data obtained by proteomic analysis of mock and upGALC cells. (A–C) Comparison of protein counts identified for (A) A2058-mock vs. A375-mock cells, (B) A2058-mock vs. A2058-upGALC cells, and (C) A375-mock vs. A375-upGALC cells. Each Venn diagram shows the breakdown of protein counts identified between the two groups.  $\Sigma$ : total number of proteins differentially expressed in the two groups. Underlined numbers: proteins expressed at significantly higher levels in the corresponding group. Numbers in italics: proteins expressed at the same level in the two groups. Numbers in bold above the  $-\text{Log}(\text{FDR})$  threshold value of 1.36 represent the number of proteins detected at a significant level in only one group, whereas those below the threshold value (bold and italics) represent the number of proteins detected in only one group but below the confidence level. (D,E) Volcano plot representation of proteins differentially expressed in A2058-mock vs. A375-mock cells (D), A2058-upGALC vs. A2058-mock cells (E), A375-upGALC vs. A375-mock cells (F).

When analyzed with the gene-set enrichment tool ShinyGO [9], A2058-mock cells showed higher levels of expression for proteins associated with KEGG pathways related to energetic metabolism when compared to A375-mock cells, including, among others, oxidative phosphorylation, mitochondrial function, and TCA cycle (Figure 3A). Accordingly, the Gene Ontology (GO) molecular function, biological process, and cellular component terms also related to energetic processes associated with mitochondrial activity were significantly enriched in the set of the 362 proteins more expressed in A2058-mock cells (Figure 3B).

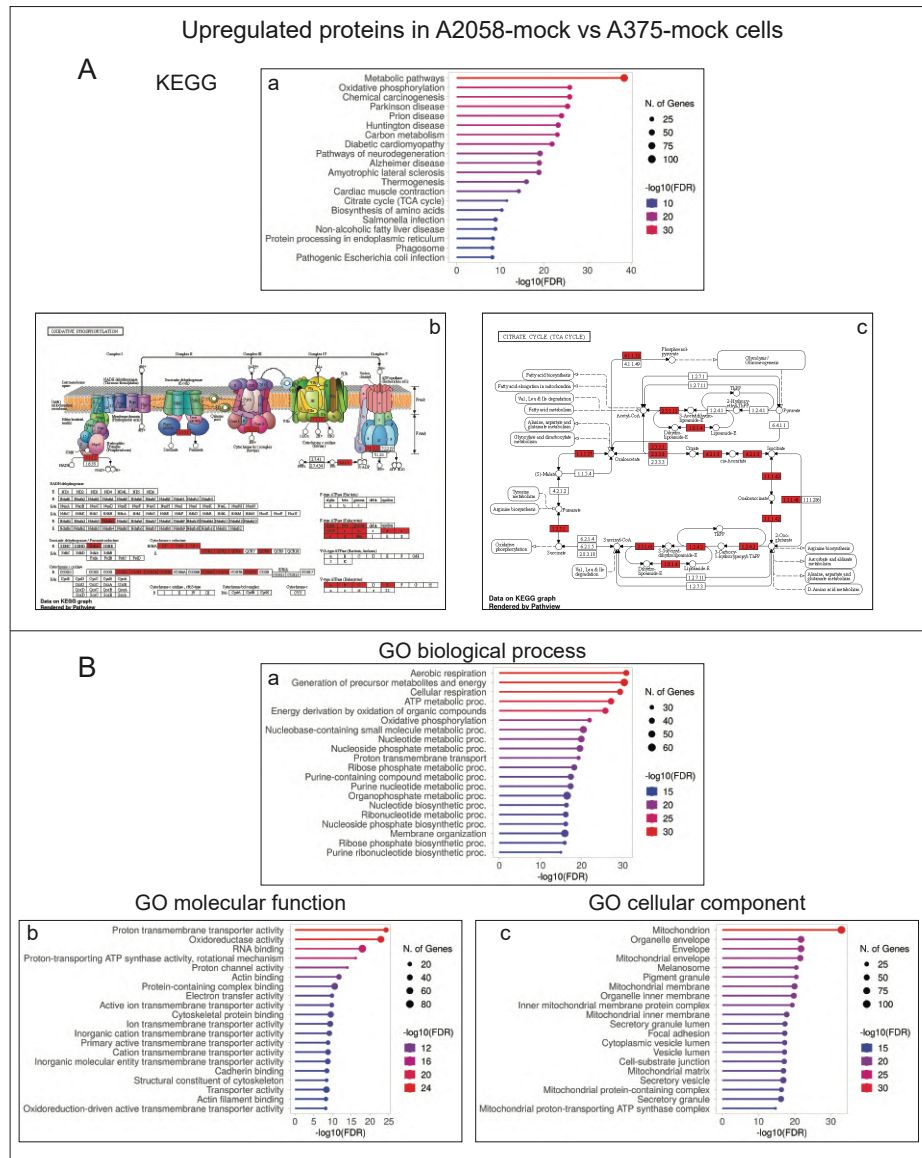


**Figure 3.** KEGG and Gene Ontology annotation of proteins expressed at higher levels in A2058-mock vs. A375-mock cell extracts. **(A)** Enriched KEGG pathways are related to energetic metabolism, including oxidative phosphorylation, mitochondrial function, and the TCA cycle (a). Pathview rendering of oxidative phosphorylation (b) and TCA cycle (c) KEGG pathways showing the proteins expressed at higher levels in A2058-mock vs. A375-mock cell extracts (in red). **(B)** Significantly enriched GO biological process (a), molecular function (b), and cellular component (c) terms are related to energetic processes associated with mitochondrial activity.

At variance, the 444 proteins expressed at higher levels in A375-mock cells were more significantly associated with the ribosome and spliceosome KEGG pathways (Figure 4A). In keeping with these findings, the corresponding enriched GO terms referred to categorizations related to mRNA binding/splicing and ribosomes (Figure 4B).

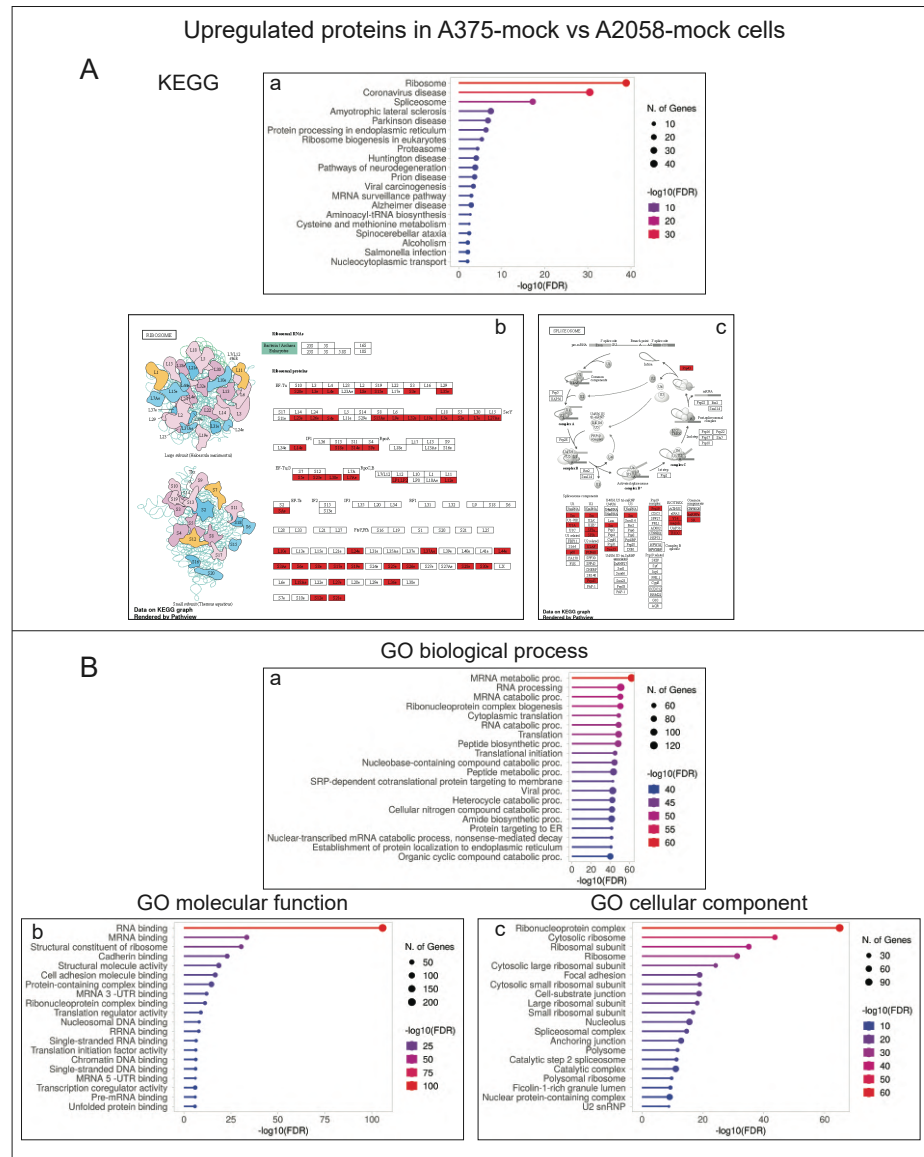


**Figure 4.** KEGG and Gene Ontology annotation of proteins expressed at higher levels in A375-mock vs. A2058-mock cell extracts. (A) The proteins expressed at higher levels in A375-mock cells are significantly associated with the ribosome and spliceosome KEGG pathways (a). Pathview rendering of the ribosome (b) and spliceosome (c) KEGG pathways showing the proteins expressed at higher levels in A375-mock vs. A2058-mock cell extracts (in red). (B) Significantly enriched GO biological process (a), molecular function (b), and cellular component (c) terms refer to categorizations related to mRNA binding/splicing and ribosomes.

Of note, A2058-mock and A375-mock cells differentially express proteins involved in the protein processing that occurs in the endoplasmic reticulum (ER). Indeed, A2058-mock

cells express higher levels of proteins belonging to the ubiquitin ligase complex, whereas A375-mock cells express higher levels of proteins related to ER-associated degradation (Figure 5).

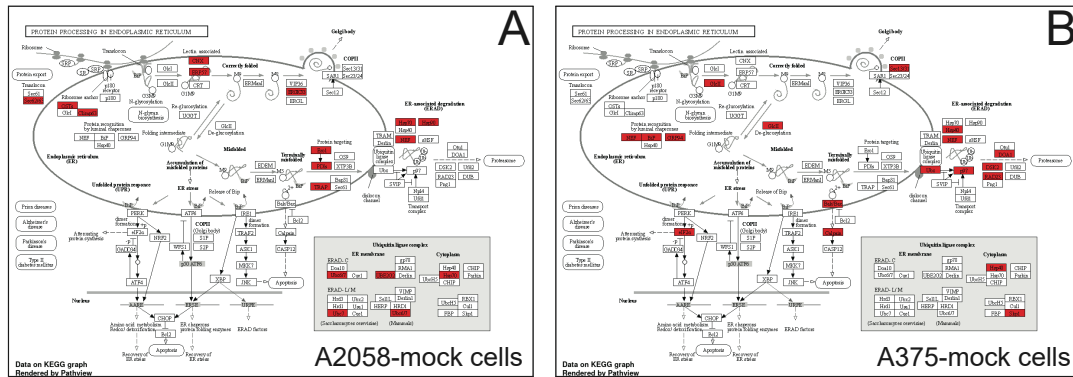


**Figure 5.** A2058-mock and A375-mock cells differentially express proteins involved in the protein processing that occurs in the ER. Pathway rendering of the protein processing in endoplasmic reticulum KEGG pathway showing the proteins expressed at higher levels in A2058-mock (A) and A375-mock (B) cell extracts (in red).

Together, these data indicate that significant differences exist in the protein landscape expressed under identical cell culture conditions by A2058 and A375 human melanoma cells, both harboring the same BRAF(V600E)-activating mutation.

### 2.3. Impact of GALC Overexpression on the Proteomic Profile of A2058 and A375 Cells

As observed for mock cells, LC-MS/MS analysis identified 1583 and 1482 proteins in A2058-upGALC and A375-upGALC cell extracts, respectively (Figure 2B,C). When compared to the corresponding control A2058-mock cells, 37 proteins were upregulated, and 14 proteins were downregulated upon GALC transduction in A2058 cells, whereas the levels of expression of 1408 proteins remained unchanged (Figure 2B,E and Supplementary Table S2). At variance, GALC overexpression in A375 cells resulted in the upregulation of the levels of 263 proteins and in the downregulation of 184 proteins, while 1052 proteins remained unchanged (Figure 2C,F and Supplementary Table S3). Thus, GALC overexpression resulted in a stronger impact on the proteomic profile of A375 cells when compared to A2058 cells ( $p < 0.0001$ , chi-square test).

ShinyGO categorization analysis of the 37 proteins upregulated in A2058-upGALC cells did not allow unambiguous identification of enriched GO terms, with just three entries associated with the “nicotinate and nicotinamide metabolism” KEGG. At variance, despite their limited number, the 14 downregulated proteins were found to belong to enriched KEGG pathways and GO terms related to mitochondrial processes, including oxidative phosphorylation, mitochondrial respiratory chain complexes, and aerobic respiration (Figure 6).

Concerning A375-upGALC cells, categorization analysis indicated that upregulated proteins were mainly associated with spliceosome and oxidative phosphorylation KEGG pathways and to GO terms related to the RNA metabolism/ribonucleoprotein complex and to various metabolic processes (Figure 7).



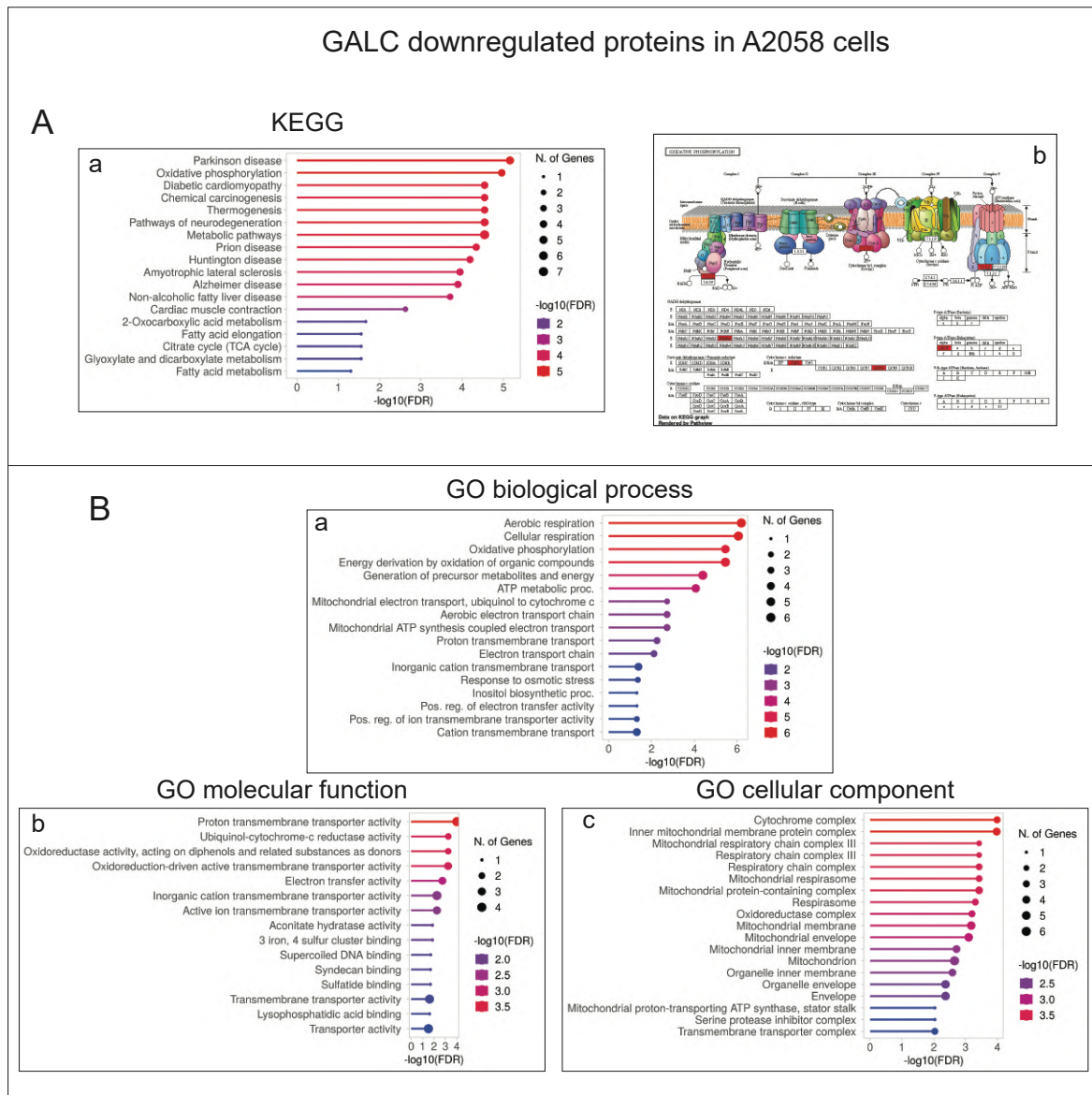
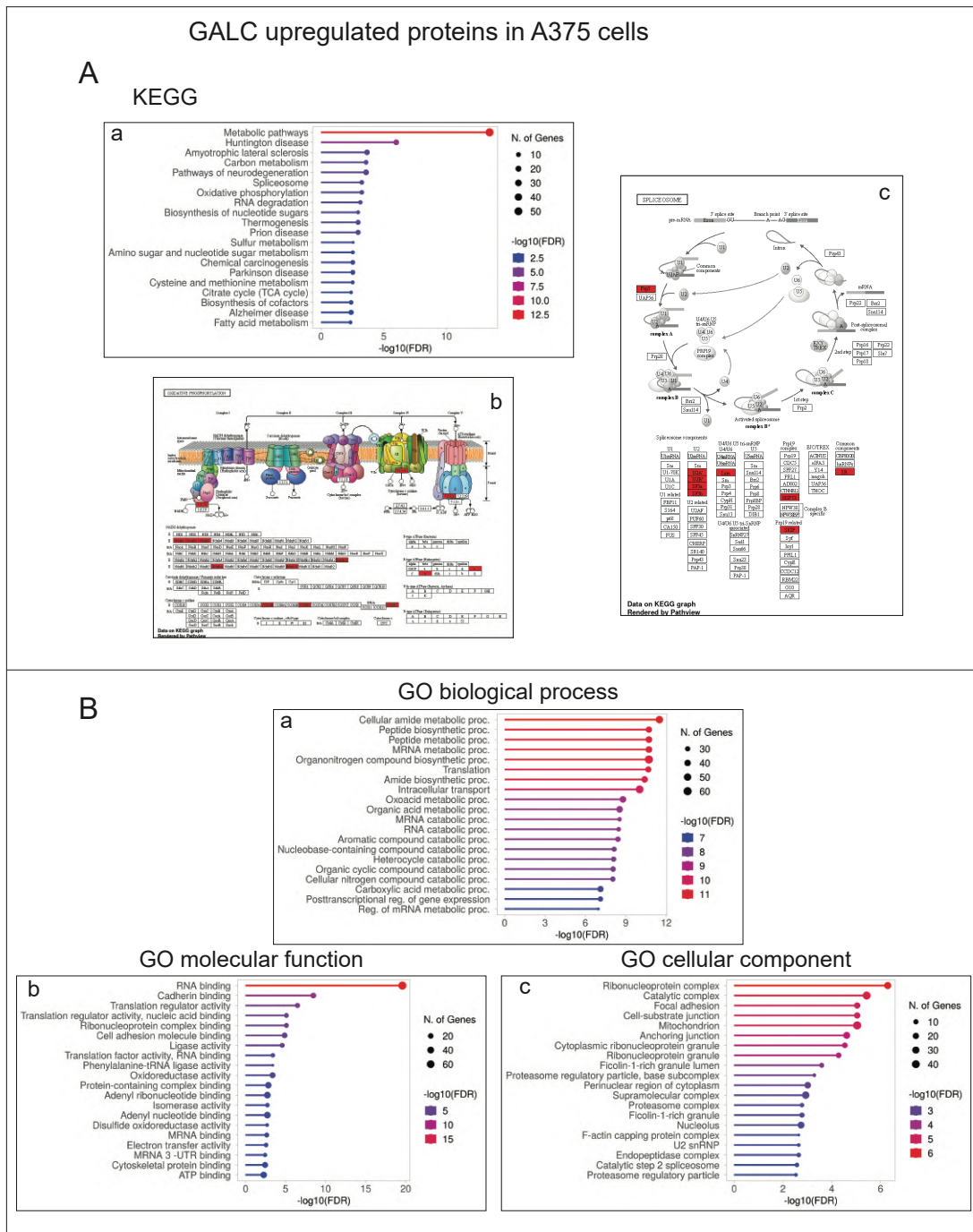


**Figure 6.** KEGG and Gene Ontology annotation of proteins downregulated following GALC overexpression in A2058-upGALC cells. **(A)** Enriched KEGG pathways are related to energetic metabolism, including oxidative phosphorylation (a). Pathview rendering of the oxidative phosphorylation KEGG pathways (b) showing the proteins expressed at higher levels in A2058-upGALC vs. mock cell extracts (in red). **(B)** Significantly enriched GO biological process (a), molecular function (b), and cellular component (c) terms are related to mitochondrial processes, including oxidative phosphorylation, mitochondrial respiratory chain complexes, and aerobic respiration.



Notably, the 184 proteins downregulated in A375-upGALC cells were also more significantly associated with the spliceosome and TCA cycle/oxidative phosphorylation KEGG pathways. Accordingly, enriched GO terms belonging to biological process, molecular function, and cellular component categorizations of these downregulated proteins referred mainly to mRNA binding/splicing as well as aerobic respiration and mitochondrion (Figure 8).

Overall, this categorization analysis suggests that *GALC* upregulation modulates the protein landscape in melanoma cells by affecting the biological processes related to RNA metabolism and mitochondria function.

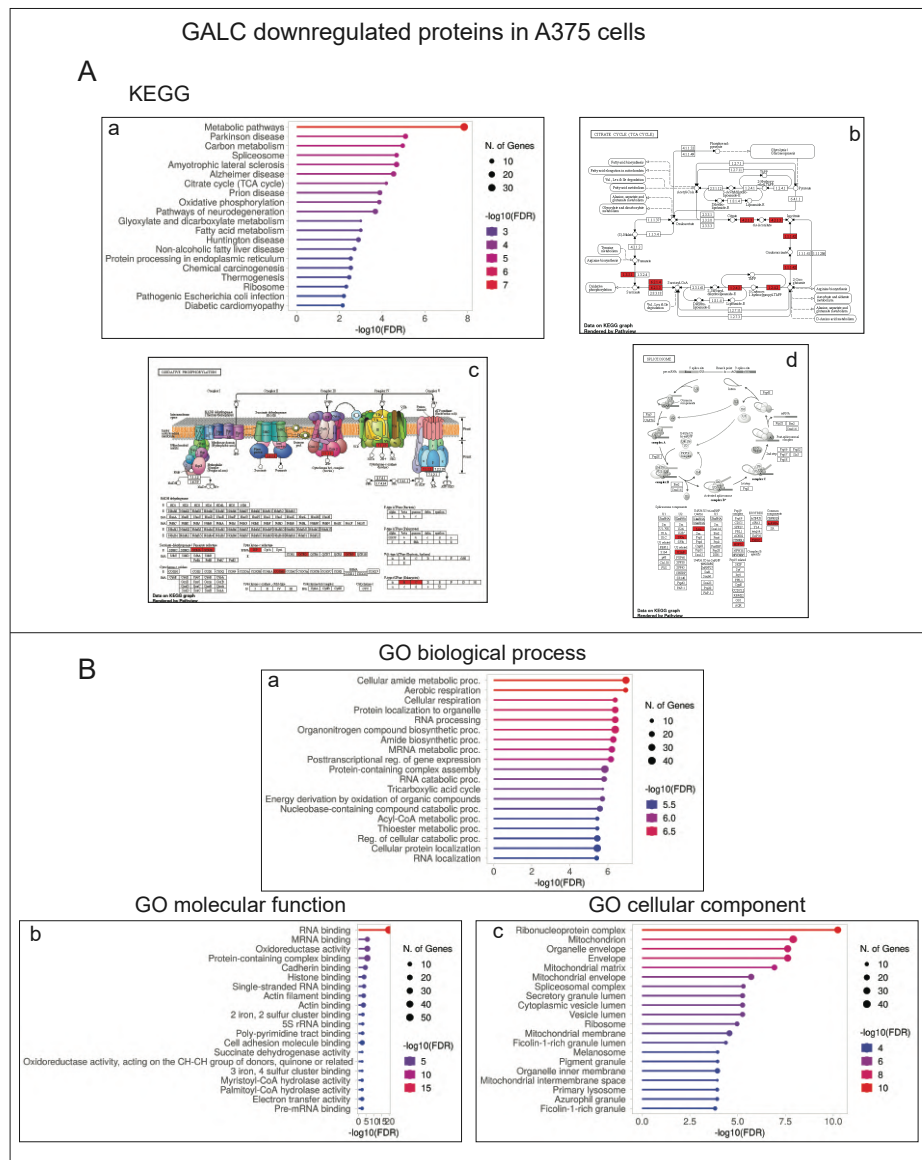


**Figure 8.** KEGG and Gene Ontology annotation of proteins downregulated following GALC overexpression in A375-upGALC cells. (A) Enriched KEGG pathways are related to metabolic pathways, including oxidative phosphorylation and spliceosome (a). Pathview rendering of TCA cycle (b), oxidative phosphorylation (c) and spliceosome (d) KEGG pathways showing the proteins expressed at lower levels in A375-upGALC vs. mock cell extracts (in red). (B) Significantly enriched GO biological process (a), molecular function (b), and cellular component (c) terms refer mainly to mRNA binding/splicing as well as aerobic respiration and mitochondrion.

Based on these premises, we investigated which proteins were downregulated or upregulated by GALC transduction in both cell lines by comparing the entries shown in Supplementary Tables S2 and S3. Twenty-five proteins appeared to be upregulated in both A2058-upGALC and A375-upGALC cells, whereas only two proteins were significantly downregulated in both GALC-overexpressing cell types. The list of these proteins and a brief description of their biological function(s) in cancer (including human melanoma when available) are shown in Table 1.

**Table 1.** List of common significantly up- and downregulated proteins upon GALC transduction in both A2058 and A375 cell lines. Each entry is completed by the name of the gene encoding for the listed protein and its known referenced biological function.

Protein	Gene	Biological Function
		Significantly upregulated
Abhydrolase domain-containing 10, depalmitoylase	<i>ABHD10</i>	A mitochondrial acyl-protein thioesterase modulating mitochondrial antioxidant ability [10].
Actin-related protein 1A	<i>ACTR1A</i>	A 42.6 kD subunit of dynactin complex associated with the centrosome and involved in microtubule-based vesicle motility, including ER-to-Golgi transport and the centripetal movement of lysosomes and endosomes. Potential biomarker in pituitary and colon cancers [11,12].
Aminopeptidase N	<i>ANPEP</i>	A membrane-bound zinc metalloprotease involved in the metabolism of regulatory peptides. It promotes angiogenesis, tumor growth, and metastasis in melanoma [13,14].
3'(2'), 5'-Bisphosphate nucleotidase 2	<i>BPNT2</i>	Member of the inositol monophosphatase family localized to the Golgi apparatus. It catalyzes the hydrolysis of phosphoadenosine phosphate to AMP. No data are available about its role in cancer.
Catenin alpha 1	<i>CTNNA1</i>	It connects cadherins located on the plasma membrane to the actin filaments, playing an important role in the cell adhesion process. CTNNA1 germLine variants are associated with hereditary gastric cancer [15].
Cytoplasmic FMR1-interacting protein 1	<i>CYFIP1</i>	It regulates cytoskeletal dynamics and protein translation. Involved in tumor metastasis [16].
CXXC motif-containing zinc-binding protein	<i>CZIB</i>	Previously referred to as C1orf123, its function remains unknown.
Eukaryotic translation initiation factor 2A	<i>EIF2A</i>	It directs the binding of methionyl-tRNAi to 40S ribosomal subunits in a codon-dependent manner. Involved in ER stress in cancer via the (PERK)-eIF2a-ATF4-CHOP signaling axis [17].
Glycogenin 1	<i>GYG1</i>	A glycosyltransferase involved in the first steps of glycogen synthesis. A target of miR-194/192 whose expression is downregulated in hepatocellular carcinoma [18].
Karyopherin subunit alpha 4	<i>KPNA4</i>	Karyopherins, or importins, are cytoplasmic proteins that recognize NLSs and dock NLS-containing proteins to the nuclear pore complex. Oncosuppressor involved in tumor immune escape [19].
Kynureninase	<i>KYNU</i>	It is involved in the biosynthesis of NAD cofactors from tryptophan through the kynurenine pathway. Overexpressed in lung adenocarcinoma, it is associated with immunosuppression and poor survival [20].
Lectin mannose-binding 1 or ER-Golgi intermediate compartment 53 kDa protein (ERGIC-53)	<i>LMAN1</i>	Membrane mannose-specific lectin that cycles between the ER, ER-Golgi intermediate compartment, and cis-Golgi, functioning as a cargo receptor for glycoprotein transport. Involved in ER stress and autophagy in human melanoma [21].
MYC-binding protein	<i>MYCBP</i>	It binds to the N-terminus of the oncogenic protein C-MYC, enhancing its transcriptional activity. Involved in EMT and progression of triple-negative breast cancer [22].
5'-Nucleotidase ecto	<i>NT5E</i>	Plasma membrane protein that catalyzes the conversion of extracellular nucleotides to membrane-permeable nucleosides. Involved in melanoma immune escape via the CD73/adenosine axis [23].
Oxysterol-binding protein	<i>OSBP</i>	Lipid transporter involved in lipid counter transport between the Golgi complex and ER membranes. Potential marker for cholangiocarcinoma metastasis [24].
Prolyl 3-hydroxylase 1	<i>P3H1</i>	Member of the collagen prolyl hydroxylase family. Localized to the ER, its activity is required for proper collagen synthesis and assembly. Highly expressed by most tumors and associated with overall survival, its knockdown hampers liver cancer cell proliferation, migration, and invasion [25].
Protein O-fucosyltransferase 1	<i>POFUT1</i>	Member of the glycosyltransferase O-Fuc family, it adds O-fucose through an O-glycosidic linkage to conserved serine or threonine residues in the epidermal growth factor-like repeats of several cell surface and secreted proteins. Tumor promoter via Notch signaling [26].

Table 1. Cont.

Protein	Gene	Biological Function
PPFIA-binding protein 1	<i>PPFIBP1</i>	Member of the LAR protein tyrosine phosphatase-interacting protein (liprin) family. Liprins interact with members of the LAR family of transmembrane protein tyrosine phosphatases. Drives tumor cell migration and invasion via the FAK/Src/JNK pathway [27].
RNA-binding motif protein 12	<i>RBM12</i>	It contains several RNA-binding motifs, potential transmembrane domains, and proline-rich regions. It plays a key role in liver cancer immunity [28].
Secreted protein acidic and rich in cysteine	<i>SPARC</i>	Cysteine-rich acidic matrix-associated protein. Involved in melanoma metastatic dissemination [29].
Signal recognition particle 72	<i>SRP72</i>	72 kDa subunit of the signal recognition particle, a ribonucleoprotein complex that mediates the targeting of secretory proteins to the ER. Involved in epithelial cancers [30].
Transglutaminase 2	<i>TGM2</i>	It catalyzes the crosslinking of proteins by epsilon-gamma glutamyl lysine isopeptide bonds. Involved in radioresistance in melanoma [31].
TOR signaling pathway regulator	<i>TIPRL</i>	Allosteric regulator of serine/threonine-protein phosphatase 2A. The TIPRL/PP2A axis affects apoptosis and proliferation of cancer cells [32].
X-prolyl aminopeptidase 1	<i>XPNPEP1</i>	Cytosolic metalloaminopeptidase that catalyzes the cleavage of the N-terminal amino acid adjacent to a proline residue. Its expression is associated with disease progression and shorter overall survival in multiple myeloma [33].
Zyxin	<i>ZYX</i>	A zinc-binding phosphoprotein that concentrates at focal adhesions and along the actin cytoskeleton. It may function as a messenger in the signal transduction pathway that mediates adhesion-stimulated changes in gene expression and may modulate the cytoskeletal organization of actin bundles. Its expression is directly related to melanoma cell spreading and proliferation and inversely related to their differentiation [34].
		Significantly downregulated
Aconitase 2	<i>ACO2</i>	It catalyzes the interconversion of citrate to isocitrate via cis-aconitate in the second step of the TCA cycle. Oncosuppressor affecting TCA cycle and mitochondrial oxidative metabolism in cancer cells [35,36].
Serpin family B member 6	<i>SERPINB6</i>	A member of the serine proteinase inhibitor superfamily. Its dysregulation is associated with autophagic and apoptotic induction in cancer cells [37].

Notably, 6 out of the 27 proteins modulated by *GALC* overexpression in both A2058-up*GALC* and A375-up*GALC* cells have been involved in melanoma biology (i.e., aminopeptidase N (CD13), lectin mannose-binding 1,5'-nucleotidase ecto (CD73), secreted protein acidic and cysteine rich, transglutaminase 2, and zyxin, encoded, respectively, by *ANPEP*, *LMAN1*, *NT5E*, *SPARC*, *TGM2*, and *ZYX* genes), 8 proteins have been involved in tumor invasion and metastatic dissemination (i.e., aminopeptidase N (CD13), cytoplasmic FMR1-interacting protein 1, catenin alpha 1, oxysterol-binding protein, prolyl 3-hydroxylase 1, PPFIA-binding protein 1, secreted protein acidic and cysteine rich, and zyxin, encoded, respectively, by *ANPEP*, *CYFIP1*, *CTNNA1*, *OSBP*, *P3H1*, *PPFIBP1*, *SPARC*, and *ZYX* genes), 4 proteins have been implicated in tumor immune escape (i.e., karyopherin subunit alpha 4, kynureninase, 5'-nucleotidase ecto (CD73), and RNA-binding motif protein 12, encoded, respectively, by *KPNA4*, *KYNU*, *NT5E*, and *RBM12* genes), and 10 proteins have been shown to play a role in ER stress responses, mitochondrial antioxidant activity, autophagy, and/or apoptosis (i.e., lectin mannose-binding 1, eukaryotic translation initiation factor 2A, signal recognition particle 72, actin-related protein 1A, abhydrolase domain-containing 10 (depalmitoylase), glycogenin 1, aconitase 2, serpin family B member 6, TOR signaling pathway regulator, and X-prolyl aminopeptidase 1, encoded, respectively, by *LMAN1*, *EIF2A*, *SRP72*, *ACTR1A*, *ABHD10*, *GYG1*, *ACO2*, *SERPINB6*, *TIPRL*, and *XPNPEP1* genes) (see Table 1 and references therein).

Next, RT-qPCR analysis was performed on A2058-up*GALC* vs. A2058-mock cells to assess the expression levels of genes encoding for various proteins up- or downregulated by *GALC* overexpression in *BRAF*-mutated melanoma cells. As shown in Supplementary Figure S2, the results of RT-qPCR analysis were congruent with proteomic data.

Finally, the correlation between *GALC* mRNA levels and the expression of the genes encoding for the 27 proteins similarly modulated by *GALC* upregulation in A2058 and A375 cells was assessed in 448 human skin melanoma samples (TCGA, Firehose Legacy) using the cBioPortal for Cancer Genomics platform [38,39]. As shown in Figure 9, the

expression levels of 14 out of the 27 genes investigated show a significant correlation with GALC expression in human melanoma specimens, congruent with the proteomic data.

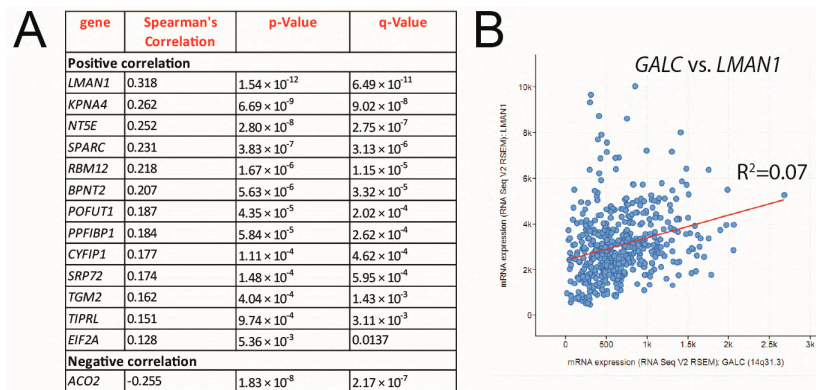


**Figure 9.** *GALC* expression in human melanoma specimens correlates with the expression of proteins identified by proteomic analysis of up*GALC* vs. mock melanoma cells. Correlation of *GALC* expression with the expression of the genes encoding for the proteins similarly modulated by *GALC* upregulation in A2058 and A375 cells was assessed in 448 human skin cutaneous melanoma samples (TCGA, Firehose Legacy) using the cBioPortal for Cancer Genomics platform (A). Correlation between *GALC* and *LMAN1* expression in human melanoma (B).

### 3. Discussion

*GALC* is a lysosomal enzyme involved in sphingolipid metabolism by removing  $\beta$ -galactose from  $\beta$ -galactosylceramide and other terminal  $\beta$ -galactose-containing sphingolipids. Recent observations indicate that this enzyme might be involved in tumor progression (reviewed in [40]). In keeping with this hypothesis, immunohistochemical data have shown that high levels of *GALC* immunoreactivity are associated with poor prognosis in colorectal cancer patients [41] and that higher *GALC* expression levels in circulating lung cancer cells correlate with a poor response to therapy, representing a possible predictor biomarker in these patients [42]. In line with these findings and with the observation that sphingolipid metabolic reprogramming plays an important role in melanoma progression [43], analysis of human specimens ranging from common nevi to stage IV melanoma demonstrated a gradual increase in *GALC* expression during tumor progression that goes along with a decrease in ceramide levels [1]. Accordingly, *Galc* silencing results in significant inhibition of the tumorigenic and metastatic activity of *Braf* wildtype murine melanoma B16-F10 cells that showed alterations in their sphingolipid profile, characterized by an increase in the intracellular levels of the oncosuppressor sphingolipid ceramide. A similar ceramide accumulation was observed in human melanoma cells following *GALC* downregulation [1].

Here, we extend these observations and demonstrate that *GALC* overexpression plays a pro-tumorigenic function on both A2058 and A375 human melanoma cells that harbor the *BRAF*(V600E)-activating mutation, which is present in approximately 50% of human melanomas [6]. A2058 and A375 cells express intermediate levels of *GALC* mRNA and protein when compared to other human melanoma cell lines (Supplementary Figure S1), being therefore suitable for assessing the impact of the upregulation of this enzyme on the biological behavior of human melanoma cells in a *BRAF*-mutated background. Indeed, our data indicate that *GALC* upregulation induces a significant increase in the proliferative potential and anchorage-independent growth of both *BRAF*-mutated human cell lines, paralleled by increased cell motility in a Boyden chamber assay and after in vitro wounding of the cell monolayer.

These findings prompted us to investigate the impact of *GALC* upregulation on the proteomic landscape of both A2058 and A375 human melanoma cells. The results of the LC-

MS/MS analysis of the cell extracts of control and *GALC*-overexpressing cells indicate that significant differences exist in the protein landscape expressed under identical cell culture conditions by the two melanoma cell lines that harbor the same driver mutation. Indeed, in keeping with the well-known heterogeneity of the proteomic landscape, even among cell lines originating from the same tumor type [8], 771 proteins (52%) out of 1437 proteins detected in both control A2058 and A375 cells were present at different levels in the two cell types. Notably, KEGG and GO categorizations indicated that A2058-mock cells express higher levels of proteins related to energy metabolism and mitochondrial activity, whereas proteins related to mRNA binding/splicing and ribosome terms are present at higher levels in A375-mock cell extracts. Experimental evidence indicates that BRAF-driven ER stress and unfolded protein response play an important role in melanoma (reviewed in [44]). In this frame, a further indication of melanoma cell heterogeneity derives from the observation that A2058-mock and A375-mock cells differentially express proteins involved in the protein processing that occurs in the ER, A2058-mock cells expressing higher levels of proteins belonging to the ubiquitin ligase complex, whereas A375-mock cells are characterized by higher levels of proteins related to the ER-associated protein degradation process.

Based on this cell heterogeneity, it is not surprising that *GALC* overexpression exerted a different impact on the proteomic landscape of the two melanoma cell lines. Indeed, *GALC* transduction in A2058 cells resulted in the up- or downregulation of the expression levels of 37 and 14 proteins, respectively, whereas it exerted a stronger impact on A375 cells (263, and 184 proteins up- or downregulated, respectively). At present, the mechanisms responsible for such differences remain unknown. It will be interesting to evaluate the impact exerted by *GALC* overexpression on the sphingolipidomic profile of the two cell lines.

Despite the differences observed between the two cell lines in terms of the number of proteins whose levels are modulated by *GALC* upregulation, categorization analysis indicates a significant enrichment in both cell lines of downmodulated proteins involved in mitochondrial functions, including oxidative phosphorylation, mitochondrial respiratory chain complexes, and aerobic respiration. Melanoma cells can shuttle between glycolysis and respiration depending upon conditions of growth, hypoxia, acidosis, and therapy, and BRAF activity has been shown to suppress oxidative phosphorylation, thus driving aerobic glycolysis in melanoma (see [45] and references therein). Thus, *GALC* appears to modulate the energetic plasticity of melanoma cells by metabolic reprogramming. In this frame, it is interesting to note that alterations in the sphingolipid metabolism via modulation of the expression levels of the lysosomal acid ceramidase affect mitochondria activity in melanoma cells [46]. Further studies will be required to elucidate the impact of *GALC* on the rewiring of energetic metabolism in melanoma.

Among the proteins whose levels of expression were affected by *GALC* overexpression in melanoma cells, 25 of them were upregulated in both A2058-up*GALC* and A375-up*GALC* cells, whereas only 2 of them were downregulated in both cell types. Of note, six proteins are known to play a significant role in human melanoma. Indeed, aminopeptidase N (CD13) promotes melanoma growth, angiogenesis, and metastatic dissemination [13,14]. Similarly, the cysteine-rich acidic matrix-associated protein (SPARC) plays a role in melanoma metastasis [29], whereas lectin mannose-binding 1 (LMAN1) is involved in melanoma ER stress and autophagy [21], and the expression of the zinc-binding, focal adhesion-associated phosphoprotein zyxin has been shown to affect melanoma cell spreading and proliferation [34]. Finally, transglutaminase 2 plays a role in melanoma radioresistance [31], whereas the plasma membrane protein 5'-nucleotidase ecto (CD73) may favor melanoma immune escape via the CD73/adenosine axis [23].

Together with CD13, SPARC, and zyxin, *GALC*-upregulated cytoplasmic FMR1-interacting protein 1 and catenin alpha 1 are also implicated in the metastatic process by regulating cytoskeletal dynamics and cell adhesion of tumor cells [15,16], PPFIA-binding protein 1 drives tumor cell migration and invasion via the FAK/Src/JNK pathway [27], ER-associated collagen prolyl 3-hydroxylase 1 plays a pivotal role in cancer cell prolifer-

ation, migration, and invasion [25], and the lipid transporter oxysterol-binding protein has been proposed as a potential marker for cholangiocarcinoma metastasis [24]. Together, these data suggest that GALC may modulate the metastatic potential of melanoma cells. In keeping with this hypothesis, *GALC* is expressed at higher levels in human melanoma metastases when compared to primary tumors, and *Galc* knockdown hampers the capacity of murine melanoma B16-F10 cells to form experimental lung metastases [1].

Immune system evasion represents a hallmark of melanoma progression [47]. Our data indicate that, besides CD73, *GALC* transduction induces an increase in the levels of the importin karyopherin subunit alpha 4, kynureninase, and RNA-binding motif protein 12, all involved in tumor immune escape [19,20,28]. In keeping with a possible role for alterations in the sphingolipid metabolism in immune evasion, sphingolipid pathway enzymes have been shown to modulate immune cell function in cancer [48], sphingomyelin appears to play a key role in tumor progression and immune evasion [49], and neutral sphingomyelinase 2 expression impairs melanoma growth by enhancing CD8+ T-cell responses [50]. Whether and how *GALC* represents a key player in modulating immune responses in melanoma remains to be investigated.

A possible role of *GALC* in ER functions in cancer is supported by the observation that *GALC* overexpression induces not only the upregulation of the levels of the overmentioned LMAN1 that functions as a cargo receptor for glycoprotein transport in the ER [21] but also of the levels of the eukaryotic translation initiation factor 2A involved in ER stress in cancer via the (PERK)-eIF2a-ATF4-CHOP signaling axis [17], the signal recognition particle 72 that mediates the targeting of secretory proteins to the ER [30], and the actin-related protein 1A implicated in the ER-to-Golgi transport and lysosome/endosome movement, representing a possible biomarker for pituitary and colon cancers [11,12].

In keeping with the hypothesis that *GALC* may modulate the energetic plasticity of melanoma cells (see above), both *GALC*-transduced A2058 and A375 cells are characterized by higher levels of the mitochondrial abhydrolase domain-containing 10 able to affect the mitochondrial antioxidant activity [10] and of glycogenin 1, a glycosyltransferase involved in the first steps of glycogen synthesis downregulated in liver cancers [18]. In addition, *GALC* upregulation causes the downregulation of the oncosuppressor aconitase 2, which affects the TCA cycle and mitochondrial oxidative metabolism in cancer cells [35,36], and of the serine protease inhibitor serpin family B member 6, whose dysregulation is associated with autophagic and apoptotic induction in cancer [37].

Finally, *GALC*-upregulated proteins include the TOR signaling pathway regulator, an allosteric regulator of the serine/threonine-protein phosphatase 2A in cancer cells [32], and the cytosolic X-prolyl aminopeptidase 1 associated with disease progression and shorter overall survival in multiple myeloma [33], together with 3'(2'), 5'-bisphosphate nucleotidase 2 and CXXC motif-containing zinc-binding protein, whose function(s) in cancer remains unexplored.

In silico analysis of transcriptomic data from 448 human skin melanoma samples performed on the cBioPortal for Cancer Genomics platform [38,39] supported the proteomic data. Indeed, the expression of 14 out of the 27 genes encoding for *GALC*-modulated proteins in both A2058 and A375 cells was significantly correlated with *GALC* mRNA levels in human melanoma specimens. Among them, three genes encode for proteins related to ER responses (i.e., LMAN1, SRP72, and EIF2A), three genes encode for proteins that play a significant role in the metastatic process (i.e., SPARC, CYFIP1, and PPFIBP1), and three genes encode for proteins involved in tumor immune escape (i.e., KPNA4, NT5E, and RBM12), thus supporting the role of *GALC* in different aspects of melanoma progression.

Previous observations have shown that *GALC* may exert a pro-oncogenic role in *Braf* wildtype murine melanoma cells [1]. The results of the present work confirm and extend these findings by demonstrating that *GALC* overexpression increases the tumorigenic potential of both A2058 and A375 human melanoma cells harboring the tumor-driving BRAF(V600E) mutation. In addition, LC-MS/MS proteomic analysis, supported by transcriptomic data mining, indicates for the first time that *GALC* may exert a pro-oncogenic



impact on the proteomic landscape in *BRAF*-mutated human melanoma cells. Previous observations have shown that *GALC* downregulation may exert profound alterations in the lipidome of murine melanoma and exert a significant increase in ceramide levels in A2058 cells [1]. Exogenous administration of ceramide affects the protein profile of different tumor cell types [51,52], and the lack of *GALC* activity alters the proteome of the central and peripheral nervous system in *Galc*-null Twitcher mice [53]. At present, we do not know whether the effects observed in *BRAF*-mutated human melanoma cells following *GALC* overexpression are due to an excess of enzyme product(s) and/or a reduction in its substrate(s). Further studies will be required to assess the effect of the modulation of *GALC* activity on the sphingolipidome of human melanoma cells and how this, in turn, may orchestrate their transcriptomic and proteomic profiles.

#### 4. Materials and Methods

##### 4.1. Cell Cultures and Lentivirus Infection

A2058 and A375 cells were purchased from ATCC, grown in Dulbecco's modified Eagle medium (DMEM; Thermo Fisher Scientific, Waltham, MA, USA) supplemented with 10% heat-inactivated fetal bovine serum (FBS), 100 U/mL penicillin, and 100 µg/mL streptomycin (Thermo Fisher Scientific) and maintained at 37 °C and 5% CO<sub>2</sub> in a humidified incubator. For *GALC* overexpression, cells were infected with a lentivirus (pLenti PGK GFP Puro (w509-5) was a gift from Eric Campeau and Paul Kaufman, Addgene plasmid #19070) harboring the human *GALC* cDNA (NM\_000153.3), thus generating A2058-up*GALC* and A375-up*GALC* cells. Cells transduced with an empty vector were used as controls (A2058-mock and A375-mock cells). For the infection protocol, cells were incubated with lentiviral particles for 7 h in a complete medium containing 8.0 µg/mL of polybrene and selected by adding puromycin (1 µg/mL) 24 h later. Next, *GALC* overexpression was confirmed by semiquantitative RT-PCR. Briefly, cells were processed, and total RNA was extracted using TRIzol Reagent according to the manufacturer's instructions (Invitrogen, Waltham, MA, USA). Contaminating DNA was digested using DNase (Promega, Madison, WI, USA), and 2.0 µg of total RNA was retro-transcribed with MMLV reverse transcriptase (Invitrogen) using random hexaprimers in a final 20 µL volume. Then, 1/10th of the reaction was analyzed by semiquantitative RT-PCR using the following primers: *GALC*, forward: ATCTCTGCATCCATGCTCCT, reverse: CTGATTAAAATGCGACCCC; *GAPDH*, forward: ACCGATTGGTCGTATTGGG, reverse: TGATTTTGGAGGGATCTCGC. The PCR products were then electrophoresed on a 2% agarose gel and visualized by ethidium bromide staining.

##### 4.2. *GALC* Activity Assay

*GALC*-mediated hydrolysis of the fluorescent *GALC* substrate LRh-6-GalCer (Nissamine-rhodaminy-6-aminohexanoylgalactosyl ceramide) following its incubation with 20 µg of cell extract or 20 µL of their conditioned medium (50×) was quantified by thin-layer chromatography (TLC) [54]. Briefly, 5 nmoles of LRh-6-GalCer in 3:2 chloroform/methanol was concentrated and dissolved in 5 µL of dimethyl sulfoxide (DMSO) and 25 µL of 0.2 M citrate phosphate buffer, pH 4.4. The enzyme source and water were added to a final volume of 100 µL and incubated overnight at 37 °C. The reaction was extracted with 1.9 mL of 3:2 *v/v* chloroform/methanol and 0.4 mL of water. The lower phase was collected and evaporated under nitrogen. Samples were spotted on glass-coated silica gel plates and developed in 25:25:25:9:16 volumes of chloroform/ethyl acetate/*n*-propanol/0.25 M KCl/methanol. The fluorescent ceramide spots (LRh-6-Cer) were visualized under an ultraviolet lamp and photographed.

##### 4.3. Cell Proliferation Assay

Cells were seeded at 10<sup>4</sup> cells/cm<sup>2</sup> in DMEM supplemented with 2.0% FBS. After 24 h (T<sub>0</sub>), fresh medium was added, and cells were counted 24–96 h thereafter [1]. The data are the mean ± SEM of three experiments in triplicate.

#### 4.4. Soft Agar Assay

Cells ( $5 \times 10^4$ ) were suspended in 2 mL of medium containing 0.3% agar and applied onto 2 mL pre-solidified 0.6% agar in 35 mm culture dishes (3 dishes per cell line). After 15 days of incubation, cell colonies were observed under a phase contrast microscope and counted [55].

#### 4.5. Wound Healing Assay

Confluent cells were scraped with a 200  $\mu$ L tip to obtain a 2 mm thick denuded area. After 24 and 48 h, wounded monolayers were photographed, and the width of the wounds was quantified by computerized analysis of the digitalized images in three independent sites per group [56]. The experiment was performed twice with similar results.

#### 4.6. Boyden Chamber Migration Assay

The chemotaxis assay was performed as described with minor modifications [57]. Briefly, cells ( $5 \times 10^4$  cells) were suspended in 50  $\mu$ L/well of serum-free DMEM and loaded in the upper compartment of a Boyden chamber containing gelatine-coated polyvinylpyrrolidone-free (PVP-free) polycarbonate filters (8  $\mu$ m pore size, Costar, Cambridge, MA, USA). A total of 30  $\mu$ L of 10% FBS-containing DMEM was placed in the lower compartment. After 5 h of incubation at 37 °C, cells that had migrated to the lower side of the filter were stained with H&E. Five random fields were counted for each triplicate sample.

#### 4.7. Mass Spectrometry

##### 4.7.1. Sample Preparation

Cell samples were lysed with RIPA buffer and denatured with TFE. The samples were subjected to DTT reduction (200 mM), IAM alkylation (200 mM), and complete trypsin protein digestion. The peptide digests were desalted on the Discovery® DSC-18 solid phase extraction 96-well plate (25 mg/well). After the desalting process, samples were vacuum-evaporated and reconstituted in the mobile phase for analysis [58]. All reagents were from Sigma-Aldrich Inc. (St. Louis, MO, USA).

##### 4.7.2. Proteomic Analysis

The digested peptides were analyzed with a UHPLC Vanquish system (Thermo Scientific, Rodano, Italy) coupled with an Orbitrap Q-Exactive Plus (Thermo Scientific). Peptides were separated by a reverse phase column (Accucore™ RP-MS 100  $\times$  2.1 mm, particle size 2.6  $\mu$ m) at a flow rate of 0.200 mL/min, with water and acetonitrile as mobile phase A and B, respectively, both acidified with 0.1% formic acid. The analysis was performed using the following gradient: 0–5 min from 2% to 5% B; 5–55 min from 5% to 30% B; 55–61 min from 30% to 90% B, and hold for one minute. At 62.1 min, the percentage of B was set to the initial condition of the run at 2% and held for about 8 min in order to equilibrate the column for a total run time of 70 min. The mass spectrometry analysis was performed in positive ion mode. The ESI source was used with a voltage of 2.8 kV. The capillary temperature, sheath gas flow, auxiliary gas, and spare gas flow were set at 325 °C, 45 arb, 10 arb, and 2, respectively. S-lens was set at 70 rf. For the acquisition of spectra, a data-dependent (ddMS2) top 10 scan mode was used. Survey full-scan MS spectra (mass range  $m/z$  381 to 1581) were acquired with resolution  $R = 70,000$  and AGC target  $3 \times 10^6$ . MS/MS fragmentation was performed using high-energy c-trap dissociation (HCD) with resolution  $R = 35,000$  and AGC target  $1 \times 10^6$ . The normalized collision energy (NCE) was set to 30. The injection volume was 3  $\mu$ L.

The mass spectra analysis was carried out using MaxQuant software (version 1.6.14). MaxQuant parameters were set as follows: trypsin was selected for enzyme specificity; the search parameters were fixed to an initial precursor ion tolerance of 10 ppm and MS/MS tolerance at 20 ppm; as fixed modification, carbamidomethylation was set, whereas oxidation was set as variable modification. The maximum missed cleavages were set to 2. Andromeda search engine searched the spectra in MaxQuant against the Uniprot\_CP\_Human\_2018

sequence database. Label-free quantification was performed, including a match between runs option with the following parameters: protein and peptide false discovery rate was set to 0.01; the quantification was based on the extracted ion chromatograms, with a minimum ratio count of 1; the minimum required peptide length was set to 7 amino acids. Statistical analyses were performed using MaxQuant software (version 1.6.14) and MetaboAnalyst software (version 5.0) (<https://www.metaboanalyst.ca/> (accessed on 24 January 2021)) [59].

#### 4.8. Analysis of MS Data

Statistics were performed using Microsoft Excel 365 and GraphPad Prism 8. *p*-values were calculated by a two-tailed uncoupled *t*-test of 4 technical replicates per sample. Setting a false discovery rate of 5% by a two-stage linear step-up procedure of Benjamini, Krieger, and Yekutieli [60] allowed us to obtain lists of significantly differentially abundant proteins whose encoding genes were given to ShinyGO for obtaining pathway analyses through KEGG and Gene Ontology databases.

#### 4.9. RT-qPCR Analysis

For the analysis of differentially expressed genes, total RNA was extracted from mock and upGALC A2058 cells as described above. RT-qPCR analysis on retro-transcribed RNA was performed using specific primers (Supplementary Table S4).

**Supplementary Materials:** The supporting information can be downloaded at: <https://www.mdpi.com/article/10.3390/ijms241310555/s1>.

**Author Contributions:** Conceptualization, D.C. and M.P.; methodology, V.D.G. and M.M.; investigation, D.C., P.C., M.C., M.B., E.S., L.M., J.G., E.G. and V.D.G.; data curation, D.C.; writing—original draft preparation, D.C. and M.P.; writing—review and editing, D.C. and M.P.; supervision, M.P.; funding acquisition, M.M. and M.P. All authors have read and agreed to the published version of the manuscript.

**Funding:** This research was supported in part by Associazione Italiana per la Ricerca sul Cancro (AIRC) IG grant no. 18493 to M.P. and by the AGING Project—Department of Excellence—DIMET, Università del Piemonte Orientale to M.M.

**Institutional Review Board Statement:** Not applicable.

**Informed Consent Statement:** Not applicable.

**Data Availability Statement:** The data presented in this study are available in the Supplementary Material.

**Acknowledgments:** The authors wish to thank Stefano Calza (University of Brescia, Italy) for his suggestions and criticisms in MS data analysis.

**Conflicts of Interest:** The authors declare no conflict of interest.

## References

1. Belleri, M.; Paganini, G.; Coltrini, D.; Ronca, R.; Zizioli, D.; Corsini, M.; Barbieri, A.; Grillo, E.; Calza, S.; Bresciani, R.; et al.  $\beta$ -galactosylceramidase promotes melanoma growth via modulation of ceramide metabolism. *Cancer Res.* **2020**, *80*, 5011–5023. [[CrossRef](#)] [[PubMed](#)]
2. Kwon, Y.W.; Jo, H.-S.; Bae, S.; Seo, Y.; Song, P.; Song, M.; Yoon, J.H. Application of Proteomics in Cancer: Recent Trends and Approaches for Biomarkers Discovery. *Front. Med.* **2021**, *8*, 747333. [[CrossRef](#)]
3. Krisp, C.; Parker, R.; Pascovici, D.; Hayward, N.K.; Wilmott, J.S.; Thompson, J.F.; Mann, G.J.; Long, G.V.; Scolyer, R.A.; Molloy, M.P. Proteomic phenotyping of metastatic melanoma reveals putative signatures of MEK inhibitor response and prognosis. *Br. J. Cancer* **2018**, *119*, 713–723. [[CrossRef](#)]
4. Harel, M.; Ortenberg, R.; Varanasi, S.K.; Mangalharra, K.C.; Mardamshina, M.; Markovits, E.; Baruch, E.N.; Tripple, V.; Arama-Chayoth, M.; Greenberg, E.; et al. Proteomics of Melanoma Response to Immunotherapy Reveals Mitochondrial Dependence. *Cell* **2019**, *179*, 236–250. [[CrossRef](#)]
5. Militaru, I.V.; Rus, A.A.; Munteanu, C.V.A.; Manica, G.; Petrescu, S.M. New panel of biomarkers to discriminate between amelanotic and melanotic metastatic melanoma. *Front. Oncol.* **2023**, *12*, 1061832. [[CrossRef](#)]
6. Ascierto, P.A.; Kirkwood, J.M.; Grob, J.-J.; Simeone, E.; Grimaldi, A.M.; Maio, M.; Palmieri, G.; Testori, A.; Marincola, F.M.; Mozzillo, N. The role of BRAF V600 mutation in melanoma. *J. Transl. Med.* **2012**, *10*, 85. [[CrossRef](#)] [[PubMed](#)]

7. Melnikova, V.O.; Bolshakov, S.V.; Walker, C.; Ananthaswamy, H.N. Genomic alterations in spontaneous and carcinogen-induced murine melanoma cell lines. *Oncogene* **2004**, *23*, 2347–2356. [[CrossRef](#)] [[PubMed](#)]
8. Betancourt, L.H.; Gil, J.; Sanchez, A.; Doma, V.; Kuras, M.; Rodriguez Murillo, J.; Velasquez, E.; Cakir, U.; Kim, Y.; Sugihara, Y.; et al. The Human Melanoma Proteome Atlas—Complementing the melanoma transcriptome. *Clin. Transl. Med.* **2021**, *11*, e451. [[CrossRef](#)] [[PubMed](#)]
9. Xijin Ge, s.; Jung, D.; Yao, R. ShinyGO: A graphical gene-set enrichment tool for animals and plants. *Bioinformatics* **2020**, *36*, 2628–2629. [[CrossRef](#)]
10. Cao, Y.; Qiu, T.; Kathayat, R.S.; Azizi, S.-A.; Thorne, A.K.; Ahn, D.; Fukata, Y.; Fukata, M.; Rice, P.A.; Dickinson, B.C. ABHD10 is an S-depalmitoylase affecting redox homeostasis through peroxiredoxin-5. *Nat. Chem. Biol.* **2019**, *15*, 1232–1240. [[CrossRef](#)]
11. Garifulin, O.M.; Kykot, V.O.; Gridina, N.Y.; Kiyamova, R.G.; Gout, I.T.; Filonenko, V.V. Application of serex-analysis for identification of human colon cancer antigens. *Exp. Oncol.* **2015**, *37*, 173–180. [[CrossRef](#)] [[PubMed](#)]
12. Peng, H.; Deng, Y.; Wang, L.; Cheng, Y.; Xu, Y.; Liao, J.; Wu, H. Identification of Potential Biomarkers with Diagnostic Value in Pituitary Adenomas Using Prediction Analysis for Microarrays Method. *J. Mol. Neurosci.* **2019**, *69*, 399–410. [[CrossRef](#)] [[PubMed](#)]
13. Aozuka, Y.; Koizumi, K.; Saitoh, Y.; Ueda, Y.; Sakurai, H.; Saiki, I. Anti-tumor angiogenesis effect of aminopeptidase inhibitor bestatin against B16-BL6 melanoma cells orthotopically implanted into syngeneic mice. *Cancer Lett.* **2004**, *216*, 35–42. [[CrossRef](#)] [[PubMed](#)]
14. Mina-Osorio, P. The moonlighting enzyme CD13: Old and new functions to target. *Trends Mol. Med.* **2008**, *14*, 361–371. [[CrossRef](#)] [[PubMed](#)]
15. Lobo, S.; Benusiglio, P.R.; Cloulet, F.; Boussemart, L.; Golmard, L.; Spier, I.; Huneburg, R.; Aretz, S.; Colas, C.; Oliveira, C. Cancer predisposition and germline CTNNA1 variants. *Eur. J. Med. Genet.* **2021**, *64*, 104316. [[CrossRef](#)]
16. Limaye, A.J.; Whittaker, M.K.; Bendzun, G.N.; Cowell, J.K.; Kennedy, E.J. Targeting the WASF3 complex to suppress metastasis. *Pharmacol. Res.* **2022**, *182*, 106302. [[CrossRef](#)]
17. Rozpędek, W.; Pytel, D.; Mucha, B.; Leszczynska, H.; Diehl, J.A.; Majsterek, I. The Role of the PERK/eIF2 $\alpha$ /ATF4/CHOP Signaling Pathway in Tumor Progression During Endoplasmic Reticulum Stress. *Curr. Mol. Med.* **2016**, *16*, 533–544. [[CrossRef](#)]
18. Morimoto, A.; Kannari, M.; Tsuchida, Y.; Sasaki, S.; Saito, C.; Matsuta, T.; Maeda, T.; Akiyama, M.; Nakamura, T.; Sakaguchi, M.; et al. An HNF4 $\alpha$ -microRNA-194/192 signaling axis maintains hepatic cell function. *J. Biol. Chem.* **2017**, *292*, 10574–10585. [[CrossRef](#)]
19. Lan, X.; Zhao, L.; Zhang, J.; Shao, Y.; Qv, Y.; Huang, J.; Cai, L. Comprehensive analysis of karyopherin alpha family expression in lung adenocarcinoma: Association with prognostic value and immune homeostasis. *Front. Genet.* **2022**, *13*, 956314. [[CrossRef](#)]
20. Fahrman, J.F.; Tanaka, I.; Irajizad, E.; Mao, X.; Dennison, J.B.; Murage, E.; Casabar, J.; Mayo, J.; Oeng, Q.; Celik, M.; et al. Mutational Activation of the NRF2 Pathway Upregulates Kynureninase Resulting in Tumor Immunosuppression and Poor Outcome in Lung Adenocarcinoma. *Cancers* **2022**, *14*, 2543. [[CrossRef](#)]
21. Lazova, R.; Klump, V.; Pawelek, J. Autophagy in cutaneous malignant melanoma. *J. Cutan. Pathol.* **2010**, *37*, 256–268. [[CrossRef](#)] [[PubMed](#)]
22. Ma, S.; Wei, H.; Wang, C.; Han, J.; Chen, X.; Li, Y. MiR-26b-5p inhibits cell proliferation and EMT by targeting MYCBP in triple-negative breast cancer. *Cell. Mol. Biol. Lett.* **2021**, *26*, 52. [[CrossRef](#)] [[PubMed](#)]
23. Yuan, C.-S.; Teng, Z.; Yang, S.; He, Z.; Meng, L.-Y.; Chen, X.-G.; Liu, Y. Reshaping hypoxia and silencing CD73 via biomimetic gelatin nanotherapeutics to boost immunotherapy. *J. Control. Release* **2022**, *351*, 255–271. [[CrossRef](#)] [[PubMed](#)]
24. Loilome, W.; Wechagama, P.; Namwat, N.; Jusakul, A.; Sripan, B.; Miwa, M.; Kuver, R.; Yongvanit, P. Expression of oxysterol binding protein isoforms in opisthorchiasis-associated cholangiocarcinoma: A potential molecular marker for tumor metastasis. *Parasitol. Int.* **2012**, *61*, 136–139. [[CrossRef](#)]
25. Li, C.; Zhang, L.; Xu, Y.; Chai, D.; Nan, S.; Qiu, Z.; Wang, W.; Deng, W. The Prognostic Significance and Potential Mechanism of Prollyl 3-Hydroxylase 1 in Hepatocellular Carcinoma. *J. Oncol.* **2022**, *2022*, 7854297. [[CrossRef](#)]
26. Li, Q.; Wang, J.; Ma, X.; Wang, M.; Zhou, L. POFUT1 acts as a tumor promoter in glioblastoma by enhancing the activation of Notch signaling. *J. Bioenerg. Biomembr.* **2021**, *53*, 621–632. [[CrossRef](#)]
27. Dong, C.; Li, X.; Yang, J.; Yuan, D.; Zhou, Y.; Zhang, Y.; Shi, G.; Zhang, R.; Liu, J.; Fu, P.; et al. PPF1BP1 induces glioma cell migration and invasion through FAK/Src/JNK signaling pathway. *Cell Death Dis.* **2021**, *12*, 827. [[CrossRef](#)]
28. Gao, C.; Shen, J.; Chen, W.; Yao, L.; Liang, X.; Zhu, R.; Chen, Z. Increased RBM12 expression predicts poor prognosis in hepatocellular carcinoma based on bioinformatics. *J. Gastrointest. Oncol.* **2021**, *12*, 1905–1926. [[CrossRef](#)]
29. Meling, M.T.; Kuniwa, Y.; Ogawa, E.; Sato, Y.; Okuyama, R. Increased expression of secreted protein acidic and rich in cysteine and tissue inhibitor of metalloproteinase-3 in epidermotropic melanoma metastasis. *J. Dermatol.* **2021**, *48*, 1772–1779. [[CrossRef](#)]
30. Faoro, C.; Ataide, S.F. Noncanonical Functions and Cellular Dynamics of the Mammalian Signal Recognition Particle Components. *Front. Mol. Biosci.* **2021**, *8*, 679584. [[CrossRef](#)]
31. Kok, J.Y.; Ekmekcioglu, S.; Mehta, K. Implications of tissue transglutaminase expression in malignant melanoma. *Mol. Cancer Ther.* **2006**, *5*, 1493–1503. [[CrossRef](#)]
32. Sun, J.; Yang, M.; Zhao, W.; Wang, F.; Yang, L.; Tan, C.; Hu, T.; Zhu, H.; Zhao, G. Research progress on the relationship between the TOR signaling pathway regulator; epigenetics; and tumor development. *Front. Genet.* **2022**, *13*, 1006936. [[CrossRef](#)] [[PubMed](#)]

33. Miettinen, J.J.; Kumari, R.; Traustadottir, G.A.; Huppunen, M.-E.; Sergeev, P.; Majumder, M.M.; Schepsky, A.; Gudjonsson, T.; Lievonen, J.; Bazou, D.; et al. Aminopeptidase Expression in Multiple Myeloma Associates with Disease Progression and Sensitivity to Melflufen. *Cancers* **2021**, *13*, 1527. [[CrossRef](#)] [[PubMed](#)]
34. Van Der Gaag, E.J.; Leccia, M.-T.; Dekker, S.K.; Jalbert, N.L.; Amodeo, D.M.; Byers, H.R. Role of Zyxin in Differential Cell Spreading and Proliferation of Melanoma Cells and Melanocytes. *J. Investig. Dermatol.* **2002**, *118*, 246–254. [[CrossRef](#)] [[PubMed](#)]
35. Ciccarone, F.; Di Leo, L.; Lazzarino, G.; Maulucci, G.; Di Giacinto, F.; Tavazzi, B.; Ciriolo, M.R. Aconitase 2 inhibits the proliferation of MCF-7 cells promoting mitochondrial oxidative metabolism and ROS/FoxO1-mediated autophagic response. *Br. J. Cancer* **2020**, *122*, 182–193. [[CrossRef](#)] [[PubMed](#)]
36. Mirhadi, S.; Zhang, W.; Pham, N.-A.; Karimzadeh, F.; Pintilie, M.; Tong, J.; Taylor, P.; Krieger, J.; Pitcher, B.; Sykes, J.; et al. Mitochondrial Aconitase ACO2 Links Iron Homeostasis with Tumorigenicity in Non-Small Cell Lung Cancer. *Mol. Cancer Res.* **2023**, *21*, 36–50. [[CrossRef](#)]
37. Jang, M.; Hara, S.; Kim, G.-H.; Kim, S.M.; Son, S.; Kwon, M.; Ryoo, I.-J.; Seo, H.; Kim, M.J.; Kim, N.-D.; et al. Dutomycin Induces Autophagy and Apoptosis by Targeting the Serine Protease Inhibitor SERPINB6. *ACS Chem. Biol.* **2021**, *16*, 360–370. [[CrossRef](#)]
38. Cerami, E.; Gao, J.; Dogrusoz, U.; Gross, B.E.; Sumer, S.O.; Aksoy, B.A.; Jacobsen, A.; Byrne, C.J.; Heuer, M.L.; Larsson, E.; et al. The cBio Cancer Genomics Portal: An open platform for exploring multidimensional cancer genomics data. *Cancer Discov.* **2012**, *2*, 401–404. [[CrossRef](#)]
39. Gao, J.; Aksoy, B.A.; Dogrusoz, U.; Dresdner, G.; Gross, B.E.; Sumer, S.O.; Sun, Y.; Jacobsen, A.; Sinha, R.; Larsson, E.; et al. Integrative analysis of complex cancer genomics and clinical Profiles Using the cBioPortal. *Sci. Signal.* **2013**, *6*, 1905–1926. [[CrossRef](#)]
40. Belleri, M.; Chiodelli, P.; Corli, M.; Capra, M.; Presta, M. Oncosuppressive and oncogenic activity of the sphingolipid-metabolizing enzyme  $\beta$ -galactosylceramidase. *Biochim. Biophys. Acta Rev. Cancer* **2022**, *1877*, 188675. [[CrossRef](#)]
41. Yang, M.; Jiang, Z.; Yao, G.; Wang, Z.; Sun, J.; Qin, H.; Zhao, H. GALC Triggers Tumorigenicity of Colorectal Cancer via Senescent Fibroblasts. *Front. Oncol.* **2020**, *10*, 380. [[CrossRef](#)]
42. Liu, D.G.; Xue, L.; Li, J.; Yang, Q.; Peng, J.Z. Epithelial-mesenchymal transition and GALC expression of circulating tumor cells indicate metastasis and poor prognosis in non-small cell lung cancer. *Cancer Biomark.* **2018**, *22*, 417–426. [[CrossRef](#)] [[PubMed](#)]
43. Pellerin, L.; Carrié, L.; Dufau, C.; Nieto, L.; Séguin, B.; Levade, T.; Riond, J.; Andrieu-Abadie, N. Lipid metabolic reprogramming: Role in melanoma progression and therapeutic perspectives. *Cancers* **2020**, *12*, 3147. [[CrossRef](#)]
44. Kong, Y.; Jiang, J.; Huang, Y.; Li, L.; Liu, X.; Jin, Z.; Wei, F.; Liu, X.; Zhang, S.; Duan, X.; et al. Endoplasmic reticulum stress in melanoma pathogenesis and resistance. *Biomed. Pharmacother.* **2022**, *155*, 113741. [[CrossRef](#)] [[PubMed](#)]
45. Huang, C.; Radi, R.H.; Arbiser, J.L. Mitochondrial metabolism in melanoma. *Cells* **2021**, *10*, 3197. [[CrossRef](#)] [[PubMed](#)]
46. Lai, M.; La Rocca, V.; Amato, R.; Freer, G.; Costa, M.; Spezia, P.G.; Quaranta, P.; Lombardo, G.; Piomelli, D.; Pistello, M. Ablation of acid ceramidase impairs autophagy and mitochondria activity in melanoma cells. *Int. J. Mol. Sci.* **2021**, *22*, 3247. [[CrossRef](#)]
47. Passarelli, A.; Mannavola, F.; Stucci, L.S.; Tucci, M.; Silvestris, F. Immune system and melanoma biology: A balance between immunosurveillance and immune escape. *Oncotarget* **2017**, *8*, 106132–106142. [[CrossRef](#)]
48. Molino, S.; Tate, E.; McKillop, W.; Medin, J.A. Sphingolipid pathway enzymes modulate cell fate and immune responses. *Immunotherapy* **2017**, *9*, 1185–1198. [[CrossRef](#)]
49. Tallima, H.; Azzazy, H.M.E.; El Ridi, R. Cell surface sphingomyelin: Key role in cancer initiation; progression; and immune evasion. *Lipids Health Dis.* **2021**, *20*, 150. [[CrossRef](#)]
50. Montfort, A.; Bertrand, F.; Rochotte, J.; Gilhodes, J.; Filleron, T.; Milhès, J.; Dufau, C.; Imbert, C.; Riond, J.; Tosolini, M.; et al. Neutral sphingomyelinase 2 heightens anti-melanoma immune responses and anti-PD-1 therapy efficacy. *Cancer Immunol. Res.* **2021**, *9*, 568–582. [[CrossRef](#)]
51. Rénert, A.-F.; Leprince, P.; Dieu, M.; Renaut, J.; Raes, M.; Bours, V.; Chapelle, J.-P.; Piette, J.; Merville, M.-P.; Fillet, M. The Proapoptotic C16-Ceramide-Dependent Pathway Requires the Death-Promoting Factor Btf in Colon Adenocarcinoma Cells. *J. Proteome Res.* **2009**, *8*, 4810–4822. [[CrossRef](#)]
52. Kota, V.; Dhople, V.M.; Fullbright, G.; Smythe, N.M.; Szulc, Z.M.; Bielawska, A.; Hama, H. 2'-Hydroxy C16-Ceramide Induces Apoptosis-Associated Proteomic Changes in C6 Glioma Cells. *J. Proteome Res.* **2013**, *12*, 4366–4375. [[CrossRef](#)]
53. Pellegrini, D.; del Grosso, A.; Angella, L.; Giordano, N.; Dilillo, M.; Tonazzini, I.; Caleo, M.; Cecchini, M.; McDonnell, L.A. Quantitative Microproteomics Based Characterization of the Central and Peripheral Nervous System of a Mouse Model of Krabbe Disease. *Mol. Cell. Proteom.* **2019**, *18*, 1227–1241. [[CrossRef](#)] [[PubMed](#)]
54. Marchesini, S.; Preti, A.; Aleo, M.F.; Casella, A.; Dagan, A.; Gatt, S. Synthesis, Spectral Properties and Enzymatic Hydrolysis of Fluorescent Derivatives of Cerebroside Sulfate Containing Long-Wavelength-Emission Probes. *Chem. Phys. Lipids* **1990**, *53*, 165–175. [[CrossRef](#)] [[PubMed](#)]
55. Ronca, R.; Di Salle, E.; Giacomini, A.; Leali, D.; Alessi, P.; Coltrini, D.; Ravelli, C.; Matarazzo, S.; Ribatti, D.; Vermi, W.; et al. Long Pentraxin-3 Inhibits Epithelial-Mesenchymal Transition in Melanoma Cells. *Mol. Cancer Ther.* **2013**, *12*, 2760–2771. [[CrossRef](#)]
56. Belleri, M.; Ronca, R.; Coltrini, D.; Nico, B.; Ribatti, D.; Poliani, P.L.; Giacomini, A.; Alessi, P.; Marchesini, S.; Santos, M.B.; et al. Inhibition of Angiogenesis by  $\beta$ -Galactosylceramidase Deficiency in Globoid Cell Leukodystrophy. *Brain* **2013**, *136*, 2859–2875. [[CrossRef](#)] [[PubMed](#)]
57. Leali, D.; Moroni, E.; Bussolino, F.; Presta, M. Osteopontin Overexpression Inhibits in Vitro Re-Endothelialization via Integrin Engagement. *J. Biol. Chem.* **2007**, *282*, 19676–19684. [[CrossRef](#)]

58. Martinotti, S.; Patrone, M.; Manfredi, M.; Gosetti, F.; Pedrazzi, M.; Marengo, E.; Ranzato, E. HMGB1 Osteo-Modulatory Action on Osteosarcoma SaOS-2 Cell Line: An Integrated Study from Biochemical and -Omics Approaches. *J. Cell. Biochem.* **2016**, *117*, 2559–2569. [[CrossRef](#)] [[PubMed](#)]
59. Manfredi, M.; Martinotti, S.; Gosetti, F.; Ranzato, E.; Marengo, E. The secretome signature of malignant mesothelioma cell lines. *J. Proteomics* **2016**, *145*, 3–10. [[CrossRef](#)]
60. Benjamini, Y.; Krieger, A.M.; Yekutieli, D. Adaptive linear step-up procedures that control the false discovery rate. *Biometrika* **2006**, *93*, 491–507. [[CrossRef](#)]

**Disclaimer/Publisher's Note:** The statements, opinions and data contained in all publications are solely those of the individual author(s) and contributor(s) and not of MDPI and/or the editor(s). MDPI and/or the editor(s) disclaim responsibility for any injury to people or property resulting from any ideas, methods, instructions or products referred to in the content.

**Highlights:**

- The overexpression of *GALC* exerts a pro-tumorigenic function on A2058 and A375 human melanoma cells harboring the BRAF<sup>V600E</sup> mutation.
- *GALC* upregulation induces a significant increase in the proliferative potential and anchorage-independent growth, paralleled by augmented cell motility.
- Liquid chromatography-tandem mass spectrometry analysis suggests that *GALC* exerted a different impact on the proteomic landscape of A2058 and A375 cell lines.
- Among the proteins whose levels of expression were affected by *GALC* overexpression, 25 of them were upregulated in both A2058 up*GALC* and A375 up*GALC* cells, whereas only 2 of them were downregulated in both cell types.
- The upregulation of *GALC* modulates the expression of proteins involved in different aspects of tumor progression, including melanoma biology, tumor invasion and metastatic dissemination, tumor immune escape, mitochondrial antioxidant activity, endoplasmic reticulum stress responses, autophagy, and apoptosis.

**Take home message:**

In the article, we have investigated the impact of *GALC* overexpression on the proteomic profile of two BRAF<sup>V600E</sup> human melanoma cell lines. The results demonstrate that, in keeping with its pro-tumorigenic activity, *GALC* modulates the expression of proteins involved in different aspects of melanoma progression.

## 5. TUMOR ANGIOGENESIS

Angiogenesis is defined as the formation of new blood vessels from pre-existing ones, (Zahedipour et al. 2021). During carcinogenesis, malignant cells require the presence of new blood vessels to support their growth and metastatic dissemination. To this aim, tumor and stromal cells secrete pro-angiogenic molecules to induce the so called “angiogenic switch” (Bergers and Benjamin 2003).

Angiogenesis is a multi-step process that is typically characterized by the budding of new capillaries from parental microvessels (sprouting angiogenesis) or, to a lesser extent, by the intravascular splitting of pre-existing capillaries (intussusceptive angiogenesis) (Lugano, Ramachandran and Dimberg 2020).

Intussusceptive angiogenesis is a dynamic intravascular process where two opposite ECs make contact and inter-endothelial junctions are formed at their edge. Within the junctions, thinning of cell membrane and cytoplasmic pressure induces splitting and separation into two vessels. Surrounding cells, i.e. mesenchymal stem cells and pericytes, invade the gap between newly formed membranes and form the intussusceptive pillar, a cylindrical microstructure that spans the lumen of small vessels and capillaries, thus increasing the complexity and number of microvascular structures within the tumor (Mentzer and Konerding 2014).

However, the most frequent and studied angiogenic process in cancer is represented by sprouting angiogenesis (fig. 5).

Sprouting angiogenesis consists in the branching of an existing vessel. ECs initiate angiogenesis after the stimulation exerted by various pro-angiogenic factors, including vascular endothelial growth factor (VEGF-A). At the same time, MMPs start to degrade the basement membrane of ECs and favor the detachment of mural cells (pericytes), allowing EC invasion into the perivascular stroma. In response to VEGF-A, tip cells (i.e., the ECs at the edge of the sprouts) drive the migration of the stalk cells in the back by producing Delta-like-4 ligand. Modulation of Notch signaling will affect the behavior of stalk cells whereas PDGF will recruit new pericytes. Finally, the formation of a vascular lumen will allow the blood flow (Lugano et al. 2020).



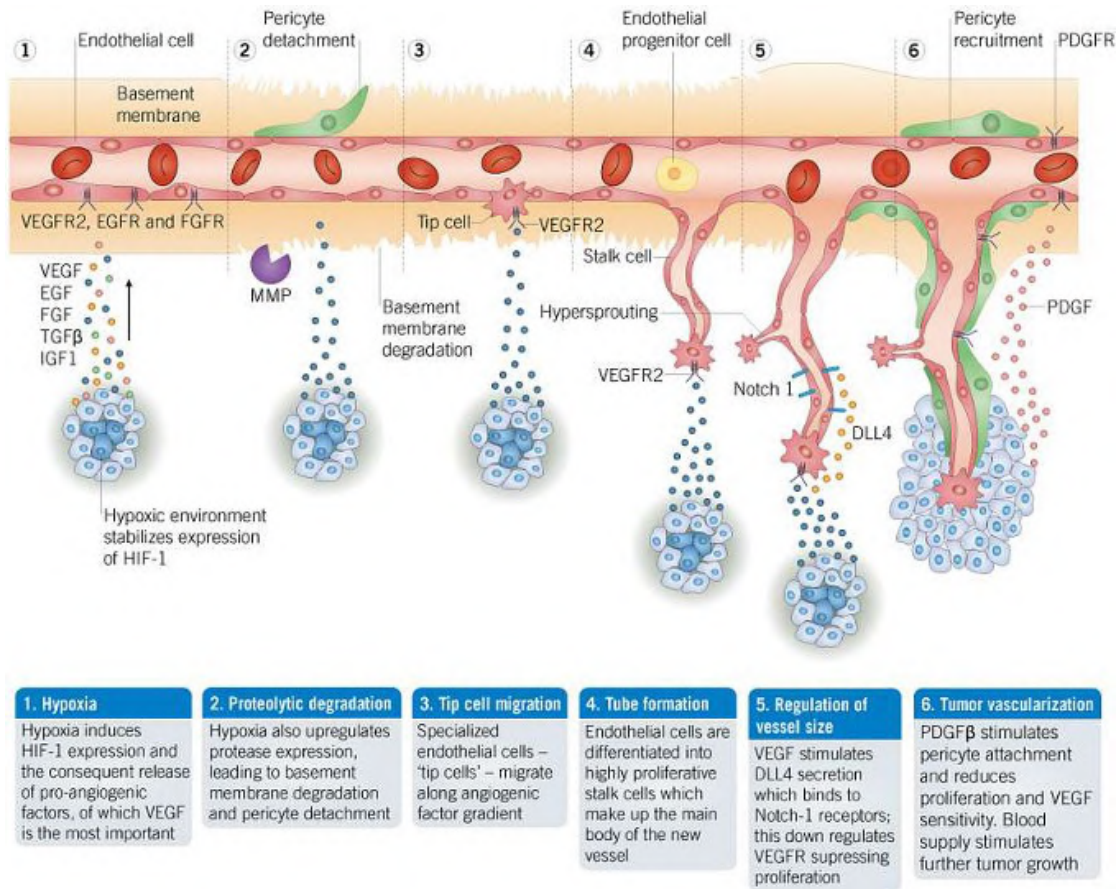


Figure 5 After activation of ECs by angiogenic stimuli, proteolytic enzymes are produced, which degrade the perivascular extracellular matrix and the basement membrane. ECs proliferate and migrate into the perivascular area, forming “primary sprouts”. Subsequent lumenation of these primary sprouts leads to formation of capillary loops, which is followed by synthesis of a new basement membrane and blood vessel maturation to complete tube-like structures through which blood can flow. From Cancer Research Product Guide, Edition 3, 2015.

## 5.1 Angiogenesis in melanoma

Melanoma displays a gradual increase in vascularity as the tumor progresses (Barnhill et al. 1992, Marcoval et al. 1997). The first evidence of the ability of melanoma to induce angiogenesis was observed following the transplantation of a human melanoma into a hamster pouch (Warren and Shubik 1966). In a subsequent study, the transplantation of malignant melanomas but not normal dermal tissue induced neo-vessel formation into cheek pouches (Hubler and Wolf 1976). Since then, various lines of evidence have shown that there is a relationship between angiogenesis and melanoma progression.

Melanoma creates a specific hypoxic microenvironment, rich in pro-inflammatory molecules that stimulate the angiogenic response. During melanoma progression, MITF regulates the expression of several genes to promote tumor survival. Among them the hypoxia-inducible

factor 1-alpha (*HIF1- $\alpha$* ) is upregulated. The expression of HIF1- $\alpha$  leads to the transcription of angiogenic factors, including VEGF-A (Viallard and Larrivée 2017). The ability of melanoma cells to build new vessels is also based on their capability to trans-differentiate into an endothelial-like cell phenotype (Wechman et al. 2020). The increased expression of VE-cadherin in highly metastatic melanoma cells enable them to form capillary-like structures that are abolished when targeting VE-cadherin with a monoclonal antibody (Braeuer et al. 2014). Therapies targeting VE-cadherin are proving effective in pre-clinical tests (Mabeta 2020).

## 5.2 Sphingolipid metabolizing enzymes modulate angiogenesis

Few studies have focused about a possible role of sphingolipid metabolism in the angiogenic process, most of the experimental evidence being related to the angiogenic potential of S1P (Wang et al. 2019).

Indeed, S1P has been found to activate complex cellular functions in the tumor microenvironment and to play an important role in endothelial barrier maintenance and tumor angiogenesis (Qiu et al. 2022). For instance, the binding of S1P to its EC receptors activates a series of signaling cascades that promotes tube formation *via* the activation of phospholipase C, ERK and PI3K-Akt signalling (Heo et al. 2009).

Scattered data indicate that also other sphingolipid-related pathways may be involved in tumor angiogenesis. Indeed, a proteomic study revealed that nSMase2 is increased in breast tumor-associated vascular cells (Bhati et al. 2008) whereas nSMase2 regulation of exosomal miR-210 increases *in vivo* metastasis in basal breast cancer by promoting local angiogenesis (Kosaka et al. 2013)

Another example is provided by ASAH1 that promotes angiogenesis *in vitro* and *in vivo* presumably by increasing the levels of HIF-1 $\alpha$  (Cho et al. 2019).

Relevant to the aims of my PhD thesis, significant alterations of microvascular endothelium were observed in the post-natal brain of GALC-deficient twitcher mice, an authentic model of globoid cell leukodystrophy. In addition, twitcher endothelium showed a reduced capacity to respond to pro-angiogenic factors, such as VEGF-A and fibroblast growth factor 2 (FGF2). Moreover, downregulation of GALC in human ECs led to decreased proliferation and hampered their motogenic response to VEGF-A. Together, these data demonstrate that GALC deficiency induces significant alterations in endothelial neovascular responses (Belleri et al.

2013). On these bases, during my PhD program I investigated the role of GALC in melanoma neovascularization.

### **5.2.1 GALC promotes angiogenesis in melanoma**

In a first set of experiments, RNAscope analysis was performed on 60 human melanoma samples to assess the relationship between *GALC* expression and vascularization at different stages of tumor progression. Morphometric analysis demonstrates that the progressive increase of *GALC* expression from common nevi to stage IV melanoma was parallel by an increase in the number of blood vessels infiltrating the tumor (fig. 5.1A-B).

These observations were confirmed when *GALC* overexpressing A2058 and A375 human melanoma cells (upGALC cells) generated in our laboratory (Belleri et al. 2020, Capoferri et al. 2023) were implanted subcutaneously in C57BL/6 mice. Histological analysis of the tumor grafts performed 7 days after implantation demonstrated a significant increase of CD31+ vessels in upGALC lesions when compared to mock controls (fig. 5.1C).

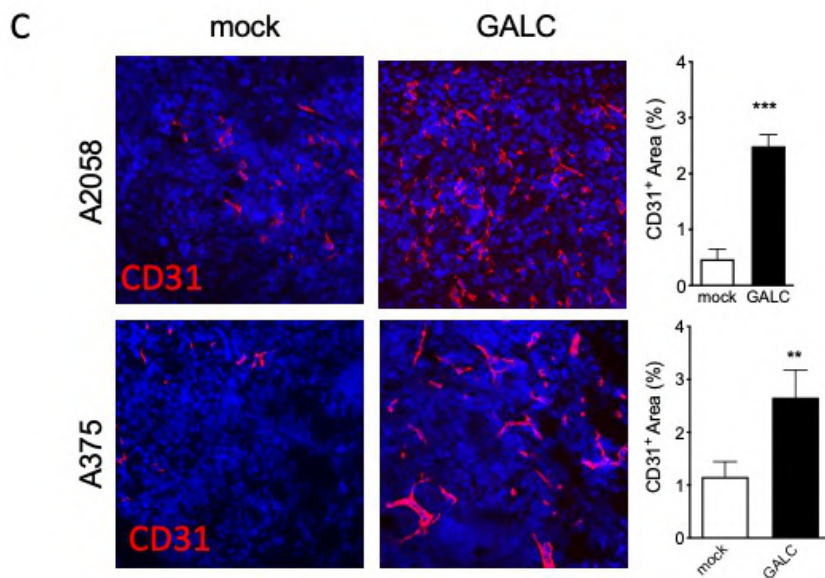
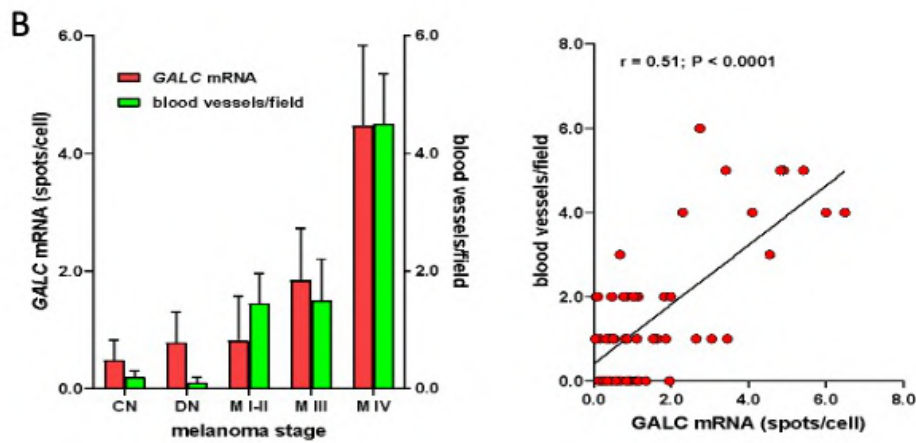
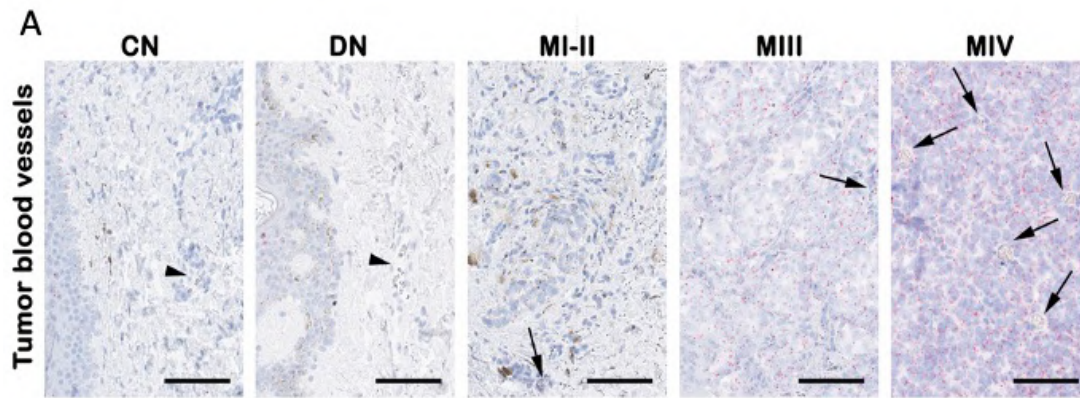


Figure 5.1 GALC expression correlates with blood vessel number in human melanoma. A, B) RNAscope analysis shows a progressive increase of GALC mRNA expression and microvessel density in histologic samples from 60 patients at different stages of melanoma progression, including common nevi (CN), dysplastic nevi (DN), melanoma stages I–II (M I–II), III (M III), and IV (M IV). Scale bar 60  $\mu$ m. C) Positive correlation between GALC expression levels and microvessel density as measured in the 60 samples independently of their tumor stage. D) Immunostaining of mock and upGALC grafts and quantification of CD31<sup>+</sup> areas.

Next, an angiogenesis protein array of the conditioned medium (CM) of upGALC A2058 cells was performed to assess whether the increased angiogenic potential of upGALC cells was due to an increased production and release of pro- and anti-angiogenic factors. As shown in fig. 5.2A, no significant alterations of the angiogenic balance seems to occur following *GALC* overexpression in melanoma cells, thus suggesting that GALC by itself may exert a pro-angiogenic function in our experimental model.

Lysosomal enzymes, including GALC, may be secreted by producing cells, being potentially available in melanoma microenvironment. To prove this hypothesis, the CM of upGALC cells was collected after 48h of starvation. Then, GALC activity was measured in the cell extract and CM of both mock and upGALC cells by a thin layer chromatography (TLC) enzymatic assay based on the conversion of the LRh-6-GalCer substrate to the LRh-6-Cer product (fig. 5.2B). The results confirm the capacity of GALC-overexpressing melanoma cells to release significant amounts of the active enzyme in the tumor microenvironment.

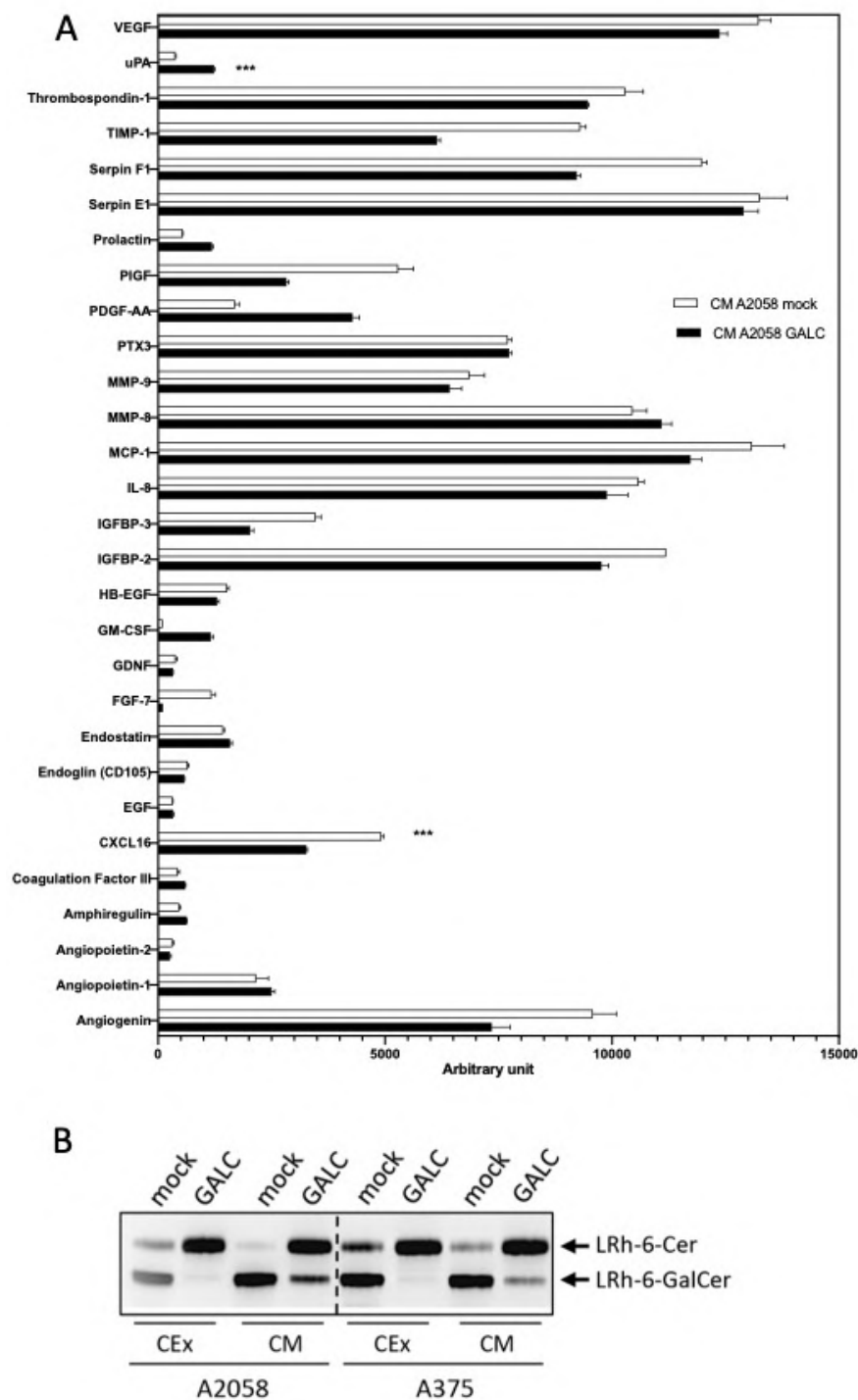


Figure 5.2 GALC overexpression does not modulate the secretion of pro-angiogenic factors in human melanoma cells. A) CM composition was characterized by an angiogenesis array (R&D system). B) GALC activity in the cell extract (CEx) and CM of mock and upGALC cells was evaluated by an enzymatic TLC assay.

On this basis, human umbilical vein endothelial cells (HUVEC) were stimulated with mock and upGALC A2058 CM in the absence or in the presence of the GALC inhibitor GCP (Marques et al. 2017). As anticipated, upGALC CM was able to induce a significant increase

of HUVEC migration and sprouting when compared to the control CM and such increase was abrogated by the GALC inhibitor (fig. 5.3A-B). In keeping with these observations, GCP abolished the angiogenic response exerted by the upGALC CM when tested in zebrafish embryo sprouting assay (fig 5.3C) or in the chick embryo CAM assay (fig. 5.3D-E). Of note, GCP did not affect VEGF-A and FGF2-mediated angiogenesis, indicating the specificity of its effect (fig. 5.3F).

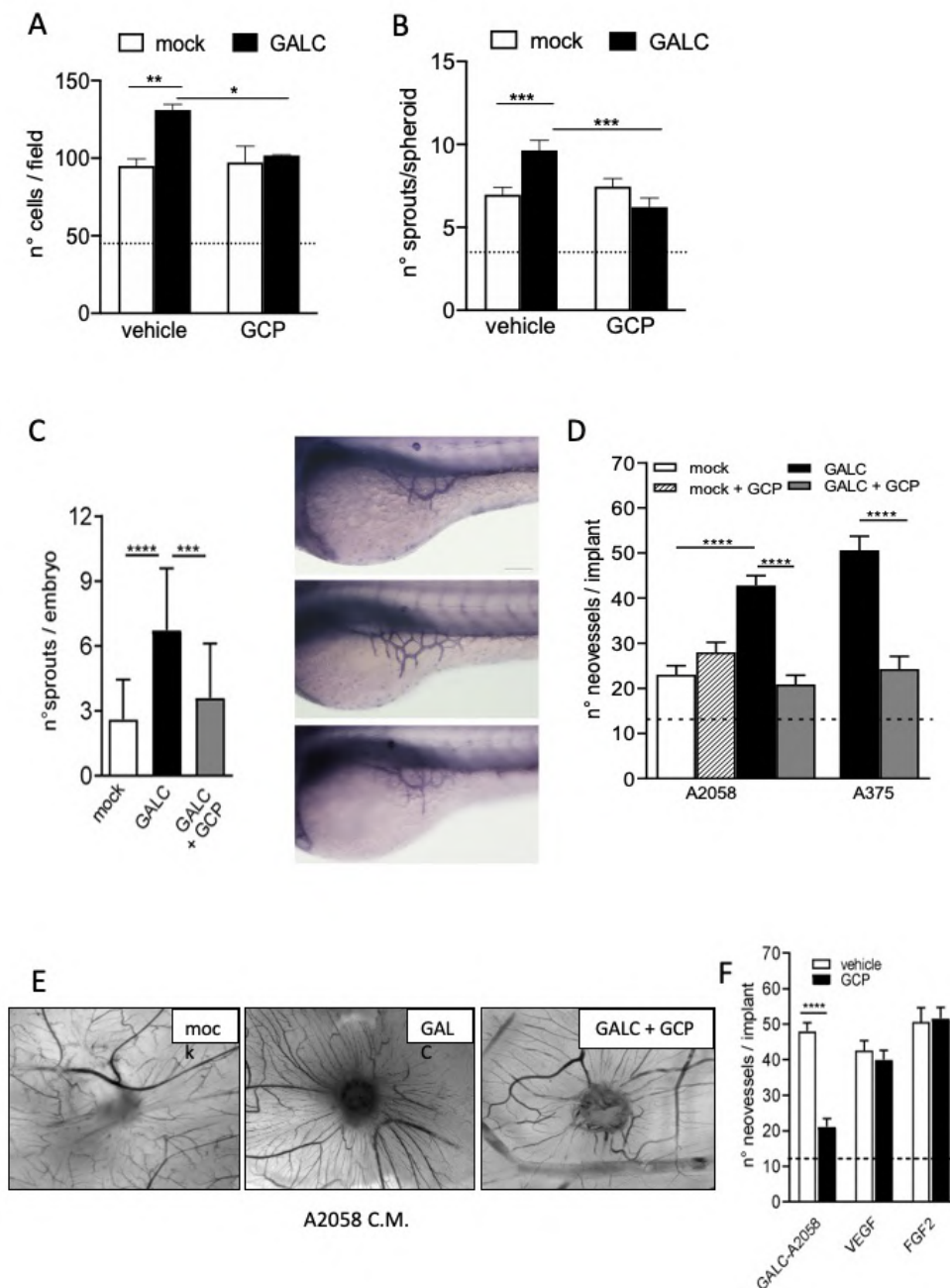


Figure 5.3 GALC promotes angiogenesis in vitro and in vivo. A) HUVEC Boyden chamber migration assay, B) HUVEC sprouting assay, C) Zebrafish sprouting assay, and D-E) CAM assay indicates that GALC exerts a pro-angiogenic activity in vitro and in vivo, both abrogated by the GALC inhibitor GCP. F) GCP did not affect neo-vessel formation triggered by VEGF-A or FGF2 in the CAM assay.

To further support a direct role of GALC activity in angiogenesis, wild-type (wt) GALC and a catalytically inactive GALC mutant harboring the R396W mutation (GALC<sup>R396W</sup>) (Deane et al. 2011) were overexpressed in HEK293T cells by lentiviral transduction. The mutation R396W is located inside the catalytic site of the enzyme, without affecting the folding and trafficking of the enzyme that is correctly expressed and secreted, as shown by Western blot analysis of GALC and GALC<sup>R396W</sup> cell lysates and CM (fig. 5.4A). As anticipated, the secreted mutant was endowed with a very limited enzymatic activity (fig. 5.4B-C) and was unable to stimulate HUVEC sprouting *in vitro* and angiogenesis *in vivo* in the CAM assay (fig 5.5D-E). Accordingly, the, inactive GALC<sup>R396W</sup> was unable to induce an angiogenic response in the CAM when overexpressed by A2058 cells (fig. 5.4F-G). Together, these data indicate that the angiogenic potential of GALC is strictly related to its enzymatic activity.



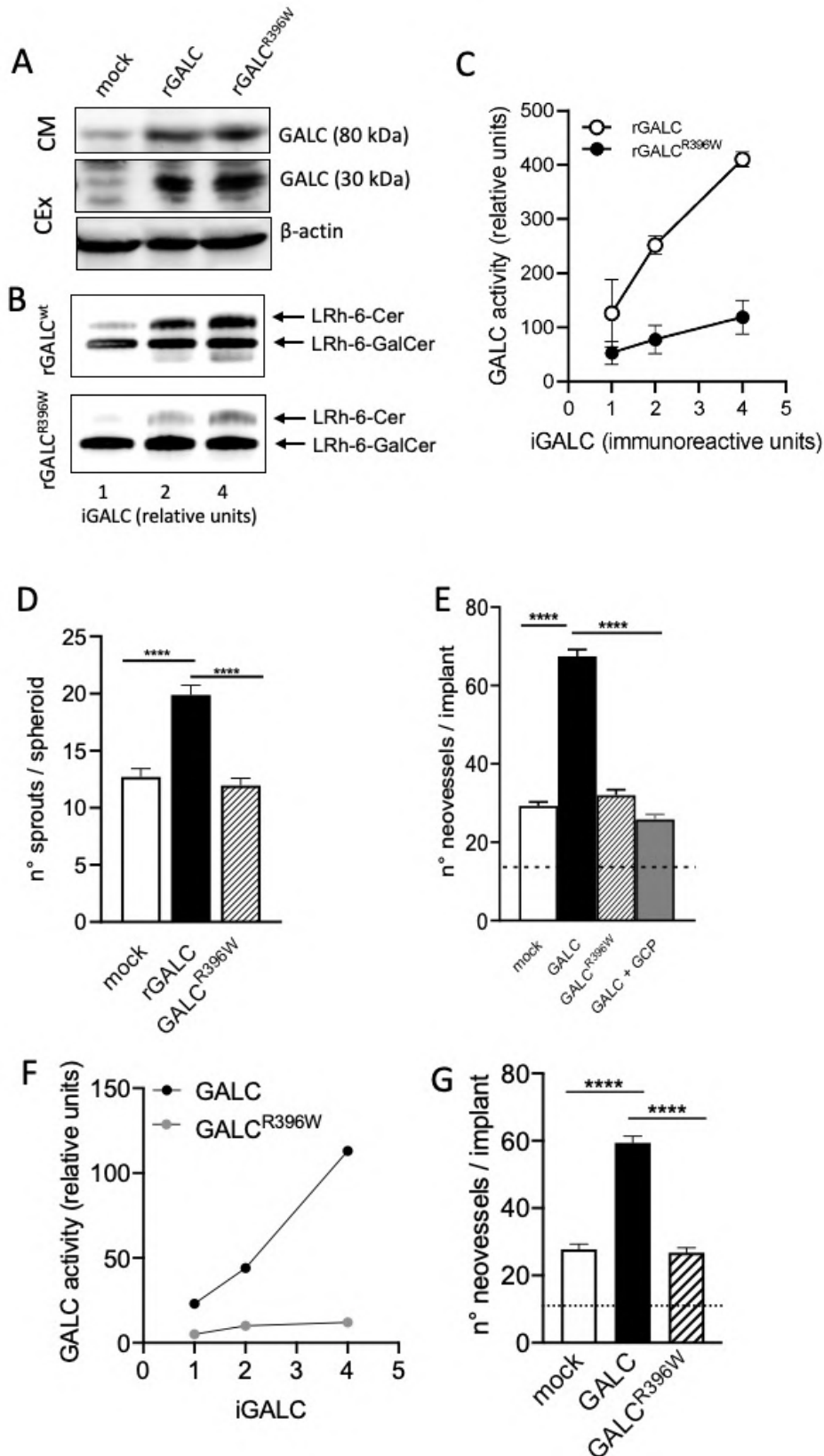


Figure 5.4 Catalytically inactive GALC failed to promote angiogenesis. A) Western blot analysis of CEx and CM confirms the overexpression of GALC<sup>wt</sup> and GALC<sup>R396W</sup> in HEK293T cells. B) and C) Residual activity of the inactive mutant was assessed by a TLC enzymatic assay. The inactive GALC<sup>R396W</sup> mutant failed to promote HUVEC sprouting (D) and neo-vessel formation in the CAM assay (E). Similar results were obtained when GALC<sup>R396W</sup> was expressed in A2058 melanoma cells (F-G).

As observed for other lysosomal enzymes, GALC tagged by a M6P residue may interact with M6PRs following its release in the extracellular environment. This will result in a receptor-driven internalization of the enzyme that will be delivered into the lysosomes (Fig. 5.5).

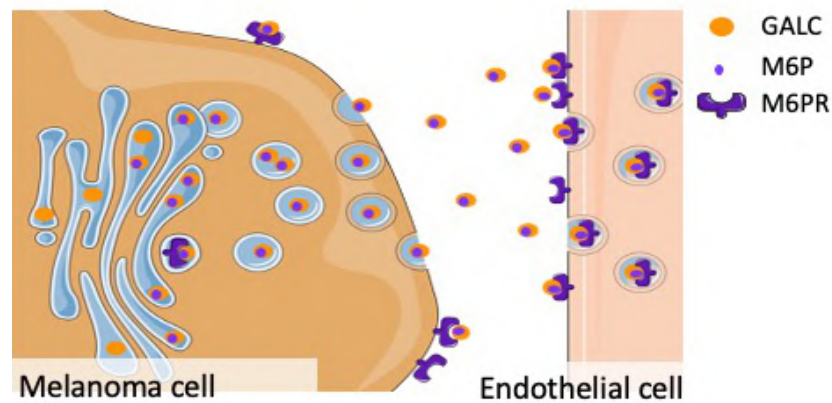


Figure 5.5 Schematic representation of GALC endocytosis by endothelial cells. M6P-tagged GALC is released from melanoma cells and it binds to M6PRs on ECs surface. The Figure was partly generated using Servier Medical Art, provided by Servier, licensed under a Creative Commons Attribution 3.0 unported license.

Accordingly, incubation of HUVECs with the A2058 upGALC CM causes a significant and progressive increase of GALC activity in their cell extract when compared to HUVECs incubated with mock CM (fig. 5.6A). Such increase is hampered by the addition of M6P to the upGALC CM (fig. 5.6B). Accordingly, RT-qPCR analysis demonstrates that HUVECs express significant levels of both cation dependent and cation independent (IGFR2) M6PRs (data not shown).

To assess whether M6PR-mediated internalization plays a non-redundant role in the angiogenic responses elicited by GALC, *in vitro* and *in vivo* angiogenesis assays were performed with upGALC CM in the absence and in the presence of M6P. In keeping with this hypothesis, M6P hampered the capacity of upGALC CM to induce HUVECs motility and sprouting and to stimulate neo-vessel formation in the CAM assay (fig. 5.6C-E). Again, no effect of M6P was exerted on the angiogenic activity of VEGF-A or FGF2, confirming the specificity of the effect (fig. 5.6F).

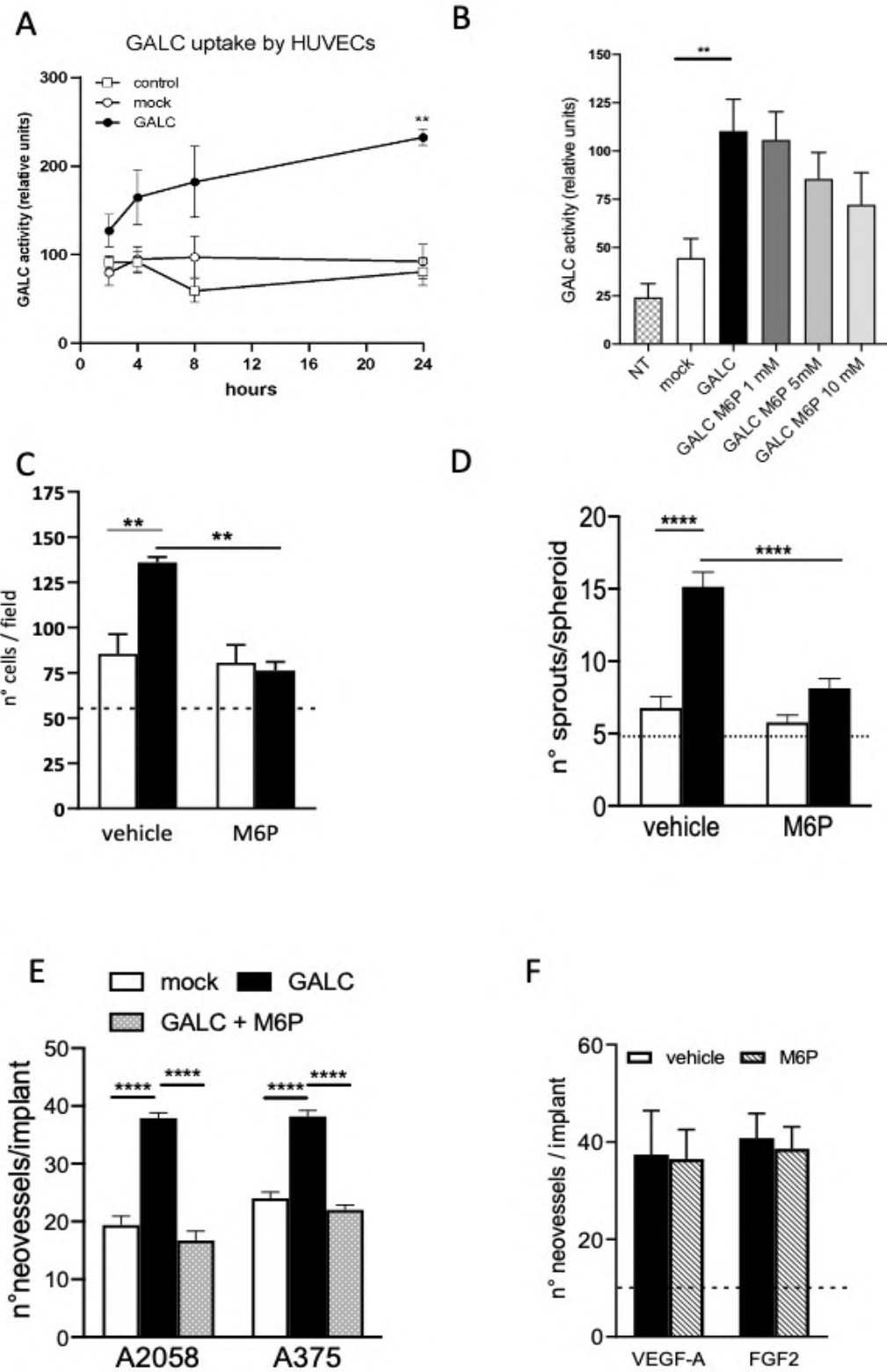


Figure 5.6 M6PR-mediated internalization mediates the angiogenic activity of upGALC CMECs. A) Kinetics of GALC uptake in HUVECs as evaluated by a TLC enzymatic assay. B) M6P prevents GALC uptake in HUVECs. M6P inhibits the capacity of A2058 upGALC CM to induce HUVEC migration (C) and sprouting (D) as well as angiogenesis in the CAM assay (E). (F) M6P did not affect VEGF-A or FGF2 mediated angiogenesis.

### 5.2.2 GALC promotes tyrosine kinase receptor signalling cascades and VEGFR2 activation in HUVECs

To identify the mechanism(s) responsible for the observed angiogenic response elicited by GALC in ECs, a human phospho-kinase array was performed on the cell extracts of HUVECs that have been incubated for 4 hours with the CM of mock or upGALC A2058 cells. As shown in fig. 5.7A, several intracellular kinases were significantly activated in HUVECs treated with upGALC CM when compared to control CM. These results were confirmed and extended by Western blot analysis of the same cell extracts (fig. 5.7B), raising the possibility that upGALC CM may induce the activation of one or more tyrosine kinase receptor(s). In keeping with this hypothesis, it was observed that the incubation of HUVECs with upGALC CM induces the phosphorylation of VEGFR2, the main pro-angiogenic tyrosine kinase receptor in ECs (fig. 5.7C). It must be pointed out that, in keeping with the angiogenesis array shown in fig. 5.2A, this occurred even though mock and upGALC CM contain the same levels of VEGF-A protein as assessed by ELISA (fig. 5.7D). Of note, both VEGFR2 and PI3K phosphorylation were abrogated upon co-treatment with the GALC inhibitor D-galactal (Dgal) (Hill et al. 2013) that, like GCP, hampered HUVEC sprouting mediated by upGALC CM (fig. 5.8A-B). Relevant to this point, no difference in *VEGF-A* gene expression was observed in HUVECs treated for 24 hours with mock or upGALC CM (data not shown), ruling out the possibility that GALC may induce *VEGF-A* upregulation in these cells.

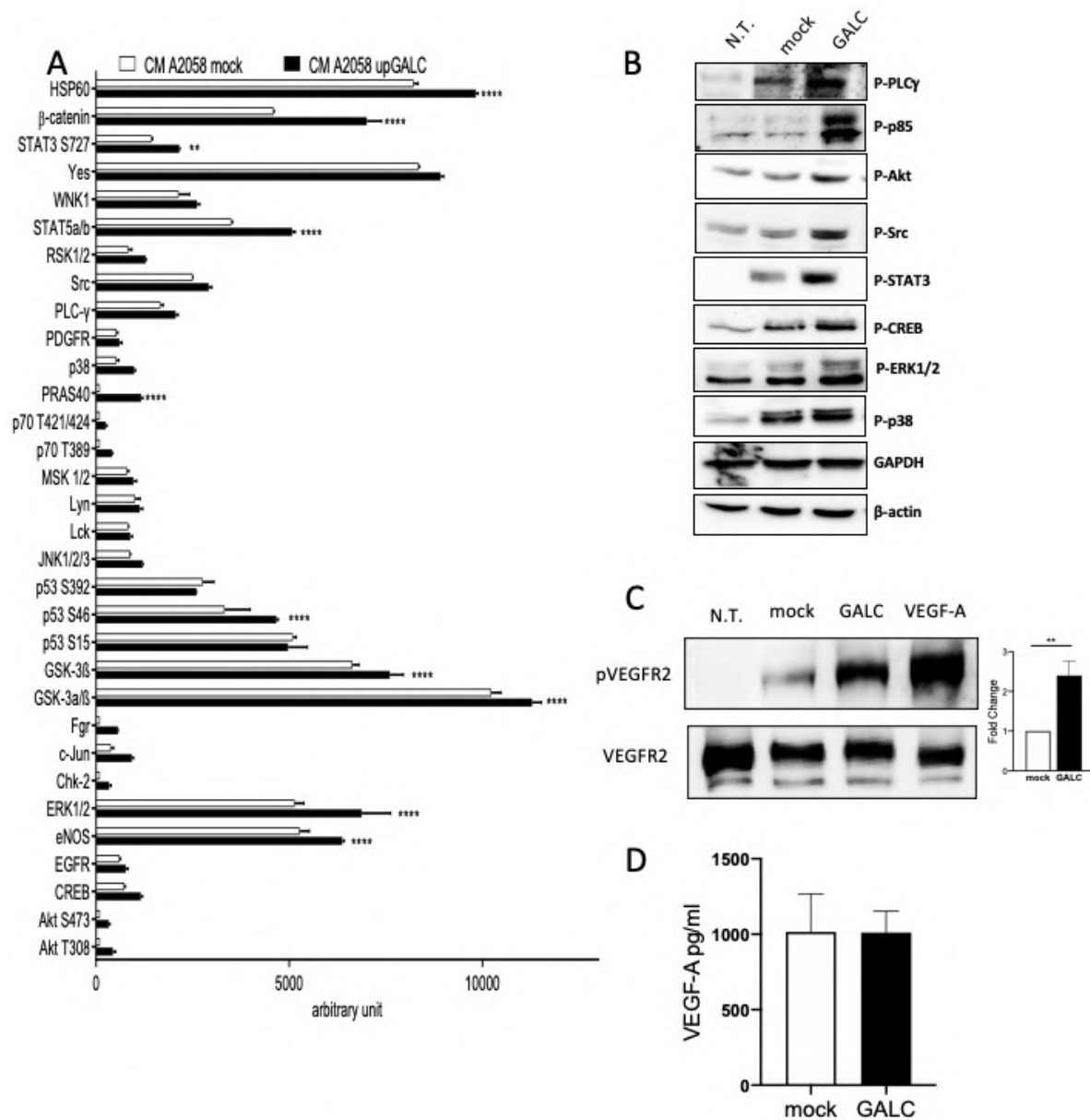


Figure 5.7 GALC activates VEGFR2 phosphorylation in ECs. A) Human phospho kinase array (R&D system) showed increased activation of several intracellular kinases in HUVECs stimulated for 4 h with upGALC CM. B) The data were confirmed and extended by Western blot analysis of the same cell extracts. C) Western blot analysis of VEGFR2 phosphorylation in HUVECs treated with upGALC (4 hours) or VEGF-A (10 min). D) VEGF-A proteins levels in mock and upGALC CM as assessed by ELISA.

Finally, to evaluate whether the capacity of upGALC CM to trigger VEGFR2 activation is mediated or not by the presence of the natural receptor ligand VEGF-A, HUVECs were co-treated with upGALC CM and the anti-VEGF-A antibody Ranibizumab. As shown in fig. 5.8C-D, Ranibizumab abolished VEGFR2 activation and HUVEC sprouting triggered by upGALC CM or recombinant VEGF-A, here used as a control.

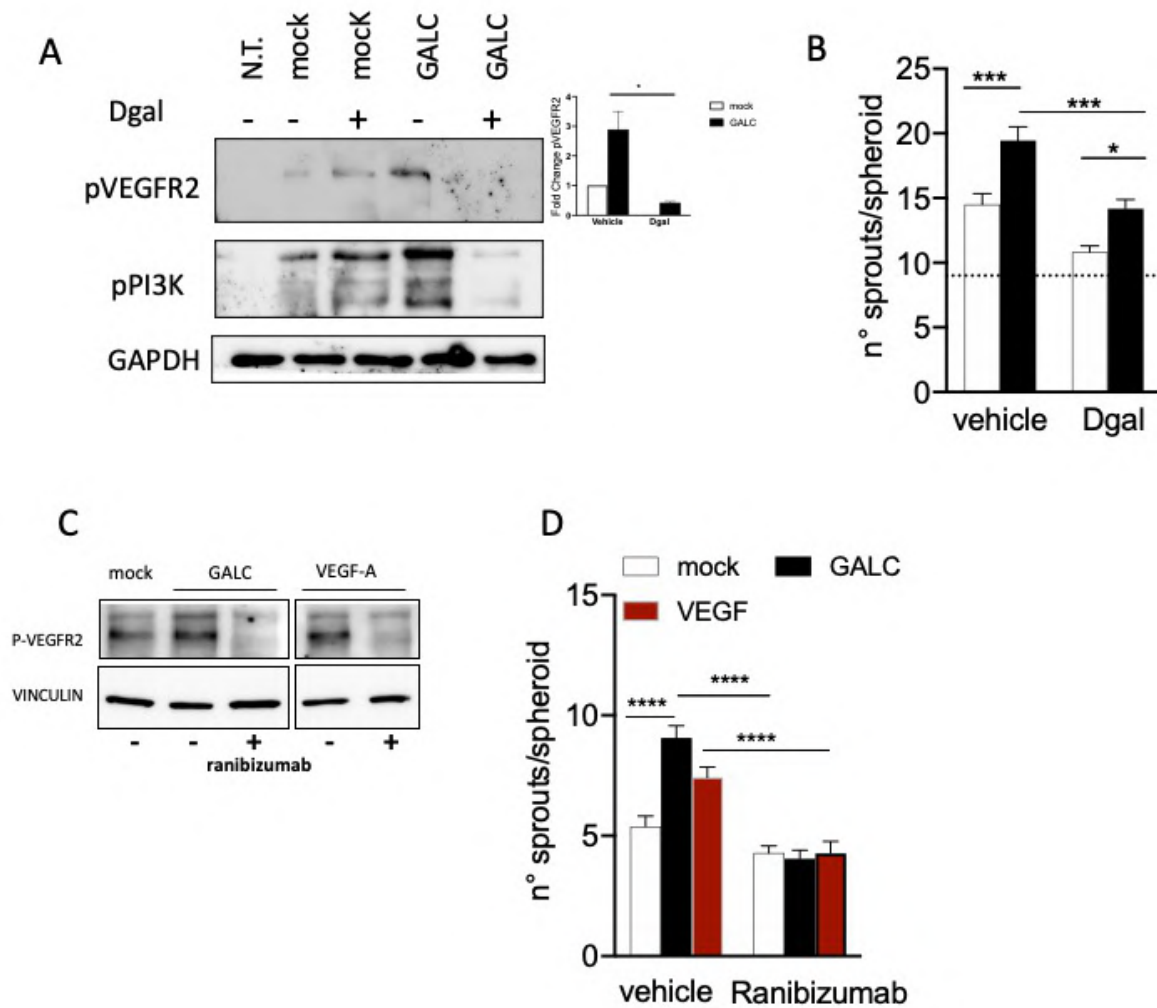


Figure 5.8. GALC activity and extracellular VEGF-A are required to promote VEGFR2 activation by upGALC CM. A) Western blot analysis shows that co-treatment of HUVECs with upGALC CM and the GALC inhibitor Dgalactose hampers VEGFR2 phosphorylation and downstream PI3K activation. B) Dgalactose abrogated also HUVEC sprouting triggered by upGALC CM. Trapping extracellular VEGF-A with the anti-VEGF-A antibody Ranibizumab inhibited GALC-mediated VEGFR2 phosphorylation (C) and sprouting (D) in HUVECs. Dgal: Dgalactose.

Together, the data indicate that enzymatically active GALC, once internalized *via* the M6P/M6PR pathway, is able to trigger VEGFR2 activation, downstream intracellular signalling, and biological responses (sprouting) in HUVECs. This capacity is strictly dependent upon the presence of VEGF-A in the extracellular environment.

## 6 DISCUSSION

Sphingolipids play a pivotal role in various physiological and pathological conditions. During my PhD program, I focused my research activity on two enzymes involved in sphingolipid metabolism: GALC and SMPD3.

The review **“Zebra-Sphinx: modelling sphingolipidoses in zebrafish”** underlines the importance of zebrafish as a versatile animal model to study sphingolipidoses. My group have investigated Krabbe disease in zebrafish and in the article **“Impact of an irreversible  $\beta$ -galactosylceramide inhibitor on the lipid profile of zebrafish embryos”**, we provide a new approach to deepen the mechanism of this neurodegenerative disease in developing organism, highlighting how GALC may exert a wider effect in the pathogenesis of the disorder. Besides its role in Krabbe disease, GALC has been studied also in tumor biology and in the review **“Oncosuppressive and oncogenic activity of the sphingolipid-metabolizing enzyme  $\beta$ -galactosylceramide”** we underline the dual role of GALC in cancer progression. Finally, the pro-oncogenic activity of GALC has been explored in the article **“The Pro-Oncogenic Sphingolipid-Metabolizing Enzyme  $\beta$ -Galactosylceramidase Modulates the Proteomic Landscape in BRAF(V600E)-Mutated Human Melanoma Cells”**.

Here I briefly discuss the work I performed during my PhD program, emphasizing the central role that sphingolipid enzymes play both in lysosomal storage diseases and in tumor progression.

Genetic deficiency of sphingolipid metabolizing enzymes leads to the occurrence of a series of pathological conditions named sphingolipidoses. The molecular and clinical features of genetic sphingolipidoses and the use of zebrafish as an animal model for the study of such diseases and for the search of novel therapeutic approaches are reviewed in the paper **“Zebra-Sphinx: modelling sphingolipidoses in zebrafish”**.

*GALC* is historically studied as a causative gene of Krabbe disease. Thus far, only a limited information is available about the effect of the modulation of GALC activity on the lipidome, mainly obtained by the analysis of tissues harvested from adult twitcher mice or genetically modified cell lines (Belleri et al. 2022). In addition, even though scattered evidence indicated that alterations of the central and peripheral nervous system may occur in human Krabbe fetuses (Suchlandt et al. 1982, Martin et al. 1981), no data are available about the effects of the lack of GALC activity on the lipidome of developing organisms. During my PhD, I evaluated

how the irreversible GALC inhibitor GCP modifies the lipid profile in zebrafish embryos. GCP has been demonstrated to exert a covalent and irreversible inhibition of the enzymatic activity of recombinant and rodent GALC (Marques et al. 2017). In the article “**Impact of an irreversible  $\beta$ -galactosylceramide inhibitor on the lipid profile of zebrafish embryos**”, *in-silico* analysis indicates that GCP shares the same pharmacophoric points in human GALC and in the zebrafish orthologues Galca and Galcb, indicating its capacity to exert an inhibitory effect by trapping the catalytic residues of the active site of the zebrafish enzymes. In keeping with this hypothesis, GCP inhibits the GALC activity present in zebrafish embryos and adult brain extracts with a potency similar to that exerted on human and murine GALC.

Taking advantage of the capacity of GCP to exert a long-lasting inhibition of GALC activity when injected in zebrafish at the 1-2 cell stage, we analyzed the lipid profile of zebrafish embryos at 96 hpf to assess a possible impact of GALC deficiency on the lipidome during the early phases of embryonic development. Untargeted lipidomic analysis identified 766 lipid species in the whole extracts of zebrafish embryos at 96 hpf in both GCP-treated and control animals. Among the various classes of lipids, GCP treatment caused a significant increase of the levels of TAG, possibly because of a reduced lipid remodeling in the yolk sac. As for sterols, while no changes in the levels of free cholesterol were observed between GCP-treated and control animals, the decrease in the levels of the CE species 22:5 and 22:6 resulted in a significant decrease in the total amount of CE following GCP treatment. This observation goes along with the decrease of CE levels that occurs in murine melanoma B16-F10 cells following shRNA mediated Galc knockdown (Belleri et al. 2020).

Notably, significant changes were observed for the levels of various classes of phospholipids following GCP treatment. They included an increase of PC, PE, and LPE levels, paralleled by a decrease of phosphatidylinositols, lyso-phosphatidylinositols, lyso-phosphatidylserines, and phosphatidylinositols-Cer. As observed for TAG changes, the effect of GCP on these phospholipid classes was restricted to defined lipid species, pointing again to a specific effect of GALC inhibition on phospholipid metabolism in zebrafish embryos. In keeping with these observations, a significant reduction of PE was observed in Galc knockdown B16 cells (Belleri et al. 2020) and alterations of the phospholipid profile and membrane turnover have been reported in the brain of twitcher mice (Weinstock et al. 2016) as a possible consequence of the tight crosstalk that occurs between phospholipid and sphingolipid metabolism [reviewed in (Rodriguez-Cuenca et al. 2017)]. Indeed, significant changes in the levels of Cer and SM were detected in GCP-treated animals.



Our data extend these observations and indicate for the first time that GALC plays a non-redundant role in lipid metabolism also during embryonic development, in line with clinical evidence about alterations of the central and peripheral nervous system of human Krabbe fetuses (Suchlandt et al. 1982, Martin et al. 1981)

Alterations of sphingolipid metabolism, exert a deep impact in melanoma progression (Bizzozero et al. 2014, Bilal et al. 2019, Shirane et al. 2014). Recently, experimental evidence pointed to an anti-tumorigenic role of nSMase2 in melanoma. nSMase2 derived-Cer delays tumor growth in C57BL/6 mice and increases CD8<sup>+</sup> lymphocytes infiltrating the tumor (Belleri et al. 2020, Montfort et al. 2021). In this thesis, the overexpression of *SMPD3* in two human melanoma cell lines harboring the BRAF<sup>V600E</sup> mutation was evaluated. Consistent with previous studies, nSMase2 does not modulate proliferation (Jabalee et al. 2020) and migration of melanoma cells (Montfort et al. 2021). As anticipated, nSMase2 upregulation in A2058 and A375 melanoma cells increased the levels of Cer and DH-Cer, paralleled by a decreased amount of SM and DH-SM. Reduced levels of HexCer and CDH may be explained by a simultaneous increase of GALC, as it was observed in some neurodegenerative diseases (Filippov et al. 2012), or Gba2, as noted in normal liver after injury (Yu et al. 2023). In a preliminary tumorigenesis assay performed on the chick embryo CAM, A2058 nSMase2 cells developed smaller lesions compared to A2058 mock grafts, consistent with the onco-suppressive role of Cer, as previously observed with murine melanoma tumors (Montfort et al. 2021, Belleri et al. 2020). In contrast to what occurs in breast cancer, where nSMase2 is related to increased local angiogenesis (Bhati et al. 2008) (Kosaka et al. 2013), here I showed that the nSMase2 lesions were less vascularized. The reduced neo-vessel formation might simply reflect the decrease in tumor growth or might represent a specific effect of Cer (Yazama et al. 2015). Further experiments will be required to elucidate this point.

Recently, Belleri et al. showed an inverse correlation between GALC and *SMPD3* expression in human melanoma, demonstrating that GALC critically modulates the oncogenic activity of melanoma cells *in vitro* and *in vivo* (Belleri et al. 2020). In the review **“Oncosuppressive and oncogenic activity of the sphingolipid-metabolizing enzyme  $\beta$ -galactosylceramide”** we have shown that GALC may exert opposite effects on tumor growth.

In line with these findings, analysis of human specimens ranging from common nevi to stage IV melanoma showed a gradual increase in *GALC* expression during tumor progression that goes along with a decrease in Cer levels (Belleri et al. 2020). Accordingly, high levels of GALC

immunoreactivity are associated with poor prognosis in colorectal cancer patients (Yang et al. 2020) and *GALC* upregulation in circulating lung cancer cells correlates with a poor response to therapy, representing a possible predictor biomarker in these patients (Liu et al. 2018).

In the article “**The Pro-Oncogenic Sphingolipid-Metabolizing Enzyme  $\beta$ -Galactosylceramidase Modulates the Proteomic Landscape in BRAF(V600E)-Mutated Human Melanoma Cells**”, we investigated the effects of *GALC* overexpression in A2058 and A375 human melanoma cells that harbor the BRAF(V600E)-activating mutation, which is present in approximately 50% of human melanomas (Ascierto et al. 2012). Our data indicate that *GALC* upregulation induces a significant increase in the proliferative potential and anchorage-independent growth of A2058 and A375 melanoma cells, paralleled by increased cell motility in a Boyden chamber assay and after *in vitro* wounding of the cell monolayer.

These findings prompted us to investigate the impact of *GALC* upregulation on the proteomic landscape of both A2058 and A375 cells. Notably, KEGG and GO categorizations indicated that A2058-mock cells express higher levels of proteins related to energy metabolism and mitochondrial activity when compared to A375 cells. Conversely, proteins related to mRNA binding/splicing and ribosome terms are present at higher levels in A375-mock cell extracts.

Based on this cell heterogeneity, it is not surprising that *GALC* overexpression exerted a different impact on the proteomic landscape of the two melanoma cell lines. Indeed, *GALC* transduction in A2058 cells resulted in the up- or downregulation of the expression levels of 37 and 14 proteins, respectively, whereas it exerted a stronger impact on A375 cells (263 and 184 proteins up- or downregulated, respectively).

Categorization analysis indicates a significant enrichment in both cell lines of downmodulated proteins involved in mitochondrial functions, including oxidative phosphorylation, mitochondrial respiratory chain complexes, and aerobic respiration. Melanoma cells can shuttle between glycolysis and respiration depending upon conditions of growth, hypoxia, acidosis, and therapy, and BRAF activity has been shown to suppress oxidative phosphorylation, thus driving aerobic glycolysis in melanoma. Thus, *GALC* appears to modulate the energetic plasticity of melanoma cells by metabolic reprogramming (Huang, Radi and Arbiser 2021). In this frame, it is interesting to note that alterations in the sphingolipid metabolism *via* modulation of the expression levels of the lysosomal acid ceramidase affect mitochondria activity in melanoma cells (Lai et al. 2021). Further studies will be required to elucidate the impact of *GALC* on the rewiring of energetic metabolism in melanoma.

Among the proteins whose levels of expression were affected by *GALC* overexpression in melanoma cells, 25 of them were upregulated in both A2058-up*GALC* and A375-up*GALC*

cells, whereas only 2 of them were downregulated in both cell types. Notably, 6 out of the 27 proteins modulated by *GALC* overexpression in both A2058- up*GALC* and A375-up*GALC* cells have been involved in melanoma biology, 4 proteins have been implicated in tumor immune escape and 10 proteins have been shown to play a role in ER stress responses, mitochondrial antioxidant activity, autophagy and/or apoptosis.

The results of the present work confirm and extend previous observations about the pro-oncogenic role of *GALC* (Belleri et al. 2020) by demonstrating that *GALC* overexpression increases the tumorigenic potential of both A2058 and A375 human melanoma cells harboring the tumor-driving BRAF(V600E) mutation.

Angiogenesis plays a pivotal role in melanoma progression. Consistent with the pro-oncogenic effects exerted by *GALC* on melanoma cells, we observed that *GALC* overexpressing A2058 and A375 cells give rise to more vascularized lesions when grafted in C57BL/6 mice. Of note, *GALC* promotes melanoma angiogenesis without affecting the secretion of angiogenic factors, including VEGF-A. Based on the observation that *GALC* can be secreted by producing cells (Nagano et al. 1998), we hypothesized *GALC* released by melanoma cells may promote tumor angiogenesis.

In keeping with this hypothesis, the CM of *GALC*-overexpressing melanoma cells contain significant levels of the enzyme and is able to induce angiogenic responses *in vitro* in HUVECs and *in vivo* in zebrafish embryos and in the chick embryo CAM. These effects were inhibited by the *GALC* inhibitors GCP and Dgal, indicating that the enzymatic activity of *GALC* is required to exert an angiogenic response. Accordingly, the enzymatically inactive *GALC*<sup>R396W</sup> mutant was devoid of a significant angiogenic potential *in vitro* and *in vivo* when expressed in HEK393T or A2058 cells.

The M6P/M6PR pathway allows the uptake and internalization of lysosomal enzymes present in the extracellular environment, including *GALC* (Nagano et al. 1998). Accordingly, we observed a progressive increase of *GALC* activity in HUVECs incubated with the CM of *GALC*-overexpressing melanoma cells and demonstrated that M6P is able to hamper the angiogenic potential of *GALC* *in vitro* and *in vivo*. Together, these data suggest that the internalization of enzymatically active *GALC* *via* its binding to M6PR is required to induce an angiogenic response in ECs. In keeping with this hypothesis, previous observations had shown that M6PR is involved in mediating proliferin-induced angiogenesis by allowing the internalization of proliferin into ECs (Volpert et al. 1996).

In this thesis, preliminary observations indicate that the activation of the prototypic angiogenic receptor VEGFR2 may mediate the angiogenic activity of GALC. Indeed, the CM of *GALC*-overexpressing melanoma cells causes the phosphorylation of this receptor and the activation of various downstream signalling pathways in HUVECs, abrogated by the GALC inhibitor Dgal. Surprisingly, a similar inhibitory effect was exerted also by the neutralizing anti-VEGF-A antibody Ranibizumab, despite the absence of significant differences in the levels of VEGF-A in the CM of *GALC*-overexpressing cells when compared to controls. At present, studies are in progress to assess the possibility that internalized GALC may modulate the lipid composition of HUVEC membranes, thus affecting the mobility of VEGFR2 on the cell surface and its capacity to interact with VEGF-A.

Together, these observations indicate for the first time that GALC may exert both autocrine and paracrine functions in human melanoma by conferring a pro-oncogenic phenotype to melanoma cells and inducing an angiogenic response in tumor endothelium.

## 7. REFERENCES

- Abed Rabbo, M., Y. Khodour, L. S. Kaguni & J. Stiban (2021) Sphingolipid lysosomal storage diseases: from bench to bedside. *Lipids Health Dis*, 20, 44.
- Airola, M. V. & Y. A. Hannun (2013) Sphingolipid metabolism and neutral sphingomyelinases. *Handb Exp Pharmacol*, 57-76.
- Airola, M. V., P. Shanbhogue, A. A. Shamseddine, K. E. Guja, C. E. Senkal, R. Maini, N. Bartke, B. X. Wu, L. M. Obeid, M. Garcia-Diaz & Y. A. Hannun (2017) Structure of human nSMase2 reveals an interdomain allosteric activation mechanism for ceramide generation. *Proc Natl Acad Sci U S A*, 114, E5549-E5558.
- Albi, E., M. Mersel, C. Leray, M. L. Tomassoni & M. P. Viola-Magni (1994) Rat liver chromatin phospholipids. *Lipids*, 29, 715-9.
- Amaria, R. N., S. M. Reddy, H. A. Tawbi, M. A. Davies, M. I. Ross, I. C. Glitza, J. N. Cormier, C. Lewis, W. J. Hwu, E. Hanna, A. Diab, M. K. Wong, R. Royal, N. Gross, R. Weber, S. Y. Lai, R. Ehlers, J. Blando, D. R. Milton, S. Woodman, R. Kageyama, D. K. Wells, P. Hwu, S. P. Patel, A. Lucci, A. Hessel, J. E. Lee, J. Gershenwald, L. Simpson, E. M. Burton, L. Posada, L. Haydu, L. Wang, S. Zhang, A. J. Lazar, C. W. Hudgens, V. Gopalakrishnan, A. Reuben, M. C. Andrews, C. N. Spencer, V. Prieto, P. Sharma, J. Allison, M. T. Tetzlaff & J. A. Wargo (2018) Neoadjuvant immune checkpoint blockade in high-risk resectable melanoma. *Nat Med*, 24, 1649-1654.
- Ascierto, P. A., J. M. Kirkwood, J. J. Grob, E. Simeone, A. M. Grimaldi, M. Maio, G. Palmieri, A. Testori, F. M. Marincola & N. Mozzillo (2012) The role of BRAF V600 mutation in melanoma. *J Transl Med*, 10, 85.
- Atilla-Gokcumen, G. E., E. Muro, J. Relat-Goberna, S. Sasse, A. Bedigian, M. L. Coughlin, S. Garcia-Manyes & U. S. Eggert (2014) Dividing cells regulate their lipid composition and localization. *Cell*, 156, 428-39.
- Baggiolini, A., S. J. Callahan, E. Montal, J. M. Weiss, T. Trieu, M. M. Tagore, S. E. Tischfield, R. M. Walsh, S. Suresh, Y. Fan, N. R. Campbell, S. C. Perlee, N. Saurat, M. V. Hunter, T. Simon-Vermot, T. H. Huang, Y. Ma, T. Hollmann, S. K. Tickoo, B. S. Taylor, E. Khurana, R. P. Koche, L. Studer & R. M. White (2021) Developmental chromatin programs determine oncogenic competence in melanoma. *Science*, 373, eabc1048.
- Barnhill, R. L., K. Fandrey, M. A. Levy, M. C. Mihm & B. Hyman (1992) Angiogenesis and tumor progression of melanoma. Quantification of vascularity in melanocytic nevi and cutaneous malignant melanoma. *Lab Invest*, 67, 331-7.
- Beckham, T. H., J. C. Cheng, P. Lu, Y. Shao, D. Troyer, R. Lance, S. T. Marrison, J. S. Norris & X. Liu (2013) Acid ceramidase induces sphingosine kinase 1/S1P receptor 2-mediated activation of oncogenic Akt signaling. *Oncogenesis*, 2, e49.
- Belleri, M., P. Chiodelli, M. Corli, M. Capra & M. Presta (2022) Oncosuppressive and oncogenic activity of the sphingolipid-metabolizing enzyme  $\beta$ -galactosylceramidase. *Biochim Biophys Acta Rev Cancer*, 1877, 188675.

- Belleri, M., G. Paganini, D. Coltrini, R. Ronca, D. Zizioli, M. Corsini, A. Barbieri, E. Grillo, S. Calza, R. Bresciani, E. Maiorano, M. G. Mastropasqua, T. Annese, A. Giacomini, D. Ribatti, J. Casas, T. Levade, G. Fabrias & M. Presta (2020)  $\beta$ -Galactosylceramidase Promotes Melanoma Growth via Modulation of Ceramide Metabolism. *Cancer Res*, 80, 5011-5023.
- Belleri, M., R. Ronca, D. Coltrini, B. Nico, D. Ribatti, P. L. Poliani, A. Giacomini, P. Alessi, S. Marchesini, M. B. Santos, E. R. Bongarzone & M. Presta (2013) Inhibition of angiogenesis by  $\beta$ -galactosylceramidase deficiency in globoid cell leukodystrophy. *Brain*, 136, 2859-75.
- Bergers, G. & L. E. Benjamin (2003) Tumorigenesis and the angiogenic switch. *Nat Rev Cancer*, 3, 401-10.
- Bhati, R., C. Patterson, C. A. Livasy, C. Fan, D. Ketelsen, Z. Hu, E. Reynolds, C. Tanner, D. T. Moore, F. Gabrielli, C. M. Perou & N. Klauber-DeMore (2008) Molecular characterization of human breast tumor vascular cells. *Am J Pathol*, 172, 1381-90.
- Bilal, F., A. Montfort, J. Gilhodes, V. Garcia, J. Riond, S. Carpentier, T. Filleron, C. Colacios, T. Levade, A. Daher, N. Meyer, N. Andrieu-Abadie & B. Ségui (2019) Sphingomyelin Synthase 1 (SMS1) Downregulation Is Associated With Sphingolipid Reprogramming and a Worse Prognosis in Melanoma. *Front Pharmacol*, 10, 443.
- Bizzozero, L., D. Cazzato, D. Cervia, E. Assi, F. Simbari, F. Pagni, C. De Palma, A. Monno, C. Verdelli, P. R. Querini, V. Russo, E. Clementi & C. Perrotta (2014) Acid sphingomyelinase determines melanoma progression and metastatic behaviour via the microphthalmia-associated transcription factor signalling pathway. *Cell Death Differ*, 21, 507-20.
- Braeuer, R. R., I. R. Watson, C. J. Wu, A. K. Mobley, T. Kamiya, E. Shoshan & M. Bar-Eli (2014) Why is melanoma so metastatic? *Pigment Cell Melanoma Res*, 27, 19-36.
- Braeuer, R. R., M. Zigler, G. J. Villares, A. S. Dobroff & M. Bar-Eli (2011) Transcriptional control of melanoma metastasis: the importance of the tumor microenvironment. *Semin Cancer Biol*, 21, 83-8.
- Capoferri, D., P. Chioldelli, M. Corli, M. Belleri, E. Scalvini, L. Mignani, J. Guerra, E. Grillo, V. De Giorgis, M. Manfredi & M. Presta (2023) The Pro-Oncogenic Sphingolipid-Metabolizing Enzyme  $\beta$ -Galactosylceramidase Modulates the Proteomic Landscape in BRAF(V600E)-Mutated Human Melanoma Cells. *Int J Mol Sci*, 24.
- Carlino, M. S., J. Larkin & G. V. Long (2021) Immune checkpoint inhibitors in melanoma. *Lancet*, 398, 1002-1014.
- CARTER, H. E. & W. J. HAINES (1947) Biochemistry of the sphingolipides; preparation of sphingolipides from beef brain and spinal cord. *J Biol Chem*, 169, 77-82.
- Cataldi, S., A. Borrelli, M. R. Ceccarini, I. Nakashidze, M. Codini, O. Belov, A. Ivanov, E. Krasavin, I. Ferri, C. Conte, F. F. Patria, T. Beccari, A. Mancini, F. Curcio, F. S. Ambesi-Impiombato & E. Albi (2020) Acid and Neutral Sphingomyelinase Behavior in Radiation-Induced Liver Pyroptosis and in the Protective/Preventive Role of rMnSOD. *Int J Mol Sci*, 21.

- Centeno, P. P., V. Pavet & R. Marais (2023) The journey from melanocytes to melanoma. *Nat Rev Cancer*, 23, 372-390.
- Chaube, R., V. M. Kallakunta, M. G. Espey, R. McLarty, A. Faccenda, S. Ananvoranich & B. Mutus (2012) Endoplasmic reticulum stress-mediated inhibition of nSMase2 elevates plasma membrane cholesterol and attenuates NO production in endothelial cells. *Biochim Biophys Acta*, 1821, 313-23.
- Cheng, J. C., A. Bai, T. H. Beckham, S. T. Marrison, C. L. Yount, K. Young, P. Lu, A. M. Bartlett, B. X. Wu, B. J. Keane, K. E. Armeson, D. T. Marshall, T. E. Keane, M. T. Smith, E. E. Jones, R. R. Drake, A. Bielawska, J. S. Norris & X. Liu (2013) Radiation-induced acid ceramidase confers prostate cancer resistance and tumor relapse. *J Clin Invest*, 123, 4344-58.
- Cho, S. M., H. K. Lee, Q. Liu, M. W. Wang & H. J. Kwon (2019) A Guanidine-Based Synthetic Compound Suppresses Angiogenesis via Inhibition of Acid Ceramidase. *ACS Chem Biol*, 14, 11-19.
- Clarke, C. J. (2018) Neutral Sphingomyelinases in Cancer: Friend or Foe? *Adv Cancer Res*, 140, 97-119.
- Clarke, C. J., J. M. Guthrie & Y. A. Hannun (2008) Regulation of neutral sphingomyelinase-2 (nSMase2) by tumor necrosis factor- $\alpha$  involves protein kinase C- $\delta$  in lung epithelial cells. *Mol Pharmacol*, 74, 1022-32.
- Clarke, C. J., K. Mediwala, R. W. Jenkins, C. A. Sutton, B. G. Tholanikunnel & Y. A. Hannun (2011) Neutral sphingomyelinase-2 mediates growth arrest by retinoic acid through modulation of ribosomal S6 kinase. *J Biol Chem*, 286, 21565-76.
- Clarke, C. J., T. G. Truong & Y. A. Hannun (2007) Role for neutral sphingomyelinase-2 in tumor necrosis factor  $\alpha$ -stimulated expression of vascular cell adhesion molecule-1 (VCAM) and intercellular adhesion molecule-1 (ICAM) in lung epithelial cells: p38 MAPK is an upstream regulator of nSMase2. *J Biol Chem*, 282, 1384-96.
- Coant, N. & Y. A. Hannun (2019) Neutral ceramidase: Advances in mechanisms, cell regulation, and roles in cancer. *Adv Biol Regul*, 71, 141-146.
- D'Angelo, G., S. Capasso, L. Sticco & D. Russo (2013) Glycosphingolipids: synthesis and functions. *FEBS J*, 280, 6338-53.
- Dai, Q., J. Liu, J. Chen, D. Durrant, T. M. McIntyre & R. M. Lee (2004) Mitochondrial ceramide increases in UV-irradiated HeLa cells and is mainly derived from hydrolysis of sphingomyelin. *Oncogene*, 23, 3650-8.
- Deane, J. E., S. C. Graham, N. N. Kim, P. E. Stein, R. McNair, M. B. Cachón-González, T. M. Cox & R. J. Read (2011) Insights into Krabbe disease from structures of galactocerebrosidase. *Proc Natl Acad Sci U S A*, 108, 15169-73.
- Degenhardt, Y., J. Huang, J. Greshock, G. Horiates, K. Nathanson, X. Yang, M. Herlyn & B. Weber (2010) Distinct MHC gene expression patterns during progression of melanoma. *Genes Chromosomes Cancer*, 49, 144-54.
- Denton, K. J., J. R. Stretch, K. C. Gatter & A. L. Harris (1992) A study of adhesion molecules as markers of progression in malignant melanoma. *J Pathol*, 167, 187-91.

- Devaux, P. F. & R. Morris (2004) Transmembrane asymmetry and lateral domains in biological membranes. *Traffic*, 5, 241-6.
- Dumoulin, F., D. Lafont, P. Boullanger, G. Mackenzie, G. H. Mehl & J. W. Goodby (2002) Self-organizing properties of natural and related synthetic glycolipids. *J Am Chem Soc*, 124, 13737-48.
- Eckhardt, M. (2010) Pathology and current treatment of neurodegenerative sphingolipidoses. *Neuromolecular Med*, 12, 362-82.
- Esch, S. W., T. D. Williams, S. Biswas, A. Chakrabarty & S. M. LeVine (2003) Sphingolipid profile in the CNS of the twitcher (globoid cell leukodystrophy) mouse: a lipidomics approach. *Cell Mol Biol (Noisy-le-grand)*, 49, 779-87.
- Filippov, V., M. A. Song, K. Zhang, H. V. Vinters, S. Tung, W. M. Kirsch, J. Yang & P. J. Duerksen-Hughes (2012) Increased ceramide in brains with Alzheimer's and other neurodegenerative diseases. *J Alzheimers Dis*, 29, 537-47.
- Filosto, S., M. Ashfaq, S. Chung, W. Fry & T. Goldkorn (2012) Neutral sphingomyelinase 2 activity and protein stability are modulated by phosphorylation of five conserved serines. *J Biol Chem*, 287, 514-522.
- Filosto, S., W. Fry, A. A. Knowlton & T. Goldkorn (2010) Neutral sphingomyelinase 2 (nSMase2) is a phosphoprotein regulated by calcineurin (PP2B). *J Biol Chem*, 285, 10213-22.
- Garbe, C., K. Peris, A. Hauschild, P. Saiag, M. Middleton, A. Spatz, J. J. Grob, J. Malvehy, J. Newton-Bishop, A. Stratigos, H. Pehamberger & A. Eggermont (2010) Diagnosis and treatment of melanoma: European consensus-based interdisciplinary guideline. *Eur J Cancer*, 46, 270-83.
- Gatt, S. & E. L. Bierman (1980) Sphingomyelin suppresses the binding and utilization of low density lipoproteins by skin fibroblasts. *J Biol Chem*, 255, 3371-6.
- Gault, C. R., L. M. Obeid & Y. A. Hannun (2010) An overview of sphingolipid metabolism: from synthesis to breakdown. *Adv Exp Med Biol*, 688, 1-23.
- Goñi, F. M. (2022) Sphingomyelin: What is it good for? *Biochem Biophys Res Commun*, 633, 23-25.
- Görögh, T., H. Rudert, B. M. Lippert, S. Gottschlich, S. Maune, K. Heidorn, J. Maass, M. Hoffmann, J. E. Meyer, I. O. Rathcke, B. J. Folz, T. Hortobagyi & J. A. Werner (1999) Transcriptional repression of the human galactocerebrosidase gene in squamous cell carcinomas of the larynx. *Int J Cancer*, 83, 750-4.
- Hannun, Y. A. & L. M. Obeid (2011) Many ceramides. *J Biol Chem*, 286, 27855-62.
- (2018) Sphingolipids and their metabolism in physiology and disease. *Nat Rev Mol Cell Biol*, 19, 175-191.
- Heering, J., N. Weis, M. Holeiter, F. Neugart, A. Staebler, T. N. Fehm, A. Bischoff, J. Schiller, S. Duss, S. Schmid, T. Korte, A. Herrmann & M. A. Olayioye (2012) Loss of the ceramide transfer protein augments EGF receptor signaling in breast cancer. *Cancer Res*, 72, 2855-66.



- Heo, K., K. A. Park, Y. H. Kim, S. H. Kim, Y. S. Oh, I. H. Kim, S. H. Ryu & P. G. Suh (2009) Sphingosine 1-phosphate induces vascular endothelial growth factor expression in endothelial cells. *BMB Rep*, 42, 685-90.
- Hill, C. H., G. M. Cook, S. J. Spratley, S. Fawke, S. C. Graham & J. E. Deane (2018) The mechanism of glycosphingolipid degradation revealed by a GALC-SapA complex structure. *Nat Commun*, 9, 151.
- Hill, C. H., S. C. Graham, R. J. Read & J. E. Deane (2013) Structural snapshots illustrate the catalytic cycle of  $\beta$ -galactocerebrosidase, the defective enzyme in Krabbe disease. *Proc Natl Acad Sci U S A*, 110, 20479-84.
- Hood, J. L., H. Pan, G. M. Lanza, S. A. Wickline & C. f. T. R. i. A. I. a. N. (C-TRAIN) (2009) Paracrine induction of endothelium by tumor exosomes. *Lab Invest*, 89, 1317-28.
- Hood, J. L., R. S. San & S. A. Wickline (2011) Exosomes released by melanoma cells prepare sentinel lymph nodes for tumor metastasis. *Cancer Res*, 71, 3792-801.
- Howe, K., M. D. Clark, C. F. Torroja, J. Torrance, C. Berthelot, M. Muffato, J. E. Collins, S. Humphray, K. McLaren, L. Matthews, S. McLaren, I. Sealy, M. Caccamo, C. Churcher, C. Scott, J. C. Barrett, R. Koch, G. J. Rauch, S. White, W. Chow, B. Kilian, L. T. Quintais, J. A. Guerra-Assunção, Y. Zhou, Y. Gu, J. Yen, J. H. Vogel, T. Eyre, S. Redmond, R. Banerjee, J. Chi, B. Fu, E. Langley, S. F. Maguire, G. K. Laird, D. Lloyd, E. Kenyon, S. Donaldson, H. Sehra, J. Almeida-King, J. Loveland, S. Trevanion, M. Jones, M. Quail, D. Willey, A. Hunt, J. Burton, S. Sims, K. McLay, B. Plumb, J. Davis, C. Clee, K. Oliver, R. Clark, C. Riddle, D. Elliot, G. Threadgold, G. Harden, D. Ware, S. Begum, B. Mortimore, G. Kerry, P. Heath, B. Phillimore, A. Tracey, N. Corby, M. Dunn, C. Johnson, J. Wood, S. Clark, S. Pelan, G. Griffiths, M. Smith, R. Glithero, P. Howden, N. Barker, C. Lloyd, C. Stevens, J. Harley, K. Holt, G. Panagiotidis, J. Lovell, H. Beasley, C. Henderson, D. Gordon, K. Auger, D. Wright, J. Collins, C. Raisen, L. Dyer, K. Leung, L. Robertson, K. Ambridge, D. Leongamornlert, S. McGuire, R. Gilderthorp, C. Griffiths, D. Manthavadi, S. Nichol, G. Barker, et al. (2013) The zebrafish reference genome sequence and its relationship to the human genome. *Nature*, 496, 498-503.
- Huang, C., R. H. Radi & J. L. Arbiser (2021) Mitochondrial Metabolism in Melanoma. *Cells*, 10.
- Hubler, W. R. & J. E. Wolf (1976) Melanoma. Tumor angiogenesis and human neoplasia. *Cancer*, 38, 187-92.
- Im, S. Y., H. M. Ko, J. W. Kim, H. K. Lee, T. Y. Ha, H. B. Lee, S. J. Oh, S. Bai, K. C. Chung, Y. B. Lee, H. S. Kang & S. B. Chun (1996) Augmentation of tumor metastasis by platelet-activating factor. *Cancer Res*, 56, 2662-5.
- Jabalee, J., R. Towle, J. Lawson, C. Dickman & C. Garnis (2020) Sphingomyelin phosphodiesterase 3 methylation and silencing in oral squamous cell carcinoma results in increased migration and invasion and altered stress response. *Oncotarget*, 11, 523-534.
- Jenkins, R. W., C. J. Clarke, D. Canals, A. J. Snider, C. R. Gault, L. Heffernan-Stroud, B. X. Wu, F. Simbari, P. Roddy, K. Kitatani, L. M. Obeid & Y. A. Hannun (2011) Regulation

- of CC ligand 5/RANTES by acid sphingomyelinase and acid ceramidase. *J Biol Chem*, 286, 13292-303.
- Jensen, S. A., A. E. Calvert, G. Volpert, F. M. Kouri, L. A. Hurley, J. P. Luciano, Y. Wu, A. Chalastanis, A. H. Futerman & A. H. Stegh (2014) Bcl2L13 is a ceramide synthase inhibitor in glioblastoma. *Proc Natl Acad Sci U S A*, 111, 5682-7.
- Keung, E. Z. & J. E. Gershenwald (2018) The eighth edition American Joint Committee on Cancer (AJCC) melanoma staging system: implications for melanoma treatment and care. *Expert Rev Anticancer Ther*, 18, 775-784.
- Kitatani, K., J. Idkowiak-Baldys & Y. A. Hannun (2008) The sphingolipid salvage pathway in ceramide metabolism and signaling. *Cell Signal*, 20, 1010-8.
- Kosaka, N., H. Iguchi, K. Hagiwara, Y. Yoshioka, F. Takeshita & T. Ochiya (2013) Neutral sphingomyelinase 2 (nSMase2)-dependent exosomal transfer of angiogenic microRNAs regulate cancer cell metastasis. *J Biol Chem*, 288, 10849-59.
- Köhler, C., D. Nittner, F. Rambow, E. Radaelli, F. Stanchi, N. Vandamme, A. Baggiolini, L. Sommer, G. Berx, J. J. van den Oord, H. Gerhardt, C. Blanpain & J. C. Marine (2017) Mouse Cutaneous Melanoma Induced by Mutant BRAf Arises from Expansion and Dedifferentiation of Mature Pigmented Melanocytes. *Cell Stem Cell*, 21, 679-693.e6.
- Lai, M., V. La Rocca, R. Amato, G. Freer, M. Costa, P. G. Spezia, P. Quaranta, G. Lombardo, D. Piomelli & M. Pistello (2021) Ablation of Acid Ceramidase Impairs Autophagy and Mitochondria Activity in Melanoma Cells. *Int J Mol Sci*, 22.
- Lee, J. H., E. Shklovskaya, S. Y. Lim, M. S. Carlino, A. M. Menzies, A. Stewart, B. Pedersen, M. Irvine, S. Alavi, J. Y. H. Yang, D. Strbenac, R. P. M. Saw, J. F. Thompson, J. S. Wilmott, R. A. Scolyer, G. V. Long, R. F. Kefford & H. Rizos (2020) Transcriptional downregulation of MHC class I and melanoma de-differentiation in resistance to PD-1 inhibition. *Nat Commun*, 11, 1897.
- Lehmann, J. M., B. Holzmann, E. W. Breitbart, P. Schmiegelow, G. Riethmüller & J. P. Johnson (1987) Discrimination between benign and malignant cells of melanocytic lineage by two novel antigens, a glycoprotein with a molecular weight of 113,000 and a protein with a molecular weight of 76,000. *Cancer Res*, 47, 841-5.
- Leonardi, G. C., L. Falzone, R. Salemi, A. Zanghì, D. A. Spandidos, J. A. Mccubrey, S. Candido & M. Libra (2018) Cutaneous melanoma: From pathogenesis to therapy (Review). *Int J Oncol*, 52, 1071-1080.
- Li, Y., Y. Xu, B. A. Benitez, M. S. Nagree, J. T. Dearborn, X. Jiang, M. A. Guzman, J. C. Woloszynek, A. Giaramita, B. K. Yip, J. Elsbernd, M. C. Babcock, M. Lo, S. C. Fowler, D. F. Wozniak, C. A. Vogler, J. A. Medin, B. E. Crawford & M. S. Sands (2019) Genetic ablation of acid ceramidase in Krabbe disease confirms the psychosine hypothesis and identifies a new therapeutic target. *Proc Natl Acad Sci U S A*, 116, 20097-20103.
- Liu, B., N. Andrieu-Abadie, T. Levade, P. Zhang, L. M. Obeid & Y. A. Hannun (1998) Glutathione regulation of neutral sphingomyelinase in tumor necrosis factor-alpha-induced cell death. *J Biol Chem*, 273, 11313-20.

- Liu, D. G., L. Xue, J. Li, Q. Yang & J. Z. Peng (2018) Epithelial-mesenchymal transition and GALC expression of circulating tumor cells indicate metastasis and poor prognosis in non-small cell lung cancer. *Cancer Biomark*, 22, 417-426.
- Liu, M., X. Yang, J. Liu, B. Zhao, W. Cai, Y. Li & D. Hu (2017) Efficacy and safety of BRAF inhibition alone versus combined BRAF and MEK inhibition in melanoma: a meta-analysis of randomized controlled trials. *Oncotarget*, 8, 32258-32269.
- Long, G. V., S. M. Swetter, A. M. Menzies, J. E. Gershenwald & R. A. Scolyer (2023) Cutaneous melanoma. *Lancet*, 402, 485-502.
- Luberto, C., D. F. Hassler, P. Signorelli, Y. Okamoto, H. Sawai, E. Boros, D. J. Hazen-Martin, L. M. Obeid, Y. A. Hannun & G. K. Smith (2002) Inhibition of tumor necrosis factor-induced cell death in MCF7 by a novel inhibitor of neutral sphingomyelinase. *J Biol Chem*, 277, 41128-39.
- Lugano, R., M. Ramachandran & A. Dimberg (2020) Tumor angiogenesis: causes, consequences, challenges and opportunities. *Cell Mol Life Sci*, 77, 1745-1770.
- Luzi, P., M. A. Rafi & D. A. Wenger (1995) Structure and organization of the human galactocerebrosidase (GALC) gene. *Genomics*, 26, 407-9.
- Mabeta, P. (2020) Paradigms of vascularization in melanoma: Clinical significance and potential for therapeutic targeting. *Biomed Pharmacother*, 127, 110135.
- Marchesini, N., C. Luberto & Y. A. Hannun (2003) Biochemical properties of mammalian neutral sphingomyelinase 2 and its role in sphingolipid metabolism. *J Biol Chem*, 278, 13775-83.
- Marcoval, J., A. Moreno, J. Graells, A. Vidal, J. M. Escribà, M. Garcia-Ramírez & A. Fabra (1997) Angiogenesis and malignant melanoma. Angiogenesis is related to the development of vertical (tumorigenic) growth phase. *J Cutan Pathol*, 24, 212-8.
- Marques, A. R., L. I. Willems, D. Herrera Moro, B. I. Florea, S. Scheij, R. Ottenhoff, C. P. van Roomen, M. Verhoek, J. K. Nelson, W. W. Kallemeijn, A. Biela-Banas, O. R. Martin, M. B. Cachón-González, N. N. Kim, T. M. Cox, R. G. Boot, H. S. Overkleeft & J. M. Aerts (2017) A Specific Activity-Based Probe to Monitor Family GH59 Galactosylceramidase, the Enzyme Deficient in Krabbe Disease. *Chembiochem*, 18, 402-412.
- Martin, J. J., J. G. Leroy, C. Ceuterick, J. Libert, P. Dodinval & L. Martin (1981) Fetal Krabbe leukodystrophy. A morphologic study of two cases. *Acta Neuropathol*, 53, 87-91.
- Mattei, S., M. P. Colombo, C. Melani, A. Silvani, G. Parmiani & M. Herlyn (1994) Expression of cytokine/growth factors and their receptors in human melanoma and melanocytes. *Int J Cancer*, 56, 853-7.
- Menaldino, D. S., A. Bushnev, A. Sun, D. C. Liotta, H. Symolon, K. Desai, D. L. Dillehay, Q. Peng, E. Wang, J. Allegood, S. Trotman-Pruett, M. C. Sullards & A. H. Merrill (2003) Sphingoid bases and de novo ceramide synthesis: enzymes involved, pharmacology and mechanisms of action. *Pharmacol Res*, 47, 373-81.
- Mentzer, S. J. & M. A. Konerding (2014) Intussusceptive angiogenesis: expansion and remodeling of microvascular networks. *Angiogenesis*, 17, 499-509.

- Meyers-Needham, M., S. Ponnusamy, S. Gencer, W. Jiang, R. J. Thomas, C. E. Senkal & B. Ogretmen (2012) Concerted functions of HDAC1 and microRNA-574-5p repress alternatively spliced ceramide synthase 1 expression in human cancer cells. *EMBO Mol Med*, 4, 78-92.
- Michaloglou, C., L. C. Vredeveld, M. S. Soengas, C. Denoyelle, T. Kuilman, C. M. van der Horst, D. M. Majoor, J. W. Shay, W. J. Mooi & D. S. Peeper (2005) BRAFE600-associated senescence-like cell cycle arrest of human naevi. *Nature*, 436, 720-4.
- Mignani, L., J. Guerra, M. Corli, D. Capoferri & M. Presta (2023) Zebra-Sphinx: Modeling Sphingolipidoses in Zebrafish. *Int J Mol Sci*, 24.
- Miller, A. J. & M. C. Mihm (2006) Melanoma. *N Engl J Med*, 355, 51-65.
- Montfort, A., F. Bertrand, J. Rochotte, J. Gilhodes, T. Filleron, J. Milhès, C. Dufau, C. Imbert, J. Riond, M. Tosolini, C. J. Clarke, F. Dufour, A. A. Constantinescu, N. F. Junior, V. Garcia, M. Record, P. Cordelier, P. Brousset, P. Rochaix, S. Silvente-Poirot, N. Therville, N. Andrieu-Abadie, T. Levade, Y. A. Hannun, H. Benoist, N. Meyer, O. Micheau, C. Colacios & B. Ségui (2021) Neutral Sphingomyelinase 2 Heightens Anti-Melanoma Immune Responses and Anti-PD-1 Therapy Efficacy. *Cancer Immunol Res*, 9, 568-582.
- Morad, S. A. & M. C. Cabot (2013) Ceramide-orchestrated signalling in cancer cells. *Nat Rev Cancer*, 13, 51-65.
- Moretti, S., C. Pinzi, A. Spallanzani, E. Berti, A. Chiarugi, S. Mazzoli, M. Fabiani, C. Vallecchi & M. Herlyn (1999) Immunohistochemical evidence of cytokine networks during progression of human melanocytic lesions. *Int J Cancer*, 84, 160-8.
- Nagano, S., T. Yamada, N. Shinnoh, H. Furuya, T. Taniwaki & J. Kira (1998) Expression and processing of recombinant human galactosylceramidase. *Clin Chim Acta*, 276, 53-61.
- Ogretmen, B. (2018) Sphingolipid metabolism in cancer signalling and therapy. *Nat Rev Cancer*, 18, 33-50.
- Park, E. S., S. J. Kim, S. W. Kim, S. L. Yoon, S. H. Leem, S. B. Kim, S. M. Kim, Y. Y. Park, J. H. Cheong, H. G. Woo, G. B. Mills, I. J. Fidler & J. S. Lee (2011) Cross-species hybridization of microarrays for studying tumor transcriptome of brain metastasis. *Proc Natl Acad Sci U S A*, 108, 17456-61.
- Peng, J., B. Chen, Z. Shen, H. Deng, D. Liu, X. Xie, X. Gan, X. Xu, Z. Huang & J. Chen (2015) DNA promoter hypermethylation contributes to down-regulation of galactocerebrosidase gene in lung and head and neck cancers. *Int J Clin Exp Pathol*, 8, 11042-50.
- Prager, B. C., Q. Xie, S. Bao & J. N. Rich (2019) Cancer Stem Cells: The Architects of the Tumor Ecosystem. *Cell Stem Cell*, 24, 41-53.
- Pralhada Rao, R., N. Vaidyanathan, M. Rengasamy, A. Mammen Oommen, N. Somaiya & M. R. Jagannath (2013) Sphingolipid metabolic pathway: an overview of major roles played in human diseases. *J Lipids*, 2013, 178910.
- Qendro, V., D. H. Lundgren, K. Rezaul, F. Mahony, N. Ferrell, A. Bi, A. Latifi, D. Chowdhury, S. Gygi, W. Haas, L. Wilson, M. Murphy & D. K. Han (2014) Large-scale proteomic characterization of melanoma expressed proteins reveals nestin and vimentin as

- biomarkers that can potentially distinguish melanoma subtypes. *J Proteome Res*, 13, 5031-40.
- Qiu, Y., J. Shen, W. Jiang, Y. Yang, X. Liu & Y. Zeng (2022) Sphingosine 1-phosphate and its regulatory role in vascular endothelial cells. *Histol Histopathol*, 37, 213-225.
- Revill, K., T. Wang, A. Lachenmayer, K. Kojima, A. Harrington, J. Li, Y. Hoshida, J. M. Llovet & S. Powers (2013) Genome-wide methylation analysis and epigenetic unmasking identify tumor suppressor genes in hepatocellular carcinoma. *Gastroenterology*, 145, 1424-35.e1-25.
- Rodriguez-Cuenca, S., V. Pellegrinelli, M. Campbell, M. Oresic & A. Vidal-Puig (2017) Sphingolipids and glycerophospholipids - The "ying and yang" of lipotoxicity in metabolic diseases. *Prog Lipid Res*, 66, 14-29.
- Ross, M. I. & J. E. Gershenwald (2011) Evidence-based treatment of early-stage melanoma. *J Surg Oncol*, 104, 341-53.
- Senkal, C. E., S. Ponnusamy, Y. Manevich, M. Meyers-Needham, S. A. Saddoughi, A. Mukhopadhyay, P. Dent, J. Bielawski & B. Ogretmen (2011) Alteration of ceramide synthase 6/C16-ceramide induces activating transcription factor 6-mediated endoplasmic reticulum (ER) stress and apoptosis via perturbation of cellular Ca<sup>2+</sup> and ER/Golgi membrane network. *J Biol Chem*, 286, 42446-42458.
- Shamseddine, A. A., M. V. Airola & Y. A. Hannun (2015a) Roles and regulation of neutral sphingomyelinase-2 in cellular and pathological processes. *Adv Biol Regul*, 57, 24-41.
- Shamseddine, A. A., C. J. Clarke, B. Carroll, M. V. Airola, S. Mohammed, A. Rella, L. M. Obeid & Y. A. Hannun (2015b) P53-dependent upregulation of neutral sphingomyelinase-2: role in doxorubicin-induced growth arrest. *Cell Death Dis*, 6, e1947.
- Shirane, K., R. Kuji, C. Tareyanagi, T. Sato, Y. Kobayashi, S. Furukawa, T. Murata, S. Kubota, Y. Ishikawa, K. Segawa & K. Furukawa (2014) Gene expression levels of  $\beta$ -galactosyltransferase 5 correlate with the tumorigenic potentials of B16-F10 mouse melanoma cells. *Glycobiology*, 24, 532-41.
- Slotte, J. P. (2013) Biological functions of sphingomyelins. *Prog Lipid Res*, 52, 424-37.
- Slotte, J. P., A. S. Härmälä, C. Jansson & M. I. Pörn (1990) Rapid turn-over of plasma membrane sphingomyelin and cholesterol in baby hamster kidney cells after exposure to sphingomyelinase. *Biochim Biophys Acta*, 1030, 251-7.
- Suchlandt, G., W. Schlote & K. Harzer (1982) [Ultrastructural findings in 9 fetuses following prenatal diagnosis of neuropilipidoses]. *Arch Psychiatr Nervenkr (1970)*, 232, 407-26.
- Swanton, C., M. Marani, O. Pardo, P. H. Warne, G. Kelly, E. Sahai, F. Elustondo, J. Chang, J. Temple, A. A. Ahmed, J. D. Brenton, J. Downward & B. Nicke (2007) Regulators of mitotic arrest and ceramide metabolism are determinants of sensitivity to paclitaxel and other chemotherapeutic drugs. *Cancer Cell*, 11, 498-512.
- Tirodkar, T. S., P. Lu, A. Bai, M. J. Scheffel, S. Gencer, E. Garrett-Mayer, A. Bielawska, B. Ogretmen & C. Voelkel-Johnson (2015) Expression of Ceramide Synthase 6 Transcriptionally Activates Acid Ceramidase in a c-Jun N-terminal Kinase (JNK)-dependent Manner. *J Biol Chem*, 290, 13157-67.

- Tohumeken, S., P. Deme, S. W. Yoo, S. Gupta, R. Rais, B. S. Slusher & N. J. Haughey (2023) Neuronal deletion of nSMase2 reduces the production of A $\beta$  and directly protects neurons. *Neurobiol Dis*, 177, 105987.
- Viallard, C. & B. Larrivée (2017) Tumor angiogenesis and vascular normalization: alternative therapeutic targets. *Angiogenesis*, 20, 409-426.
- Visigalli, I., S. Ungari, S. Martino, H. Park, M. Cesani, B. Gentner, L. Sergi Sergi, A. Orlacchio, L. Naldini & A. Biffi (2010) The galactocerebrosidase enzyme contributes to the maintenance of a functional hematopoietic stem cell niche. *Blood*, 116, 1857-66.
- Volpert, O., D. Jackson, N. Bouck & D. I. Linzer (1996) The insulin-like growth factor II/mannose 6-phosphate receptor is required for proliferin-induced angiogenesis. *Endocrinology*, 137, 3871-6.
- Wang, J., J. Li, J. Gu, J. Yu, S. Guo, Y. Zhu & D. Ye (2015) Abnormal methylation status of FBXW10 and SMPD3, and associations with clinical characteristics in clear cell renal cell carcinoma. *Oncol Lett*, 10, 3073-3080.
- Wang, P., Y. Yuan, W. Lin, H. Zhong, K. Xu & X. Qi (2019) Roles of sphingosine-1-phosphate signaling in cancer. *Cancer Cell Int*, 19, 295.
- Warren, B. A. & P. Shubik (1966) The growth of the blood supply to melanoma transplants in the hamster cheek pouch. *Lab Invest*, 15, 464-78.
- Wechman, S. L., L. Emdad, D. Sarkar, S. K. Das & P. B. Fisher (2020) Vascular mimicry: Triggers, molecular interactions and in vivo models. *Adv Cancer Res*, 148, 27-67.
- Wegner, M. S., S. Schiffmann, M. J. Parnham, G. Geisslinger & S. Grösch (2016) The enigma of ceramide synthase regulation in mammalian cells. *Prog Lipid Res*, 63, 93-119.
- Weinstock, N. I., L. Wrabetz, M. L. Feltri & D. Shin (2016) Metabolic profiling reveals biochemical pathways and potential biomarkers associated with the pathogenesis of Krabbe disease. *J Neurosci Res*, 94, 1094-107.
- Won, J. S., A. K. Singh & I. Singh (2016) Biochemical, cell biological, pathological, and therapeutic aspects of Krabbe's disease. *J Neurosci Res*, 94, 990-1006.
- Yang, M., Z. Jiang, G. Yao, Z. Wang, J. Sun, H. Qin & H. Zhao (2020) GALC Triggers Tumorigenicity of Colorectal Cancer via Senescent Fibroblasts. *Front Oncol*, 10, 380.
- Yazama, H., K. Kitatani, K. Fujiwara, M. Kato, M. Hashimoto-Nishimura, K. Kawamoto, K. Hasegawa, H. Kitano, A. Bielawska, J. Bielawski & T. Okazaki (2015) Dietary glucosylceramides suppress tumor growth in a mouse xenograft model of head and neck squamous cell carcinoma by the inhibition of angiogenesis through an increase in ceramide. *Int J Clin Oncol*, 20, 438-46.
- Yu, S., K. Wang, Q. Li, Y. Wei, Y. Li, Q. Zhang, P. Huang, H. Liang, H. Sun, H. Peng, X. Huang, C. Liu, J. Zhou, J. Qian & C. Li (2023) Nonalcoholic steatohepatitis critically rewires the ischemia/reperfusion-induced dysregulation of cardiolipins and sphingolipids in mice. *Hepatobiliary Surg Nutr*, 12, 3-19.
- Zahedipour, F., P. Zamani, K. Jamialahmadi, M. R. Jaafari & A. Sahebkar (2021) Vaccines targeting angiogenesis in melanoma. *Eur J Pharmacol*, 912, 174565.

- Zanfani, A., E. Dreassi, A. Berardi, P. Piomboni, E. Costantino-Ceccarini & A. Luddi (2014) GC-EI-MS analysis of fatty acid composition in brain and serum of twitcher mouse. *Lipids*, 49, 1115-25.
- Zhang, Q., H. Seltmann, C. C. Zouboulis & J. B. Travers (2006) Activation of platelet-activating factor receptor in SZ95 sebocytes results in inflammatory cytokine and prostaglandin E2 production. *Exp Dermatol*, 15, 769-74.
- Zhang, Z., S. Imani, M. D. Shasaltaneh, H. Hosseinfard, L. Zou, Y. Fan & Q. Wen (2019) The role of vascular mimicry as a biomarker in malignant melanoma: a systematic review and meta-analysis. *BMC Cancer*, 19, 1134.
- Zhao, Y., Y. Guo, Z. Wang, Z. Xiao, R. Li, A. Luo, C. Wu, Z. Jing, N. Sun, X. Chen, H. Du & Y. Zeng (2015) GALC gene is downregulated by promoter hypermethylation in Epstein-Barr virus-associated nasopharyngeal carcinoma. *Oncol Rep*, 34, 1369-78.
- Zizioli, D., M. Guarienti, C. Tobia, G. Gariano, G. Borsani, R. Bresciani, R. Ronca, E. Giacomuzzi, A. Preti, G. Gaudenzi, M. Belleri, E. Di Salle, G. Fabrias, J. Casas, D. Ribatti, E. Monti & M. Presta (2014) Molecular cloning and knockdown of galactocerebrosidase in zebrafish: new insights into the pathogenesis of Krabbe's disease. *Biochim Biophys Acta*, 1842, 665-75.
- Šála, M., K. R. Hollinger, A. G. Thomas, R. P. Dash, C. Tallon, V. Veeravalli, L. Lovell, M. Kögler, H. Hřebabeký, E. Procházková, O. Nešuta, A. Donoghue, J. Lam, R. Rais, C. Rojas, B. S. Slusher & R. Nencka (2020) Novel Human Neutral Sphingomyelinase 2 Inhibitors as Potential Therapeutics for Alzheimer's Disease. *J Med Chem*, 63, 6028-6056.

## **9. RINGRAZIAMENTI**

Un sentito ringraziamento al professor Presta per avermi guidato durante questi tre anni e a tutto il gruppo GALC che mi ha aiutato nella realizzazione di questo lavoro.

Ringrazio anche il professor Bruno Segù per avermi accolto nel suo laboratorio e tutto il team melasphinx per avermi fatto sentire a casa.

Un grazie di cuore anche a tutta la sezione di oncologia per i consigli ricevuti.

Un immenso grazie a Nico che mi è stato accanto in tutto questo percorso e alla mia famiglia per aver portato tanta pazienza.



**MODULO DI EMBARGO DELLA TESI**  
**(da compilare solo se si richiede un periodo di segretezza della tesi)**

Il/La sottoscritto/a Marzia Corli Nato/a il 23/06/1993 a Treviso Bresciano, provincia di Brescia  
Dottorato di Ricerca in Precision Medicine

**DICHIARA**

- che il contenuto della tesi **non può essere immediatamente consultabile per il seguente motivo: presenza di dati non ancora pubblicati.**

La motivazione deve essere dettagliata e controfirmata obbligatoriamente dal Primo Supervisore di tesi  
(Brevetto, segreto industriale, motivi di priorità nella ricerca, motivi editoriali, altro)

- che il testo completo della tesi potrà essere reso consultabile dopo:

- 6 mesi dalla data di conseguimento titolo
- 12 mesi dalla data di conseguimento titolo

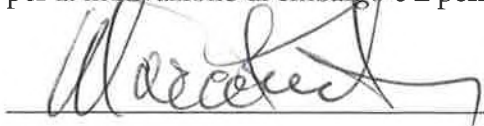
- che sarà comunque consultabile immediatamente l'abstract della tesi, che viene caricato in Esse3, profilo studente.

Luogo e Data  
Brescia, 08/01/2024

Firma del Dichiarante

  
\_\_\_\_\_

Controfirma del Primo Supervisore di tesi  
per la motivazione di embargo e il periodo.

  
\_\_\_\_\_